



Copyright Undertaking

This thesis is protected by copyright, with all rights reserved.

By reading and using the thesis, the reader understands and agrees to the following terms:

1. The reader will abide by the rules and legal ordinances governing copyright regarding the use of the thesis.
2. The reader will use the thesis for the purpose of research or private study only and not for distribution or further reproduction or any other purpose.
3. The reader agrees to indemnify and hold the University harmless from and against any loss, damage, cost, liability or expenses arising from copyright infringement or unauthorized usage.

IMPORTANT

If you have reasons to believe that any materials in this thesis are deemed not suitable to be distributed in this form, or a copyright owner having difficulty with the material being included in our database, please contact lbsys@polyu.edu.hk providing details. The Library will look into your claim and consider taking remedial action upon receipt of the written requests.

**RESILIENCE-BASED SEISMIC PERFORMANCE OF
INDIVIDUAL BUILDINGS AND COMMUNITY
PORTFOLIOS**

HAZANFAR ALI ANWAR

PhD

The Hong Kong Polytechnic University

2022

The Hong Kong Polytechnic University
Department of Civil and Environmental Engineering

**Resilience-based seismic performance of individual
buildings and community portfolios**

Ghazanfar Ali ANWAR

A thesis submitted in partial fulfilment of the requirements for the degree
of Doctor of Philosophy

August 2022

CERTIFICATE OF ORIGINALITY

I hereby declare that this thesis is my work and that, to the best of my knowledge and belief, it reproduces no material previously published or written, nor material that has been accepted for the award of any other degree or diploma, except where due acknowledgment has been made in the text.

_____ (Signed)

ANWAR Ghazanfar Ali (Name of student)

This thesis is dedicated to my parents
Mr. Muhammad Anwar Ghumman & Mrs. Rehana Kousar

ABSTRACT

The vulnerability of the built environment to natural hazards has increased in recent decades due to the growing population, increased construction activities, and climate change, among others. This exposure to natural hazards and resulting consequences are projected to increase substantially by the end of the century. The existing building portfolios and infrastructure systems are already vulnerable to extreme events and are likely to be increased in the future due to the aging of existing structures, non-conformance to updated codes, and changing future hazard scenarios. This is evident from past hazards such as the 1994 Northridge and 1995 Kobe earthquakes, in which the buildings provided intended life safety function but still incur huge damage to the structures resulting in significant socioeconomic and environmental consequences due to repair activities and reduced functionality of buildings. The reduced functionality due to the relatively un-organized recovery process of building portfolios as observed in recent hazards including the 2004 Sumatra-Andaman earthquake and tsunami and 2005 hurricane Katrina has further highlighted the need to assess and possibly enhance the performance of the community building portfolios.

Hence, it is essential to develop frameworks and methodologies that can better predict the socioeconomic and environmental consequences of extreme events. These uncertain consequences could be assembled into meaningful performance indicators including risk, resilience, and sustainability. Also, there is a need to better assess these performance indicators on buildings and community portfolio-level. Furthermore, there is a need to improve the performance of considered infrastructure systems and the built environment by considering different mitigation alternatives. Finally, a decision-

making framework is required to provide optimal solutions to reduce the uncertain consequences given the least mitigation costs.

This thesis aim to provide methodologies and frameworks for the mathematical modeling of buildings and community portfolios by considering risk, resilience, and sustainability performance indicators under seismic hazard scenarios. The highlighted problems and research gaps are addressed in this thesis in different chapters, divided into two parts and three stages. Part 1 is focused on providing mathematical models for individual buildings and part 2 is focused on community building portfolios. Each part is further divided into three stages depending upon the type of problem addressed. For instance, stage 1 of each part is focused on the performance assessment methodologies under seismic hazard considering multiple performance indicators, stage 2 is focused on the performance enhancement frameworks and methods under seismic hazard by implementing conventional retrofit tools and techniques, and stage 3 is focused on developing decision-making methodologies by implementing strategies established in the first two stages and including multi-criteria optimization and decision-making methods.

Hence, the proposed frameworks include performance assessments, enhancements, and decision-making for buildings and community building portfolios under seismic hazard scenarios considering various methodologies, theories, algorithms, tools, and techniques including a building-level framework for risk, resilience, and sustainability assessment, seismic resilience enhancement considering conventional retrofit techniques, performance-based assessment and enhancement methodologies, resilience assessment framework on a community building portfolio-level considering utility networks, interactions, and access to essential facilities, and

the performance-based assessment and enhancement methodologies for surrogate-based optimization and decision-making of buildings on a community level.

These assessments, enhancement, and decision-making frameworks are illustrated on individual buildings and on community portfolios to demonstrate their potential, significance, and applicability. Finally, the conclusions and recommendations are made and future works, prospects, and potential future directions are suggested.

LIST OF PUBLICATIONS

Journal articles

Anwar, G.A., Dong, Y.*, & Ouyang, M. (2022). Systems thinking approach to community buildings resilience considering utility networks, interactions, and access to essential facilities. *Bulletin of Earthquake Engineering*, 1-29. <https://doi.org/10.1007/s10518-022-01557-y>

Anwar, G.A., & Dong, Y.* (2022). Surrogate-based decision-making of community building portfolios under uncertain consequences and risk attitudes. *Engineering Structures*, 268, 114749. <https://doi.org/10.1016/j.engstruct.2022.114749>

Zhou, Z., **Anwar, G. A.***, & Dong, Y. (2022). Performance-based bi-objective retrofit optimization of building portfolios considering uncertainties and environmental Impacts. *Buildings*, 12(1), 85. <https://doi.org/10.3390/buildings12010085>

Anwar, G. A., Dong, Y.*, & Li, Y. (2020). Performance-based decision-making of buildings under seismic hazard considering long-term loss, sustainability, and resilience. *Structure and Infrastructure Engineering*, 17(4), 454-470. <https://doi.org/10.1080/15732479.2020.1845751>

Anwar, G. A., & Dong, Y.* (2020). Seismic resilience of retrofitted RC buildings. *Earthquake Engineering and Engineering Vibration*, 19(3), 561-571. <https://doi.org/10.1007/s11803-020-0580-z>

Anwar, G. A., Dong, Y.*, & Zhai, C. (2020). Performance-based probabilistic framework for seismic risk, resilience, and sustainability assessment of reinforced

concrete structures. *Advances in Structural Engineering*, 23(7), 1454-1472.
<https://doi.org/10.1177/1369433219895363>

Zheng, Y., Dong, Y., Chen, B., & **Anwar, G. A.** (2019). Seismic damage mitigation of bridges with self-adaptive SMA-cable-based bearings. *Smart Structures and Systems*, 24(1), 127-139. <https://doi.org/10.12989/sss.2019.24.1.127>

Conference papers

Anwar, G. A., and Dong, Y. (2022). Probabilistic building portfolio recovery modelling under macroeconomic conditions. *Proceedings of the 13th International Conference on Structural Safety and Reliability (ICOSSAR 2021)*, Shanghai, P.R. China, Jun 21-25, 2021

Anwar, G. A., and Dong, Y. (2022). Gaussian process-based optimization framework for community building portfolios considering resilience and sustainability objectives. *The International Symposium on Reliability Engineering and Risk Management (ISRERM)*, Hannover, Germany.

Anwar, G. A., and Dong, Y. (2021). Socio-economic and environmental constraints-based community resilience assessment. *Engineering Mechanics Institute Conference/ Probabilistic Mechanics and Reliability Conference*, Columbia University, New York City, Virtually.

Anwar, G. A., and Dong, Y. (2020). Restoration modelling of Water Network under seismic hazard: Role of Electrical and Power Network. *Proceedings of the 5th International Conference on Civil, Structural and Transportation Engineering*, Niagara Falls, Canada, Virtually.

Anwar, G. A., and Dong, Y. (2019), Economic Loss Evaluation Comparing Component and System-Level Fragility Assessment Methods. *First Eurasian Conference on OpenSEES Hong Kong*, Hong Kong, China

ACKNOWLEDGMENTS

I would like to express my deepest gratitude to my chief supervisor Dr. You Dong, for his utmost guidance and support during my entire Ph.D. tenure at The Hong Kong Polytechnic University (PolyU). The kind of leadership, management, and supervision he has provided throughout this time is truly unique and has been extremely helpful for my career building. This work would not have been possible without his leadership, guidance, and support. I am immensely grateful for his patience, kindness, empathy, and support during all these years. I am also grateful and fortunate to get an opportunity to work under his kind supervision. Best supervisor ever!

I would also like to thank and extend my appreciation to my co-supervisor Dr. Songye Zhu, university professors, external examiners, university staff, and everyone else who played a part in this journey with me. Also, I would like to thank Ms. Elsie Cheung for always being willing to go a step further in helping research students.

I also would like to extend thanks and gratitude to my very nice group members Dr. Peng Yuan, Dr. Ruiwei Feng, Dr. Hongyuan Guo, Dr. Yaohan Li, Dr. Anastasios Giouvanidis, Menghan Zhao, Jing Qian, Deming Zhu, Li Lai, Yu Zhang, Jiabin Zhang, Fuhao Deng, and Qian Wu. It is a pleasure to be a part of such a helping and supportive group.

Furthermore, I would also like to extend my thanks to all my friends who have truly made me feel at home. I will always remember those tea and lunch sessions with Numan Malik, Dr. Mustesin Ali Khan, and Dr. Aatif Ali Khan. Also the unlimited amount of gatherings with Husnain Tansar, Mudasir Hussain, Abdullah, Naeem, Asad

Ali, Waseem, and Danish. You guys have made me feel at home and have made this Ph.D. journey easier and more fulfilling.

Also, I would like to extend appreciation to my brothers Jehanzaib Anwar, Farhan Anwar, Furqan Anwar, my beautiful sister Urooj Fatima, and my loving wife Sana Arshad. I love you guys more than anything!

Finally, I would like to express my deepest gratitude to my parents Mr. Muhammad Anwar Ghumman and Mrs. Rehana Kausar. I have no words to express the unconditional love and support I have from my parents and it has always been a driving force for me in my life. My parents have always been my motivation and truly give meaning to my life. This work has not have been possible without the unconditional love and support of my parents. Love you always!

CONTENTS

CERTIFICATE OF ORIGINALITY	i
ABSTRACT.....	iii
LIST OF PUBLICATIONS	vi
ACKNOWLEDGMENTS	ix
CONTENTS.....	xi
LIST OF FIGURES	xviii
LIST OF TABLES	xxvi
CHAPTER 1 INTRODUCTION	1
1.1 Background and motivation.....	1
1.2 Scope and objectives	4
1.3 Thesis outline.....	5
1.4 Contributions	9
CHAPTER 2 LITERATURE REVIEW	12
2.1 Introduction	12
2.2 Resilience and sustainability	14
2.3 Performance enhancements strategies	17

2.4	Resilience assessment of community buildings	21
2.5	Optimization and decision-making.....	25
2.6	Research Gaps	29
CHAPTER 3 PERFORMANCE-BASED PROBABILISTIC FRAMEWORK FOR SEISMIC RISK, RESILIENCE, AND SUSTAINABILITY		31
3.1	Introduction	31
3.2	Sustainability and resilience under seismic hazard	32
3.2.1	Seismic sustainability	32
3.2.2	Seismic resilience	33
3.3	Integrated performance-based engineering	35
3.3.1	Hazard analysis	37
3.3.2	Structural analysis.....	37
3.3.3	Damage analysis	38
3.3.4	Seismic risk assessment.....	39
3.3.5	Seismic sustainability and resilience assessment.....	39
3.4	Illustrative example	42
3.4.1	Description and modeling of the investigated building	42
3.4.2	Structural vulnerability	44

3.4.3	Performance, seismic loss, and sustainability.....	47
3.4.4	Downtime and resilience	53
3.5	Summary.....	59
CHAPTER 4 SEISMIC RESILIENCE OF RETROFITTED BUILDINGS		61
4.1	Introduction	61
4.2	Seismic resilience assessment	62
4.2.1	Developing collapse fragilities from pushover.....	63
4.2.2	Consequence assessment	65
4.2.3	Seismic resilience assessment.....	67
4.3	Illustrative example	70
4.3.1	Developing collapse fragilities from pushover.....	71
4.3.2	Consequence assessment	74
4.3.3	Seismic resilience assessment.....	78
4.4	Conclusions	82
CHAPTER 5 PERFORMANCE-BASED DECISION-MAKING OF BUILDINGS UNDER SEISMIC HAZARD		84
5.1	Introduction	84
5.2	Multi-criteria decision-making framework	85

5.2.1	Performance-assessment module (PAM).....	85
5.2.2	Sustainability-assessment module (SAM).....	88
5.2.3	Resilience-assessment module (RAM).....	90
5.3	Performance-based decision-making.....	95
5.3.1	Criteria evaluation.....	96
5.3.2	TOPSIS	97
5.4	Illustrative example	99
5.4.1	Performance and sustainability assessment module	101
5.4.2	Resilience assessment module	107
5.4.3	Performance-based decision-making module (PB-MCDM)	111
5.5	Conclusions	115
CHAPTER 6 SEISMIC RESILIENCE OF COMMUNITY BUILDINGS		118
6.1	Introduction	118
6.2	Community resilience framework	119
6.3	Component damage and recovery	120
6.3.1	Component damage assessment.....	122
6.3.2	Component recovery assessment.....	123

6.4	Network modeling and functionality assessment	126
6.4.1	Network connectivity modeling.....	127
6.4.2	Capacity, demand, and supply modeling	129
6.4.3	Interdependencies and functionality assessment of buildings	131
6.5	Community resilience assessment	136
6.5.1	Community functionality	136
6.5.2	Access to essential facilities	138
6.5.3	Community resilience	139
6.6	Illustrative example	140
6.6.1	Defining hazard scenarios.....	141
6.6.2	Component damage and recovery assessment.....	142
6.6.3	Network modeling and functionality assessment	143
6.6.4	Community resilience assessment	146
6.7	Conclusions	152

CHAPTER 7 PERFORMANCE-BASED RETROFIT OPTIMIZATION OF COMMUNITY BUILDINGS..... 155

7.1	Introduction	155
7.2	Optimization Framework for Community Building Portfolios	156

7.3	Performance-Based Community Objectives Assessment.....	159
7.3.1	Building-Level Damage Assessments	160
7.3.2	Building-Level Consequence Assessments	161
7.3.3	Portfolio-Level Performance Objectives Assessment	163
7.4	Bi-Objective Evolutionary Optimization.....	163
7.4.1	Fast Non-Dominated Sorting and Crowding Distances.....	165
7.4.2	Selection, Crossover, and Mutation.....	166
7.4.3	New Population Generation.....	168
7.5	Illustrative Example.....	169
7.5.1	Performance-Based Assessment	171
7.5.2	Bi-Objective Evolutionary Optimization.....	175
7.6	Conclusions	182

**CHAPTER 8 BAYESIAN OPTIMIZATION AND DECISION-MAKING OF
COMMUNITY BUILDINGS..... 184**

8.1	Introduction	184
8.2	Proposed optimization and decision-making framework	185
8.3	Performance-based expensive black-box	188
8.4	Efficient multi-objective surrogate-based optimization	190

8.4.1	Generating initial dataset for individuals.....	191
8.4.2	Building a Gaussian process model.....	192
8.4.3	Sample functions via spectral sampling.....	195
8.4.4	Evaluating Pareto-optimal solutions from sampled functions.....	196
8.4.5	Generating new points to query expensive black-box function...	197
8.4.6	Updating the dataset of individuals	198
8.5	Utility Decision Theory under Uncertainty	198
8.6	Illustrative example	200
8.6.1	Performance-based expensive black-box.....	202
8.6.2	Surrogate-based efficient multi-objective optimization	205
8.6.3	Decision making under Uncertainty	212
8.7	Conclusions	215
CHAPTER 9 CONCLUSIONS AND FUTURE WORK		218
9.1	Conclusions	218
9.2	Future directions	221
REFERENCES.....		224

LIST OF FIGURES

Figure 1-1 Organization and outline of the thesis based on performance assessment, enhancement, and decision-making of buildings	9
Figure 3-1 Resilience assessment under hazards	34
Figure 3-2 PEER PBEE methodology incorporating sustainability and resilience	36
Figure 3-3 Probabilistic sustainability and resilience quantification framework	42
Figure 3-4 Vertical member design and layout of 8-story building.....	43
Figure 3-5 (a) IDA results and (b) Fragility curves of the investigated RC building ..	45
Figure 3-6 Time histories of inter-story drifts at (a) story-5 under SLE scenario, (b) story-5 under DLE scenario, and (c) story-6 under MCE scenario and time histories of maximum accelerations at (d) story-8 under SLE scenario, (e) story-3 under DLE scenario, and (f) story-1 under MCE scenario	46
Figure 3-7 EDPs for earthquake scenarios (a) Peak inter-story drift ratios and (b) peak floor acceleration	47
Figure 3-8 Distributions for repair loss associated with structural and non-structural components at (a) SLE, (b) DLE, and (c) MCE	50
Figure 3-9 CO ₂ emissions under three earthquake scenarios.....	53
Figure 3-10 Downtime for the slow and fast track at levels (a) SLE, (b) DLE, and (c) MCE.....	56

Figure 3-11 Distributions of resilience at investigated 100, 200, and 300 days under DLE.....	58
Figure 3-12 Expected resilience under 1000 days investigated period under (a) SLE, (b) DLE, and (c) MCE.....	58
Figure 4-1. The methodology for assessing seismic resilience using a nonlinear static procedure.....	63
Figure 4-2. Functionality states and recovery considering structural and non-structural damage, impeding delays, sequence of repairs, and utility availability.....	69
Figure 4-3. Building plan and structural details.....	71
Figure 4-4. Capacity curve for (a) reference structure, (b) reinforced concrete jacketing, (c) FRP overlays, and (d) steel jacketing.....	73
Figure 4-5. Collapse fragilities for (a) FRP overlays, (b) reinforced concrete jacketing, and (c) steel jacketing	74
Figure 4-6. Fragility and consequence functions for considered structural columns ..	75
Figure 4-7. The social consequence in terms of expected fatalities given IM.....	77
Figure 4-8. Consequences (a) Economic in terms of monetary loss, and (b) Environmental in terms of kgCO ₂ emissions.....	78
Figure 4-9. Expected resilience of a reference un-retrofitted building under given scenarios.....	80

Figure 4-10. Seismic hazard scenario of 0.32g showing (a) functionality curves, and (b) seismic resilience	81
Figure 5-1 Main modules of the proposed framework	85
Figure 5-2 Illustration of building restoration after an earthquake event	95
Figure 5-3 Illustration for computing EAC: (a) Derivative of hazard curve, (b) consequence curve, and (c) integration of slope of hazard and consequences given IM	97
Figure 5-4 Building model and layout of 4-story building	100
Figure 5-5 Collapse fragility curves for building with retrofit options	103
Figure 5-6 Expectation of probabilistic loss curves: (a) Economic and (b) social	104
Figure 5-7 Long-term loss under investigated time interval: (a) Economic and (b) Social	104
Figure 5-8 Long-term loss curves: (a) Economic and (b) Social.....	106
Figure 5-9 Environmental loss: (a) Total embodied energy and (b) long-term equivalent carbon emissions	107
Figure 5-10 Downtime assessment flowchart.....	108
Figure 5-11 Functionality states repair sequence at (a) FLE, (b) DLE, and (c) MCE	110

Figure 5-12 Expected resilience for (a) FLE, DLE, and MCE scenarios under different investigated time intervals and (b) DLE scenario with and without utility system and impeding factors.....	111
Figure 5-13 Relative closeness coefficient ranking retrofit alternatives based on PB-MCDM linking loss, sustainability, and resilience	113
Figure 5-14 Relative closeness coefficient ranking retrofit alternatives against risk attitude of decision-makers	113
Figure 6-1 The proposed framework for community resilience assessment	120
Figure 6-2 The augmented adjacency matrix representation of multi-networks	128
Figure 6-3 The illustration of functionality assessment of building i via systems thinking	133
Figure 6-4 The illustration of network capacity, demand, supply and functionality modeling	136
Figure 6-5 Inherent resilience and access to essential facilities (a) during the investigated time, and (b) in terms of percentage of buildings being able to access the facilities within certain distances	139
Figure 6-6 Spatial distributions of building portfolios, WN system, and EPN system	140
Figure 6-7 Spatial distribution of median (a) PGA under 95-year (b) PGV under 95-year, and considered four hazard scenarios	141

Figure 6-8 Recovery under four hazard scenarios for (a) WN, and (b) EPN	143
Figure 6-9 WN repair during the investigated time under design hazard scenario ...	144
Figure 6-10 EPN repair during the investigated time under four hazard scenarios...	144
Figure 6-11 Functionality assessment of a community building portfolios under the design hazard scenario during the investigated time of (a) 0 days, (b) 100days, (c) 300 days, and (d) 500 days	146
Figure 6-12 Community functionality assessment of building portfolios under the design hazard scenario	147
Figure 6-13 Community full functionality assessment showing the effect of utility dependence for different hazard scenarios of (a) 475-year, (b) 95-year, and (c) 2475-year.....	148
Figure 6-14 Loss of resilience (LoR) due to supply and demand of utilities for (a) Non-essential facilities, and (b) Essential facilities	149
Figure 6-15 Inherent resilience of a community via access to essential facilities.....	150
Figure 6-16 Access to EI under design hazard scenario during the investigated time of (a) 0 days, (b) 60 days, (c) 100 days, and (d) 150 days	151
Figure 6-17 Access to essential facilities for (a) CB, (b) ER, (c) MC, and (d) EI.....	152
Figure 6-18 Community resilience assessment under the four hazard scenarios	152
Figure 7-1 Bi-objective retrofit optimization framework for community building portfolio considering uncertainties.	157

Figure 7-2 Evolutionary optimization terminologies in the context of community building portfolio.	158
Figure 7-3 Performance objectives assessment of community building portfolio utilizing performance-based assessment methodology.....	159
Figure 7-4 Damage state assessment under seismic hazard.....	161
Figure 7-5 Illustration of fast non-dominated sorting and crowding distances.	166
Figure 7-6 Illustrative community consisting of building communities.....	170
Figure 7-7 Damage states distributions of community building portfolio under given hazard.....	172
Figure 7-8 Damage states of community building portfolio under a given hazard. ..	173
Figure 7-9 Performance indicators of community building portfolio under a given hazard scenario.....	174
Figure 7-10 Performance indicator distributions of community building portfolio given hazard scenario for (a) Risk, (b) Downtime, and (c) Sustainability	175
Figure 7-11 Pareto-optimal solutions of performance indicators against retrofit costs for (a) Risk, (b) Downtime, and (c) Sustainability	178
Figure 7-12 Mean values of buildings at different retrofit levels in a population along with considered four retrofit programs.	179
Figure 7-13 Distributions of risk performance indicator under four retrofit programs.	181

Figure 7-14 Distributions of downtime performance indicator under four retrofit programs.	181
Figure 7-15 Distributions of sustainability performance indicator under four retrofit programs.	182
Figure 8-1 Proposed efficient multi-objective performance-based optimization and decision-making framework for community building portfolios under uncertain consequences and risk attitudes	186
Figure 8-2 Proposed methodology for efficient surrogate-based optimization for community building portfolio	191
Figure 8-3 The community building portfolio with different structural systems under seismic hazard.....	201
Figure 8-4 The probability density functions of the repair costs under four hazard scenarios.....	203
Figure 8-5 Community building portfolios repair costs under hazard scenario of (a) 95-year, (b) 475-year, (c) 975-year, and (d) 2475-year	203
Figure 8-6 Cumulative distribution functions of community building portfolios for (a) casualties, (b) repair costs, (c) equivalent carbon emissions, and (d) embodied energy	204
Figure 8-7 Community building portfolios recovery under design hazard scenario during the investigated time of (a) 00 days, (b) 200 days, (c) 400 days, and (d) 600 days	205

Figure 8-8 Community building portfolios recovery during the investigated time for hazard scenario of (a) 95-year, (b) 475-year, (c) 975-year, and (d) 2475-year	205
Figure 8-9 Approximate Pareto-optimal solution showing retrofit cost versus repair cost under design hazard scenario	207
Figure 8-10 Community building portfolio repair costs under the design hazard scenario against the retrofit cost of (a) 0 million USD, (b) 5 million USD, (c) 10 million USD, and (d) 15 million USD.....	208
Figure 8-11 Approximate Pareto-optimal solution showing retrofit cost versus repair cost (a) under four hazard scenarios, and (b) Expected annual consequences	209
Figure 8-12 Approximate Pareto-optimal solutions for considered performance objectives in terms of EACs	210
Figure 8-13 The efficiency of the proposed optimization approach against the conventional genetic algorithm in terms of hyper improvement and computational time per iteration	212
Figure 8-14 The expected utility against the retrofit costs considering risk attitudes	214
Figure 8-15 The highlighted approximate Pareto-optimal solutions for considered performance objectives in terms of EACs given risk perceptions with maximum expected utility.....	215

LIST OF TABLES

Table 3-1 Fragility curves and repair costs of the damageable components	48
Table 3-2 Damage ratios corresponding to different damage states	51
Table 3-3 Repair actions of damageable components at different damage states	51
Table 3-4 Material take-offs and CO ₂ emissions of different building materials.....	52
Table 3-5 Probabilistic repair times of damageable components	54
Table 4-1. Fragility functions and consequence functions of damageable components	76
Table 4-2. Impeding factors for delay and utility disruption curves.....	81
Table 5-1. Functionality states definition considering structural, non-structural damage, and utility availability	94
Table 5-2. Fragility and consequence functions of damageable components	102
Table 5-3. Environmental consequence functions of damageable components	106
Table 5-4. Impeding factors for delay and utility disruption curves.....	109
Table 5-5. Rankings of retrofit alternatives against given scenarios	115
Table 6-1 Summary of physical infrastructure systems and key components' damage and recovery assessment	121

Table 6-2 The computational procedure for connectivity modeling	133
Table 7-1 Statistical moments of damage states of community building portfolio given hazard.....	172
Table 7-2 Statistical moments of risk performance indicator under considered retrofit programs.	180

CHAPTER 1 INTRODUCTION

1.1 Background and motivation

A community building portfolio is an essential part of the built environment that sustains many important community functions such as providing housing, commercial activities, education, health, and emergency services, among others. In addition, the community buildings provide infrastructure to sustain social well-being and economic activities (Roohi et al., 2020). These functions can be hindered in a hazardous event due to the damage to community buildings. Recent post-hazard damage assessments such as Hurricane Katrina in 2005, Wenchuan Earthquake in 2008, and Superstorm Sandy in 2012 have highlighted the increased vulnerability of the built environment. Major earthquakes have also highlighted significant damage to community buildings with the housing sector alone representing 50 percent of the total economic consequence (Alisjahbana and Kiremidjian, 2020). The recovery process of the building infrastructure system is also complex, usually not centrally planned, comparatively takes longer, and includes various stakeholders and decision-makers (Wang et al., 2020). It is therefore important to have science-based tools and decision-making frameworks to assess and enhance community buildings.

Also, the existing building infrastructure around the world is at risk of poor performance in an earthquake event due to inadequate structural detailing and inefficient seismic design provisions implemented during the design and construction of these buildings (Gautam and Chaulagain, 2016). The seismic loss can be significant

for the deficient existing buildings, particularly in low-to-medium seismicity regions where the seismic codes have not been adopted. This also highlights the importance of improving the performance of existing structures to reduce seismic consequences and increase resilience.

The design codes provide life safety performance objectives under design hazard scenarios but to evaluate other performance objectives, performance-based methodologies are usually implemented (Porter, 2003). Performance-based methods can be utilized along with optimization techniques to assess and possibly enhance the performance of buildings and infrastructure systems (Kim et al., 2011; Dong et al., 2014; Wang et al., 2019). The performance may be assessed in terms of meaningful socioeconomic and environmental consequences including repair costs, downtime of buildings, and equivalent carbon emissions, among others (Broccardo et al., 2015). These multiple and sometimes conflicting consequences require a multi-objective optimization and decision-making approach to enhance community performance considering sustainability and resilience.

Bruntland Report (Keeble, 1988) describes sustainability as the “development that meets the needs of the present without compromising the ability of future generations to meet their own needs”. Architecture 2030 (2019) estimates the building industry in the U.S. consumes almost 49% of the energy and contributes 47% of the total equivalent CO₂ emissions. Previously, the operational energy consumption was nearly 88% as compared to the embodied energy consumption of 12%, but the ratio has been significantly reduced more recently due to the advancements in operational efficiency, to a point where embodied energy contribution is a significant factor in overall sustainability. Therefore, it is increasingly becoming important to assess and

reduce embodied impacts in sustainable design tools. In infrastructure development, sustainability is achieved by reducing social, economic, and environmental impacts on the life-cycle of a structure (Frangopol et al., 1997; Wang et al., 2018). However, these sustainability assessments often only consider high probability, low consequence events and might fail in enhancing sustainability in the regions, where extreme events cannot be ignored (Dong et al., 2014; Gencturk et al., 2016). The extreme events impart damage to the structure resulting in additional social, economic, and environmental consequences referred to herein as seismic sustainability. Thus, it is of vital importance to incorporate sustainability in the performance-based assessment and decision-making of civil infrastructure.

Disaster assessment studies related to 1994 Northridge, California, and 1995 Kobe, Japan indicate that the consequences of a disaster are not limited to the immediate aftermath, but will continue during the recovery phase referred to herein as lack of resilience (Kilanitis and Sextos, 2019). Resilience addresses parameters such as robustness, functionality, and downtime (Lounis and McAllister, 2016). The recovery of a building is multi-disciplinary and depends on various factors such as additional delays for financing and management, utility availability, and the sequence of repairs. The additional delays due to impeding factors, and the dependencies on the utilities may impact the downtime of a building, hence overall seismic resilience. Hence, a logical sequence of repairs, utility availability, and additional delays due to inspections, mobilization, financing for accurate estimation of downtime, and resilience of a building is required for accurate estimation of resilience.

Considering the aforementioned discussion, it is imperative to develop assessment, enhancement, and decision-making methodologies for the built

environment considering various approaches including performance-based methods, optimization, and multi-criteria decision-making, among others. Also, considering the immediate and continuing impacts of the extreme events along with their consequences on the environment, the performance-based assessment, enhancement, and decision-making methodologies should be focused in terms of meaningful performance indicators including resilience and sustainability. The development of these methodologies on building and portfolio-level are discussed in this thesis.

1.2 Scope and objectives

The scope of this thesis includes developing performance-based assessment, enhancement, and decision-making methodologies on building and community portfolio-level considering risk, resilience, and sustainability-related indicators. The specific objectives are listed as follows:

1. Develop a performance-based probabilistic framework for seismic risk, resilience, and sustainability assessment of reinforced concrete structures by utilizing component-level detailed finite element and performance models. Subsequently, utilizing the framework for efficient retrofit selection based on the seismic resilience of deficient buildings retrofitted with the conventional mitigation approaches.
2. Propose a performance-based multi-criteria decision-making framework for buildings under seismic hazard considering long-term loss, sustainability, and resilience to provide rankings for considered retrofit alternatives considering the entire hazard curve and multiple socioeconomic and environmental performance indicators.

3. Formulate a system thinking approach to assess the resilience of buildings on a community level considering utility networks, interactions, and access to essential facilities to develop an efficient recovery and resilience assessment framework.
4. Propose a multi-objective surrogate-based optimization and decision-making framework for community building portfolios under uncertain consequences and risk attitudes to develop an efficient technique for performance-enhancement and multi-criteria decision-making on a community level under uncertain consequences and risk attitudes.

1.3 Thesis outline

This thesis consists of nine chapters divided into two parts and each part into three stages as shown in Figure 1-1. The first chapter provides the introduction of the thesis, followed by the literature review chapter, and the last chapter provides the conclusion and future work. Chapters' three to eight provide the frameworks, methodologies, and illustrative examples related to performance-based assessment, enhancement, and decision-making considering risk, resilience, and sustainability performance indicators.

The first part of the thesis is from chapter 3 to chapter 5 which focused on (1) building-level assessment, enhancement, and decision-making strategies, and the second part is from chapter 6 to chapter 8 and is focused on (2) community-level assessment, enhancement, and decision-making strategies. Each part further consists of three stages: (1) stage 1 is comprised of developing and implementing an assessment framework, (2) stage 2 is focused on developing and implementing an enhancement framework considering retrofit alternatives, and (3) stage 3 is focused on the multi-

criteria decision-making strategies to provide rankings and optimal decisions considering risk, resilience and sustainability performance indicators.

A summary of each chapter is as follows:

Chapter 1 provides an introduction of the thesis which comprises of background and motivation of the thesis, overall aim and specific objectives, thesis organization, and main contributions of the thesis.

Chapter 2 provides a literature review related to the risk, resilience, and sustainability performance indicators, performance-based assessment methodologies, performance enhancement-related strategies, optimization strategies, and multi-criteria decision-making methods on individual building and community portfolio levels.

Chapter 3 provides a building-level performance assessment framework for risk, resilience, and sustainability assessment of reinforced concrete buildings. The uncertainties associated with structural performance and consequence functions are incorporated. Distributed repair loss, equivalent carbon emissions, and downtime are calculated. The residual functionalities are determined probabilistically, and resilience is quantified for an investigated time period. The proposed approach is illustrated on a non-ductile RC frame structure.

Chapter 4 provides a building-level performance enhancement framework considering conventional retrofit alternatives to improve the seismic resilience of existing structures. The social, economic, and environmental consequences are evaluated and compared for a reference non-retrofitted, and a retrofitted building. It is concluded that applying retrofit techniques reduces the probability of collapse, social,

economic, and environmental consequences. The repair times of a building's components are also reduced, hence improving the seismic resilience.

Chapter 5 provides a building-level multi-criteria decision-making framework considering the entire seismic hazard curve to rank considered retrofit alternatives based on seismic risk, resilience, and sustainability performance indicators. The social, economic, and environmental consequences are determined for the investigated building by considering different retrofit alternatives and utilized in the decision-making process. A reinforced concrete building with three retrofit alternatives is selected as an illustrative example, and based on this example, it can be concluded that the framework can be used for the ranking of retrofit alternatives against different criteria.

Chapter 6 provides a community-level framework for resilience assessment of building portfolios considering functionality from utility networks, interactions, and access to essential facilities. The framework is developed following a synthesis paradigm of systems thinking. Subsequently, the framework is applied to a community consisting of building portfolios, water, and power systems. The building functionality states are defined, and the community resilience is assessed via community functionality and access to essential facilities.

Chapter 7 provides a community-level performance enhancement framework for building portfolios considering conventional retrofit alternatives under a pre-hazard scenario considering socioeconomic and environmental consequences. Performance-based assessment methodology is utilized to assess performance objectives in terms of risk, downtime, and sustainability. Then, the performance objectives are optimized by

utilizing an evolutionary optimization approach for given retrofit levels for each building in a community. The proposed methodology is implemented on an illustrative community and Pareto-optimal solutions are developed. Finally, the Pareto-optimal solutions are utilized to assess four different retrofit programs to enhance the community performance.

Chapter 8 provides a community-level performance optimization and decision-making framework by utilizing efficient surrogate-based optimization and utility decision theory-based multi-criteria decision-making methods. The proposed framework provides approximate Pareto-optimal solutions by utilizing performance-based method, Gaussian process models, spectral sampling, and genetic optimization. Later, utility decision theory is implemented to determine ideal solutions among the approximate Pareto-optimal solutions.

Chapter 9 presents the conclusions and provides possible future directions.

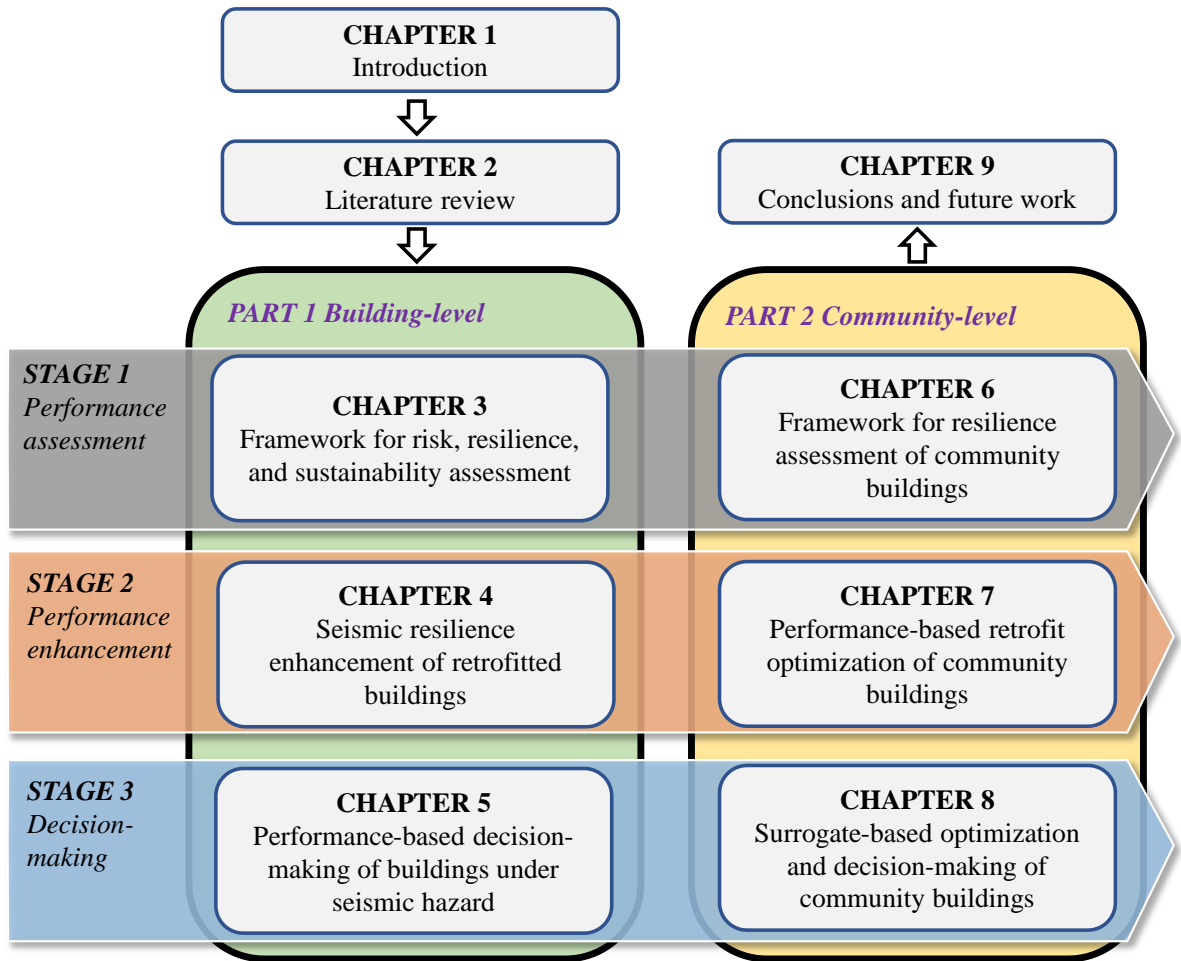


Figure 1-1 Organization and outline of the thesis based on performance assessment, enhancement, and decision-making of buildings

1.4 Contributions

The major contributions of the thesis are as follows:

1. A probabilistic performance-based approach is proposed to aid the development of next-generation performance-based engineering incorporating both resilience and sustainability. Subsequently, the approach is utilized for retrofit selection based on the seismic resilience of deficient buildings retrofitted with the conventional mitigation approaches. The component-based methodology is

considered for the sustainability and resilience assessment by compiling nonlinear numerical and building performance models. The collapse fragilities are developed from the pushover, time histories, and incremental dynamic analyses, and the resulting socioeconomic, and environmental consequences are determined. Also, the resilience of buildings is assessed by developing a downtime assessment methodology incorporating a sequence of repairs, impeding factors, and utility availability. Finally, different functionality states are developed to assess the performance during the investigated time.

2. A performance-based multi-criteria decision-making framework is developed by utilizing a performance-based approach coupled with seismic loss, sustainability, and resilience for the selection of different retrofit alternatives. To achieve this, a component-based probabilistic approach is utilized for the seismic loss, sustainability, and resilience assessment from a long-term perspective. The resulting socioeconomic and environmental consequences are converted to expected annual consequences by considering the full range of seismic hazards and are utilized as a multi-criterion in the technique for order preference by similarity to the ideal solution to rank considered retrofit alternatives for performance enhancements.
3. A community-level seismic resilience assessment framework is proposed considering utility networks, interactions, and access to essential facilities. The resilience of community building portfolios is achieved by utilizing the dependencies and interdependencies of utility networks, and by considering geospatial access to services by utilizing inherent resilience and access to essential facilities. The proposed approach provides important insights into

community resilience such as building functionality, utility demand, and supply, access to essential facilities, among others.

4. To support decision-making on a community level, a multi-objective decision-making framework considering multiple performance objectives is proposed. The methodology considers performance-based assessment, multi-objective optimization, and a decision-making method to evaluate, enhance and provide decision-support considering community performance. The contributions include considering a performance-based black-box to evaluate the socio-economic and environmental consequences by considering all the possible hazard scenarios, a surrogate-based multi-objective optimization approach to inexpensively approximate the Pareto-optimal solutions, and a utility theory-based decision-making considering multiple performance-objectives over an entire hazard curve and under different risk attitudes.

CHAPTER 2 LITERATURE REVIEW

2.1 Introduction

Most of the building stock is privately owned and the decision-making related to the choices including the type of construction, and up-gradation, among others, is partially decentralized (i.e., buildings construction and up-gradation-related activities are not entirely centrally planned by a government body or community stakeholders). The stakeholders and decision-makers must work in collaboration and form an organizational structure to reduce the hazard impacts (Godschalk, 2003). Different levels of organizational structure perform different functions. For instance, the construction of main roads and bridges is decided at a state level, the mitigation support may be provided at a state or country level. The planning to assess the hazards, characterize the built environment, assess the performance, and identify possible mitigation alternatives can be performed on a community level (Koliou et al., 2017). Hence, it is important to consider the performance of buildings on a building as well as portfolio level for possible collective assessments, enhancements, and decision-making.

The performance of buildings is usually assessed in terms of engineering demand parameters (Fajfar, 2000; Ghobarah, 2001; Huang et al., 2017; Guo et al., 2021). These parameters provide engineering information that is difficult to comprehend for community stakeholders and decision-makers. For instance, given a possible hazard scenario, engineering demand parameters for a particular building may

include story drifts, spectral accelerations, deflections, and curvatures, among others (Moehle, 2006; Jeong et al., 2012; Lemma et al., 2021). These parameters are checked against the allowable limits to verify the acceptable performance of a building under hazards (FEMA, 2005; Zheng et al., 2019; Guan M. EERI et al., 2021; Jalayer et al., 2021).

More recently, demand parameters that may be more meaningful to the community stakeholders are being utilized to better assess the performance of a community (Giouvanidis and Dong, 2020; Chen et al., 2021). The utilized demand parameters may include total casualties, total repair costs, and total repair time under a given hazard scenario that gives a meaningful performance assessment parameter that community stakeholders can understand (Dong and Frangopol, 2016a; Hashemi et al., 2019; Anwar et al., 2020). The demand parameters are usually correlated with the discrete damage states of buildings via fragility functions which are lognormal cumulative distribution functions, providing the probability of exceeding damage states given intensity measures. Different damage states provide contributions of a varying percent to the assessment of demand parameters which are discussed in various methods available in literature including FEMA, HAZUS, among others (HAZUS, 2003; FEMA-P-58, 2012; Vettore et al., 2020). These demand parameters can provide an intuitive understanding of the performance of buildings under a hazard and are utilized in this research to assess and enhance community performance.

The collective demand parameters are assessed by utilizing performance indicators. The performance indicators considered in the literature include risk, resilience, and sustainability (Rodriguez-Nikl, 2015; McAllister and Moddemeyer, 2018; Yang and Frangopol, 2018). The risk performance indicator is related to the

immediate impact of extreme events and has been extensively utilized to assess the performance of buildings under hazard scenarios (Barbat et al., 2010; Erdik, 2017; Battarra et al., 2018). These immediate impacts may include the total number of casualties, total waste generated, and total repair costs on a community level, among others.

The resilience performance indicator is related to the consequences arising due to the non-functionality of buildings such as population outmigration, and business interruptions, among others (Miles and Chang, 2006; Miles et al., 2018; Donà et al., 2019). Resilience is often measured in relation to the downtime and functionality assessments of buildings (Burton et al., 2017; Feng et al., 2017; Lin and Wang, 2017a; Masoomi and van de Lindt, 2018; Hassan and Mahmoud, 2020; Sen et al., 2021). However, the sustainability performance indicator considers consequences that may compromise the ability of future generations to meet their needs (Zinke et al., 2012; Asprone and Manfredi, 2015). For instance, the release of potential global warming gases during the repair activities from a hazard event would impact the environment negatively and may impact future generations. These performance indicators can cover a wide range of consequences, provide more meaningful and intuitive information, and can be utilized to make decisions and enhance performance.

2.2 Resilience and sustainability

The first step towards a resilient community is to understand individual infrastructure components and their relation to a whole community. Numerous studies exist in the literature proposing frameworks for the resilience assessment of individual buildings and community portfolios. For instance, Broccardo et al. (2015) presented a

probabilistic resilience assessment methodology of civil systems, and Burton et al. (2015) proposed a performance-based methodology for the recovery process associated with a building community. A methodology for recovery modeling by aggregating building-level restoration using probabilistic damage assessment was later developed for community building portfolios (Lin and Wang, 2017b; Lin and Wang, 2017a). Similar approaches were developed for the functionality recovery and resilience assessments for the built environment (Koliou et al., 2017; Masoomi and van de Lindt, 2018; Masoomi et al., 2020) and few studies utilized detailed component-based damage and consequence assessment approaches to quantify resilience (Dong and Frangopol, 2016a; Hashemi et al., 2019).

Sustainability addresses social, economic, and environmental issues and their impact on future generations (Zhao et al., 2014; Sabatino et al., 2015). Structures constructed in hazard-prone regions need to be resilient also to fulfill sustainability objectives (Zheng et al., 2018; Wen et al., 2019). Resilience and sustainability have vast similarities and should be considered together for a resilient and sustainable built environment (Bocchini et al., 2014; Rodriguez-Nikl, 2015). Frameworks for resilience and sustainability assessment of the built environment have also been developed over the last few years (Marchese et al., 2018) and studies are available that have incorporated sustainability in hazard-prone regions as well (Asprone and Manfredi, 2015; Gencturk et al., 2016).

However, a computational platform incorporating seismic sustainability and resilience using a detailed component-level damage assessment model is limited. Moreover, there is an increasing trend to incorporate uncertainties in seismic sustainability and resilience assessment procedures. The uncertainties in the prediction

models arise because of the inability to accurately predict hazards, structural modeling uncertainties, and uncertainty in the damage assessments, among others. Additionally, there are uncertainties associated with consequences resulting from repair actions, downtime, and carbon emissions, among others. The cumulative result of these inherent uncertainties makes precise evaluation difficult and should also be incorporated while addressing the sustainability and resilience of the building environment.

Limited studies are available investigating seismic sustainability and resilience of buildings utilizing physics-based building fragilities and component-level damage assessment considering uncertainties as well. For instance, Hashemi et al. (2019) investigated seismic sustainability and resilience of limited-ductile buildings. A multi-axis hybrid simulation was performed and CFRP retrofit was investigated on a soft-story building. Structural damage states were defined experimentally, and performance-based methodology was used to incorporate resilience into the life-cycle sustainability approach.

There is a further need to incorporate comprehensive structural and non-structural components in the component-based performance assessment methodology. Additionally, there exist uncertainties in seismic sustainability and resilience and a probabilistic platform is required to present results realistically. In comparison, this thesis evaluates seismic sustainability and resilience probabilistically considering the uncertainties in the framework by not just utilizing the lognormal or normal distributions of repair cost, repair times, and equivalent carbon emissions but also incorporates Gaussian process surrogate models for uncertainty propagation and assessment.

2.3 Performance enhancements strategies

Repair, rehabilitation, and retrofitting are utilized to improve the performance of existing buildings. Recently, it has become an important construction activity, considering that the amount of money spent globally on the repair and rehabilitation of existing structures is higher than on new constructions (Ma et al., 2017). The retrofitting techniques include adding lateral force-resisting systems or upgrading the existing elements for structural performance improvement (Zheng et al., 2019). The upgrading of existing elements can be implemented by either reducing the demands on a lateral force-resisting or improving the capacity, achieved by modifying strength, stiffness, ductility properties, or through any of these combinations (Thermou and Elnashai, 2006).

Ductility depends on the detailing of structural components and therefore, its retrofitting would require improving beam-column joints and rebar reinforcements, which can be disruptive and expensive. Hence this type of retrofitting is rarely used in the low-to-medium seismicity region (Calvi, 2013). A more desirable approach for ductility-related retrofitting is to reduce the demands on the structure by modifying or replacing lateral force-resisting members. This study is related to improving the strength and stiffness of existing lateral force-resisting members by using Reinforced Concrete Jacketing (RCJ), Steel Jacketing (SJ), and Fiber-Reinforced-Polymer (FRP) wrapping around columns, which is a commonly utilized approach (Billah and Alam, 2014).

Performance-based assessment is adopted for the seismic upgrading evaluations of existing buildings. Performance is expressed in terms of discrete performance levels

defined as immediate occupancy, life safety, and collapse prevention. The performance levels are correlated with social, economic, and downtime losses, but these correlations are observation-based or empirical and are site-specific (Whitman et al., 1997). This approach to risk reduction requires threshold limit state values which cannot be precisely determined for various types of buildings, since they depend on several factors, such as structural configurations, design criteria, importance factors, and level of detailing, among others (Qian and Dong, 2020). The recovery time of a building, which is a key input in the seismic resilience assessment, is also related to building performance levels, which are mostly presented in crude terms (e.g., the most widely used HAZUS risk-assessment platform assumes the building achieves full functionality within one year, irrespective of the amount of damage and hazard scenario).

Numerous studies have adopted a performance-based seismic assessment approach for risk and resilience evaluation (Dong and Frangopol, 2015b; Zheng et al., 2018; Kilanitis and Sextos, 2019; Giouvanidis and Dong, 2020; Li et al., 2020a), also linking to seismic sustainability (Bocchini et al., 2014; Dong et al., 2014; Rodriguez-Nikl, 2015). A component-level approach incorporating seismic loss, sustainability, and resilience has also been investigated by many researchers (Dong and Frangopol, 2016a; Anwar et al., 2019; Asadi et al., 2019; Hashemi et al., 2019). Tirca et al. (2016) investigated improvement in seismic resilience through local modifications of the components of office buildings. Incremental Dynamic Analysis (IDA) was used to develop damage fragilities, and functionality curves developed by Cimellaro et al. (2010a) were used to evaluate seismic resilience. Guo et al. (2017) studied the seismic resilience of a frame building retrofitted with self-centering walls with friction devices. The performance of a building was compared through Engineering Demand Parameters

(EDPs), but a quantification framework for seismic resilience was not considered. Similar studies can be found in the literature for seismic resilience improvements considering seismic retrofit (Pekcan et al., 2014; Khanmohammadi et al., 2018; Rousakis, 2018; Vona et al., 2018; Anelli et al., 2019), but none utilizes a performance-based quantification framework of resilience assessment.

Molina Hutt et al. (2016) propose a seismic loss and downtime assessment approach for increasing seismic resilience for tall buildings by utilizing IDA, which employs a series of time history analyses with increasing intensity measure levels, and which can be computationally expensive, particularly for complex structural models, high-rise buildings, and in cases where buildings have to be analyzed several times. According to the authors' best knowledge, seismic resilience assessment of deficient reinforced concrete buildings retrofitted with conventional mitigation approaches has not been investigated in detail and further investigations are required considering uncertainties, and especially through assembly-based quantification of functionalities by utilizing component fragility functions, consequence functions, and collapse fragilities. Additionally, the risk assessment indicators only consider the robustness of a structure, while the resilience indicator also considers the recovery of a building.

Numerous studies also aimed at incorporating seismic sustainability or resilience in the performance assessment framework but most of the studies consider seismic loss, sustainability, or resilience individually and not in the context of decision-making (Decò et al., 2013; Feese et al., 2014; Padgett and Li, 2014; Dong and Frangopol, 2016b; Dong et al., 2016; Chhabra et al., 2017; Akiyama et al., 2020; Giouvanidis and Dong, 2020; Liu et al., 2020). For instance, Dong and Frangopol (2015b) presented a framework for highway bridges, incorporating loss and resilience under the mainshock

and aftershock sequence. Han et al. (2017), and Tesfamariam and Goda (2015) performed a seismic loss assessment of non-ductile reinforced concrete structures incorporating a mainshock aftershock sequence. Feese *et al.* (2014) evaluated seismic repair cost and environmental consequences of commercial buildings utilizing a system-level approach of loss estimation. Bocchini *et al.* (2014) proposed a unified approach for sustainability and resilience in an integrated perspective due to the similarities and common characteristics. Frangopol and Soliman (2016) discussed the integration of risk, resilience, and sustainability into life-cycle management. Yang and Frangopol (2018) proposed a novel concept of lifetime resilience to bridge the gap between sustainability and resilience, among others (Zinke et al., 2012; McAllister and Moddemeyer, 2018; Caspeepe et al., 2020). Dong and Frangopol (2016a) studied the seismic performance of base-isolated and conventional buildings using a component-level approach and quantified sustainability and resilience considering slow-track and fast-track repair strategies.

Fewer studies have also incorporated component-level assessment for damage and consequence evaluation (Chhabra et al., 2017; Hashemi et al., 2019). For instance, Asadi et al. (2019) discussed decision-making incorporating seismic sustainability and resilience. Previous seismic loss and resilience assessment studies focused on a single hazard (Dong and Frangopol, 2017b), multiple hazards (Kameshwar et al., 2019), and/or mainshock-aftershock (Dong and Frangopol, 2015b), but the stochastic occurrence of the multiple earthquakes is not well investigated, especially for decision-making. The low-intensity seismic events may occur multiple times during the service life of a structure, while high-intensity events may only occur once due to the low probability of occurrence of such events. The stochastic nature of frequency and

magnitude of low-intensity seismic hazard may result in higher accumulative consequences due to multiple earthquakes during the investigated time interval, termed herein as long-term consequences (Li et al., 2020a; Li et al., 2020b). The long-term consequences are evaluated based on the occurrence model of earthquakes. The Poisson process with an occurrence rate λ is generally utilized to model the stochastic occurrence of earthquakes, which has been widely used in earthquake engineering (Rackwitz, 2002; Yeo and Cornell, 2009).

2.4 Resilience assessment of community buildings

Seismic risk assessment on a regional scale is widely investigated in the literature (Whitman et al., 1997; Kircher et al., 2006; Silva et al., 2014; Newman et al., 2017), but, contrarily, seismic resilience assessment is relatively a recent development with a conceptual framework originally proposed by Bruneau et al. (2003) and later illustrated on community buildings (Cimellaro et al., 2010a; Cimellaro et al., 2010b). Various other researchers have attempted to propose methodologies to assess the resilience of buildings on a community level (Burton et al., 2015; Miles et al., 2018). For instance, Feng et al. (2017) proposed a functional interdependence model to measure functionality recovery as a measure of the resilience of community buildings, Lin and Wang (2017a) proposed stochastic functionality recovery of community buildings as discrete-state, continuous-time markov chain; Masoomi et al. (2020) proposed functionality recovery of buildings considering utility networks, Alisjahbana and Kiremidjian (2020) proposed housing recovery model using a stochastic queuing model, among others (Gonzalez et al., 2020; Logan and Guikema, 2020). All these resilience assessment methodologies are limited to functionality recovery curves and

there is rarely an attempt to connect socioeconomic consequences into performance indicators that can be more meaningful to the stakeholders (Nozhati et al., 2019; Hassan and Mahmoud, 2020). Additionally, there is also a need to consider the environmental consequences in the community assessment and enhancement frameworks considering climate change concerns.

The end goal of these assessment methodologies is to perform decision-making but there are only a few resilience frameworks for building portfolios that provide such decision support. For instance, Masoomi and van de Lindt (2018) proposed a community resilience based design methodology for the built environment by considering population outmigration performance objective, and Kameshwar et al. (2019) proposed a decision support framework for community resilience by considering the Bayesian network. However, these decision support frameworks provide a generalized decision-making approach and considered a few performance indicators, mostly functionality recovery only. There is a need to consider multiple performance indicators for community buildings optimization, prioritization, and decision-making considering pre-hazard mitigation alternatives.

In the past, community recovery has been investigated following a reductionism approach (Dong and Frangopol, 2015b; Dong and Frangopol, 2016b; Dong and Frangopol, 2016a; Yang and Frangopol, 2019; Giouvanidis and Dong, 2020; Li et al., 2020a; Li et al., 2020b; Qian and Dong, 2020) by evaluating the functionality recovery of building portfolios in a hazard event and integrating over investigated time to evaluate resilience. However, the functionality of individual buildings not only depends on their damage states but also on the availability of utilities such as water and electricity. Hence, there exist interactions between buildings and utility systems

referred to herein as dependencies and/or interdependencies. To apply systems thinking, building portfolios and utility systems should be considered in a holistic manner (i.e., a model of an interacting physical infrastructure system consisting of relevant systems and key community components such as building portfolios). The individual building recovery and resilience assessment lack explicit modeling of such relationships, and therefore, resilience assessment at a community level is expected.

Numerous studies investigated community resilience by considering building portfolios under hazards (Miles and Chang, 2006; Cimellaro et al., 2010b; Cimellaro et al., 2010a; Cimellaro and Piqué, 2016; Miles et al., 2018), exploring various methods such as analytical formulations, agent-based modeling, among others (Ouyang, 2014). For instance, Burton et al. (2015) proposed a performance-based community recovery framework and applied it to a residential community (Burton et al., 2017). Lin and Wang (2017) formulated discrete-state continuous-time Markov Chains for the stochastic post-disaster recovery assessment of building portfolios. These studies provide substantial insights into the community recovery and resilience against earthquakes but follow a reductionism approach where interactions among the components are ignored.

Few studies have considered these interactions in the recovery modeling of building portfolios. For instance, Kameshwar et al. (2019) proposed a decision-support framework utilizing the Bayesian network, incorporating transportation, water network, and electrical power networks in a multi-hazard context. Masoomi et al. (2020) proposed a post-earthquake functionality assessment of buildings, considering the connectivity from utility networks, but the bidirectional coupling relationship (i.e., interdependency) between the water and electrical power networks, and their

dependence on buildings were not explored. These relationships could affect the demand and supply of utilities and can also provide additional insights about the community recovery and resilience.

The two major approaches to evaluate community resilience include (a) evaluating the socioeconomic, institutional, and infrastructure capacity of a community, and (b) assessing functionality recovery of physical infrastructure systems (Cutter, 2020). The former is not hazard-specific and is a qualitative measure of resilience that relies on the socioeconomic performance indicators to prepare for anticipated hazards, adapt to changing conditions, and to recover rapidly (Cutter et al., 2014; Cutter, 2016). The latter aims for the physical infrastructure systems to have robustness (the ability to sustain damage) and recover from the hazard rapidly (Bruneau et al., 2003; Ouyang et al., 2012; Ouyang and Wang, 2015; Akiyama et al., 2020; Anwar and Dong, 2020; Dong and Frangopol, 2020). This approach is widely adopted in infrastructure resilience and the central idea of this approach is to improve functionality recovery by upgrading the physical infrastructure systems. The functionality curve is integrated over an investigated time after an earthquake event and the resulting value is often considered as a measure of its resilience (Koliou et al., 2017). The limitation is that the single numeric outcome is challenging to comprehend, less meaningful to the decision-makers, and unable to capture the geospatial variations of people and services. These variations such as lack of access to essential facilities can contribute to population outmigration indicating its correlation to the resilience of a community when recovering from disruptions (Aldrich, 2012). Access to essential facilities after an extreme event is as essential as the robustness and rapidity of the physical infrastructure systems (Logan and Guikema, 2020), and thus can be utilized as an indicator to assess community

resilience. According to the best of the authors' knowledge, there have been few studies providing a holistic model to assess community resilience considering bidirectional interactions of utility and building portfolios under seismic hazards by considering novel resilience indicators such as community functionality, inherent resilience, and access to essential facilities. Furthermore, the community building portfolios have been seldom considered along with its interactions with critical infrastructure systems for functionality and resilience assessments.

2.5 Optimization and decision-making

The decision-making for retrofit alternatives, considering seismic loss, sustainability and resilience can be challenging due to the possibility of conflicting (i.e., improving one criterion may worsen another criterion or one criterion may be a benefit criterion, preferring higher values, while another may be a cost criterion, preferring lower values) and disproportionate nature of criteria (i.e., some criteria may have a greater influence on the decision-making) (Bocchini et al., 2014; Asadi et al., 2019). For instance, some sustainable materials may be less resilient; a strategy to repair over replacement might be sustainable but may have high seismic loss potential (Brown et al., 2011; McAllister and Moddemeyer, 2018), among others. Sustainability and resilience are considered benefit performance indicators with preferred high values, while seismic loss is a cost performance indicator with preferred lower values. Additionally, long-term consequences can result in disproportionate losses and can influence decision-making (Ligabue et al., 2018). Technique for order preference by similarity to ideal solutions (TOPSIS) is a multi-criteria decision-making (MCDM) method developed by Hwang and Yoon (1981), and has been used in road pavements (Chang et al., 2005), bridge

construction (Zavadskas et al., 2007), loss assessment for civil infrastructure (Faber and Stewart, 2003), among others (Qian and Dong, 2020). TOPSIS considers different alternatives at a Euclidian distance away from the ideal solution, and the shortest distance of any alternative from the ideal solution is considered the most acceptable solution (Mateo, 2012). Caterino *et al.* (2009), among others, used multi-criteria decision-making methods for seismic retrofit selection but seismic sustainability and resilience were not considered. According to the best of the authors' knowledge, there have been no investigations considering long-term uncertain consequences in the multi-criteria decision-making incorporating risk attitudes of the decision makers, and by considering seismic loss, sustainability, and resilience for retrofit selection of buildings.

The performance assessment and enhancements considering multiple performance indicators against community-level retrofit costs require a multi-objective optimization approach. The community building portfolios consist of numerous buildings with different structural systems, functionalities, and different retrofit strategies that cannot be selected manually for optimized performance. In the last two decades, the evolutionary multi-objective optimization approach has become increasingly popular because this technique does not require derivative information and is relatively easier to implement in a variety of settings such as optimizing the dynamic response of structural systems, design optimization, life-cycle optimization, among others in the context of structural engineering (Dong et al., 2014; Dong and Frangopol, 2017a). The method was first proposed by Holland (1975), inspired by Darwin's evolutionary theory of the origin of species. Later, many multi-objective evolutionary algorithms were developed (Schaffer, 1985; Horn et al., 1994; Konak et al., 2006), the two most widely adopted being the strength Pareto evolutionary algorithm (Zitzler et al., 2001) and non-

dominated sorting genetic algorithm (Deb et al., 2002). In a community building portfolio under a hazard scenario, few researchers have employed one of these methods on a community level to solve the optimization problem in a pre-hazard scenario. For instance, Zhang and Nicholson (2016) proposed bi-objective optimization considering risk in terms of population dislocation and structural costs. However, sustainability-related indicators and uncertainties have not been explored.

A community building portfolio consists of a number of buildings with different code configurations, structural systems, dimensions, and stories, among others. Hence, formulating an objective function with derivative information may not be practical. Contrarily, numerical optimization approaches are gaining traction due to the advancements in computer simulations (Larson et al., 2019; Gambella et al., 2021; Pardalos et al., 2021). The numerical optimization problems where derivative information is not directly available are referred to as black-box optimization problems (Guirguis et al., 2019). In the case of community building portfolios, it can be computationally expensive to query an objective function from a black box which makes these conventional numerical optimization techniques undesirable.

The solution is to develop sequential sampling techniques by establishing a cheap surrogate model from a finite number of points from an expensive black-box objective function (Forrester and Keane, 2009). This surrogate-based optimization technique utilizes Gaussian process models to sample points by utilizing acquisition functions. The Gaussian process models have shown good performance and have been utilized in multi-objective settings with existing optimization algorithms (Rasmussen, 2003a; Knowles, 2006; Voutchkov and Keane, 2010). There also have been improvements in the algorithms in terms of acquisition functions such as the use of hypervolume

functions, utilizing expected Euclidian distances, among others (Emmerich et al., 2011; Hupkens et al., 2014; Emmerich et al., 2016).

The approximated Pareto-optimal solutions provide multiple optimal solutions in terms of considered performance objectives. The relationships between the pre-hazard mitigation costs and resulting performance enhancements can be identified and an ideal solution can be selected (Sabatino et al., 2015; Dong and Frangopol, 2017a). However, selecting an ideal solution from the Pareto-optimal may not be straight forward task due to many factors. For instance, performance enhancements may be in terms of reducing casualties or equivalent carbon emissions during repair, among others and it is difficult to assign a cost-benefit approach to select an ideal solution considering multiple different performance objectives (Frangopol et al., 2017).

The decision may be further complicated due to different rates of returns, hazard scenarios with varying intensities and probability of occurrences, and inherent risk perceptions of decision-makers due to uncertain consequences (Cheng and Frangopol, 2021). A risk-seeking decision-maker may prefer a low mitigation cost solution in exchange for high future consequences, whereas a risk-averse decision-maker may prefer low uncertainty and is more inclined toward reducing future consequences (Dong and Frangopol, 2015a; Gong and Frangopol, 2020). Hence, the information provided by approximated Pareto-optimal solutions is inadequate for decision-making under uncertain consequences. Hence, an efficient surrogate-based optimization and decision-making framework for community building portfolios considering socioeconomic and environmental consequences under risk perceptions is needed. According to the best of the authors' knowledge, there have been no studies providing an efficient performance-based multi-objective Bayesian optimization framework for community building

portfolios by utilizing Gaussian process surrogates, spectral sampling techniques, and by considering multiple performance indicators including risk, resilience, and sustainability as performance objectives and under uncertainties.

2.6 Research Gaps

The literature review chapter provides details related to the need for performance-based assessment methods to evaluate socioeconomic and environmental consequences in terms of meaningful and novel performance indicators including risk, resilience, and sustainability. The scope of the literature review is limited to buildings and building portfolios on a community-level, and under seismic hazard scenarios. The literature review is conducted related to the performance assessment, enhancement, and decision-making of buildings and building portfolios under seismic hazard scenarios with increased attention towards resilience. The findings in terms of the research gaps are as follows:

1. There is an apparent need to integrate resilience and sustainability into the performance-based assessment frameworks to establish a comprehensive methodology capable of incorporating detailed component-based performance models to provide meaningful performance indicators for decision-makers and stakeholders under uncertain consequences.
2. The resilience assessment of buildings retrofitted with conventional mitigation approaches is required to be investigated by developing detailed component-level recovery assessment strategies. Since the conventionally conducted risk assessments are not capable of providing information related to the additional consequences during the recovery from an extreme event.

3. Furthermore, there are no studies available extending the next-generation performance-based assessment methodologies for decision-making especially considering the long-term consequences. Hence, establishing a multi-criteria decision-making framework incorporating seismic risk, sustainability, and resilience for retrofit selection is required.
4. Additionally, it is more desirable to think about resilience on a community level. In this respect, there have been no studies providing a holistic model to assess community resilience considering dependencies and interdependencies of utility networks and building portfolios under seismic hazards by considering novel resilience indicators such as community functionality, inherent resilience, and access to essential facilities.
5. Finally, for performance enhancement and decision-making, efficient surrogate-based optimization and decision-making framework for community building portfolios considering socioeconomic and environmental consequences under risk perceptions is required for possible performance enhancements on a community level.

The following chapters (i.e., chapter 3 to chapter 8) address the aforementioned research gaps, and the last chapter provides the overall conclusion and findings resulting from the addressed research gaps.

CHAPTER 3 PERFORMANCE-BASED PROBABILISTIC FRAMEWORK FOR SEISMIC RISK, RESILIENCE, AND SUSTAINABILITY

3.1 Introduction

Recent earthquakes have highlighted additional losses due to the lack of resilience of damaged structures. Environmental impact, as a performance indicator, has also received increased attention within performance-based earthquake engineering. In this chapter, a combined probabilistic framework is proposed to assess seismic risk, sustainability, and resilience of a non-ductile reinforced concrete frame structure. The framework utilizes a three-dimensional inelastic fiber-based numerical modeling approach to develop limit states associated with performance levels. The decision variables (i.e. repair cost, downtime, and equivalent carbon emissions) are quantified at both component- and system-level and are compared considering seismic risk, sustainability, and resilience. Additionally, the proposed approach considers uncertainties in the building performance and consequence functions of structural and non-structural components. Fast-track and slow-track schemes are utilized as a repair strategy and probabilistic resilience is quantified given the investigated time period. The proposed approach can aid the development of next-generation performance-based engineering incorporating both resilience and sustainability.

3.2 Sustainability and resilience under seismic hazard

3.2.1 Seismic sustainability

Sustainability, as defined in the report of Brundtland, (1987) is “meeting the needs of the present generation without compromising the ability of future generations to meet their own needs”. Sustainability assessment includes social, economic, and environmental impacts distributed over the life-cycle of a building (e.g., construction, maintenance, demolition, and aging). In this study, seismic sustainability is emphasized by considering the socio-economic and environmental impacts resulting from earthquake hazards. Environmental indicator (e.g., equivalent carbon emissions) is used to evaluate environmental impacts. The social impact of seismic sustainability is determined by calculating the total repair time of a building under seismic hazard. Mathematically, the sustainability impact of earthquake hazard can be computed as:

$$SI = C_{SM|C} \cdot p_{C|IM} + C_{SM|NC} \cdot (1 - p_{C|IM}) \quad 3-1$$

$$C_{SM|NC} = \sum_{Comp} \sum_{DS} C_{SM,Comp|DS} \cdot p_{DS,Comp|IM} \quad 3-2$$

where $C_{SM|C}$ and $C_{SM|NC}$ is the consequence (e.g., economic loss, equivalent CO₂ emissions, repair time) given collapse and non-collapse of a building; IM is the intensity measure; $p_{C|IM}$ is the probability of collapse under IM ; $C_{SM,Comp|DS}$ is the sustainability metric given a damage state of a given component with the building; and $p_{DS,Comp|IM}$ is the probability of a damage state associated with a component under a given IM .

The carbon emissions due to repair (i.e. non-collapse condition) are accounted for, by calculating the probability of damage states (i.e. $p_{DS,Comp|IM}$) utilizing fragility functions of considered structural and non-structural components. The consequences associated with different repair actions are weighted with relevant probability of being in damage states to determine the desirable sustainability impact of a particular component (i.e. $\sum_{DS} C_{SM,Comp|DS} \cdot p_{DS,Comp|IM}$). A similar procedure is carried out for all the components and the desirable consequences given non-collapse of a building are evaluated (i.e. $C_{SM|NC}$). The consequence given the collapse of a building is determined considering construction materials (e.g. concrete, reinforcing steel, bricks) used during the construction phase and the relevant sustainability impact of construction materials can be determined. The total sustainability impact (e.g. equivalent carbon emissions) is evaluated by adding consequences for collapse and non-collapse of a building weighted as represented in Equation (3-1).

3.2.2 Seismic resilience

Resilience is represented by its functionality and can be associated with four attributes: *robustness*: the ability to withstand an extreme event without complete failure; *rapidity*: the ability to recover from an extreme event efficiently and effectively; *redundancy*: reserve or substitutive structural components or systems; and *resourcefulness*: efficiency in identifying problems, prioritizing solutions, and mobilizing (Bruneau et al., 2003). Mathematically, resilience can be evaluated by integrating the functionality curve over time.

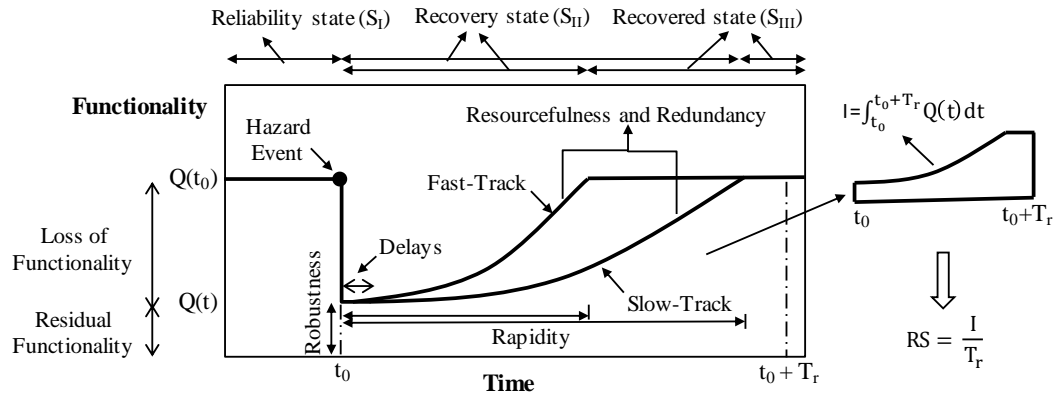


Figure 3-1 Resilience assessment under hazards

$$RS = \frac{1}{T_r} \int_{t_0}^{t_0+T_r} Q(t) dt \quad 3-3$$

equivalent CO₂ emissions) given collapse and non-collapse of a building; IM is the intensity measure; $p_{C|IM}$ where $Q(t)$ is the functionality; t_0 is the time of occurrence of the extreme event and T_r is the time of investigation of functionality. As shown, the three functionality states associated with the functionality are proposed defined as follows:

1. Reliability state (S_I): Pre-event functionality state where a building is considered to have baseline functionality (i.e., the building is functional or in an original state before the occurrence of a hazard event);
2. Recovery state (S_{II}): Post-event functionality state where the building is considered to have a loss of functionality depending upon the robustness of the building, and time-variant functionality regain as a result of repair efforts. Two types of repair schemes are defined for functionality recovery (i.e., series repair scheme where a building is repaired one story at a time termed as slow-track and parallel repair scheme where all the stories are repaired simultaneously

termed as fast-track). The repair efforts are an attribute of resourcefulness and redundancy of the system; and

3. Recovered state (S_{III}): building functionality after the recovery efforts (i.e., building regains loss of functionality)

In the reliability state, the building has baseline functionality and at t_0 the building changes from baseline functionality to residual functionality as a result of physical damage and loss of services of a building. After a hazard event, the state changes from reliability state to recovery state, which includes the delay time (i.e., the time required for inspection, engineering mobilization, review and/or redesign, financing, contractor mobilization and permitting, etc.) and the time-variant functionality improvement. Subsequently, repair actions are performed, and the building regains its functionality to reach a recovered state. The resilience can be calculated by taking integral from a hazard event to the investigated time period.

3.3 Integrated performance-based engineering

The PBEE methodology is carried out in four stages (i.e., hazard, structural, damage, and loss analysis), providing Decision Variables (DVs) meaningful to the stakeholders. The methodology focuses on probabilistic procedures to incorporate uncertainties in all phases of the process.

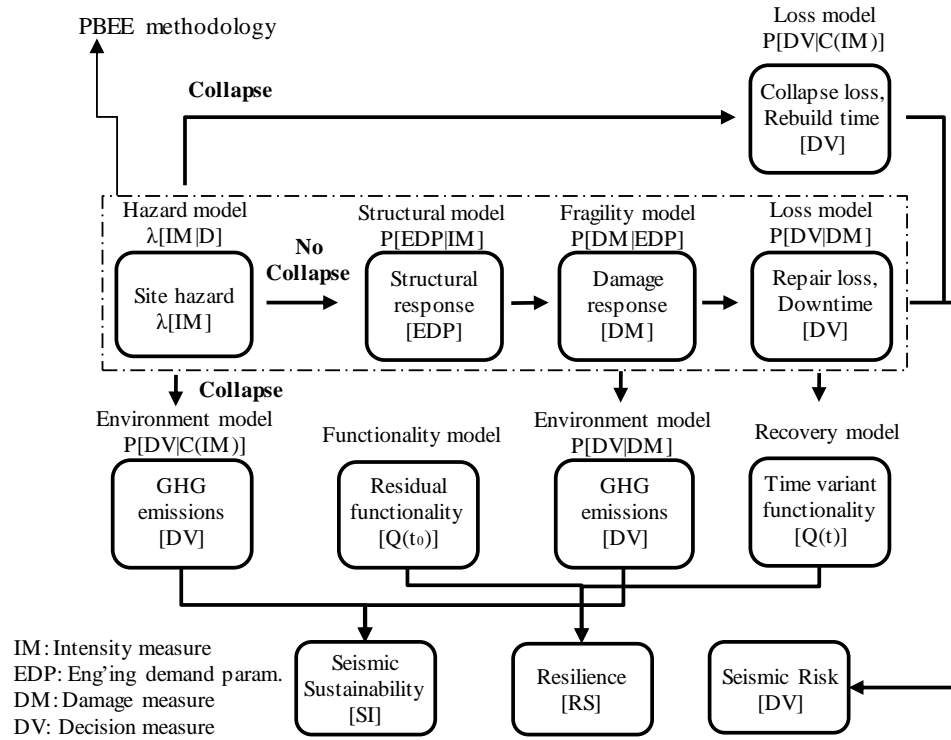


Figure 3-2 PEER PBEE methodology incorporating sustainability and resilience

Each stage of the PBEE methodology is carried out individually to arrive at DVs. For a given earthquake scenario, following equations are utilized to calculate expected total loss, total repair time, and total sustainability impact (e.g. environmental indicator in terms of equivalent carbon emissions).

$$L_{T|IM} = L_{C|IM} + L_{NC|IM} \quad 3-4$$

$$RT_{T|IM} = RT_{C|IM} + RT_{NC|IM} \quad 3-5$$

$$SI_{T|IM} = SI_{C|IM} + SI_{NC|IM} \quad 3-6$$

where $L_{T|IM}$ is a total monetary loss DV; $L_{C|IM}$ and $L_{NC|IM}$ are losses for collapse and non-collapse; $RT_{T|IM}$ is a total building repair time DV; $RT_{C|IM}$ and $RT_{NC|IM}$ are repair times for collapse and non-collapse; $SI_{T|IM}$ is the total seismic sustainability impact

(e.g., equivalent carbon emissions); and $SI_{C|IM}$ and $SI_{NC|IM}$ are seismic sustainability impact for collapse and non-collapse cases. The detailed process of PBEE incorporating resilience and sustainability is introduced in the following section.

3.3.1 Hazard analysis

PBEE methodology requires the selection of suits of earthquake records representative of the potential scenarios, a structural system may experience. The representative earthquake records for dynamical analysis are selected based on the criteria, such as magnitude, source mechanism, source to site distance, rupture directivity, and local site conditions, among others. Several ground motion databases are available for ground motion selection, such as the PEER ground motion database, and the European strong-motion database.

3.3.2 Structural analysis

Structural analysis is performed to evaluate the response of the structure under seismic hazards. Nonlinear time history analysis is performed to determine engineering demand parameters (EDP) (such as element forces, deformations, floor accelerations, drifts, etc.). Element forces and drifts are considered more suitable for structural components, while peak floor accelerations and peak floor velocities are usually considered for non-structural components. The variation in hazard is incorporated by considering a number of analyses with given intensity measures to get the mean and variance of EDPs. The probability of collapse $p_{C|IM}$ can be determined using collapsed data from Incremental Dynamic Analysis (IDA) (Vamvatsikos and Cornell, 2002), and the probability of having no global collapse can be determined using the total probability theorem.

$$p_{NC|IM} = 1 - p_{C|IM} \quad 3-7$$

A lognormal cumulative distribution function is used to fit the probability of collapse under a given EDP (Sfahani et al., 2015). Fragility curves for IO, LS, and CP can also be generated similarly as follows:

$$p_{C|IM} = \Phi \left(\frac{\ln(x/\theta)}{\beta} \right) \quad 3-8$$

where Φ is the standard normal cumulative distribution function (CDF); θ is the median of the collapse fragility function (i.e., Intensity measure (IM) with 50% probability of collapse); and β is the dispersion or standard deviation of $\ln IM$.

3.3.3 Damage analysis

Damage analysis is performed to determine physical damage at the component level using structural responses in terms of EDPs. The probabilistic EDPs are incorporated with the damage fragility curves to calculate the Probability of Exceedance (PoE) of damage states. Damage measures (DM) in terms of different damage levels or damage states are typically defined as fragility functions to quantify the damage. The damage fragility functions for structural and non-structural components can be developed using experimental testing, analytical modeling, and/or expert opinion. Component fragility functions are usually divided into fragility groups and performance groups depending upon the EDPs effect on component damage.

3.3.4 Seismic risk assessment

Loss analysis is performed to determine direct economic losses and downtime. The PoEs obtained from damage analysis are used to determine losses using consequence functions, which are likely values of repair to replacement cost ratio, repair time, etc. Limit state fragilities are utilized along with the hazard model to determine the probability of collapse of a building and related consequences are evaluated. Fragility functions utilized in the fragility model are used along with the repair actions to evaluate related consequences for the non-collapse of a building. The uncertainties of the consequence functions are included depending upon the variability in each of the DV. The Monte Carlo process is used to generate a large number of EDPs for the statistically consistent demand sets given a limited set of input EDPs. These demand sets generated using Monte Carlo simulations are used with fragility and consequence functions to calculate statically distributed DVs. Losses due to collapse and non-collapse of a building are added to determine seismic risk due to earthquake scenario.

3.3.5 Seismic sustainability and resilience assessment

In this section, the seismic sustainability and resilience assessment incorporated in the proposed framework is outlined. Step 1 starts with building a detailed finite element model. A suite of earthquake ground motions is selected, and IDA is performed to develop fragilities at immediate occupancy (IO), life safety (LS), collapse prevention (CP), and collapse (C) limit states. In Step 2, three hazard scenarios are considered with 50%, 10%, and 2% probability of exceedance in 50 years of a structure. Non-linear time history analyses are performed to evaluate structural responses (e.g., story drifts, floor accelerations, and velocities). Drift-sensitive structural components, drift-sensitive

non-structural components, and acceleration-sensitive non-structural components are identified, and component-level damage assessment is performed using fragility functions determined from literature (FEMA, 2012; Dong and Frangopol, 2016). Monte Carlo simulations are conducted, and monetary losses and downtime are evaluated using consequence functions.

In Step 3, repair actions are determined for the considered structural and non-structural components following the repair descriptions provided in fragility specifications of FEMA methodology (FEMA, 2012). Monte Carlo simulations are performed to probabilistically determine equivalent carbon emissions related to the relevant materials. The relationship between equivalent carbon emissions and the materials is extracted from (Chau et al., 2012; Dong and Frangopol, 2016). Seismic sustainability is thus evaluated by quantifying equivalent carbon emissions using the probability of damage and collapse scenarios utilizing Equations (3-1) and (3-2).

In Step 4, probabilistic seismic resilience can be quantified utilizing the residual functionality of a building and its recovery to pre-event functionality state at the end of recovery time. The residual functionality is mapped against the different building limit states developed in Step-1; with baseline functionality at no damage and zero functionality at building collapse. Intermediate functionalities are assigned to different damage states to account for uncertainties. Recovery functions can be linear, trigonometric, and exponential and depend on the community's resourcefulness and rapidity. Under an earthquake event, the building will suffer structural and non-structural damage, and the building will change its state from full functionality to some residual functionality depending upon the robustness of a structure. Recovery functions are used to track time-variant functionality improvement and after the downtime, the

building will achieve full functionality. The time-variant functionality over an investigated period can thus be determined, and resilience can be computed by integrating the time-variant functionality using Equation (3-3).

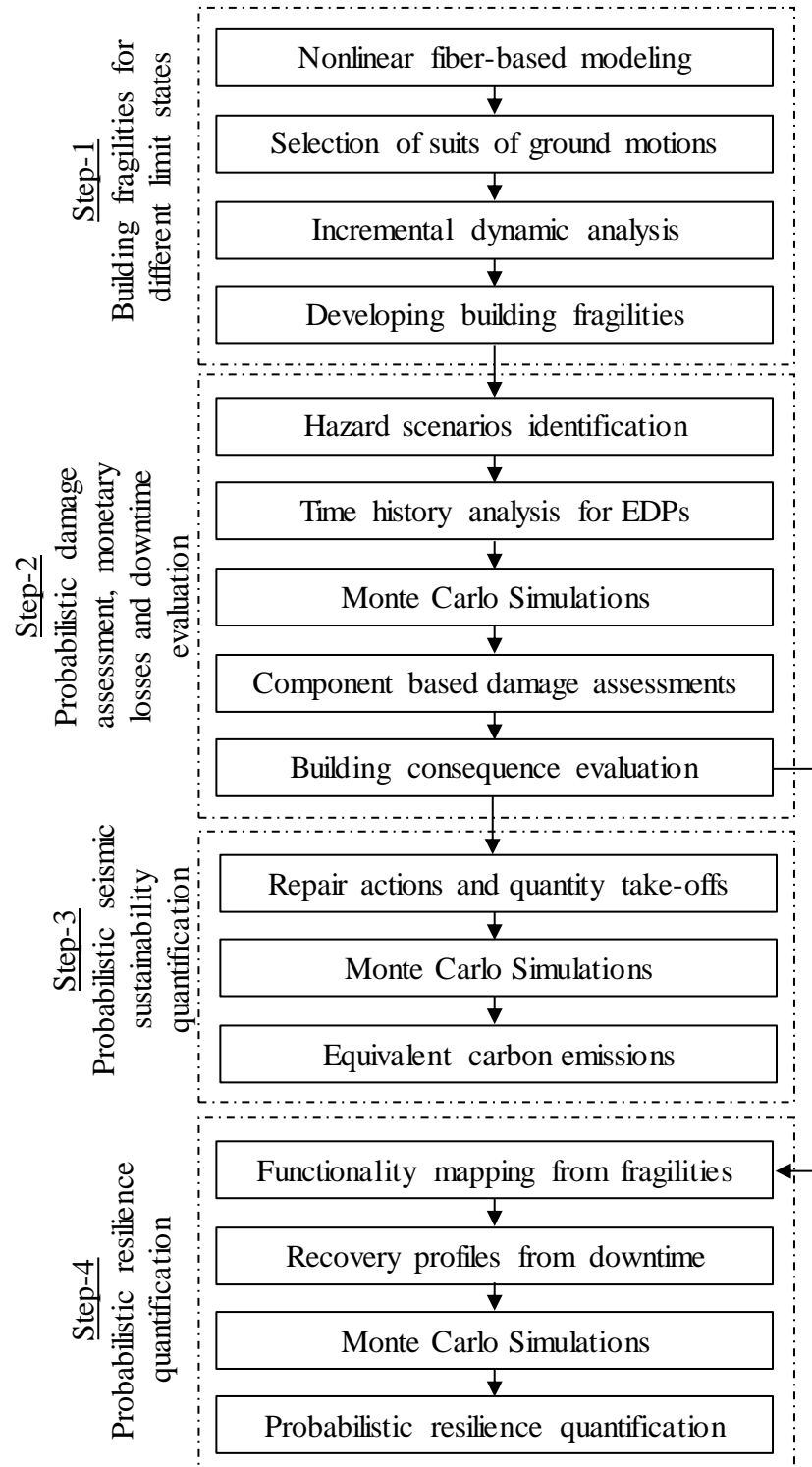


Figure 3-3 Probabilistic sustainability and resilience quantification framework

3.4 Illustrative example

3.4.1 Description and modeling of the investigated building

The developed integrated performance-based assessment methodology for seismic sustainability and resilience quantification is applied to an eight-story non-ductile RC moment-resisting frame structure. The selected building is located in the earthquake-prone region and was not designed considering earthquake design guidelines, as standard practice before the implementation of earthquake codes. The non-ductile structures may perform poorly during a natural hazard since they are not designed according to the revised building codes. The building has a ground floor height of 5 *m* and a typical story height is 3.5 *m*, design details for critical elements along with the layout are shown in the following Figure.

The building was constructed before 1991 when UBC (1997) recommended seismic zone ‘0’ for most of the low-to-medium seismicity regions. Recent seismic hazard studies revised the seismic zones in many regions of the world, however existing building stock may be vulnerable to seismic risk. The considered building was designed only under the gravity and wind loads without considering seismic provisions. Gravity loads considered in the design process include self-weight, superimposed dead load of 4.0 kN/m², and a live load of 2.0 kN/m². The live load of 4.8 kN/m² was considered for the staircase areas and exit ways. The considered building is a residential structure and was assigned risk category II. Concrete strength of 20 MPa and mild steel with a yield strength of steel of 240 MPa were used in the design. Slab thickness of 0.2m was used

considering serviceability requirements and column dimensions were appropriately selected.

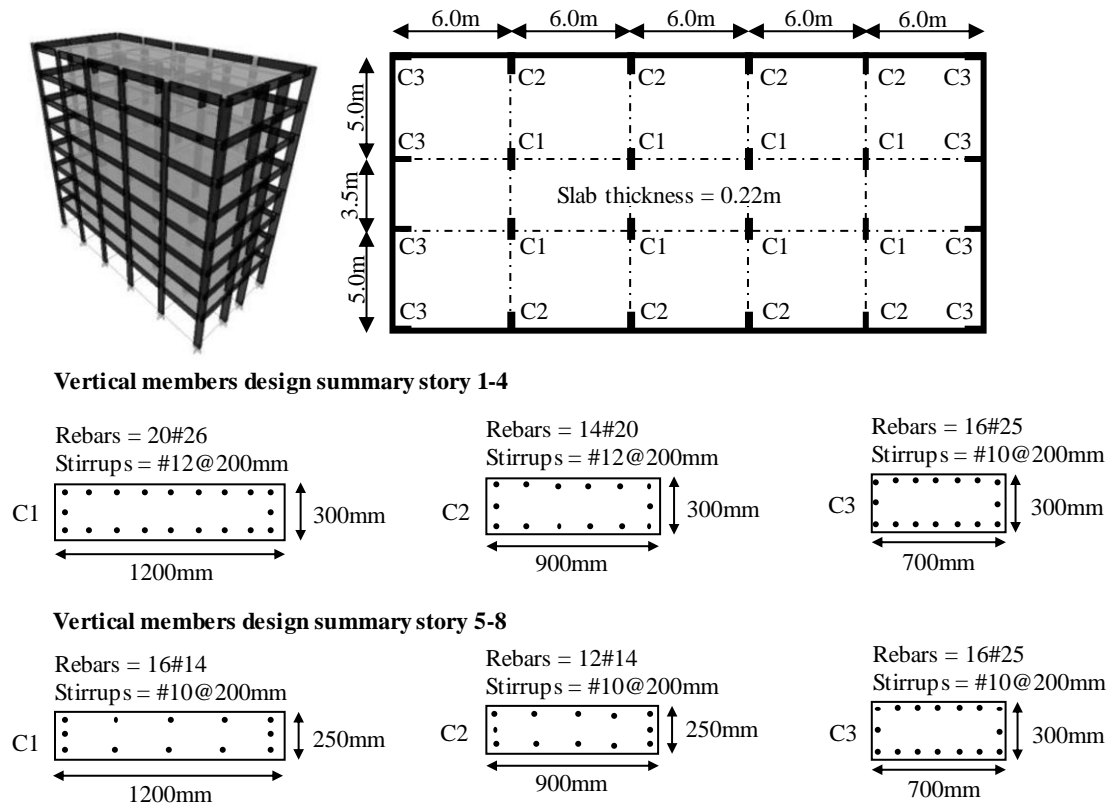


Figure 3-4 Vertical member design and layout of 8-story building

Fiber-based modeling technique is used for the performance evaluation of non-ductile structures under earthquake hazards. Incremental dynamic analysis was performed using nonlinear analysis software. Nonlinear material properties are used to represent concrete and steel behavior. The nonlinear concrete confinement model is used with a crushing strain of 0.02 and a confinement factor of 1.05 depending upon the reinforcement detailing. A bilinear elastoplastic model with kinematic strain hardening is used for mild steel with a strain hardening parameter of 0.005, yield strength of 264 MPa, and modulus of elasticity of 200 GPa. Structural members are modeled using Cubic Elasto-Plastic Frame (CEPF) elements, which are capable of

modeling concrete cracking and steel yielding. CEPF elements are also capable of effectively modeling nonlinear geometric and material properties in space frames (Mwafy and Elkholy, 2017).

3.4.2 Structural vulnerability

IDA analysis was performed using carefully selected twenty far-field earthquake records based on epicentral distance, magnitude, soil conditions, PGA, and a/v ratios. ASCE (2013) gives limit states with respect to Inter-story Drift Ratios (IDR) for each performance criteria. An IDR of 0.5%, 1%, and 2% is considered for IO, LS, and CP performance limit states, while numerical instability due to excessive nonlinear deformations in the structure is considered for the collapse limit state (Li et al., 2014; Vamvatsikos and Cornell, 2002). Building fragility curves developed using IDA are shown in the following Figure. The extracted fragility curves provide probability of exceedance of the given limit states given the intensity measures. The fragility curves for the IO, LS, CP seems steeper as compared to the moment resisting frames designed in accordance to the recent design codes with implemented seismic provisions. This could be due to several factors. For instance, in the illustrative example, UBC (1997) was utilized and seismic provisions were not considered. Also, concrete strength of 20 MPa was considered with comparatively higher superimposed and live loads, making building heavier and hence more prone to the seismic loads. Hence, the fragility curves may appear steeper as compared to ductile moment resisting reinforced concrete frames that are designed according to the latest seismic design codes and have sufficient ductility to absorb the lateral loads

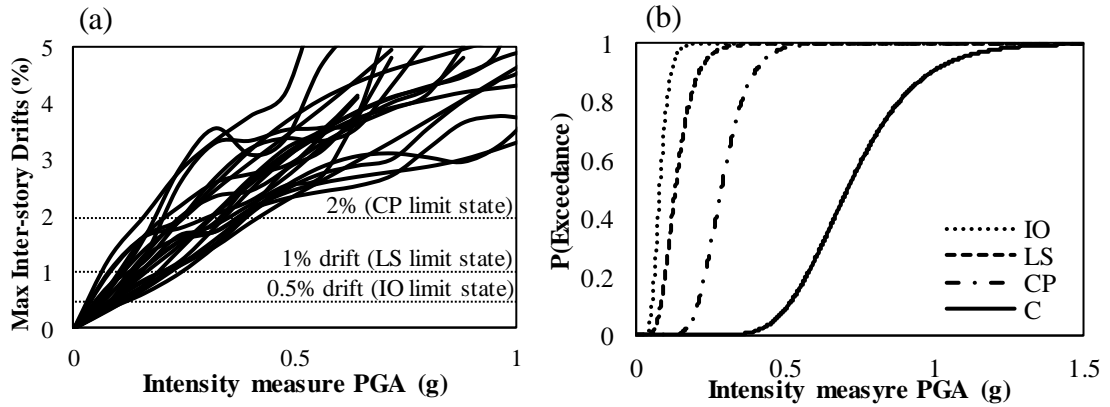


Figure 3-5 (a) IDA results and (b) Fragility curves of the investigated RC building

Loma Prieta-Emeryville 1989 with a magnitude of 6.93 and a duration of 28 seconds is selected for seismic sustainability and resilience assessment. The hypothetical seismic scenarios (i.e., service level earthquake (SLE) with a 50% probability of occurrence in the 50-year life of a structure, design level earthquake (DLE) with 10% probability of occurrence, and maximum considered earthquake (MCE) with 2% probability of occurrence) are then assumed. The earthquake record is selected for illustrative purposes. Generally, record-to-record variability and uncertainty should be considered and a wide range of realizations considering uncertainties must be generated to account for ground motion variations. Time history analysis is performed, and results are plotted for maximum IDRs and accelerations. Maximum IDR of 1.02%, 2.47%, and 3.67% is observed at story-5 and story-6 for three earthquake scenarios. Similarly, maximum floor accelerations of 0.276g, 0.448g, and 0.570g are observed at story-8, story-3, and story-1, respectively.

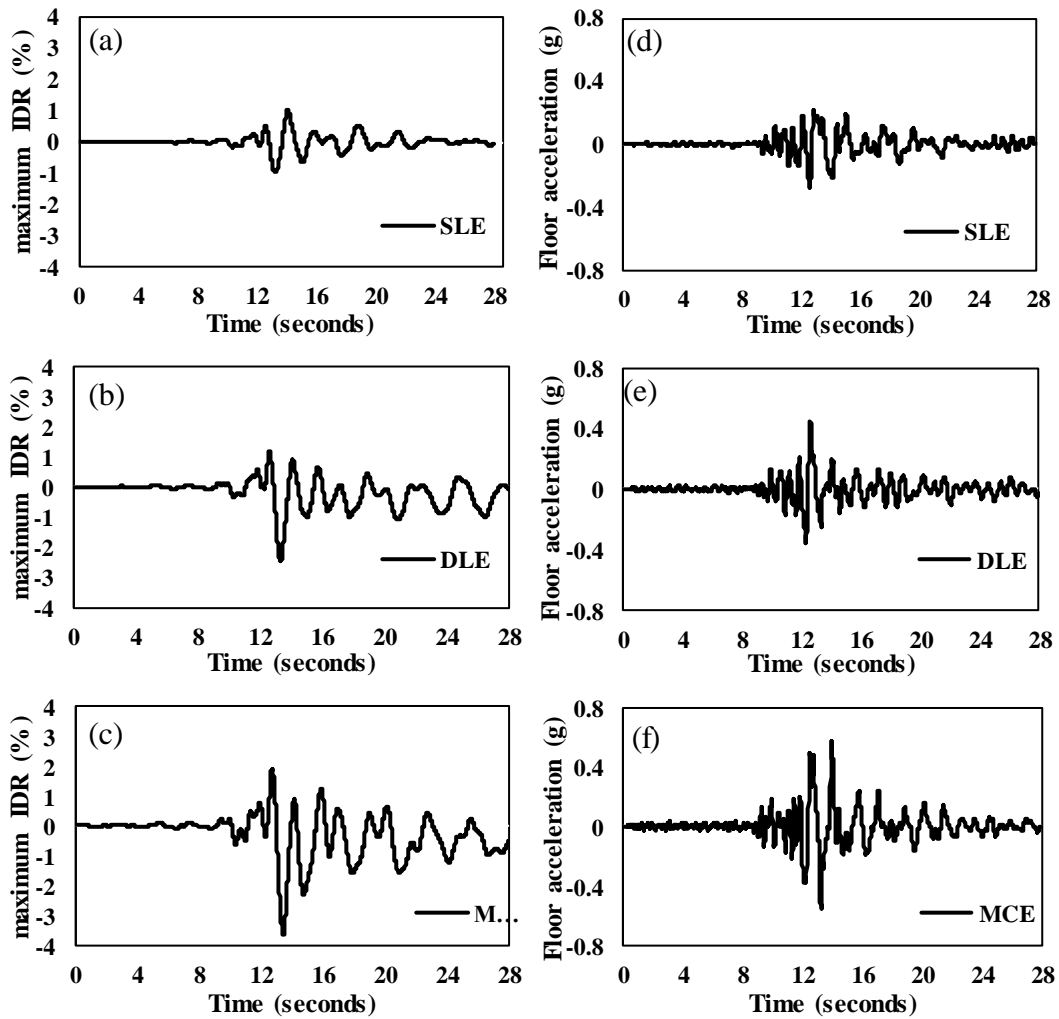


Figure 3-6 Time histories of inter-story drifts at (a) story-5 under SLE scenario, (b) story-5 under DLE scenario, and (c) story-6 under MCE scenario and time histories of maximum accelerations at (d) story-8 under SLE scenario, (e) story-3 under DLE scenario, and (f) story-1 under MCE scenario

As shown, it can be observed that the increasing intensity of earthquake scenarios results in increasing demands on a structure. Peak IDRs increased by 58.48% for DLE and 32.63% for MCE. Similarly, for peak floor accelerations, an increase of 38.36% for DLE and 23.33% for MCE is observed.

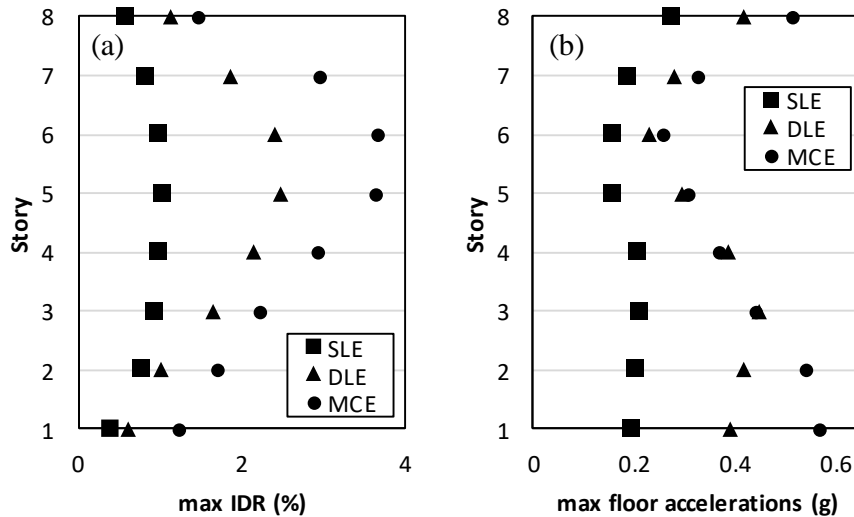


Figure 3-7 EDPs for earthquake scenarios (a) Peak inter-story drift ratios and (b) peak floor acceleration

3.4.3 Performance, seismic loss, and sustainability

Seismic loss and sustainability in terms of dollar, downtime, and equivalent carbon emissions are assessed considering structural and non-structural components. Damageable components are identified and divided into two performance groups (i.e., drifts-based performance group and acceleration-based performance group). The drifts-based performance group includes drift-sensitive structural components and drift-sensitive non-structural components, while the acceleration-based performance group includes acceleration-sensitive non-structural components. The fragility functions of the damageable components are represented using lognormal distributions with median and dispersion values. Table 3-1 shows various structural and non-structural damageable components considered in this example with uncertainty incorporated repair costs at different damage states. The damageable components fragility curves and repair costs are collected from Cardone and Perrone (2017) and FEMA (2012).

Table 3-1 Fragility curves and repair costs of the damageable components

Components	DS	No. per floor	EDP	Fragility functions		Repair cost (USD)	
				median	dispersion	median	dispersion
Structural components							
External joints	DS1	16	IDR (%)	1.75	0.40	2090	0.39
	DS2			2.25	0.40	3180	0.32
	DS3			3.22	0.40	3860	0.30
OMRF columns	DS1	24	IDR (%)	1.50	0.40	2090	0.39
	DS2			1.75	0.40	3180	0.32
	DS3			2.00	0.40	3860	0.30
Non-structural infill components							
Masonry infill	DS1	10	IDR (%)	0.15	0.5	570	0.22
	DS2			0.40	0.5	1200	0.44
	DS3			1.75	0.35	5760	0.52
Exterior masonry infill with windows	DS1	16	IDR (%)	0.1	0.5	570	0.30
	DS2			0.3	0.5	1020	0.46
	DS3			1.75	0.4	4320	0.52
Interior masonry infill with doors and windows	DS1	12	IDR (%)	0.2	0.50	510	0.28
	DS2			0.5	0.40	960	0.46
	DS3			1.75	0.35	4650	0.52
Aluminum-framed window	DS1	30	IDR (%)	1.6	0.29	69.6	0.2
	DS2			3.2	0.29	348	0.2
	DS3			3.6	0.27	696	0.2
Non-structural MEP components							

Conveying cold water	DS1	67.5* 1000l	PFA	1.5	0.4	50	0.76
	DS2	f	(g)	2.6	0.4	500	0.4
Conveying hot water	DS1	954* 1000l	PFA	0.55	0.4	50	0.76
	DS2	f	(g)	1.1	0.4	500	0.41
Sanitary waster piping	DS1	545* 1000l	PFA	1.2	0.5	80	0.58
	DS2	f	(g)	2.4	0.5	560	0.34
Electrical service and distribution (Switchgear)	DS1	3.6* AP 225	PFA (g)	1.28	0.4	1940	0.16
Electrical service and distribution (Distribution panel)	DS1	3.6* AP 225	PFA (g)	2.16	0.45	1940	0.16

*DS1 = Damage state 1, DS2 = Damage state 2 and DS3 = Damage state 3

*PFA = Peak floor accelerations

*MEP=Mechanical, electrical and plumbing

*OMFR = ordinary moment resisting frame

*lf = linear foot

Fragility functions and repair functions for different damage states are presented for considered damageable components. The number of components per floor is also given. It can be noted that Mechanical, electrical, and plumbing (MEP) components are acceleration sensitive, while non-structural infills and structural components are drift sensitive. The repair loss of the components is calculated using Equation (3-2). The loss distributions for all the components are determined using Monte Carlo simulations and aggregated for structural and non-structural repair losses. The following Figure shows structural and non-structural repair losses under considered seismic scenarios.

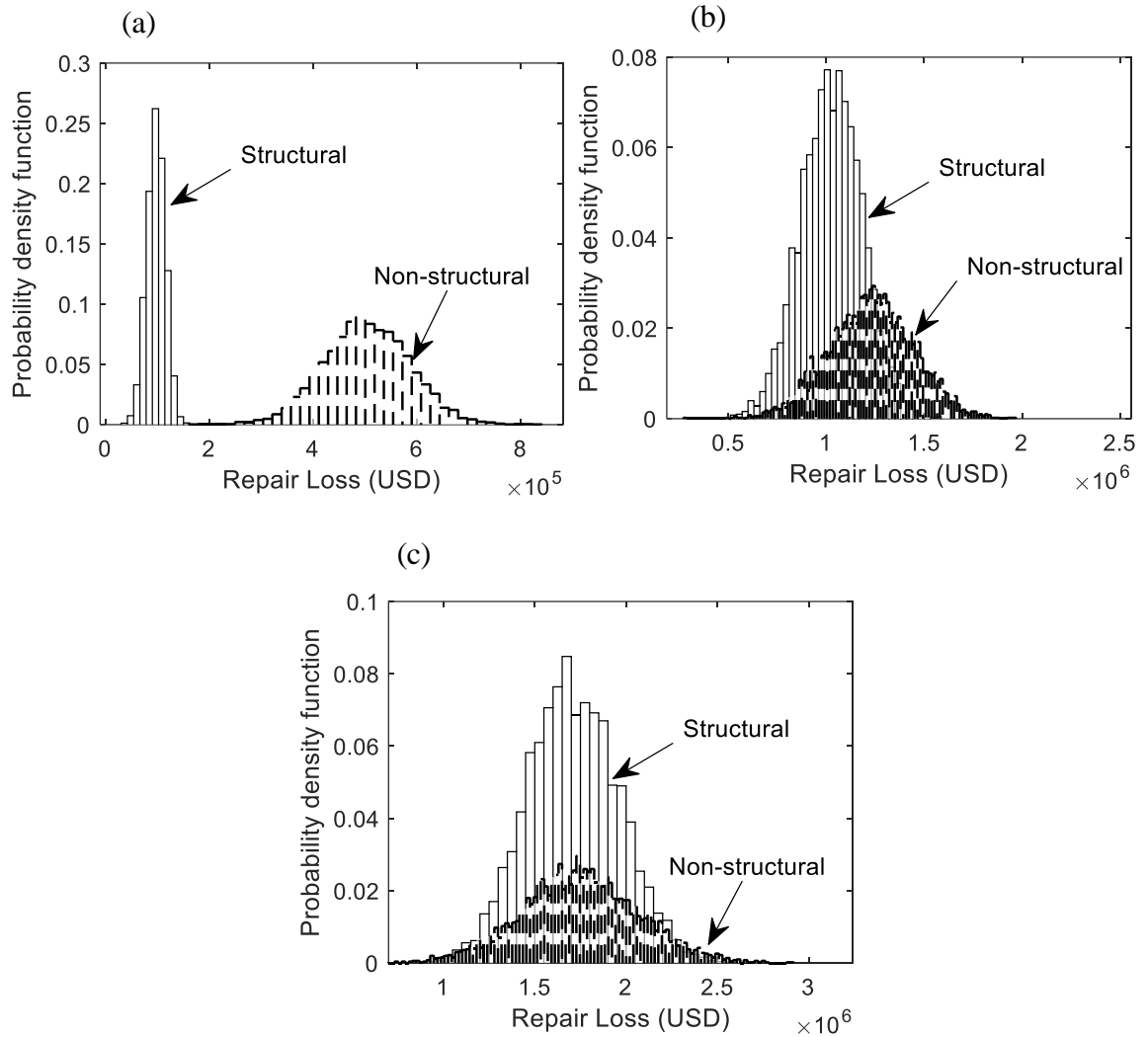


Figure 3-8 Distributions for repair loss associated with structural and non-structural components at (a) SLE, (b) DLE, and (c) MCE

The total expected losses for SLE, DLE, and MCE level earthquakes are 6.03×10^5 , 2.25×10^6 , and 3.47×10^6 USD, respectively. As indicated, the repair losses for the non-structural components are much larger at the SLE level, but as the intensity of earthquake ground motion increases, the structural losses significantly increase along with the non-structural components. Since its non-ductile structure with stringent drift performance limit states, structural losses are also higher. The collapse cost determined at three earthquake levels is 1.72×10^0 , 5.01×10^4 , and 9.93×10^5 USD, respectively.

Results indicate negligible collapse losses at SLE, 2.18%, and 22.25% of the total losses at DLE and MCE. It shows that most of the structural and non-structural losses are at a low probability of collapse, even at MCE level earthquake for a building designed without considering earthquake forces, the losses due to collapse contribute to 22.25%. The repair to replacement cost ratio for three earthquake levels is 15.51%, 57.84%, and 89.19%. The higher repair to replacement ratio can be due to non-ductile code configurations of the evaluated RC frame structure. It is observed that most of the damage is from non-structural infills, structural components also contribute to the repair loss considerably, while repair loss due to MEP components is negligible.

Table 3-2 Damage ratios corresponding to different damage states

Damage State	Damage ratio (%)	Central damage ratio
Slight Structural Damage (IO)	1.25-7.50	3.5
Moderate Structural Damage (LS)	7.5-20	10
Severe Structural Damage (CP)	20-90	65
Collapse (C)	90-100	95

Environmental impact in terms of greenhouse gases (GHG) is assessed by quantifying equivalent CO₂ emissions associated with the repair activities. Repair actions of damageable components for different damage states shown in Table 3-3 are used to quantify materials during repair activities. The material types of damageable building components, material take-off and the relevant distributions of equivalent carbon emissions are shown in Table 3-4.

Table 3-3 Repair actions of damageable components at different damage states

Components	Damage states	Repair actions
Structural components		
External joints and OMRF Columns	DS1	Patch new plaster and paint
	DS2	Restore concrete 1 inch beyond the exposed reinforcing steel, Patch new plaster and paint
	DS3	Replace component
Non-structural infill components		
Masonry Infill	DS1	Patch new plaster and paint
	DS2	Restore broken bricks, patch new plaster and paint
	DS3	Reinstall windows and doors, restore all bricks, patch new plaster and paint
Non-structural MEP components		
Conveying cold water, hot water and sanitary piping	DS1	Fix minor leakage
	DS2	Fix one pipe break per 1000 feet
Electrical service and distribution (Switchgear and distribution panel)	DS1	Fix inoperability

The material take-offs are based on the building drawings and repair actions, and the carbon emission values are based on the study conducted by Chau et al. (2012) and Dong and Frangopol (2016). Monte Carlo simulations are performed and equivalent CO₂ emissions are quantified for all the damageable components and aggregated to get total emissions. The equivalent CO₂ emissions for SLE, DLE, and MCE are shown in the following Figure.

Table 3-4 Material take-offs and CO₂ emissions of different building materials

Material type	SLE	DLE	MCE	Type of PDF	CO ₂ emissions (kg CO ₂ /kg)	
	kg	kg	kg		Median	β
Concrete	1.27 x10 ⁴	1.84 x10 ⁵	3.22 x10 ⁵	uniform	0.045	0.06
Steel	9.96 x10 ²	1.68 x10 ⁴	3.04 x10 ⁴	lognormal	0.460	0.4
Plaster	1.08 x10 ⁵	1.81 x10 ⁵	2.22 x10 ⁵	lognormal	0.023	0.4
Paint	8.84 x10 ³	1.33 x10 ⁴	1.57 x10 ⁴	lognormal	1.665	0.4
Brick	3.54 x10 ⁵	9.60 x10 ⁵	1.31 x10 ⁶	lognormal	0.042	0.4
Glass	4.15 x10 ²	4.05 x10 ³	6.27 x10 ³	normal	0.184	0.4
Plywood	3.17 x10 ²	4.84 x10 ³	7.50 x10 ³	lognormal	0.192	0.4

* β = dispersion values

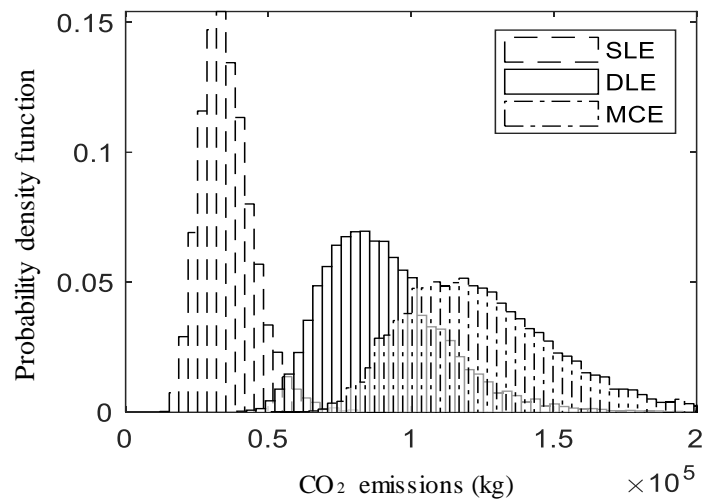


Figure 3-9 CO₂ emissions under three earthquake scenarios

3.4.4 Downtime and resilience

Repair times associated with damageable components are shown in Table 3-5. Repair times are represented as worker days required to complete repairs while building

downtime is the total time required for a building to complete all repairs. Downtime is calculated using two schemes (i.e., parallel (fast-track) and series (slow-track)). In practice, neither parallel nor series configuration is utilized but it covers a wide range of downtime, and actual downtime is presumed to be within this range. In addition to repair times for actual building repair activities, additional time called delay time is also considered in the downtime assessment. Delay time is an additional time required for inspection, engineering mobilization, review and/or redesign, financing, contractor mobilization and permitting, etc. The delay times can vary considerably and can range from weeks to months (Hutt et al., 2015). The repair times of damageable components are collected from FEMA (2012).

Table 3-5 Probabilistic repair times of damageable components

Components	Damage state	Repair time (Worker-days)	
		median	dispersion
Structural components			
External joints	DS1	18.9	0.46
	DS2	28.7	0.40
	DS3	35.3	0.39
OMRF columns	DS1	18.9	0.46
	DS2	28.7	0.40
	DS3	35.3	0.39
Non-structural infill components			
Masonry infill	DS1	18.9	0.46
	DS2	28.7	0.40
	DS3	35.3	0.39

Exterior masonry infill with windows	DS1	5	0.4
	DS2	10	0.4
	DS3	15	0.4
Interior masonry infill with doors and windows	DS1	5	0.4
	DS2	12	0.4
	DS3	17	0.4
Aluminum-framed window	DS1	0.18	0.3
	DS2	0.72	0.3
	DS3	1.44	0.3
Non-structural MEP components			
Conveying cold water	DS1	0.307	0.80
	DS2	0.281	0.48
Conveying hot water	DS1	0.370	0.80
	DS2	0.281	0.48
Sanitary waster piping	DS1	0.424	0.63
	DS2	3.02	0.42
Electrical service and distribution (Switchgear)	DS1	2.18	0.3
Electrical service and distribution (Distribution panel)	DS1	2.18	0.3

Slow track and fast track repair schemes can provide a reasonable estimate of lower and upper bounds of a building downtime and can be calculated by dividing the total repair time with the total number of workers available per floor for repairs and adding delay times. The consequence functions for structural and non-structural

components are based on (Cardone and Perrone, 2017; Dong and Frangopol, 2016; FEMA, 2012).

The following Figure shows the downtime at three earthquake levels for slow track and fast track. The expected downtime for the slow track at three levels is 567, 1735, and 2621 days, respectively; similarly, for the fast track is 90, 362, and 486 days. The difference between slow and fast track depends on the number of stories along with other factors, as the number of stories increases, the difference in the slow-track and fast-track increase considerably (Almufti and Willford, 2013).

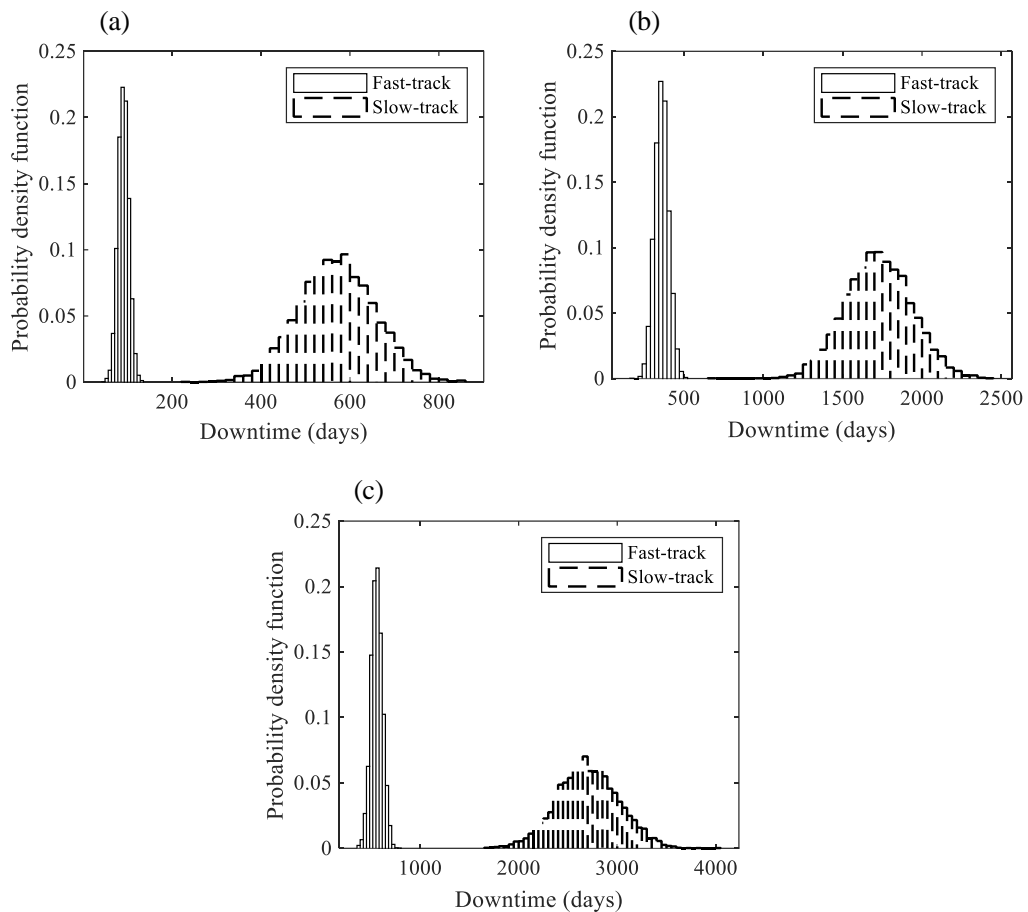


Figure 3-10 Downtime for the slow and fast track at levels (a) SLE, (b) DLE, and (c) MCE

At the SLE level, most of the downtime is due to the non-structural repair of infills, while for DLE and MCE levels, downtime due to structural repair is dominant. The distribution of downtime is utilized for the resilience assessment. Performance limit states (i.e., IO, LS, CP, and collapse) are considered for the determination of residual functionality. Residual functionality also considered as the robustness of a building system can be quantified from the building performance limit states. The uncertainties associated with functionality are incorporated using a triangular distribution with lower bound, upper bound, and mode corresponding to IO, LS, and CP as (0.7, 0.9, 0.8), (0.4, 0.6, 0.5), and (0, 0.2, 0), respectively (Dong and Frangopol, 2016). The residual functionality corresponding to no damage is 1 and for the collapse of a building is 0. Monte Carlo simulations are performed for the uncertainty modeling of residual functionality against different limit states and corresponding expected values for three levels are determined (i.e., 0.52, 0.22, and 0.15 for SLE, DLE, and MCE). Residual functionalities are used to calculate resilience under investigated time intervals using Equation (3-1). The calculated resilience at an investigated time interval of 100, 200, and 300 days is shown as follows for fast-track and slow-track.

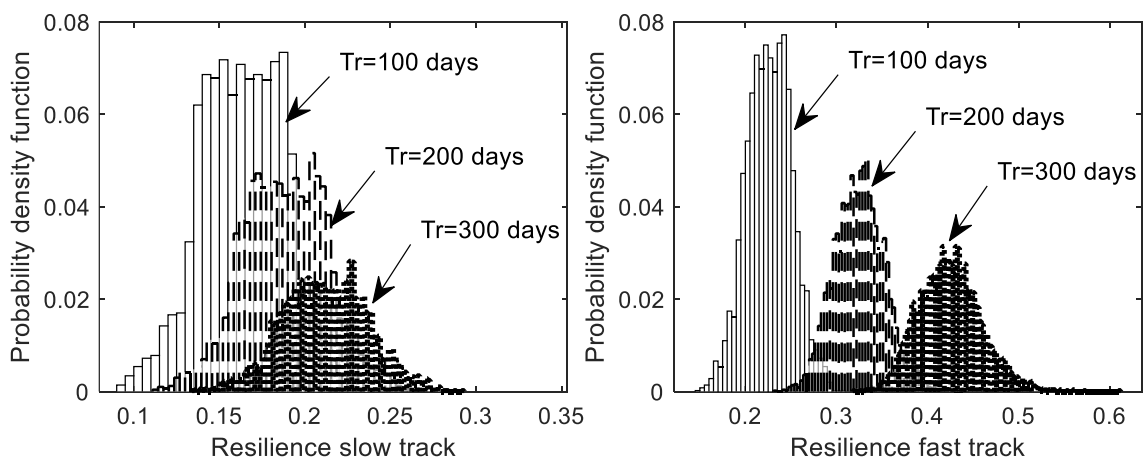


Figure 3-11 Distributions of resilience at investigated 100, 200, and 300 days under DLE

The expected values of resilience are plotted as follows for the investigated time period of 1,000 days.

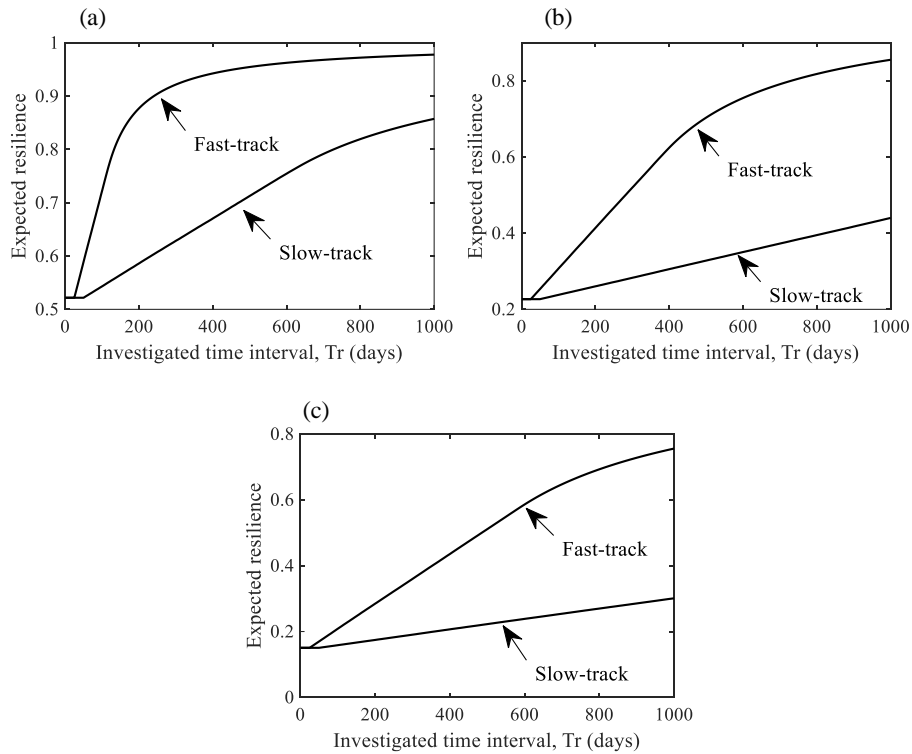


Figure 3-12 Expected resilience under 1000 days investigated period under (a) SLE, (b) DLE, and (c) MCE

As indicated, the residual functionalities are substantially low for DLE and MCE. The reduced residual functionality shows poor earthquake performance during an earthquake event. The comparatively large differences between slow-track and fast-track downtimes increase the bounds, but still, useful information can be deduced about the recovery profile of a building. The expected resilience of 0.975, 0.85, and 0.75 is

observed for fast-track at an investigated time period of 1000 days, while for slow-track the expected resilience observed is 0.86, 0.42, and 0.31, respectively.

3.5 Summary

The chapter provides a probabilistic framework to compute seismic sustainability and resilience using performance-based assessment methodology. Following conclusions are drawn.

1. The performance-based methodology is used for the repair and downtime assessment of non-ductile RC buildings. Monetary losses due to non-collapse account for 99.99%, 97.82%, and 77.75% of the total losses at three earthquake scenarios. The total repair losses for structural and non-structural components at three levels are 9.72×10^4 , 1.02×10^6 , 1.71×10^6 USD and 5.06×10^5 , 1.23×10^6 , 1.76×10^6 USD. Non-structural infills contribution to repair loss is found to be significant with 83%, 51%, and 46% of the total repair loss. Losses due to structural components also dominate with 45% and 49% at DLE and MCE.
2. The equivalent carbon emissions for three earthquake levels equal 3.447×10^4 , 8.696×10^4 , and 1.222×10^5 kg, respectively. The emissions are dominated by bricks and paint material with 89%, 74%, and 69% of the total emissions at three earthquake scenarios. Repair to replacement ratio for economic loss at three scenarios is 15.51%, 57.84%, and 89.19% while, for environmental is 10.59%, 26.80%, and 37.39%. In the considered example, it is environmentally friendly to repair a structure even at MCE earthquake scenario.
3. Resilience quantification using performance-based assessment methodology can be used as an indicator for measuring the robustness and recovery of

building infrastructure. Based on results, the non-ductile building suffers a high loss of functionality and is not able to gain even 50% of the functionality at DLE and MCE for slow-track after 1000 days of investigated time period, showing poor performance not only during an earthquake but during the recovery time as well. Fast-track scheme shows considerably better recovery performance but for that community must have high resourcefulness and rapidity attributes.

4. Downtime assessment plays an important role in the resilience assessment of individual multi-story buildings and thus should be investigated further to improve quantification of resilience, since neither series nor parallel repair schemes would be adopted for the repair of an actual building after an earthquake. The results conclude huge variability in slow-track and fast-track resilience and should follow a logical repair strategy for downtime assessment to reduce variability.
5. Future research is needed to incorporate record-to-record variability using large suits of earthquake records for assessment purposes. Improved uncertainty modeling and functionality mapping should be developed for better predicting residual functionality during and after an earthquake.

CHAPTER 4 SEISMIC RESILIENCE OF RETROFITTED BUILDINGS

4.1 Introduction

Existing buildings can be at greater seismic risk due to non-conformance to current design codes and may require structural retrofitting to improve building performance. The performance of buildings is measured in terms of immediate consequences due to direct damage, but the continuing impacts related to recovery are not considered in the seismic retrofit assessment. This chapter introduces a framework of retrofit selection based on the seismic resilience of deficient buildings retrofitted with the conventional mitigation approaches. The assembly-based methodology is considered for the seismic resilience assessment by compiling a nonlinear numerical model and a building performance model. The collapse fragility is developed from the capacity curve, and the resulting social, economic, and environmental consequences are determined. The seismic resilience of a building is assessed by developing a downtime assessment methodology incorporating a sequence of repairs, impeding factors, and utility availability. Five functionality states are developed for the building functionality given investigated time intervals, and a functionality curve for each retrofit is determined. It is concluded that seismic resilience can be used as a performance indicator to assess the continuing impacts of a hazard for the retrofit selection.

4.2 Seismic resilience assessment

The framework begins by selecting building and retrofit methods used for investigating and enhancing seismic resilience. The first step is to develop the nonlinear models for the reference un-retrofitted and the retrofitted buildings. The nonlinear model should be able to effectively capture the steel yielding, concrete crushing, strength, and stiffness degradation. The capacity curve representing base shear given lateral displacement can then be developed from the nonlinear static analysis procedure and is used to estimate the deficiencies in the lateral force-resisting system.

The capacity curves are developed by applying a series of lateral loads with increasing magnitude and recording the lateral displacements. Increasing the lateral loads in each iteration will eventually cause elements to start to yield, and, as a result of each yielding of structural members, the redistribution of loads will take place (Su et al., 2019). The model is revised in each iteration by adjusting the member yielding, strength, and stiffness degradation, and the process continues till the yield pattern and strength and stiffness degradation for the whole structure is identified. The maximum base shear and the lateral displacements are identified and compared with the design loads and a strength factor is determined. If the strength factor is greater than one or within the desirable limits of the codes, the structure is considered safe; otherwise structural retrofitting is required. The capacity curves are developed for the retrofitted models using the same procedure (i.e., pushover analysis). If the strength factors are not desirable, then the retrofit techniques are revised and the process is repeated to achieve the desirable preliminary performance. The methodology is presented in a flowchart as shown below.

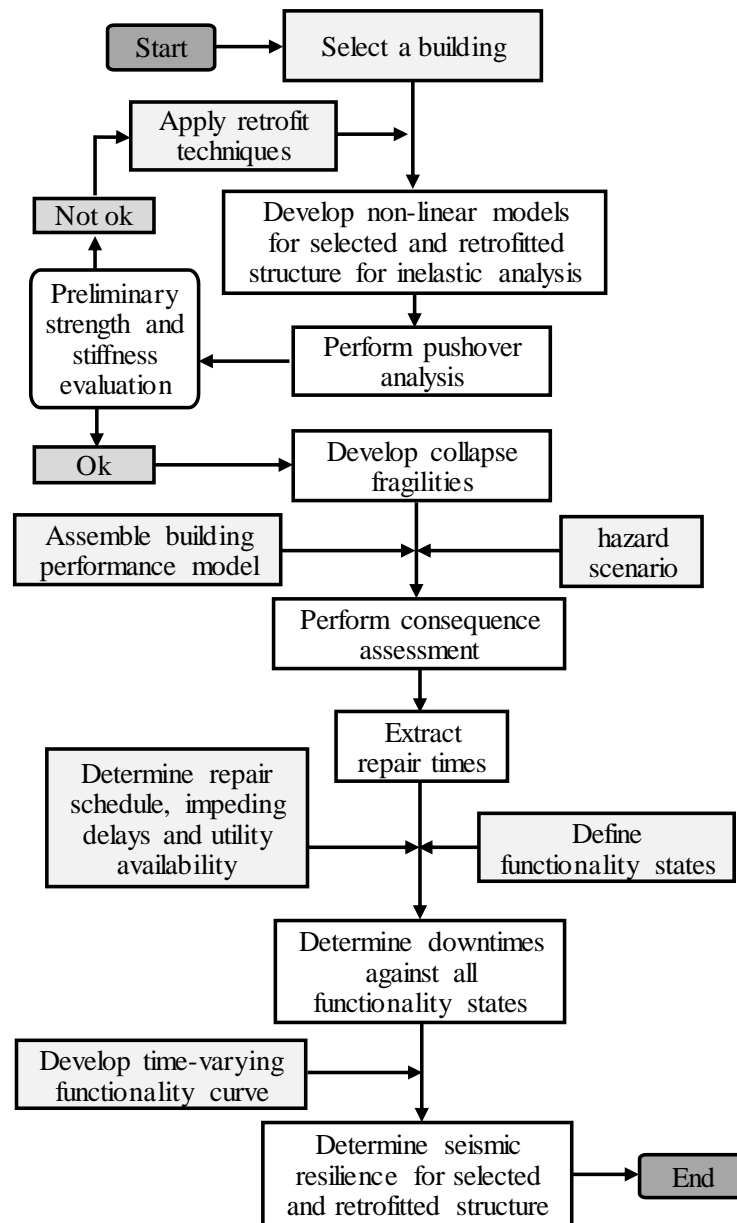


Figure 4-1. The methodology for assessing seismic resilience using a nonlinear static procedure

4.2.1 Developing collapse fragilities from pushover

If the retrofit techniques satisfy the preliminary strength and stiffness requirements, the next step is to develop the collapse fragilities and building performance model. Vamvatsikos and Cornell (2006) investigated a series of single-degree-of-freedom

systems with a wide range of time periods through incremental dynamic analysis. The resulting hysteresis loops were converted to backbone curves ranging from simple bilinear to quadrilinear, comprising an elastic, hardening, softening, and a residual plateau segment that ends at a zero-strength. The relationship between the characteristic segments of IDA curves were linked to the backbone curves of many systems, suggesting that nonlinear static analysis procedure (i.e., pushover analysis) can be used to estimate nonlinear dynamic response. In this chapter, the pushover analysis is used to estimate nonlinear IDA results by utilizing the static pushover to incremental dynamic analysis (SPO2IDA) tool. FEMA-P-58 (2012) recommends that this tool can be used to develop collapse fragilities for low-rise buildings dominated by the fundamental mode of vibration. This method can bypass the computationally expensive part of the methodology and can rapidly generate the collapse fragility. Following are the steps to develop collapse fragility using the SPO2IDA tool.

1. Develop a suitable nonlinear mathematical model of a structure for the pushover analysis.
2. Perform a nonlinear static analysis procedure to develop capacity curve in the principle building direction.
3. Approximate the capacity curve into quadrilinear curve by identifying four control points each indicating the endpoint and the start point of the four defined segments
4. Execute the SPO2IDA tool and input the control points and relevant information (e.g., building weight, building height, fundamental time period, etc.), and extract the median collapse capacity.

5. Construct the collapse fragility using a lognormal cumulative distribution function with a dispersion of 0.6.

4.2.2 Consequence assessment

The collapse fragility analysis provides information on the probability of collapse given an intensity measure. It is more interesting for decision-makers to obtain more meaningful information (e.g., economic loss in terms of dollars, casualties in terms of numbers, equivalent carbon emissions, etc.). In the consequence assessment, collapse fragility and the probability of damage to components of a building are converted to social, economic, and environmental consequences. For that purpose, a building performance model is assembled, comprising fragility functions and consequence functions for damageable structural and non-structural components. Fragility functions determine the probability of exceeding given damage states for each damageable component. Consequence functions use the probabilities of components being in different damage states and determine the social, economic, or environmental consequences. The following steps can determine economic and environmental consequences given a hazard scenario.

1. Define a hazard scenario against which consequences are to be determined
2. Evaluate EDPs from the developed nonlinear mathematical model.
3. Determine the probability of exceeding different damage states for all the damageable components.

4. Utilize the probability of exceeding different damage states for all the damageable components, and the collapse fragility to determine consequences using the total probability theorem.

The social consequences (i.e., injuries, fatalities) can be determined as

$$S_{m|IM} = \varnothing_C T_{rand} f(p|T_{rand}) P_T P_R P_{C|IM} \quad 4-1$$

where $S_{m|IM}$ is the social metric of seismic sustainability; \varnothing_C is the casualty function, which depends on the type of construction and can be determined using historical casualties from past earthquakes; T_{rand} is the randomly generated time of the day and day of the week for a particular realization; $f(p|T_{rand})$ is the time-dependent population model; P_T is the total population of a building; $p_{C|IM}$ is the probability of collapse of a building given IM; and P_R is the population at risk depending upon the failure mode of a building.

The economic and environmental consequences can be determined as

$$C_{L|IM} = \sum_{DS} \int_0^{\infty} C_{L|DS} P_{DS|EDP} f_{EDP|IM} dEDP \cdot (1 - p_{C|IM}) + C_{L|C} \cdot p_{C|IM} \quad 4-2$$

where $C_{L|IM}$ is the total consequence given IM; $C_{L|C}$ is the consequence given probability of collapse; $p_{C|IM}$ is the random value of a consequence loss function of a component for a given damage state; $P_{DS|EDP}$ is the probability of damage state given EDP; and $f_{EDP|IM}$ is the probability density function of EDP given IM.

The resulting socioeconomic and environmental consequences may include considerable variations due to the uncertainties in the variables in different stages of the analysis and it is essential to consider these uncertainties for better understanding of the consequences and the existing variations. This would be discussed in more detail in the subsequent chapters but is important to highlight that mean alone cannot provide complete picture and these meaningful consequences can have significant variations that may hinder effective decision support and should be considered accordingly.

4.2.3 Seismic resilience assessment

Seismic resilience is the ability of a structure to absorb damage without suffering collapse and to recover from the earthquake hazard efficiently. The building with greater seismic resilience would have less damage in the immediate aftermath of an earthquake and would recover faster. The functionality of a building after an earthquake and its recovery can be used as a performance indicator for assessing seismic resilience. The functionality curve provides the functionality state given the investigated time interval and its recovery to full functionality after a hazard event. Seismic resilience can be mathematically evaluated by integrating the functionality curve over time.

In this chapter five functionality states are developed depending upon the structural and non-structural damage and utility availability. The mapping of the functional states and the recovery to full functionality is presented in a flowchart shown in Figure 4-2. Five functionality states are represented mathematically by a designated weighting factor. Full-Functionality (FF) is assigning a weighting factor of 1, and the Restricted-Entry (RE) is given a weighting factor of 0.2. The remaining functionality states are assigned weighting factors between 0.2 and 1 with an increment of 0.2. After

an earthquake event, the process starts with the inspection of a building, which is performed by a professional building inspector. In this chapter, the structural and non-structural damage is computed using fragility functions to quantify the extent of damage to the building. Depending on the extent of damage and the information about the utility availability, the initial functional state of a building can be determined. For example, if the building has experienced moderate to extensive structural damage, the building is tagged in the Restricted-Entry (RE) functional state (i.e., the occupants are not allowed to enter the premises before the necessary repairs). The logical sequence of repair is designed in the next step to bring the building functionality to a pre-hazard state. Before the building repairs, additional delays, called impeding delays, will occur due to financing, engineering reviews, permitting, contractor mobilization, and sometimes long lead times.

The building is tagged as Restricted-Entry (RE) if it suffers moderate to extensive structural damage, and if the building only suffers non-structural damage, then the building is in Restricted-Use (RU) functional state. The building will be recovered to full functionality after the impeding delays, necessary non-structural repairs, and availability of all the utilities. If minor or no damage is observed, then, depending upon the availability of utilities, a building is assigned as one of the remaining three functional states. If no utility is available, the building is in Re-Occupancy (RO) functional state (i.e. the building space can be occupied for shelter purposes but cannot be utilized for its intended purpose). If only critical utilities are available (i.e. electricity and water), then the building is Baseline-Functional (BF), and the building will achieve Full-Functionality (FF) after the availability of all the utilities.

The repair time required for the repair of each damaged structural and non-structural component can be determined from Equation (4-2). The downtime for each functional state can be determined by considering the repair schedule (i.e., sequence of repairs determined from the repair times of all the damageable components), impeding delays (i.e., financing, engineering review and permitting, contractor mobilization, and long lead times) and the utility availability. The impeding delays and the utility availability are considered in this chapter through the lognormal distribution function developed by Almufti and Willford (2013) in the REDi Rating System (Resilience-based Earthquake Design Initiative for the Next Generation of Building). The functionality curve can be developed after determining the downtime for each functional state, and the seismic resilience can be evaluated.

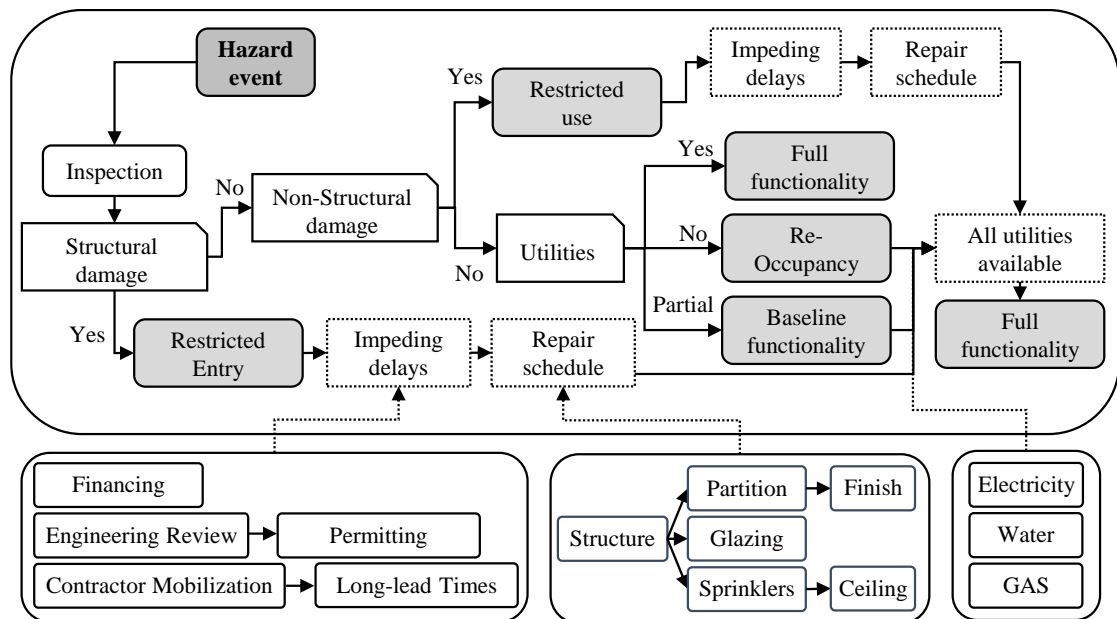


Figure 4-2. Functionality states and recovery considering structural and non-structural damage, impeding delays, sequence of repairs, and utility availability

4.3 Illustrative example

The non-ductile reinforced concrete building selected for this illustrative purpose is a two-story intermediate moment-resisting frame building with a total height of 8.5m. The residential building is designed according to the building codes implemented at the time of its design and construction, which largely ignored seismic provisions, and in which only wind loads are considered in the design of a building against the lateral loads. The concrete strength of 20Mpa and a mild steel with yield strength of 240 MPa is used for the design, resulting in large cross-sections, increased weight, and stiffness. Three retrofitting techniques, namely, Reinforced Concrete Jacketing (RCJ), Steel Jacketing (SJ), and Fiber Reinforced Polymer (FRPs) overlays are considered for improving the performance of a non-ductile building. The considered seismic retrofit techniques require modifying the existing lateral force-resisting components (i.e., column in the considered example). The enhancement of the cross-sections follows FEMA-547 (2006) and ASCE-41-13 (2013) recommendations, which explicitly highlight the detailing, construction practices, and seismic evaluation of existing buildings. The layout and the design details of a building are shown in Figure 4-3.

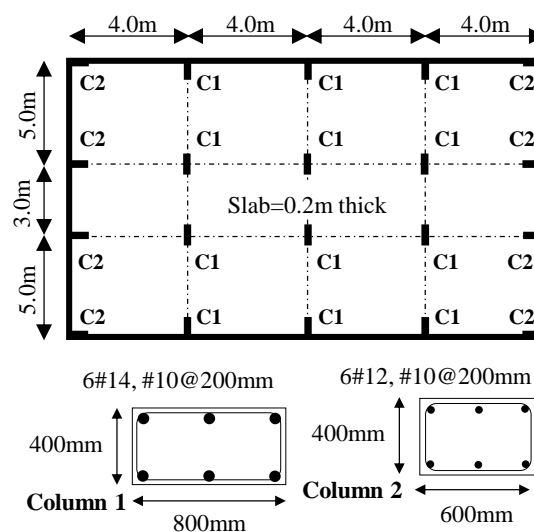


Figure 4-3. Building plan and structural details

Ten fiber-based nonlinear models are developed, one for the reference unretrofitted structure and nine models for the retrofitted structures (i.e., three retrofit models for each retrofit technique). The numerical models are developed in an open-source nonlinear analysis platform ZEUS-NL (Jeong and Elnashai, 2005). The built-in nonlinear material models are used to represent concrete and steel behavior. The nonlinear concrete material model with a crushing strain of 0.02 and a confinement factor of 1.05 is used depending upon the reinforcement details. A bilinear elastoplastic model with kinematic strain hardening is used for the steel material modeling. The material and geometric nonlinearities, P-delta effects, and large displacements are considered. The models for the reinforced concrete jacketing, steel jacketing, and FRP overlays are represented by modeling sections of the columns into reinforcing steel, confined, and unconfined concrete regions. The element cross-sections are divided into a number of fibers to effectively monitor the stresses and strains of different sections of elements. A uniaxial constant confinement concrete model is utilized for the reinforced concrete jacketing, a bilinear steel model with constant strain hardening is utilized for the steel jacketing, and a uniaxial trilinear fiber-reinforced plastic model is used for the fiber-reinforced polymer overlays.

4.3.1 Developing collapse fragilities from pushover

Pushover analysis is performed on a model by applying an increasing inverted triangular lateral loads pattern, representing the deformation of a building under the fundamental mode, and evaluating the maximum lateral displacements. Information on the structure's strength, stiffness, and ductility can be extracted from the resulting

capacity curve of a building, and a strength factor can be determined to evaluate the performance of a building and retrofit methods (Elkady and Lignos, 2015). Following Figure shows the capacity curve of the reference building and the considered retrofit techniques. The capacity curve gives important information about member yielding, stiffness, and ultimate strength of a building structure. The ultimate strengths are compared with the design strength, and the strength factor is determined, which is the ratio of the design strength to ultimate strength. If the strength factor is more than one, then the building is satisfactory; otherwise retrofit techniques are used to improve the strength factor. The non-ductile reinforced concrete building is designed only to resist gravity and wind loads, since before 1991 the region was classified as zone '0', and the lateral seismic loads were not considered during the design process. According to the revised zone classification of the region, UBC's (1997) static lateral force procedure provides a required design strength of 655 kN, and the ultimate strength determined from the capacity curve is 605 kN. Since the ultimate strength is less than the required design strength of a building, the reference building is not conforming to the design requirement of the current code of practice (i.e., UBC (1997)). RCJ retrofit with retrofit thickness of 50mm, 75mm, and 100mm gives the strength factors of 2.69, 3.13, and 3.57. Similarly, the strength factors for the FRP retrofit for one, two and three layers are 1.54, 2.01, and 2.12. And the strength factors for the SJ retrofit with steel jacket thicknesses of 3mm, 5mm, and 10mm are 2.40, 2.99 and 3.98. It is interesting to note that steel jacketing has greater impact in increasing the lateral capacity of a building, while FRPs provide comparatively the least improvement in the ultimate lateral capacity. Nonetheless, all the considered retrofit techniques provide satisfactory strength factors (i.e., greater than one).

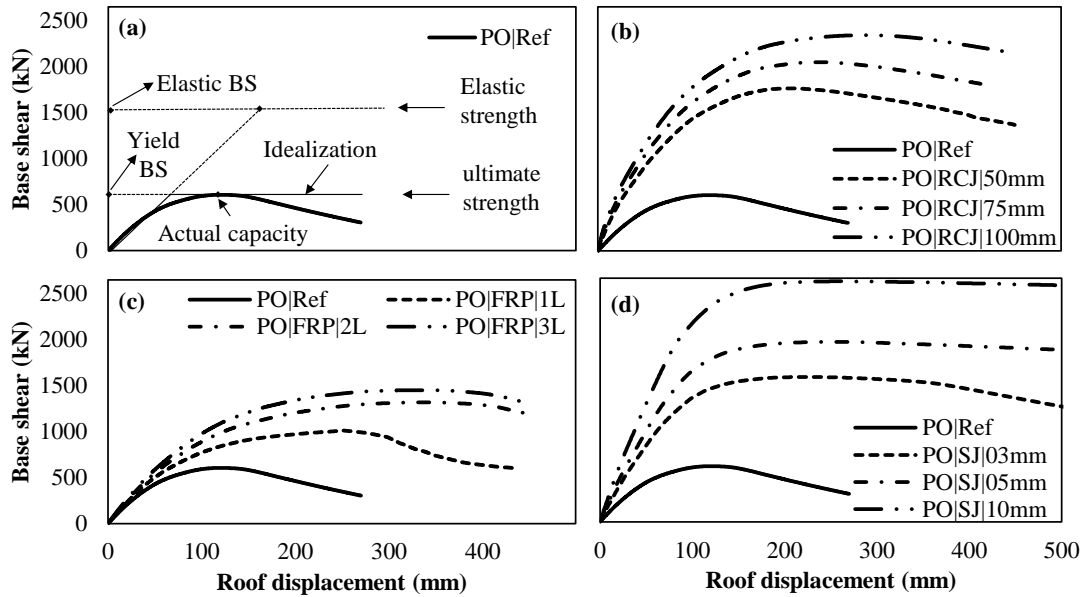


Figure 4-4. Capacity curve for (a) reference structure, (b) reinforced concrete jacketing, (c) FRP overlays, and (d) steel jacketing

The capacity curves are converted into idealized curves, a bilinear approximation is provided in Figure 4-4a, and more details on idealization from the capacity curve can be obtained from Elnashai and Di Sarno (2008). The four segments of the idealized curve will give four control points, which are used as an input in the SPO2IDA tool, and the median and dispersion values for the collapse fragilities are evaluated. The lognormal cumulative distribution function is then used to develop collapse fragilities for each model. The following Figure shows the collapse fragilities developed by using pushover analysis. It is noted that SJ retrofit reduces the probability of collapse significantly, RCJ retrofit also significantly reduces the probability of collapse, while for the FRP retrofit, the reduction in the probability of collapse is not significant. Nonetheless, the probability of collapse is reduced for all the considered retrofit techniques.

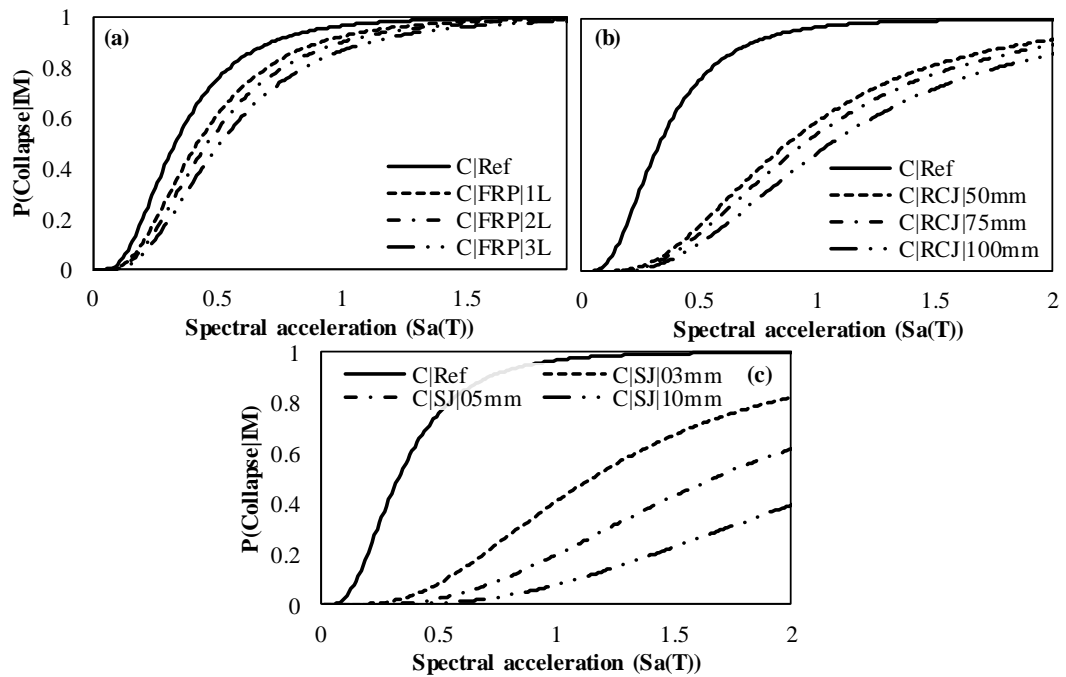


Figure 4-5. Collapse fragilities for (a) FRP overlays, (b) reinforced concrete jacketing, and (c) steel jacketing

4.3.2 Consequence assessment

Consequence assessment starts with selecting a hazard scenario and assembling a building performance model. The hazard scenario with a design PGA of 0.16g is selected for the case of this illustrative example. To investigate the variation of social, economic, and environmental consequences with varying intensity measures, four hazard scenarios are considered for the consequence assessment (i.e. half the design hazard scenario, twice the design hazard scenario, and four times the design hazard scenario). Three retrofit techniques (i.e. FRPs with 1 layer, RCJ with 75mm of jacket thickness, and SJ with 3mm of jacket thickness) are considered for the consequence and resilience assessment.

The building performance model consists of fragility functions and consequence functions. Fragility functions relate the structural analysis results to the damage, and consequence functions translate the damages into social, economic, and environmental consequences. The fragility and consequence functions utilized in this example are extracted from (Mitrani-Reiser, 2007; FEMA-P-58, 2012; Hashemi et al., 2019), and are shown in Table 4-1. Additionally, for the illustration purposes, fragility and consequence functions for the structural damageable component (i.e., structural columns) is shown in Figure below. The fragility functions for the three damage states are shown as a cumulative distribution functions, while the corresponding consequence function is represented as probability distribution function. The fragility function will give probability of exceedance of given damage state and the corresponding consequence function will provide the resulting economic loss in terms of USD.

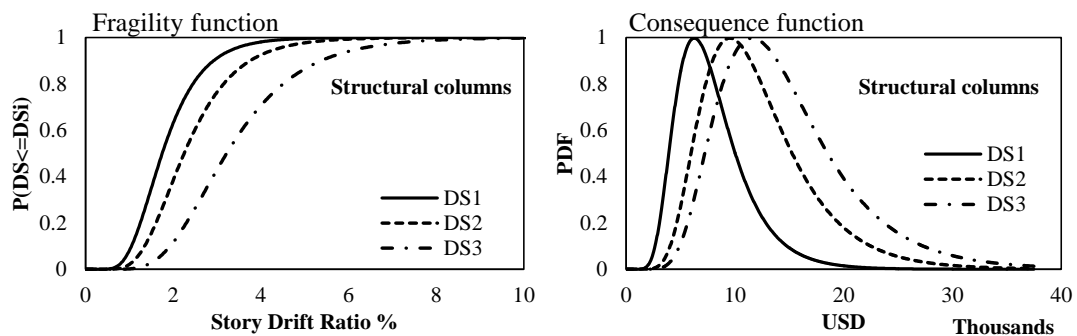


Figure 4-6. Fragility and consequence functions for considered structural columns

The fragility and consequence functions for various types of retrofitted structural components are not yet available in the literature. Therefore, in this illustrative example, conventional fragility and consequence functions are utilized for the retrofitted buildings.

Table 4-1. Fragility functions and consequence functions of damageable components

Component	Quantity per floor	Damage state	Fragility functions		Consequence functions			
					Economic (USD)		Environmental (kgCO ₂)	
			Median	CoV	Median	CoV	Median	CoV
Structural columns	20 units	DS ₁	1.75	0.40	6270	0.39	1.794	0.4
		DS ₂	2.25	0.40	9540	0.32	1.794	0.4
		DS ₃	3.22	0.40	11580	0.30	19.73	0.4
Partition	6 m ² x 22	DS ₁	0.39	0.17	115	0.20	12.72	0.4
		DS ₂	0.85	0.23	679	0.10	25.52	0.4
Finish	6 m ² x 44	DS ₁	0.39	0.17	115	0.20	1.336	0.4
		DS ₂	0.85	0.23	321	0.10	2.686	0.4
Glazing	2.8 m ² x 5.654	DS ₁	4.00	0.36	564	0.17	96.30	0.4
		DS ₂	4.60	0.36	564	0.17	183.2	0.4
Ceiling	232 m ² x 0.22	DS ₁	0.35	0.40	4541	0.40	1.023	0.4
		DS ₂	0.55	0.40	37612	0.50	5.846	0.4
		DS ₃	0.80	0.40	70769	0.55	19.73	0.4
Sprinklers	4 m x 8.8	DS ₁	0.32	1.40	1154	0.37	58.07	0.4

The components are divided into drift-sensitive and acceleration-sensitive components. The components partitions, finishes, and glazing are sensitive to lateral story drifts, and ceiling and sprinklers are sensitive to floor accelerations. The social consequences are determined by constructing a population model and defining casualty function and the population at risk. The time-dependent population model represents the percentage of people present during the time of the day, and day of the week for a

given realization. The casualty function for the reinforced concrete residential construction indicates that 90% will suffer casualties in the event of collapse, and 10% will suffer a major injury in the case of reinforced concrete frame structure (FEMA-P-58, 2012). The following Figure shows the social losses in terms of the total number of expected fatalities given four scenarios. The social losses for the reference un-retrofitted building have the highest number of expected fatalities. Applying retrofit reduces the social losses, with SJ and RCJ being the most effective in reducing the social consequences.

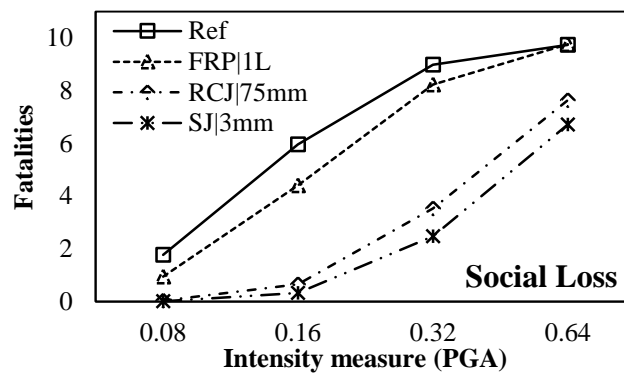


Figure 4-7. The social consequence in terms of expected fatalities given IM

To evaluate the economic and environmental losses, structural analyses of nonlinear building models are performed and engineering demand parameters (i.e., story drifts and accelerations) are extracted for each story, correlated with damage through fragility functions and consequences through consequence functions. The total economic and environmental consequences determined from Equation (4-2) are shown in the Figure below. The economic and environmental consequences increase with increasing IM levels. The un-retrofitted structure has the highest consequences, reduced using retrofit techniques. Comparatively, the percent reduction in the social, economic, and environmental consequences is highest for the 0.16g and 0.32g hazard scenario,

and lowest for the 0.08g and 0.64g hazard scenario. In the given illustrative example, SJ and RCJ are more effective in reducing the consequences for the design and twice the design seismic hazard scenario.

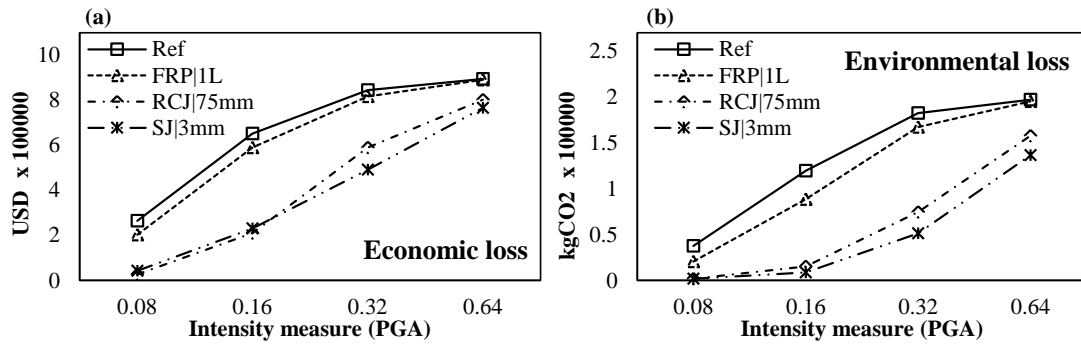


Figure 4-8. Consequences (a) Economic in terms of monetary loss, and (b) Environmental in terms of kgCO₂ emissions

4.3.3 Seismic resilience assessment

The first step in evaluating seismic resilience is to extract the repair times for all the damageable components of a building. Table 4-2 shows the repair time functions given damage state, utilized to determine repair times for all the components for a given story. The next step is to develop a logical repair sequence for the downtime of a building. The building repair starts with repairing the structural components serially (i.e., structural components of the first story are repaired first, before moving to the higher stories). Not all non-structural components can be repaired simultaneously (e.g., to repair ceilings the sprinklers need to be repaired first, and to do finishes, partitions needed to be repaired). In the example considered, partition, glazing, and sprinklers are simultaneously repaired in parallel, followed by finish and ceilings. Additional delays due to impeding factors (i.e., delays due to inspection, engineering mobilization,

financing, contractor mobilization, and permitting), and utilities (i.e., water, gas, and electricity) are considered using lognormal cumulative distribution functions. The utility disruption curves represent the restoration of utilities to the building and are determined from previous earthquake data and simulation studies (Almufti and Willford, 2013). The utility disruptions depend on the amount of local damage to the distribution system and are considered through repair rate (RR), which is computed based on the peak ground velocity at a building site. The related lognormal distribution function is selected for repair rates greater or less than 0.2 repairs/Km, as shown in Table 4-2.

In a pre-hazard state, the building is performing its intended purpose and is in a full functional state (i.e., all the utilities are available and no structural or non-structural damage hinders the normal intended functions). After an earthquake event, the building can be in any functional state, depending upon the structural and non-structural damage and utility availability. The functionality state recovery times can be evaluated, and a functionality recovery curve can be generated, which gives the propagation of functional states to full functionality given the investigated time interval. The functionality curve can be utilized to develop resilience using Equation (4-3). The resilience of a reference building determined for the given four scenarios is shown in the following Figure. It is observed that for a hazard scenario with a maximum PGA of 0.08g, the building showed better resilience, but for the rest of the hazard scenarios, it showed poor resilience. In the hazard scenario of 0.64, the building has negligible expected resilience even at 500 days of investigated time interval, showing that the building has collapsed and cannot be repaired.

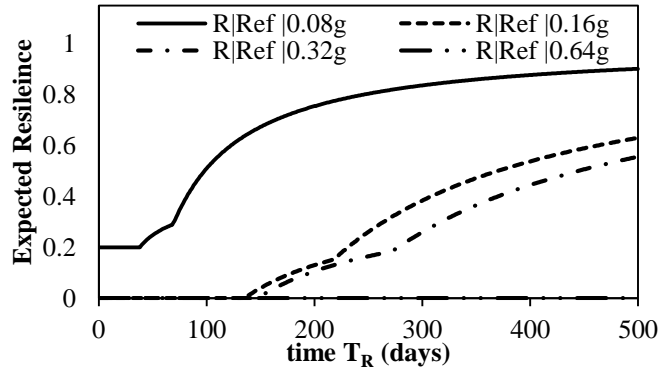


Figure 4-9. Expected resilience of a reference un-retrofitted building under given scenarios

Applying the retrofit reduces the damage, hence improving the functionality curves and seismic resilience. The following Figure shows the functionality curves and the resulting seismic resilience of the reference building along with the retrofit techniques applied. The reference un-retrofitted building at a PGA of 0.32g takes an expected 272.5 days to achieve full functionality, which is reduced to 260.5, 107, and 85.5 days after applying FRP, RCJ, and SJ retrofits. The improvement in seismic resilience in the case of FRP retrofit techniques is negligible, while significant improvement is observed for the RCJ, and SJ retrofit techniques. Since, seismic resilience is a function of collapse fragility, EDPs, fragility functions, and the consequence functions. It is observed that applying RCJ and SJ can effectively reduce the collapse fragility and the demands on EDPs as compared to FRPs. As a result, the seismic resilience for RCJ and SJ is larger compared with the FRP retrofit alternative.

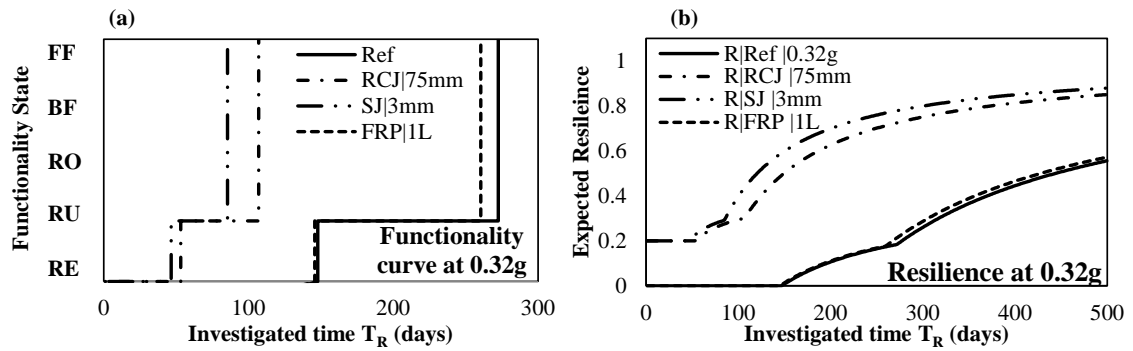


Figure 4-10. Seismic hazard scenario of 0.32g showing (a) functionality curves, and (b) seismic resilience

Table 4-2. Impeding factors for delay and utility disruption curves

Impeding Factors and utility system	Mitigation measures	Damage conditions	median	CoV	
Inspection	BORP Equivalent	-	1 day	0.54	
Engineering Mobilization	Engineer on contract	Minor	2 weeks	0.32	
		Extensive	4 weeks	0.54	
Financing	Pre-arranged credit	-	1 week	0.54	
Contractor Mobilization	GC on contract	Minor	3 weeks	0.66	
		Extensive	7 weeks	0.35	
Permitting	GC on contract	Minor	1 week	0.86	
		Extensive	8 weeks	0.32	
Electricity system	-	-	3 days	1.0	
Water system	RR ≤ 0.2 repairs/Km	-	4 days	0.5	
	RR > 0.2 repairs/Km	-	21 days	1.0	
Natural system	gas	RR ≤ 0.2 repairs/Km	-	10 days	0.5
			RR > 0.2 repairs/Km	42 days	0.6

4.4 Conclusions

This chapter presents a performance-based methodology for evaluating seismic resilience under conventional structural retrofit techniques. The following conclusions can be drawn.

1. Pushover analysis provides important information on a structure's strength, stiffness, and ductility, which can be used for preliminary evaluation of a building and the suitability of the considered retrofit technique. The strength factor determined from the capacity curve for the reference un-retrofitted building was 0.92, indicating non-conformance with the current building codes, and hence, structural modifications are required to improve the performance of a building.
2. Three retrofit techniques, namely, RCJ, SJ and FRPs, were used for improving the performance of a deficient building. Capacity curves for the retrofit buildings showed improved strength factors, hence improving the overall seismic performance of a building. The SJ retrofit technique significantly improved the performance of a building, followed by the RCJ retrofit. The FRPs also improved the performance above the acceptable code performance, but comparatively the performance improvement was not significant.
3. The social, economic, and environmental consequences for the reference and retrofit buildings were assessed in term of casualties, monetary loss in USD, and equivalent carbon emissions. The consequences were reduced significantly

by applying SJ jacketing, followed by the RCJ. In the case of FRP retrofit, the reduction in consequences were not significant.

4. The seismic resilience assessment considers component-level repair time of a building considering sequence of repairs, utility repair times, and impeding delays for the downtime assessment of a building. Five discrete functionality states were considered for developing the functionality repair curve to evaluate seismic resilience. Among the considered retrofit alternatives, SJ and RCJ showed better seismic resilience, while FRPs and the un-retrofitted building showed poor seismic resilience.

CHAPTER 5 PERFORMANCE-BASED DECISION- MAKING OF BUILDINGS UNDER SEISMIC HAZARD

5.1 Introduction

It is of vital importance to incorporate sustainability and resilience in the performance-based decision-making of civil infrastructure under seismic hazards. However, a performance-based engineering framework utilizing a component-level approach, integrating seismic loss, sustainability, and resilience in a multi-criteria decision-making (MCDM) is not yet extensively developed particularly for retrofit selection in a long-term perspective. This chapter introduces a framework utilizing a performance-based approach to couple seismic loss, sustainability, and resilience in the decision-making framework for the selection of different retrofit alternatives. A component-based probabilistic approach is developed for the seismic loss, sustainability, and resilience assessment in a long-term perspective. The resulting social, economic, and environmental consequences are converted to expected annual consequences (EACs) by considering the full range of seismic hazards and are utilized as a multi-criterion in the technique for order preference by similarity to ideal solution (TOPSIS). The proposed long-term performance-based multi-criteria decision-making (PB-MCDM) framework considers five consequences, which include cost, casualties, equivalent carbon emissions, embodied energy, and repair time. Based on the illustrative example, it may be concluded that incorporating seismic sustainability and resilience in the PB-

MCDM approach in a long-term perspective can provide ideal solutions and better decision-making against retrofit alternatives.

5.2 Multi-criteria decision-making framework

The proposed framework consists of four main modules: (1) Performance-assessment module (PAM), (2) Sustainability-assessment module (SAM), (3) Resilience-assessment module (RAM), and (4) Decision-Making module (PB-MCDM) is shown below.

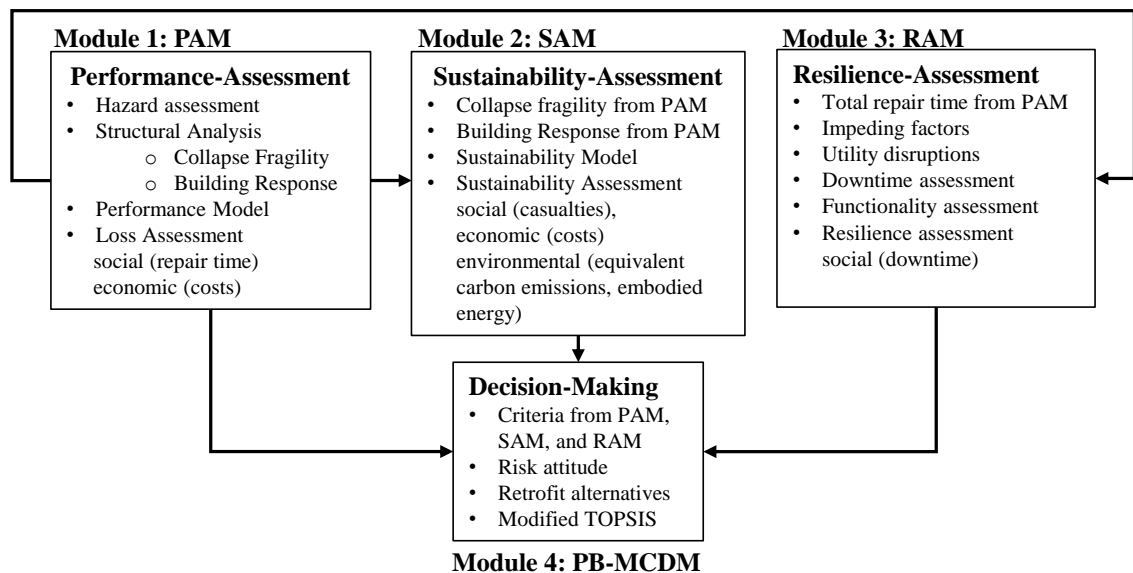


Figure 5-1 Main modules of the proposed framework

5.2.1 Performance-assessment module (PAM)

The performance-assessment module utilizes four stages (i.e., hazard assessment, structural analysis, performance model, and loss assessment) to quantify consequences.

The hazard assessment stage requires developing a hazard model to evaluate intensity

measures (IM), the structural analysis stage requires building a structural model to determine collapse fragility and building response, the performance model stage requires assembling fragility and consequence functions, and the loss assessment stage requires evaluating seismic losses. The horizontal ground shaking effect of an earthquake is directly correlated with the seismic loss and is considered in hazard assessment (Calvi et al., 2006). A structural model is used to predict the building response in terms of Engineering Demand Parameters (EDPs) which are correlated with the structural and non-structural damage (Zheng and Dong, 2019). Uncertainties in the hazard and structural model result in a distribution of EDPs, which can be assumed as lognormally distributed (Hashemi et al., 2019). Regressions can be performed for the analytical representation of the response quantities as a continuous function of IM as follows:

$$u_{EDP|IM} = \alpha_1 (IM)^{\alpha_2} \quad 5-1$$

$$\alpha_{ln(EDP)|IM} = \sum_{i=1}^n \beta_i (IM)^{i-1} \quad 5-2$$

where $u_{EDP|IM}$ is the median value of the response EDP given IM; $\alpha_{ln(EDP)|IM}$ is the lognormal coefficient of variation; and α_1 , α_2 , and β_i are regression constants.

Loss assessment utilizes damage state probabilities and collapse fragility to compute decision variables (e.g., repair time, repair cost). Collapse fragility can be determined from the maximum drift EDPs using a set of earthquake records and limit state function. Limit state function provides maximum drift EDP beyond which collapse occurs, and collapse fragility can be developed through fragility fitting (Baker, 2015). Total probability theorem is used to calculate the total loss in terms of repair time and/or repair cost as follows:

$$l_{LT|IM} = l_{LR|IM,NC} (1 - p_{C|IM}) + l_{LC|C} p_{C|IM} \quad 5-3$$

where $l_{LT|IM}$ is the total loss in terms of cost or time given IM; $l_{LR|IM,NC}$ is the loss in terms of repair cost or time conditioned on non-collapse probability; $l_{LC|C}$ is the loss given probability of collapse; and $p_{C|IM}$ is the probability of collapse of a building given IM.

Collapse loss is calculated by evaluating the replacement value of a building given collapse of a building or irreparability due to excessive residual drifts. Non-collapse loss mathematically presented in Equation (5-4), is calculated using the component-based assessment method.

$$l_{LR|IM,NC} = \sum_{DS} \int_0^{\infty} l_{LR|DS} p_{DS|EDP} f_{EDP|IM} dEDP \quad 5-4$$

where $l_{LR|DS}$ is the random value of a consequence loss function of a component for a specific damage state; $p_{DS|EDP}$ is the probability of damage state given EDP; and $f_{EDP|IM}$ is the probability density function of EDP given IM.

The proposed long-term loss can be determined by summing the losses from individual earthquakes during the investigated time period t_{max} as follows:

$$l_{(LT)LT|t_{max}} = \sum_{k=1}^{N(t_{max})} l_{LT,k|IM} e^{-rT_k} \quad 5-5$$

where $l_{(LT)LT|t_{max}}$ is the total loss for the k th hazard; T_k is the arrival time of the hazard; and r is the financial discount rate used to convert future losses to present. The expected number of earthquakes during the investigated time period can be determined from a

Poisson process $\{N(t_{max}), t_{max} > 0\}$ with $E[N(t_{max})] = \lambda t_{max}$, a widely used occurrence model (Rackwitz 2002; Yeo and Cornell 2009), and the expected long-term loss is determined as follows:

$$E[l_{(LT)L_T|t_{max}}] = \frac{L\lambda}{r} (1 - e^{-rt_{max}}) \quad 5-6$$

where $E[l_{(LT)L_T|t_{max}}]$ is the expected long-term loss; L is the total loss under single hazard and can be determined from Equation (5-3); λ is the frequency of the earthquake given IM determined from hazard curve; and t_{max} is the investigated time interval.

It is important to note that the social losses such as casualties including fatalities and injuries are based on simplified mathematical tools and models, and more advance models in social science field exists and the overall estimation of social losses involve many factors including disparities among communities, socioeconomic status, ethnicity, household income, geographic reasons, and among others. Nonetheless, for the purpose of this framework, simplified social loss models are considered which is in accordance with the state of art in the earthquake engineering field. Also, the consideration of these factors is outside the scope of this work but is worth mentioning that advance social loss models under extreme events exists and could be incorporated to better assess the social losses under extreme events.

5.2.2 Sustainability-assessment module (SAM)

Sustainability is defined in terms of its three pillars (i.e., social, economic, and environmental). The social consequences are evaluated through casualties (i.e., fatalities and/or injuries) arising due to the collapse or extensive damage of a building,

and are determined herein using the time-dependent population model, casualty functions, and population at risk for fatality or injury. The social consequences of an earthquake are mathematically formulated as follows:

$$S_{m|IM} = \phi_C T_{rand} f(p|T_{rand}) p_T p_R p_{C|IM} \quad 5-7$$

where $S_{m|IM}$ is the social metric of seismic sustainability; ϕ_C is the casualty function, which depends on the type of construction and can be determined using historical casualties from the past earthquakes; T_{rand} is the randomly generated time of the day and day of the week for a particular realization; $f(p|T_{rand})$ is the time-dependent population model; p_T is the total population of a building; and p_R is the population at risk depending upon the failure mode of a building.

The environmental consequences (e.g., equivalent carbon emissions, embodied energy) of a building can be determined by defining new consequence functions, correlating environmental consequences with the building damage and collapse fragility. The total environmental consequences can also be computed using Equations (5-3) and (5-4), where l would represent the environmental consequence of an earthquake for seismic sustainability. The long-term seismic sustainability can be evaluated by summing the consequences related to seismic sustainability from individual seismic hazards conditioned on the probability of occurrences during the service life of a building as follows:

$$S_{(LT)L_T|t_{max}} = \sum_{k=1}^{N(t_{max})} S_{ELT,k|IM} \quad 5-8$$

where $S_{ELT,k|IM}$ is the seismic sustainability for the k th hazard. The expected number of earthquakes during the investigated time period can be determined from a Poisson

process as $\{N(t_{max}), t_{max} > 0\}$ with $E[N(t_{max})] = \lambda t_{max}$. The occurrence rate associated with high-intensity events is smaller than low-intensity events. Considering the occurrence rate, the expected long-term seismic sustainability can be formulated as follows:

$$E[S_{(LT)LT|t_{max}}] = S\lambda t_{max} \quad 5-9$$

where $E[S_{(LT)LT|t_{max}}]$ is the expected long-term seismic sustainability and S is the seismic sustainability under a single hazard. The economic metric of sustainability is affected by the discount rate and can be determined using Equation (5-6).

5.2.3 Resilience-assessment module (RAM)

Resilience is the ability to prepare for anticipated hazards, adapt to changing conditions, and withstand and recover rapidly from disruptions (Koliou et al., 2017). Seismic resilience herein refers to the ability of a building to sustain the impact (i.e., robustness), and recover rapidly from seismic hazards. After an earthquake event, it takes time for recovery efforts to bring the building back to full functionality, resulting in additional consequences. Downtime assessment is a critical step in determining the resilience of a building but is considered empirically in the past research. In this module, total recovery time considers both the repair and rebuilding time. The rebuilding time is computed as the product of collapse probability and the total construction time of a building. For the repair time, the sequence of repairs is considered, and the total repair time of a building is determined. REDi methodology (Almufti and Willford, 2013) is then adopted which provides a rational basis to calculate downtime of a building (i.e., total repair time and the additional delays due to impeding factors and utilities). The adopted methodology

is improved, and additional time required for planning and execution of the repair efforts is included through quick assessment impeding and the utility availability curves (Anwar and Dong, 2020). The impeding factors include delays from inspection, financing, engineering and contractor mobilization, and permitting, etc., and utilities may include water, gas, and electricity. Five functionality states are defined in this framework depending upon the structural and non-structural damage, and the availability of utility. Each structural and non-structural damageable component is defined using fragility function, which is assigned to a repair class defining the severity of the damage. The damage severity of structural and non-structural components is determined by quantifying the damage of component using Equation (5-10) and correlating with the repair class (e.g., a building component with n damage states can be in minimum, moderate or maximum repair class category). The repair class refers to the severity of component damage and it could impact the impeding factors. The building functionality state can then be determined considering the utility availability, impeding factors, and total repair time as follows:

$$DS_{Dam} = \frac{\sum_{i=1}^n i \cdot DS_i}{\sum_{i=1}^n DS_i}, \begin{cases} \text{if } DS_{Dam} = i & \text{then "minimum repair class"} \\ \text{if } i < DS_{Dam} < n & \text{then "moderate repair class"} \\ \text{if } DS_{Dam} = n & \text{then "maximum repair class"} \end{cases}$$

5-10

where DS_{Dam} is the average damage state of a component with n damage states; and DS_i is the number of components in damage state i .

$$\tau_{FF} = \max\{f(u_{elc}), f(u_{wtr}), f(u_{gas}), \tau_{RT|IM}\} + \max \begin{cases} f(D_{Ins}) + f(D_{Fin}) \\ f(D_{Ins}) + f(D_{Eng.mob}) + f(D_{perm}) \\ f(D_{Ins}) + f(D_{Con.mod}) + f(D_{LLt}) \end{cases}$$

5-11

$$\tau_{BF} = \max\{f(u_{elc}), f(u_{wtr}), \tau_{RT|IM}\} + \max \begin{cases} f(D_{Ins}) + f(D_{Fin}) \\ f(D_{Ins}) + f(D_{Eng.mob}) + f(D_{perm}) \\ f(D_{Ins}) + f(D_{Con.mod}) + f(D_{LLt}) \end{cases} \quad 5-12$$

$$\tau_{RO} = \begin{cases} \text{IF } \tau_{RT|IM} > 0 \\ \max \begin{cases} f(D_{Ins}) + f(D_{Fin}) \\ f(D_{Ins}) + f(D_{Eng.mob}) + f(D_{perm}) \\ f(D_{Ins}) + f(D_{Con.mod}) + f(D_{LLt}) \\ \text{ELSE } 0 \end{cases} + \tau_{RT|IM} \end{cases} \quad 5-13$$

$$\tau_{RU} = \begin{cases} \text{IF } \tau_{TH|Ext.Dam} \geq \tau_{SRT|IM} \geq 0 \\ \max \begin{cases} f(D_{Ins}) + f(D_{Fin}) \\ f(D_{Ins}) + f(D_{Eng.mob}) + f(D_{perm}) \\ f(D_{Ins}) + f(D_{Con.mod}) + f(D_{LLt}) \\ \text{ELSE } 0 \end{cases} + \tau_{SRT|IM} \end{cases} \quad 5-14$$

$$\tau_{RE} = \begin{cases} \text{IF } \tau_{SRT|IM} \geq \tau_{TH|Ext.Dam} \\ \max \begin{cases} f(D_{Ins}) + f(D_{Fin}) \\ f(D_{Ins}) + f(D_{Eng.mob}) + f(D_{perm}) \\ f(D_{Ins}) + f(D_{Con.mod}) + f(D_{LLt}) \\ \text{ELSE } 0 \end{cases} + \tau_{SRT|IM} \end{cases} \quad 5-15$$

where τ is the relevant downtime to achieve given functional state (definitions of functional states are presented in Table 5-1); $f(u_{elc})$, $f(u_{wtr})$, and $f(u_{gas})$ are probabilistic repair times functions for electricity, water, and gas utilities, illustratively presented in the following Figure; $f(D_{Ins})$, $f(D_{Fin})$, and $f(D_{LLt})$ are probabilistic repair time functions for inspection, financing and long lead times; $f(D_{Eng.mob})$, $f(D_{Con.mod})$, and $f(D_{perm})$ are probabilistic repair times functions for engineering mobilization, contractor mobilization, and permitting; $\tau_{RT|IM}$ is the total repair time of a building determined from Equations (5-3) and (5-4), and adjusted for the sequence of repairs; $\tau_{SRT|IM}$ is the total structural repair time of a building; and $\tau_{TH|Ext.Dam}$ is the threshold repair time against extensive damage determined from Equations (5-3) and (5-4) and Equation (5-10). Functionality curve represents the

propagation of functionality state after an earthquake to its pre-earthquake state. A typical functionality curve representing five functionality states and the median recovery time to the pre-hazard state after an earthquake event, along with the median repair times for impeding delays, building repairs, and utility availability is also presented.

To illustrate this, consider a simple case of an earthquake event where 10 damageable columns in each story of a building are in damage state i . The story with the highest average damage has 2,5,3 columns in damage states 1, 2, and 3. The average damage state of that story calculated using Equation (5-10), is 2.1 indicating a moderate repair class, and therefore relevant impeding curves can be selected. Assuming inspection, financing, and permitting would take 1, 4, and 5 days, and engineering mobilization, contractor mobilization, and long lead times would take 4, 4, and 10 days. Electricity, water, and gas utilities will be restored at 5, 20, and 40 days. The repair times for all damageable components is determined from Equations (5-3) and (5-4) and considering repair schedule, the total repair time of a building is 30 days. The full functionality will be achieved at 55 days and the baseline functionality will be achieved at 45 days after an earthquake which is determined as:

$$DS_{Dam} = \frac{(1 \times 2) + (2 \times 5) + (3 \times 3)}{10} = 2.1 \quad \left\{ \begin{array}{l} \text{since } i < DS_{Dam} < n \\ \text{then "moderate repair class"} \end{array} \right.$$

$$\tau_{FF} = \max\{5, 20, 40, 30\} + \max \begin{cases} 1 + 4 \\ 1 + 4 + 5 \\ 1 + 4 + 10 \end{cases} = 40 + 15 = 55 \text{ days}$$

$$\tau_{BF} = \max\{5, 20, 30\} + \max \begin{cases} 1 + 4 \\ 1 + 4 + 5 \\ 1 + 4 + 10 \end{cases} = 30 + 15 = 45 \text{ days}$$

Table 5-1. Functionality states definition considering structural, non-structural damage, and utility availability

Functionality States			Structural Damage	Non-Structural Damage	Utility Availability
5	FF	Full Functionality	No damage or Repaired	No damage or Repaired	All available (e.g., water, electricity, gas)
4	BF	Baseline Functionality	No damage or Repaired	No damage or Repaired	Critical ones (e.g., water and electricity)
3	RO	Re-Occupancy	No damage or Repaired	No damage or Repaired	No
2	RU	Restricted Use	No damage or Repaired	Damaged or under-repair	No
1	RE	Restricted Entry	Damaged or under-repair	Damaged or under-repair	No

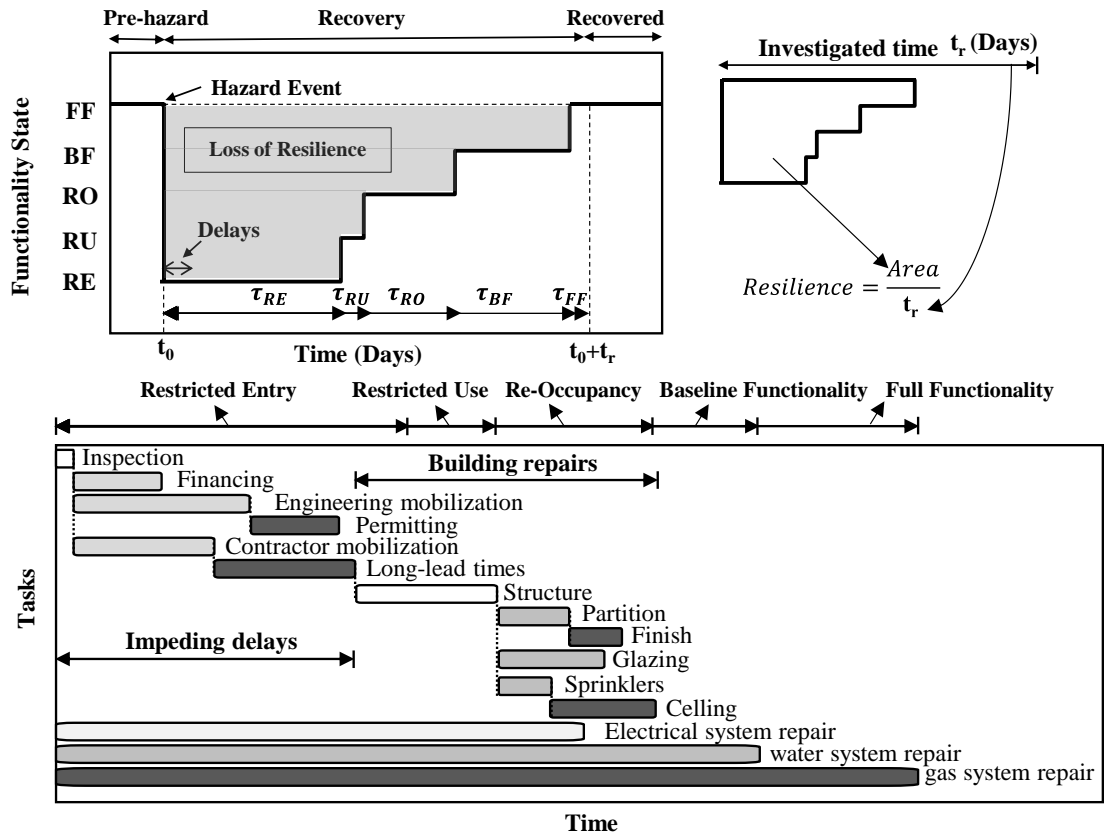


Figure 5-2 Illustration of building restoration after an earthquake event

5.3 Performance-based decision-making

The proposed PB-MCDM utilizes performance-based engineering and TOPSIS for decision-making. The consequences developed in the seismic loss, sustainability, and resilience modules are converted into attributes in criteria evaluation and the retrofit options are ranked based on the decision-making method. The steps are explained in the subsequent sections.

5.3.1 Criteria evaluation

TOPSIS is a multi-criteria decision-making method, which requires multiple criteria to be ranked based on the closeness to the ideal solution. In this methodology, the proposed modules are used to assess social, economic, and environmental consequences. The multi-criteria are the consequences determined in the previous modules. To incorporate the entire range of hazard scenarios in decision-making, the consequences are translated to EACs for seismic loss, sustainability, and resilience. The EAC provides a single value of consequence by considering all hazard scenarios with the probability of occurrence. The mathematical formulation of EAC is computed by integrating consequence and hazard curve (Krawinkler et al., 2006; Cardone et al., 2017) as follows:

$$EAC = \int_0^{\infty} C_{T|IM} \left| \frac{\partial \lambda_{IM}}{\partial IM} \right| dIM \quad 5-16$$

where $C_{T|IM}$ is the expected value of total consequence given IM and λ_{IM} is the mean annual frequency of exceedance of a given IM determined from the hazard curve.

The computation of EACs requires a hazard curve and a consequence curve. The hazard curve gives the mean annual frequency of exceedance of IM, and consequence curves give social, economic, or environmental consequences for a given IM, and can be determined using Equations (5-3) and (5-7). For the long-term consequences refer to Equations (5-6) and (5-9). In general, a closed-form solution to the integral Equation (5-16) cannot be determined, and therefore a numerical integration approach is utilized (Eads et al., 2013). The slope of the hazard curve can be determined using the numerical approach, IM time step can be selected, and the

integration of slope of hazard curve and consequence curves is achieved for each time step, and EAC can be determined as illustrated below.

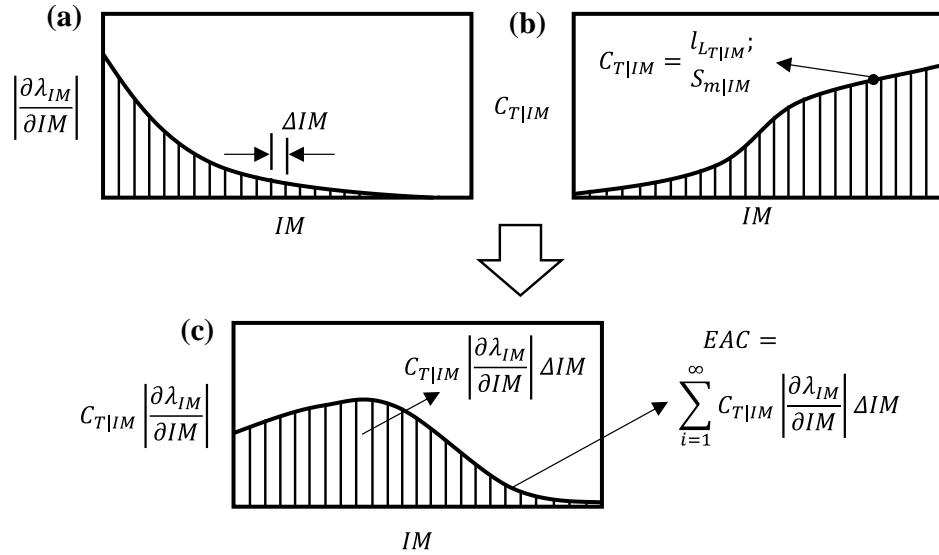


Figure 5-3 Illustration for computing EAC: (a) Derivative of hazard curve, (b) consequence curve, and (c) integration of slope of hazard and consequences given IM

5.3.2 TOPSIS

Seismic loss, sustainability, and resilience are characterized into attributes, which include cost attribute from seismic loss, casualties, equivalent carbon emission, embodied energy attribute from seismic sustainability, and repair time attribute from resilience assessment. The formulated weighted normalized decision matrix for attributes in terms of EACs and retrofit options in terms of alternatives is calculated by:

$$v_{ab} = \frac{w_a x_{ab}}{\sqrt{\sum_{b=1}^m x_{ab}^2}} \quad \text{where } b = 1, \dots, m; a = 1, \dots, n \quad 5-17$$

where v_{ab} is an element of matrix normalized to the weights referred to as normalized decision matrix; w_a is the weights for an attribute a ; and x_{ab} is an element of a matrix showing EAC of attributes for retrofit alternatives b .

The least ideal and the most ideal solutions are computed using Equations (5-19) and (5-20) referred herein as the most acceptable solution v^* , and least acceptable solution v^- .

$$v^* = \{v_1^*, \dots, v_n^*\} = \{(\max_b v_{ab} | a \in I'), (\min_b v_{ab} | a \in I'')\} \quad 5-18$$

$$v^- = \{v_1^-, \dots, v_n^-\} = \{(\min_b v_{ab} | a \in I'), (\max_b v_{ab} | a \in I'')\} \quad 5-19$$

where I' and I'' are positive and negative attributes, respectively. The measured five attributes are considered as negative attributes since it is favorable to reducing cost, casualties, emissions, and repair time of a building. The ideal and the negative-ideal solutions for each attribute are used to calculate the Euclidean distances referred to as the separation measures from an ideal solution D_b^* and the separation measure from the non-ideal solution D_b^- calculated by:

$$D_b^* = \sqrt{\sum_{a=1}^n (v_{ab} - v_a^*)^2} \text{ where } b = 1, \dots, m; a = 1, \dots, n \quad 5-20$$

$$D_b^- = \sqrt{\sum_{a=1}^n (v_{ab} - v_a^-)^2} \text{ where } b = 1, \dots, m; a = 1, \dots, n \quad 5-21$$

Finally, to determine the relative closeness to the ideal solution and ranking of the retrofit alternatives from best to worse, Equation (5-22) is used as follows:

$$p_b = \frac{D_b^-}{(D_b^* + D_b^-)} \text{ where } b = 1, \dots, m; 0 < p_b < 1.0 \quad 5-22$$

The conventional TOPSIS method is normalized, resulting in a narrow gap between performance measures, which may lead to a loss in information. Additionally, different stakeholders may have different risk attitudes in decision-making. To solve the narrow gap problem for the performance measures and to add risk-attitude in the TOPSIS, the normalized decision matrix is modified as follows:

$$v_{ab} = 1 - \left[\frac{(v^* + D_2) - x_{ab}}{(v^* + D_2) - (v^- - D_1)} \right]^{Ra} \quad \text{where } b = 1, \dots, m; a = 1, \dots, n \quad 5-23$$

where D_1 and D_2 are values to achieve a wider gap in the performance measures ; v_{ab} is an element of a normalized matrix; x_{ab} is an element of a matrix showing EAC of attributes for retrofit alternatives b ; and Ra can be interpreted as a reflecting risk attitude.

5.4 Illustrative example

The proposed framework consisting of four modules (i.e., performance assessment, sustainability assessment, resilience assessment, and PB-MCDM) is illustrated on a reinforced-concrete residential building. The reference building and the retrofit alternatives are designed for illustration of the proposed framework. The designed building is an intermediate four-story moment resisting frame structure with three bays in the x-direction and five bays in the y-direction, the width of the bay is 4 m and typical story height is 3.5 m. The gravity loads considered in the design of a building include self-weight of a building, super-imposed dead load of 4.0 kN/m², and live load of 2.0 kN/m² for the slabs. The concrete strength of 24 MPa and a steel strength of 240 MPa is considered in the strength design of structural components. The structural design of a building is based on the ACI-318 (2011) code of practice, and the seismic design is

based on the IBC (2012). The design level earthquake of 0.398g is considered for the lateral design of a building, extracted from the hazard curve. The fragility and consequence functions for residential building type are extracted from previous studies (Mitrani-Reiser, 2007; FEMA-P-58, 2012; Hashemi et al., 2019). For instance, Hashemi et al. (2019) provided the relevant fragility functions for both structural and non-structural components of a reinforced concrete building, and FEMA-P-58 (2012) provided an extensive database for fragility and consequence functions along with spreadsheets which is used to extract structural and nonstructural components, the quantities and the relevant fragility and consequence functions. FEMA 547 (2006) discussed various retrofitting techniques for global strength and stiffness deficiencies with focus on vertical members to improve lateral stability. Three retrofit methods are designed and implemented following the FEMA 547 (2006) and ASCE (2013) recommendations. The building layout and structural details are shown below.

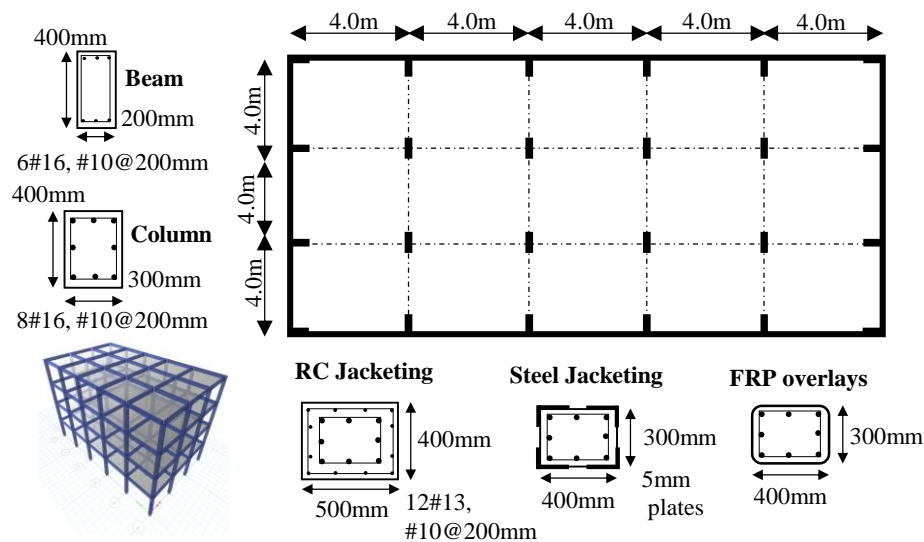


Figure 5-4 Building model and layout of 4-story building

5.4.1 Performance and sustainability assessment module

The first step of the PAM module is hazard assessment. PGAs (Peak Ground Accelerations) at FLE (Frequent Level Earthquake), DLE (Design Level Earthquake), and MCE (Maximum Considered Earthquake) scenarios are extracted from the hazard curve (i.e., 0.137g, 0.398g, and 0.778g, respectively). Building performance model developed in PAM consists of fragility functions, consequence functions, and population model. The population model shows the variation of percentage of population present during the time of a day and day of a week. Random time of the day and day of the week is determined using a stochastic process and is utilized in each realization for the casualty assessment. Fragility functions relate the EDPs with the probability of damage state, and consequence functions translate those probabilities to repair loss and repair time for each component. Table 5-2 shows the fragility and consequence functions for structural and non-structural components. Structural members are drift-sensitive structural components; ceiling and sprinklers are acceleration-sensitive non-structural components (i.e., the damage in these components is triggered due to floor accelerations); and the remaining non-structural components are drift-sensitive. The total cost and total time are inclusive of repair cost and repair times determined from damage assessment, and the replacement time and replacement cost from the probability of collapse. The replacement cost (i.e., the total cost required to replace the structure in case of collapse) is estimated to be 2 million USD, and the total replacement time (i.e., the total time required to replace the structure in case of collapse) is estimated to be 280 days. The replacement cost and time are estimated from the quantity estimation tools provided in FEMA-P-58 (2012), and from the relevant studies (Asadi et al., 2019; Hashemi et al., 2019), adjusted for inflation.

Table 5-2. Fragility and consequence functions of damageable components

Component	Quantity per floor	Damage state	Fragility functions		Consequence functions			
					Repair cost (USD)		Repair time (Days)	
			Median	CoV	Median	CoV	Median	CoV
Structural members	21 units	DS ₁	1.75	0.40	6270	0.39	18.9	0.46
		DS ₂	2.25	0.40	9540	0.32	28.7	0.40
		DS ₃	3.22	0.40	11580	0.30	35.3	0.39
Partition	6 m ² x 50	DS ₁	0.39	0.17	115	0.20	0.136	0.30
		DS ₂	0.85	0.23	679	0.10	0.797	0.30
Finish	6 m ² x 100	DS ₁	0.39	0.17	115	0.20	0.135	0.51
		DS ₂	0.85	0.23	321	0.10	0.376	0.61
Glazing	2.8 m ² x 12.85	DS ₁	4.00	0.36	564	0.17	0.582	0.29
		DS ₂	4.60	0.36	564	0.17	0.582	0.40
Ceiling	232 m ² x 0.5	DS ₁	0.35	0.40	4541	0.40	5.699	0.63
		DS ₂	0.55	0.40	37612	0.50	47.05	0.40
		DS ₃	0.80	0.40	70769	0.55	88.40	0.40
Sprinklers	4 m x 20	DS ₁	0.32	1.40	1154	0.37	1.227	0.80

A set of 20 far-field earthquake records are utilized for the collapse fragility assessment. The vertical structural elements are retrofitted with reinforced concrete (RCJ), steel jacketing (SJ) and fiber-reinforced polymer (FRP) overlays to improve lateral stability. In RCJ, all the columns are retrofitted with the 75 mm reinforced concrete jacket, a steel jacket of 3 mm thickness is used for SJ, and fiber-reinforced

polymer overlays with a thickness of 0.33 mm were used for FRP retrofit. The number of collapses per twenty simulations is recorded given IM with increasing intensity. A lognormal distribution is fitted using maximum likelihood function (Baker, 2015) and collapse fragilities are developed for reference building and retrofit options. The reference building ($C|Ref$) and the retrofit with Fiber-Reinforced Polymer ($C|FRP$) have considerably higher probability of collapse as compared to Reinforced-Concrete Jacketing ($C|RCJ$) and Steel-Jacketing retrofit ($C|SJ$), nonetheless it is observed that, the probability of collapse is reduced using retrofit. Seismic loss assessment is performed to determine social and economic consequences. Following Figure shows social and economic loss curves for a reference building developed using Equations (5-3) and (5-4) and Equation (5-7).

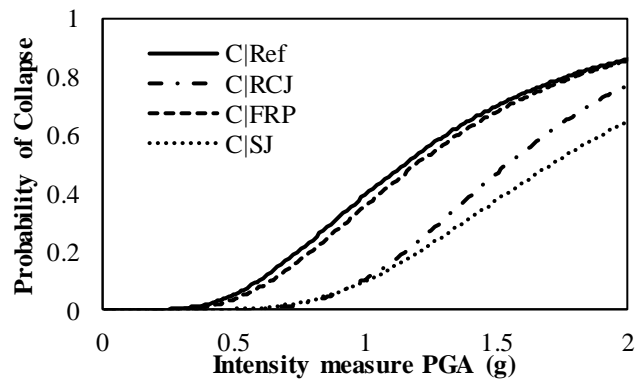


Figure 5-5 Collapse fragility curves for building with retrofit options

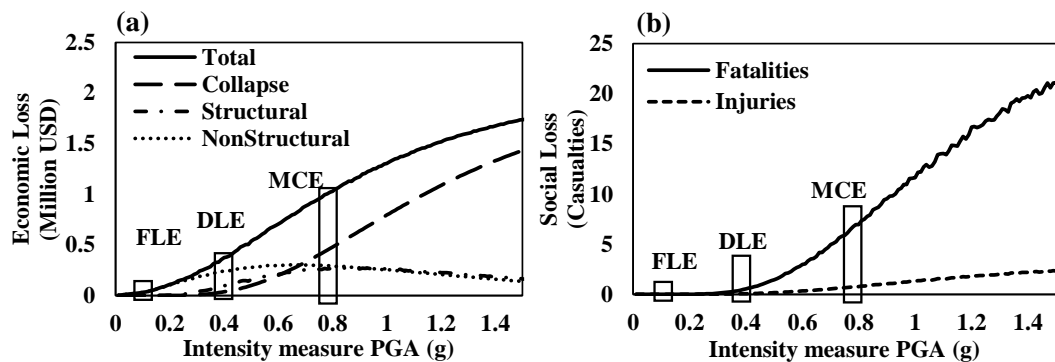


Figure 5-6 Expectation of probabilistic loss curves: (a) Economic and (b) social

It is observed that the repair losses increase with increasing IM levels up to 0.65g, and then start decreasing, while collapse losses continue to increase with increasing IM. However, it is important to note that, the total economic losses increase with the increasing IM levels. The expected total economic losses determined from the economic loss curves are 0.054, 0.375, and 1.03 million USD, for the considered three scenarios (i.e., FLE, DLE, and MCE). As shown, the economic losses are dominated by structural and nonstructural damage at low IM levels due to the high probability of non-collapse, while at high IM levels the economic losses are dominated by collapse losses due to high probability of collapse. The casualties are conditioned on the probability of collapse; therefore, an increasing trend is observed for social consequences with increasing IM. The mean annual frequency of earthquake hazard (λ) for the three scenarios, determined from the hazard curve is 0.0139, 0.0021, and 0.0004. The inflation rate is assumed as 3% yearly and the expected long-term economic and social loss is determined using Equations (5-6) to (5-9), for the investigated period.

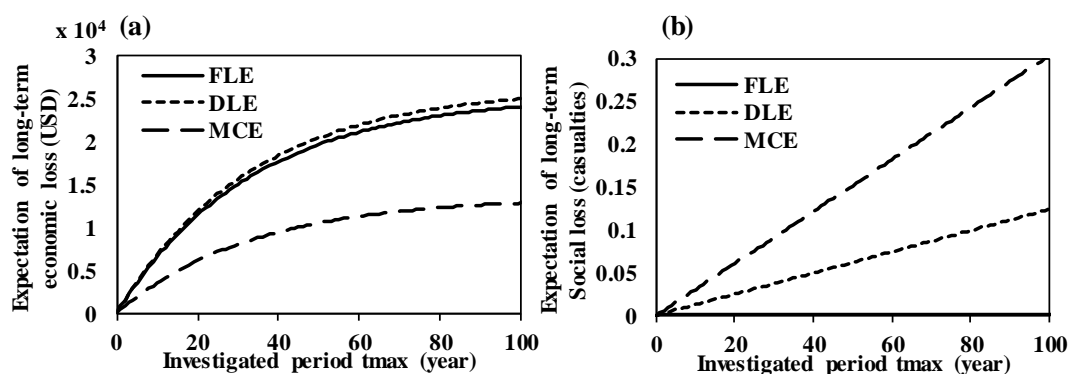


Figure 5-7 Long-term loss under investigated time interval: (a) Economic and (b) Social

In the 50-year service life of a building, the expected long-term economic loss for the three scenarios is 1.969×10^4 , 2.045×10^4 , and 1.050×10^4 USD, and it increases with the increasing service life of a structure. On the contrary, the DLE scenario experiences higher long-term economic losses as compared to FLE and MCE scenarios, indicating that the DLE scenario is likely to cause higher accumulative economic loss during the service life of a structure. The long-term consequences are a function of the probability of occurrence, intensity, and consequences of an event. In the considered example, the long-term economic consequences are highest for the DLE event, and long-term social consequences are highest for the MCE event. The following Figure shows the long-term economic and social loss curves given IM for three different service lives of a structure. The reduced long-term economic losses in the MCE scenario are due to the low probability of occurrence of a seismic event at high IM levels. The long-term social losses increase with increasing IM with the highest social loss at 0.77g, and it decreases afterward because the probability of occurrence starts to decrease significantly. It is interesting to note that, high long-term economic losses are observed at low IM values, while for long-term social loss, the IM levels are closer to the MCE scenario. The social losses are conditioned only on the collapse case, while economic losses are conditioned on both collapse and non-collapse cases. At low IM levels, the economic consequences are more sensitive to structural and non-structural damage due to the high probability of non-collapse. The sensitivity to damage at low IM levels can also be observed in similar research (Ramirez et al., 2012; Hashemi et al., 2019).

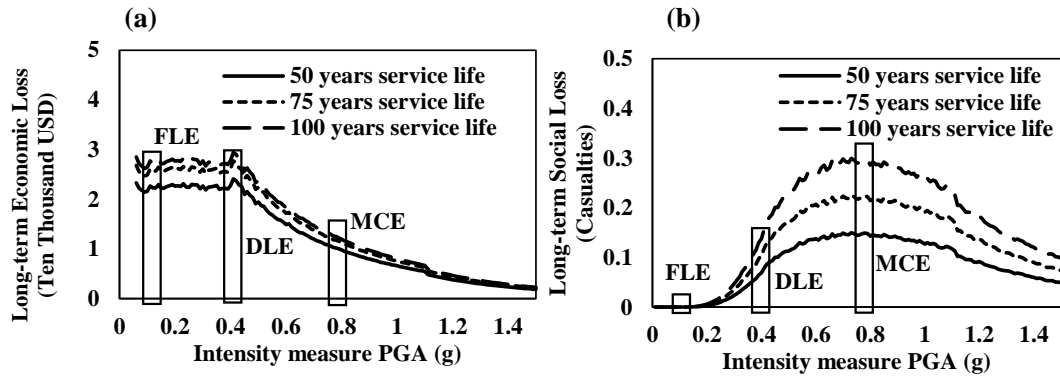


Figure 5-8 Long-term loss curves: (a) Economic and (b) Social

The parameters used in the seismic sustainability model are shown in Table 5-3. Social loss curves for casualties and environmental loss curves for total embodied energy are shown below. It is observed that increasing the service life of a structure results in a higher long-term environmental loss, and the MCE scenario has the highest, while the DLE scenario has the lowest long-term environmental loss. A similar trend is observed for the environmental consequence (i.e., at low IM levels consequences are sensitive to damage, and at high IM levels the consequences are more sensitive to collapse).

Table 5-3. Environmental consequence functions of damageable components

Components	Damage state	Environmental consequence functions			
		Carbon emission (kgCO ₂)		Embodied energy (MJ)	
		Median	CoV	Median	CoV
Structural members	DS ₁	1.794	0.4	16.00	0.4
	DS ₂	1.794	0.4	432.0	0.4
	DS ₃	19.73	0.4	500.0	0.4
Partition	DS ₁	12.72	0.4	226.0	0.4

	DS ₂	25.52	0.4	453.0	0.4
Finish	DS ₁	1.336	0.4	25.29	0.4
	DS ₂	2.686	0.4	50.84	0.4
Glazing	DS ₁	96.30	0.4	1679	0.4
	DS ₂	183.2	0.4	3314	0.4
Ceiling	DS ₁	1.023	0.4	17.53	0.4
	DS ₂	5.846	0.4	104.9	0.4
	DS ₃	19.73	0.4	349.9	0.4
Sprinklers	DS ₁	58.07	0.4	839.3	0.4

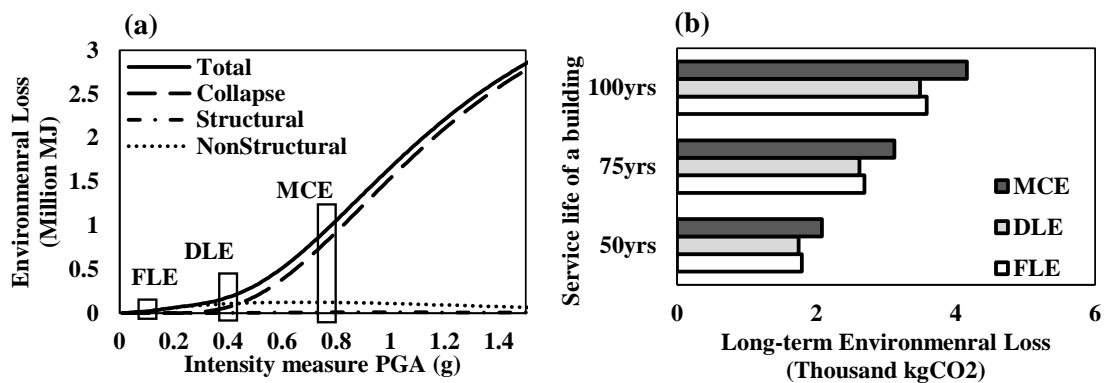


Figure 5-9 Environmental loss: (a) Total embodied energy and (b) long-term equivalent carbon emissions

5.4.2 Resilience assessment module

In the structural and non-structural repair assessment, three sequences of repairs are considered in a repair schedule shown below (i.e., (1) structural repair, partition and then finishes, (2) structural repair and then glazing, and (3) structural repair, sprinklers and then ceilings), and the maximum repair time is determined using CPM. The

structural components are repaired serially, while non-structural components are repaired in parallel. Three sequences of impeding factors are also considered.

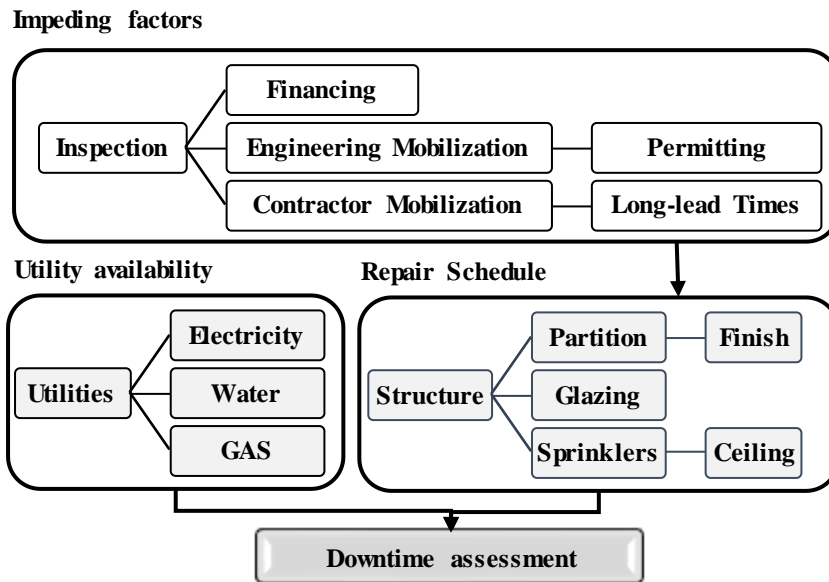


Figure 5-10 Downtime assessment flowchart

The repair time of all the components at each story is determined using Equations (5-3) and (5-4) and the maximum repair time can be calculated using critical path analysis as follows:

$$\tau_{RT} = \max \begin{cases} \tau_{Str} + \tau_{Par} + \tau_{Fin} \\ \tau_{Str} + \tau_{Glz} \\ \tau_{Str} + \tau_{Spr} + \tau_{Cel} \end{cases} \quad 5-24$$

where τ_{Str} is the structural repair time; τ_{Par} is the repair time of the partition component; τ_{Fin} is the repair time of finishes; τ_{Glz} is the repair time of the glazing component; τ_{Spr} is the repair time of sprinklers; and τ_{Cel} is the repair time of the ceiling component.

In the considered example, the path with the longest repair time is the critical path of a building under given IM. The CPM is repeated for all the IM levels and repair time loss curves are developed. Lognormal distribution curves are utilized for incorporating impeding factors and utility availability, synthesized from the REDi (Almufti and Willford, 2013) as shown in Table 5-4.

Table 5-4. Impeding factors for delay and utility disruption curves

Impeding Factors and utility system	Mitigation measures	Other conditions	Median	CoV	
Inspection	BORP Equivalent	-	1 day	0.54	
Engineering Mobilization	Engineer on contract	Minor damage	2 weeks	0.32	
		Extensive damage	4 weeks	0.54	
Financing	Pre-arranged credit	-	1 week	0.54	
Contractor Mobilization	GC on contract	Minor damage	3 weeks	0.66	
		Extensive damage	7 weeks	0.35	
Permitting	GC on contract	Minor damage	1 week	0.86	
		Extensive damage	8 weeks	0.32	
Electricity system	-	-	3 days	1.0	
Water system	RR ≤ 0.2 repairs/Km	-	4 days	0.5	
	RR > 0.2 repairs/Km	-	21 days	1.0	
Natural system	gas	RR ≤ 0.2 repairs/Km	-	10 days	0.5
			RR > 0.2 repairs/Km	42 days	0.6

The impeding factors, utility availability curves, and structural and non-structural damage conditions are mapped against different functional states and the amount of time spent in each functional state is used to model building restoration after an earthquake event. The other conditions in Table 5-4, indicating minor and extensive damage would result in different engineering mobilization, contractor mobilization, and permitting delay times for minor and extensive damage states of a building. The time required to achieve different functional states is determined from Equations (5-11) to (5-15), and the functionality recovery curve can be determined for a given hazard scenario. The resulting functionality recovery sequence for the three scenarios with and without impeding factors and utility availability is shown below.

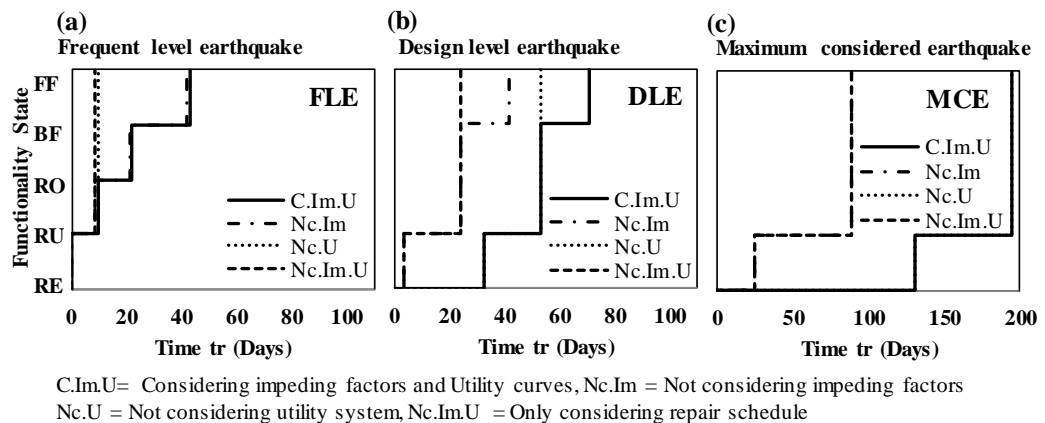


Figure 5-11 Functionality states repair sequence at (a) FLE, (b) DLE, and (c) MCE

In this illustrative example, it is observed that considering impeding factors and utility availability results in a longer time period to achieve full functionality. The availability of utility has a larger impact on determining resilience at the FLE scenario, while impeding factors have a larger impact on resilience for the MCE scenario, and considering utility system has no impact on resilience and recovery profile for the MCE scenario. The expected resilience for the FLE, DLE, and MCE scenarios and the effect

of utility availability and impeding factors are shown in the following Figure. The FLE and DLE scenarios perform better in terms of time to recovery as compared to the MCE. It is observed that for the DLE scenario, utilities have a negligible impact on the seismic resilience of a reference building, while not-considering impeding factors would affect the seismic resilience. The expected resilience for the investigated time interval of 200 days is 0.930, 0.789, and 0.285, and the expected long-term resilience for the building with 50-year service life, for three scenarios is 0.645, 0.083, and 0.0058, respectively.

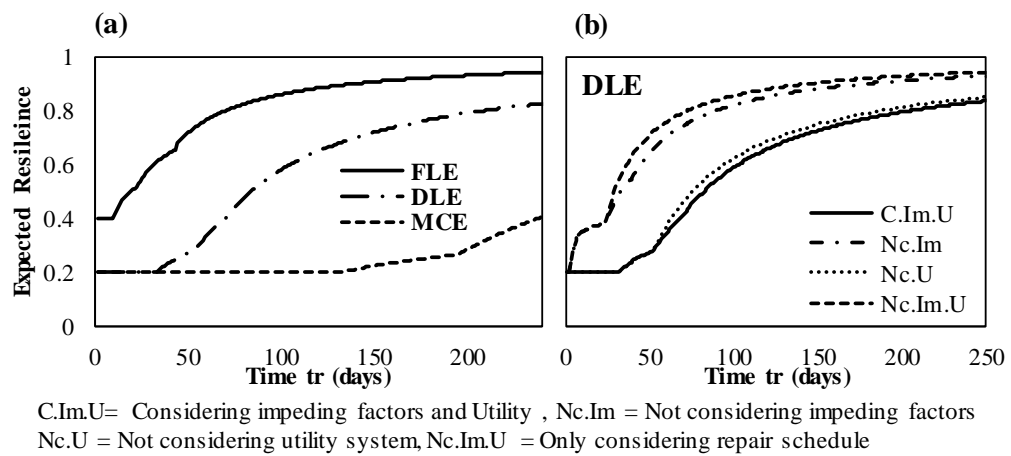


Figure 5-12 Expected resilience for (a) FLE, DLE, and MCE scenarios under different investigated time intervals and (b) DLE scenario with and without utility system and impeding factors

5.4.3 Performance-based decision-making module (PB-MCDM)

TOPSIS used in the PB-MCDM utilizes five criteria from seismic loss, sustainability, and resilience, for retrofit selection. The EACs are determined for each criterion for all retrofit options. The ease of applicability of the selected retrofit option is also considered in TOPSIS, with FRPs being the most practical solution as it causes the least

disruption during its application and has good compatibility with the retrofitted structural member. RCJ also has good compatibility, but it causes lots of disruption, since it requires removing concrete cover, exposing reinforcing steel, drilling, applying new steel cage and concreting, etc. Steel jacketing also causes a significant amount of disruption and is relatively incompatible with the reinforced concrete structural members.

The developed decision-making framework is effectively applied to utilize EACs to prioritize the considered retrofit alternatives. The resulting relative closeness coefficient for retrofit alternatives using the conventional TOPSIS method is shown in the following Figure. FRP retrofit has the highest closeness coefficient and is considered the best retrofit option among considered alternatives, RCJ has a slightly lower closeness coefficient and is the second preferable choice, while steel jacketing is the least acceptable solution among the selected retrofit alternatives. Considering long-term consequences results in different closeness coefficients, in which RCJ is considered the most acceptable solution and the SJ is considered as the least acceptable solution. It is noted that RCJ has the lowest social impact with the least number of casualties. Environmental impact is lower as well as compared to the FRP jacketing but economically FRPs perform better as compared to RCJ and SJ. The repair times for FRPs are also lowest, showing faster recovery and better performance in terms of resilience. In this example, equal weighting factors are assigned to all five criteria, but the presented framework can be utilized for cases where different weighting factors are required.

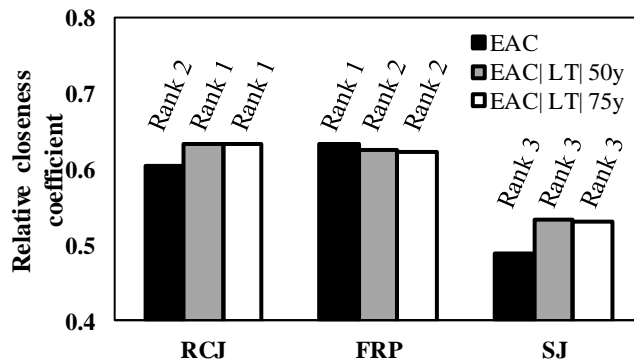


Figure 5-13 Relative closeness coefficient ranking retrofit alternatives based on PB-MCDM linking loss, sustainability, and resilience

From the long-term perspective, the RCJ has the lowest social and environmental loss, while FRPs have the lowest economic loss and downtime. The following Figure shows long-term EAC against 50 years of building service life under different risk attitudes of the decision-maker. The factor $Ra = 1$ is used for risk-neutral, $Ra = 0.5$ for the risk-averse, and $Ra = 2$ is used for the risk-seeking attitude.

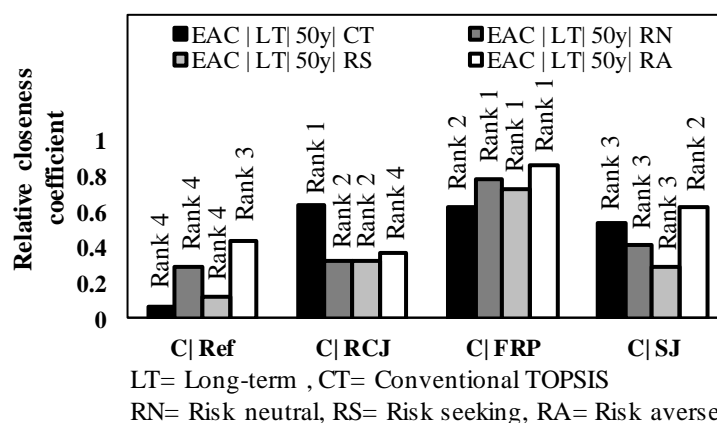


Figure 5-14 Relative closeness coefficient ranking retrofit alternatives against risk attitude of decision-makers

It is observed that, for a building with a service life of 50 years and considering long-term consequences, RCJ is ranked the best choice under conventional TOPSIS. Adopting modified TOPSIS with a wider gap among performance measures and incorporating risk attitude results in different relative closeness coefficients. RCJ ranked second best choice after FRPs, considering the neutral and risk-seeking attitude of the decision-makers, and the least acceptable choice while considering the risk-averse attitude of a decision-maker. Some building owners or stakeholders might give more importance to the social consequences, or environmental consequences, which might also change the outcome of the relative closeness coefficient. Hence it is worth noting that the framework is sensitive to the selection of weighting factors, investigated period, and risk attitudes, which can be inherently subjective. Nonetheless, the weighting factors, investigated period and the risk-attitude can be determined through the judgement of the stakeholders and professionals, through empirical evidence, and/or by conducting surveys.

The framework can then be utilized for the decision-making by considering all the relevant scenarios for the considered options and making decisions probabilistically. Table 5-5 shows rankings of retrofit options with number 1 being the most acceptable solution and 4 being the least acceptable solution, against conventional TOPSIS, modified TOPSIS, three different risk-attitudes, and long-term under service life of 50 years and 75 years. 50 years and 75 years' service life of a building is considered as the most likely scenarios for residential buildings, and considering the given twelve scenarios, the probability of RCJ being the most ideal solution is 66.67%. FRPs have an equal likeliness of 33.33% at being the first, second, and third most ideal solution. The probability of SJ being in the third rank is 66.67% and the reference

building is ranked the least ideal solution with a probability of 83.33%. The proposed framework can therefore be utilized to prioritize the retrofit alternatives considering possible scenarios under conflicting and disproportionate criteria.

Table 5-5. Rankings of retrofit alternatives against given scenarios

Scenario	not considering long-term				Long-term 50 years				Long-term 75 years			
	CT	RN	RS	RA	CT	RN	RS	RA	CT	RN	RS	RA
No-retrofit	4	4	4	4	4	4	4	3	4	4	4	3
RC jacket	2	2	1	1	1	3	2	4	1	3	2	4
FRP jacket	1	1	2	2	2	1	1	1	2	1	1	1
Steel jacket	3	3	3	3	3	2	3	2	3	2	3	2

CT = Conventional TOPSIS, RN = Risk neutral, RS= Risk seeking, RA=Risk averse

5.5 Conclusions

This chapter presents a performance-based multi-criteria decision-making framework considering seismic loss, sustainability, and resilience from a long-term perspective.

The following conclusions can be drawn:

1. The proposed PB-MCDM framework can be utilized to rank alternatives by evaluating social, economic, and environmental consequences based on the seismic risk, resilience, and sustainability which are important performance indicators for investigating the performance of buildings under hazard. The methodology can be developed for other structural systems, retrofit, and hazard types, and additional consequences can be added for the decision-making.

2. In the illustrative example, SJ retrofit showed the lowest probability of collapse, followed by RCJ, while FRPs showed a slightly lower probability of collapse compared to the reference building, nonetheless, all the retrofit options provide a lower probability of collapse. It is also observed that collapse fragility is responsible for the consequences at higher IM levels, while social, economic, and environmental consequences at low IM levels depend on the non-collapse case.
3. The modified REDi methodology provided a better estimation of the functionality state and the progression to full functionality. In the illustrative example, the investigated building under FLE and DLE scenarios is associated with better expected long-term resilience, while with relatively poor resilience under the MCE scenario.
4. The seismic resilience of a building was evaluated through component-level repair time assessment, considering the sequence of repairs, incorporating impeding delays and availability of utilities. The various parameters associated with impeding and utilities, affecting the downtime of a building were considered through lognormal cumulative functions providing better downtime estimation of each functional state.
5. TOPSIS was used to rank retrofit alternatives under conflicting and disproportionate criteria. Twelve relevant scenarios for the reference building considering risk attitude, and with and without long-term consequences were studied and RCJ was found the best alternative with the probability of 66.67% of being the ideal solution.
6. Not considering long-term consequences results in FRP being the best retrofit option with ease of applicability, low cost of repair, better recovery time, and

the overall resilience. RCJ was found to be the second-best option with the lowest casualties, embodied energy, and equivalent carbon emissions. SJ was ranked the least attractive retrofit alternative considering social, economic, and environmental consequences.

7. In a long-term perspective, RCJ was found to be the most-acceptable retrofit option, with the lowest social and environmental long-term losses. FRP was found to be the second-best choice, with the lowest economic long-term loss and reduced long-term repair time. The SJ was found to be the third favorable retrofit option with high long-term economic loss and environmental consequences.

CHAPTER 6 SEISMIC RESILIENCE OF COMMUNITY BUILDINGS

6.1 Introduction

The functionality of community buildings not only depends on the damage to individual buildings but also on the interactions with other infrastructure systems. This chapter incorporates these interactions by applying systems thinking approach to analyze community resilience. The proposed framework starts with identifying the physical infrastructure systems and key components in a community. Then, the hazard scenarios are defined, and the component damage and recovery are assessed by utilizing fragility and consequence functions. After that, a network model, considering the interdependencies between the utility networks and the dependency of utility networks on the community buildings, is introduced to evaluate the component-level building functionality. Finally, community resilience is assessed by proposing community-level indicators including inherent resilience, community functionality, and access to essential facilities. The proposed model is illustrated on a community consisting of building portfolios, water, and electric power systems under four hazard scenarios. It is concluded that the systems thinking approach considered at a community level provides important insights to the community resilience such as building functionality, utility demand, and supply, access to essential facilities, among others.

6.2 Community resilience framework

To introduce the proposed community resilience assessment framework, this section mainly takes building portfolios and two physical infrastructure systems including the water (WN) system and the electrical power (EPN) system as an example for illustrative purposes. The building portfolios consist of components including residential buildings (RB), commercial buildings (CB), educational institutes (EI) consisting of schools, colleges, and universities, medical care facilities (MC) consisting of clinics and hospitals, and emergency response facilities (ER) consisting of fire stations, police stations, and emergency operation centers. The WN system consists of pipelines, water tanks, reservoirs, and pumping plants. The EPN system consists of generators, electrical wires, and an electric substation.

The framework for community resilience assessment comprises of three main parts: (1) component damage and recovery assessment, (2) network modeling and functionality assessment by considering interactions (i.e., dependencies and interdependencies), and (3) community resilience assessment by evaluating indicators such as inherent community resilience, community functionality, and access to essential facilities. The component damage and recovery assessment aim to develop recovery profiles for individual components. Since the functionality depends on the recovery of various interacting components, the network modeling approach is employed to evaluate the dependencies and interdependencies of components. The final step is to evaluate the community resilience by considering performance indicators that can provide meaningful information. In this step, the inherent resilience of a community, which is independent of hazard scenario is measured as the shortest distances from non-essential facility to access the essential facilities. Then, individual components'

recovery assessment is utilized to estimate community functionality and access to essential facilities. Finally, these community-level performance indicators are utilized to assess community resilience. The next sections provide further demonstration of the three main parts of the framework.

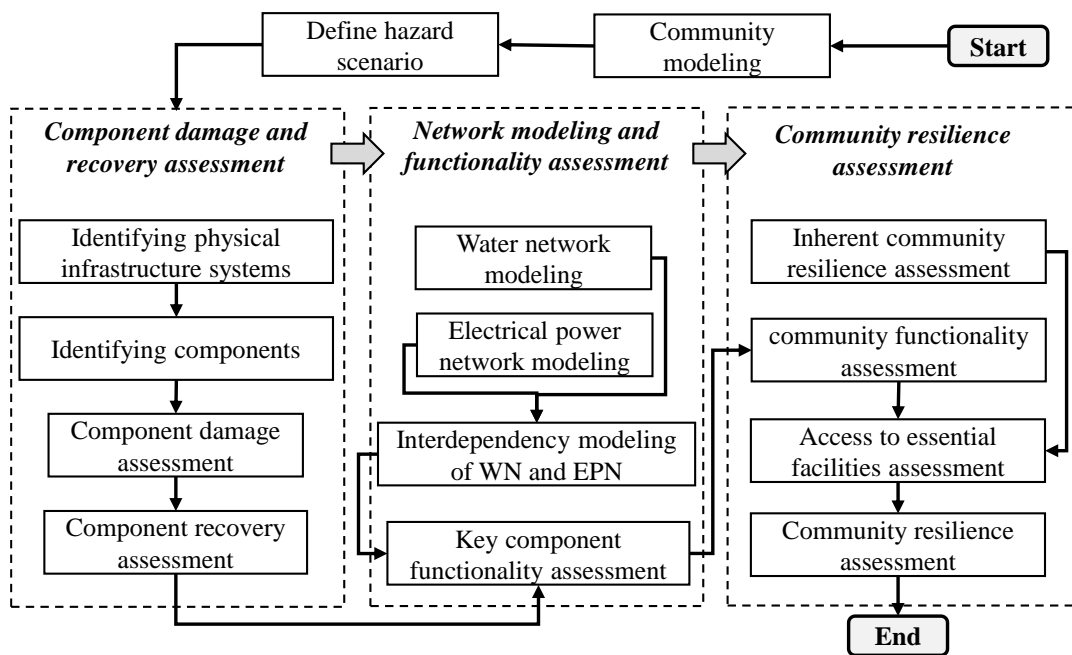


Figure 6-1 The proposed framework for community resilience assessment

6.3 Component damage and recovery

The first step towards assessing community resilience is to identify physical infrastructure systems and key community components (i.e., building portfolios). The building portfolios consist of different types of buildings including essential and non-essential buildings. The non-essential buildings (i.e., RBs) serve the purpose of providing shelter, while the essential buildings provide educational, medical, and emergency-related services, among others. The WN system provides water service to the buildings through pipelines that receive water from the reservoir through

components such as water tanks and pumping plants. The EPN system provides electricity to the buildings from the electric substation through the electrical wires. After identifying the components in a community, the component damage, downtime, and recovery assessment are performed, explained in subsequent subsections. The summary of the considered components and data required for the component damage, downtime, and recovery assessment are shown in Table 6-1.

Table 6-1 Summary of physical infrastructure systems and key components' damage and recovery assessment

Physical infrastructure systems and key components	Components	Damage assessment	Recovery assessment
Water network	Reservoir	Fragility (HAZUS, 2003)	Consequence (HAZUS, 2003)
	Pumping plant	Fragility (HAZUS, 2003)	Consequence (HAZUS, 2003)
	Water tank	Fragility (HAZUS, 2003)	Consequence (HAZUS, 2003)
	Pipelines	Repair rate (HAZUS, 2003; ALA, 2001; O'Rourke & Deyoe, 2004)	Repair time from pipe breaks and leaks (HAZUS, 2003; ALA, 2001; O'Rourke & Deyoe, 2004)
Electrical power network	Substation	Fragility (HAZUS, 2003)	Consequence (HAZUS, 2003)
	Pole towers	Fragility (HAZUS, 2003)	Consequence (HAZUS, 2003)
	Power lines	Fragility (HAZUS, 2003)	Consequence (HAZUS, 2003)

Building portfolios	building	Fragility (HAZUS, 2003; FEMA, 2012)	Consequence (HAZUS, 2003; FEMA, 2012; Almufti and Willford, 2013)
---------------------	----------	-------------------------------------	---

6.3.1 Component damage assessment

The component damage is evaluated by defining discrete damage states which are based on the level of damage after an earthquake event. In this chapter, four damage states (i.e., slight, moderate, extensive, and complete) are defined and the probability of exceeding each damage state given the intensity measure (IM) of an earthquake is determined from the fragility functions.

The damage state probabilities provide the probability of exceeding each damage state given IM. To evaluate a specific damage state, a probabilistic method is proposed herein. In this method, a specific damage state of a component is determined by utilizing a random generating function, and the probability of being in each damage state is formulated as:

$$DS_k^i = \begin{cases} \text{if } \emptyset_{|0Rn}^i > p_{DS_1|IM}^i; DS_0^i \\ \text{if } p_{DS_2|IM}^i < \emptyset_{|0Rn}^i \leq p_{DS_1|IM}^i; DS_1^i \\ \text{if } p_{DS_3|IM}^i < \emptyset_{|0Rn}^i \leq p_{DS_2|IM}^i; DS_2^i \\ \text{if } p_{DS_4|IM}^i < \emptyset_{|0Rn}^i \leq p_{DS_3|IM}^i; DS_3^i \\ \text{if } \emptyset_{|0Rn}^i \leq p_{DS_4|IM}^i; DS_4^i \end{cases} \quad 6-1$$

where DS_k^i is the k damage state of component i given IM; k represents a discrete number ranging from 0 to 4 for four damage states; $\emptyset_{|0Rn}^i$ is a function generating a

random number ranging from 0 to 1; and $p_{DS_k|IM}^i$ is the probability of exceeding damage state k .

6.3.2 Component recovery assessment

6.3.2.1 Downtime and recovery assessment of buildings

The severer the damage, the longer it takes to prepare for the recovery efforts and the actual repair work. The downtime of a component is defined as the total time it takes to repair a component including the time required for starting the repair work. Thus, the downtime consists of two parts: (1) delay time, and (2) repair time. The repair time is the time from the start of actual repairs to completion and the delay time is an additional time required for the management of actual repairs. For instance, in the case of the building portfolios, the total delay time for a building can be determined as (Almufti and Willford, 2013):

$$TDT^i = DT_{Ins}^i + \max \left\{ \begin{array}{l} DT_{Fin}^i \\ DT_{Enm}^i + DT_{Per}^i \\ DT_{Com}^i \end{array} \right. \quad 6-2$$

where TDT^i is the total delay time for building i ; DT_{Ins}^i is the delay time due to inspection; DT_{Fin}^i is the delay time due to financing; DT_{Enm}^i is the delay time due to engineering mobilization; DT_{Per}^i is the delay time due to permitting; and DT_{Com}^i is the delay time due to contractor mobilization. The Downtime is the sum of total delay time and repair time determined as:

$$DWT^i = IRT^i + TDT^i \quad 6-3$$

where DWT^i is the downtime of component i ; and IRT^i is the repair time of component i . The repair time for each building can be determined by utilizing consequence functions. The consequence function is also a lognormal CDF providing a repair time against the damage state of a building (FEMA-P-58, 2012; Hutt et al., 2015; Molina Hutt et al., 2016).

6.3.2.2 Pipelines recovery assessment

The recovery of the WN pipelines is determined by evaluating the repair rate which is the number of repairs required per kilometer of pipeline under a given IM (O'Rourke and Deyoe, 2004). In the case of buried pipelines, the repairs required (i.e., the total number of breaks and leaks) are sensitive to peak ground velocity (PGV), and for the case of liquefaction, the repairs required are sensitive to peak ground displacement (PGD) (Honegger and Eguchi, 1992; O'Rourke and Ayala, 1993). The community is geographically divided into many sectors to better understand community profile, identify the distribution of components such as pipelines, and assign resources in a hazard event such as the number of workers for repair works, among others. In the proposed methodology, the total number of required repairs are determined per sector as:

$$RR = 0.0001 \cdot Wn_S \cdot C_T \cdot (IM_{PGV})^{2.25} \quad 6-4$$

$$RR_L = p_{liq|IM} \cdot Wn_S \cdot C_T \cdot (IM_{PGD})^{0.56} \quad 6-5$$

where RR is the total number of repairs required including breaks and leaks in given sector S ; Wn_S is the cumulative length of the pipelines in a given sector; RR_L is the number of repairs required given liquefaction scenario; $p_{liq|IM}$ is the probability of

liquefaction; IM_{PGV} is PGV IM; IM_{PGD} is the PGD IM; and C_T is the pipeline type multiplier that is 1 for the brittle pipes and 0.3 for the ductile pipes (HAZUS, 2003).

HAZUS assumes that in the case of PGV IM, the total number of required repairs includes 80% leaks and 20% breaks, while in the case of liquefaction, the total number of required repairs includes 20% leaks and 80% breaks (HAZUS, 2003). The total repair time for the pipelines can be determined as:

$$PRT_S = \frac{1}{W_S} \sum_{pt=1}^n (L_S^{pt} \cdot LF^{pt} + B_S^{pt} \cdot BF^{pt}) \quad 6-6$$

where PRT_S is the total repair time in days for pipelines in a sector S ; W_S is the number of workers assigned to a sector for repair work; B_S^{pt} is the number of estimated breaks of a pipeline type pt ; L_S^{pt} is the number of estimated leaks in pipeline pt given sector S ; BF^{pt} is the repair factor for the breaks that depends on the pipe type, size, among others; and LF^{pt} is the repair factor for the leaks. Note that the HAZUS methodology implemented herein is a simplified approach for repair time estimation for water pipelines, and can be better modeled utilizing improved methodologies (Nurre et al., 2012; Xu et al., 2019).

6.3.2.3 Other network components recovery assessment

The recovery for other WN components including pumping plants, water tanks, the reservoirs is evaluated by utilizing consequence functions (HAZUS, 2003). The damage states for electric substations and distribution circuits are also determined from fragility functions and the resulting repair time is evaluated from the consequence functions, respectively (HAZUS, 2003; FEMA-P-58, 2012). Note that due to limited

repair resources there also exists delay time for WN and EPN systems, and advanced models can be incorporated to estimate the delay times for the physical infrastructure systems as well (Fang et al., 2016; Bristow and Hay, 2017; Liu and Song, 2020). However, the delay times for the building portfolios can be considerable since the recovery of the building is not centrally planned, may have a high financial burden, takes considerably longer, and also involves many stakeholders (McAllister, 2015). Hence, in this work, the delay times for the building portfolios are considered.

6.4 Network modeling and functionality assessment

The physical infrastructure systems and building portfolios are interconnected, and the failure of one component may affect the functionality of another. The failure propagation and the dependence of various components in the physical infrastructure systems are modeled through network dependencies and interdependencies (Ouyang et al., 2019). These interactions may result in the propagation of failure due to the connections between the components. The failure of components in one physical infrastructure system may affect the functionality of components in other systems. For instance, the WN has an infrastructure interdependency with EPN, therefore, a failure of the component in the EPN will affect the functionality of the WN and vice versa. Similarly, the functionality of building portfolios has infrastructure dependence on the WN and EPN. As a result, the failure of the WN or EPN components will affect the functionality of buildings. The subsequent subsections discuss the dependency and interdependency modeling and its effect on the functionality assessment of building portfolios.

6.4.1 Network connectivity modeling

The network of the physical infrastructure systems is modeled through the proposed augmented adjacency matrix. The augmented adjacency matrix consists of two types of submatrices: (1) the adjacency matrices, and (2) the interaction matrices. The adjacency matrix models a physical infrastructure system as a network referred herein as a network system, and the interaction matrix models a dependency of one network on another. For instance, the following Figure shows two physical infrastructure systems represented as system k1 and system k2. These two network systems are modeled as an adjacency matrix A^{k1} and A^{k2} , respectively. The interactions between systems (i.e., dependency and/or interdependency) are modeled by interaction matrix $A^{k1,k2}$ (dependence of k1 on k2) and $A^{k2,k1}$ (dependence of k2 on k1).

The adjacency matrix is a two-dimensional $n*n$ matrix, where n is the total number of nodes in network k . Network k is modeled in terms of nodes and edges, where nodes represent the components including water tanks, substation, pipelines, generators, among others, and edges represent the bidirectional connectivity representing interdependency within the network. The network k is modeled through the adjacency matrix $A^{(k)}$ formulated as:

$$A^{(k)} = \begin{bmatrix} a_{11}^{(k)} & & \dots & & a_{1n}^{(k)} \\ & \ddots & & \ddots & \\ \vdots & & a_{ij}^{(k)} & & \vdots \\ & & \ddots & \ddots & \\ a_{n1}^{(k)} & & \dots & & a_{nn}^{(k)} \end{bmatrix}, k = 1, \dots, K, (i, j \in k; i, j = 1, \dots, n^{(k)}) \quad 6-7$$

where i and j are the nodes of network k ; $a_{ij}^{(k)}$ is the network edge representing a bidirectional relationship (i.e., interdependency) connecting nodes i and j ; and $n^{(k)}$ is

the total number of nodes in a network. The connectivity of edges within a network is determined as:

$$a_{ij}^{(k)} = \begin{cases} \text{if } (i \neq j) \text{ and "link" = yes; } 1 \\ \text{if } (i \neq j) \text{ and "link" } \neq \text{yes; } 0 \\ \text{if } (i = j); 0 \end{cases} \quad 6-8$$

where "link" = yes when node i has a bidirectional relationship with node j .

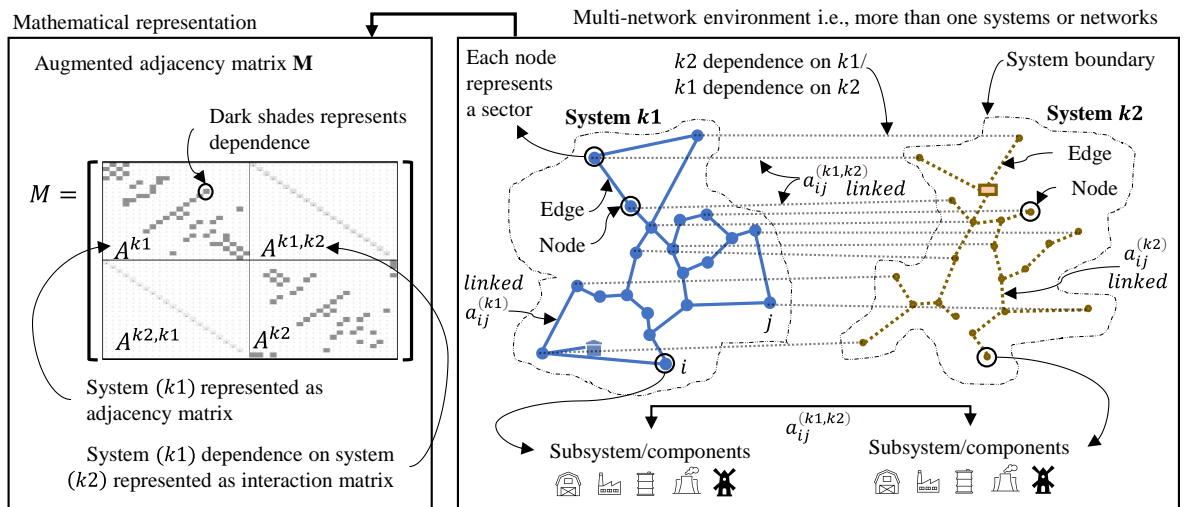


Figure 6-2 The augmented adjacency matrix representation of multi-networks

In the case of K interdependent networks, where the networks have dependencies (i.e., unidirectional relationship) and interdependencies (i.e., bidirectional relationship) with each other, the interaction matrix between any two networks is formulated as:

$$A^{(k1,k2)} = \begin{bmatrix} a_{11}^{(k1,k2)} & \dots & a_{1n}^{(k1,k2)} \\ \vdots & a_{ij}^{(k1,k2)} & \vdots \\ a_{n1}^{(k1,k2)} & \dots & a_{nn}^{(k1,k2)} \end{bmatrix}, \quad k1, k2 = 1, \dots, K, (i, j \in k1, k2; i, j = 1, \dots, n^{(k1,k2)}) \quad 6-9$$

where $k1, k2$ are the two interdependent networks; and $a_{ij}^{(k1,k2)}$ represents the edge connecting node i on network $k1$ with node j in network $k2$. The adjacency matrix and the interaction matrix are combined into an augmented adjacency matrix M as:

$$M = \begin{bmatrix} A^{(1)} & \dots & A^{(1,k)} & \dots & A^{(1,K)} \\ \vdots & \ddots & \vdots & \ddots & \vdots \\ A^{(k,1)} & \dots & A^{(k)} & \dots & A^{(k,K)} \\ \vdots & \ddots & \vdots & \ddots & \vdots \\ A^{(K,1)} & \dots & A^{(K,k)} & \dots & A^{(K)} \end{bmatrix} \quad 6-10$$

where $A^{(k)}, k = 1, \dots, K$ is the adjacency matrix of network k ; and $A^{(K,k)}$ is the interaction matrix representing the dependency of network K on network k .

After an earthquake event, the edges will be disrupted and the interactions between the nodes of inter and intra-network will break because of the damage to components. After the recovery of components, the nodes in the networks will be connected again. This network repair is formulated by updating the augmented adjacency matrix during the investigated time after an earthquake event. The updating is based on the recovery of components (i.e., the two nodes are connected by an edge if all the required components of the two nodes are repaired). Therefore, depending upon the recovery of components within a multi-network environment, the augmented adjacency matrix is updated, and the network connectivity and community functionality during the investigated time can be tracked.

6.4.2 Capacity, demand, and supply modeling

There exist numerous studies which build on the concept of adjacency matrix to evaluate capacity, demand, and supply for water and electrical power networks. For instance, Guidotti et al. (Guidotti et al., 2016) explored the role of network

dependencies of water and electrical power networks by evaluating pressure and demand criteria for water network. Sharma et al. (Sharma and Gardoni, 2022) proposed a concept of tensors for mathematical modeling of interdependent infrastructure systems, also provided classification and mathematical modeling of infrastructure interdependencies (Sharma et al., 2021), and evaluated the time-varying performance of electrical infrastructure under hazard (Sharma and Gardoni, 2018). This chapter considers these methodological improvements in the network modeling and evaluates the capacity, demand, and supply of utilities by considering the adjacency and interaction matrices and demands from the building portfolios.

The base capacity and demand of a network system can be determined as:

$$C^{(k)}(t) = f[A^{(k)}(t), \phi_c^{(k)}] \quad 6-11$$

$$D^{(k)}(t) = f[A^{(k)}(t), \phi_D^{(k)}, IM^{(k)}] \quad 6-12$$

where $C^{(k)}(t)$, $D^{(k)}(t)$ are the base capacity and demand of network system k , $\phi_c^{(k)}$, $\phi_D^{(k)}$ are the model parameters for the respective capacity and demand models, and IM is the intensity measure at each node of a network system. The respective capacities of a network at nodes and edges are allocated as:

$$C^{(k)}(t) = \begin{cases} \text{if } (i \neq j) \text{ and link} = \text{"yes"}; \text{Transmission Capacity } C_{ij}^{(k)}(t) \\ \text{if } (i \neq j) \text{ and link} \neq \text{yes}; 0 \\ \text{if } (i = j); \text{Generation Capacity } C_{ii}^{(k)}(t) \end{cases}$$

6-13

The generation capacity is provided at the nodes, and the transmission capacity is provided at the edges of a network. Then, the base capacity and demand models can be utilized to evaluate the supply for a network as:

$$S^{(k)}(t) = f[A^{(k)}(t), C^{(k)}(t), D^{(k)}(t), \emptyset_S^{(k)}] \quad 6-14$$

where $\emptyset_S^{(k)}$ are the supply parameters and $S^{(k)}(t)$ is the time-varying supply of a network system k .

6.4.3 Interdependencies and functionality assessment of buildings

The components or a network as a whole serve one or more functions. These functions may depend on the recovery and interactions of other components. For instance, for a building to provide safe drinking water, it should be useable and the components providing water should be in a recovered state and connected to the source providing water. Similarly, to get electricity, the electric substations should be recovered and the relevant electric wires connecting a particular building should also be in the recovered state.

The dependence of functions on other components is modeled by interaction matrices. For instance, a water network system consists of pumps that require electricity from the distribution circuit components of an electrical power network. This dependence can be modeled by updating the capacity and demand as follows:

$$C'^{(k1,k2)}(t) = f[A^{(k1,k2)}(t), \Omega_C^{(k1,k2)}, C^{(k1)}, C^{(k2)}] \quad 6-15$$

$$D'^{(k1,k2)}(t) = f[A^{(k1,k2)}(t), \Omega_D^{(k1,k2)}, D^{(k1)}, D^{(k2)}] \quad 6-16$$

where $C^{(k1,k2)}(t)$ is the updated capacity of network system k1 due to the dependence of network system k2, $\Omega_C^{(k1,k2)}$ is the strength of dependency of k1 on k2, $D^{(k1,k2)}(t)$ is the updated demand, and $\Omega_D^{(k1,k2)}$ is the strength of dependency for demand.

The availability of water and electricity to building i , considering the interdependency of WN and EPN, is modeled by proposing a utility availability factor $U_k^i(t)$ which is an input variable for modeling the functionality of this building. The building will be able to get water supply if it is connected to water reservoirs through pipeline distribution and other components necessary to deliver water including water tanks, pumping plants, among others. Similarly, the electricity supply depends on the functionality of the substations and the network of wires connecting the substations to the buildings. Hence, the utility availability factor is a functionality contribution from the utility networks ranging from 0-100% and is determined by calculating the ratio of updated supply and demand for a particular node of a particular network, where 0% indicates no utility availability and 100% indicates that the supply of particular utility is fulfilling the demand of the building.

The utility availability factor is also affected by the interdependency of WN and EPN. For instance, if WN is connected to building i but the EPN is not connected, the utility availability factor will provide reduced functionality contribution for the WN as well depending upon the dependence strength of WN on EPN. The procedure to evaluate the building functionality by considering the component interactions in a systems thinking platform by considering water and electrical power network is visually illustrated in following Figure.

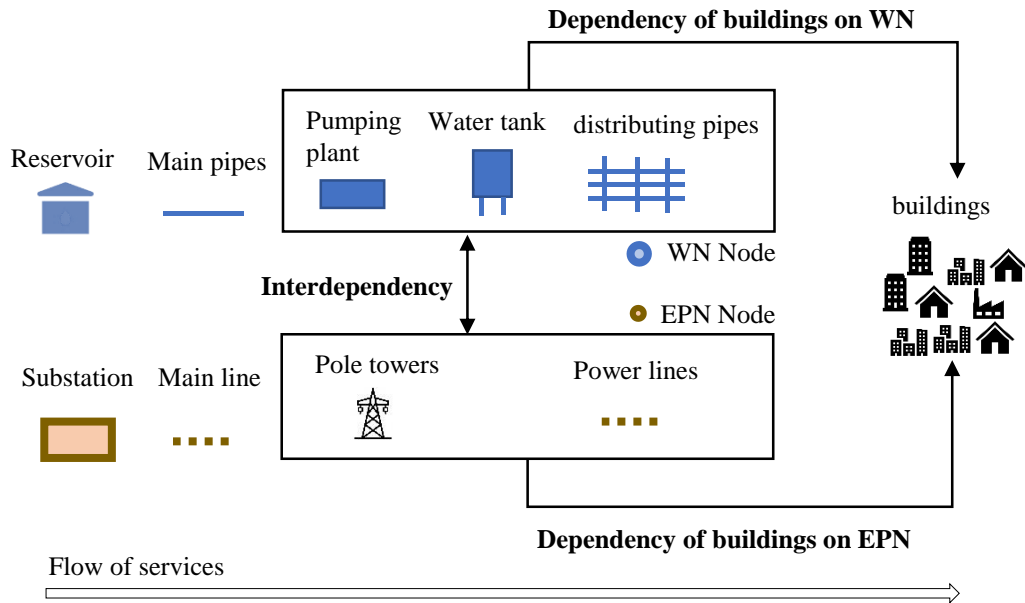


Figure 6-3 The illustration of functionality assessment of building i via systems thinking

Also, to assess the building utility supply and demand, it is important to consider the connectivity of utility from source to building i through various components. The computational procedure for the connectivity modeling of water and electricity supply to building i is presented in Table 6-1 which includes three steps: (1) defining the components for all the considered networks and modeling a network by utilizing the augmented adjacency matrix, (2) applying the find (\bullet) function to determine the connectivity of nodes, and (3) applying the depth-first search dfs (\bullet) function to determine the connectivity of building i with the source providing water or electricity. The nodes connected to the source are the nodes which will have water or electricity supply and building i available at that node will be connected to the water or electricity supply.

Table 6-2 The computational procedure for connectivity modeling

Step 1: Define global variables which will be used to perform computations on the adjacency matrix.

```
n = number of nodes in a network
Ak = adjacency matrix
count = 0
component = [ ]
visited = [false] x n
```

Step 2: Applying find() function to determine which nodes are connected to which edges.

```
Function find ()
For (i=0; i < n; i++):
if !visited [i]:
count ++
dfs(i)
return count
```

Step 3: Applying depth-first search dfs() function to determine which nodes are connected with the source providing the utility and which nodes are not connected with the source providing utility.

```
Function dfs (at)
visited [at] = true
component[at] = count
for next in g[at]:
if !visited [next]:
dfs (next)
```

The damage state of a building and utility availability factor is then utilized to evaluate the functionality state of a building (Lin and Wang, 2017a; Masoomi et al., 2020). The functionality state can provide the building condition with respect to the available utility supply and the extent of damage to the building. The higher the extent of damage, the lower the functionality, and similarly the reduction in utility supply will also reduce the functionality. The illustration of the capacity, demand, and supply of utilities, and the resulting functionality state of building *i* is shown in the following Figure. The progression of functionality states of buildings during the investigated time

after an earthquake event will provide a sense of community recovery. In this chapter, six functionality states are defined depending upon the damage state and utility availability as:

$$BFN^i = \begin{cases} \text{if } DS_0^i \cap U_{WN}^i \cap U_{EPN}^i; FF^i = 100\% \\ \text{if } DS_0^i \cap [U_{WN}^i \cup U_{EPN}^i]; BF^i = 80\% \\ \text{if } DS_1^i \cup DS_0^i; RO^i = 60\% \\ \text{if } DS_2^i; RU^i = 40\% \\ \text{if } DS_3^i; RE^i = 20\% \\ \text{if } DS_4^i; NU^i = 00\% \end{cases} \quad 6-17$$

where BFN^i is the functionality state of building i after an earthquake event; FF^i is the full functionality of a building and is given 100% weighting factor, since the building is in a no-damage state DS_0^i , and all the utilities are available (i.e., electricity U_{EPN}^i and water utility U_{WN}^i); BF^i is the baseline functionality where the building is in a no-damage state and the utilities are partially available (i.e., either electricity U_{EPN}^i or water utility U_{WN}^i); RO^i is the re-occupancy functionality state where the building is in the slight or no-damage state; RU^i is the restricted use building functionality state where the building is in moderate damage state DS_2^i and should be used with caution; RE^i is the restricted entry building functionality state where the building is in an extensive damage state DS_3^i and its use is restricted; and NU^i is the collapsed or not useable functionality state where the building is in a complete damage state DS_4^i and is not usable anymore. After the delay time, the repair works will start, and the building functionality will improve depending upon the downtime of the building and the utility availability (Cimellaro et al., 2010b; Cimellaro and Piqué, 2016).

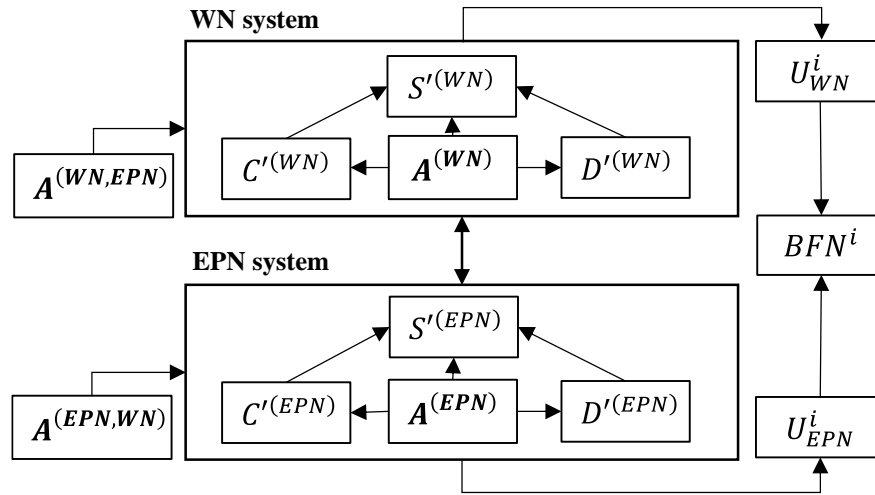


Figure 6-4 The illustration of network capacity, demand, supply and functionality modeling

6.5 Community resilience assessment

The community building portfolios consist of numerous buildings of different importance factors, occupancy categories, and structural systems, among others. It is important to have community-level indicators to assess community resilience under hazards. In this chapter, two community-level indicators are proposed to track the performance of a community during the investigated time after an earthquake event which includes: (1) community functionality and (2) access to essential facilities. These community-level performance indicators are then utilized to evaluate community resilience.

6.5.1 Community functionality

To assess the community functionality, the component functionality of all individual buildings is determined and summed up in the community functionality indicator in

terms of the percentage of buildings in the considered functionality states during the investigated time. For instance, the community-level full functionality (FF) indicator will provide the percentage of buildings in the full functional state during the investigated time. This indicator can provide information related to the complete recovery of a community from a hazard event. Since the community is defined to be recovered from an earthquake event after 90% of the buildings in a community have achieved full functionality (Koliou et al., 2017). The Re-Occupancy (RO) functionality state serves a critical function of providing temporary residence to the population after an earthquake event. Similarly, other community functionality state indicators will provide insights related to their respective functionality states. Mathematically, the community functionality indicator can be written as:

$$CFI_j(t) = \frac{\sum_{i=1}^n F_j^i(t)}{n}, j \in 1 \dots 6 \quad 6-18$$

where n is the total number of buildings in a community, $F_j^i(t)$ is the functionality state indicator for a particular functionality state j of a building i during the investigated time t , and j represents functionality state (i.e., 1 for full functionality and 6 for not useable functionality state). The $F_j^i(t)$ is determined based on the community functionality state of interest. For instance, to determine the full functionality state of a community, the $F_1^i(t)$ is determined as:

$$F_j^i(t) = \begin{cases} 1, & BFN^i(t) = 100\% \\ 0, & BFN^i(t) \neq 100\% \end{cases} \quad 6-19$$

6.5.2 Access to essential facilities

This proposed indicator is related to the inherent resilience which measures the nearest distance of a residential building to the essential facilities including commercial buildings, hospitals, schools, fire stations, among others. The nearest distances to essential facilities are measured for all the buildings and a cumulative distribution curve representing the access to essential facilities of a community is developed as a measure of its inherent resilience. The shorter distances would mean the facilities can be accessed in less time and hence higher inherent resilience.

However, after an earthquake event, the shortest distances would change due to the functionality loss of essential buildings. The functionality during the investigated time will provide corresponding access to essential facilities as a measure of community resilience. This additional community-level indicator will provide further insights on the community resilience under hazard in addition to the physical infrastructure systems and key components recovery.

The concept of inherent resilience and access to essential facilities is illustratively presented below. As shown, a particular essential facility can be accessed by at least 50% of the residential community at a distance of approximately 400 meters before an earthquake event, and after a hazard event during the investigated time the distances are increased due to reduced functionality of buildings and then restored after downtime. This dynamics can be tracked as a measure of resilience as shown, where different curves show different access to essential facility information at a given time after an earthquake event.

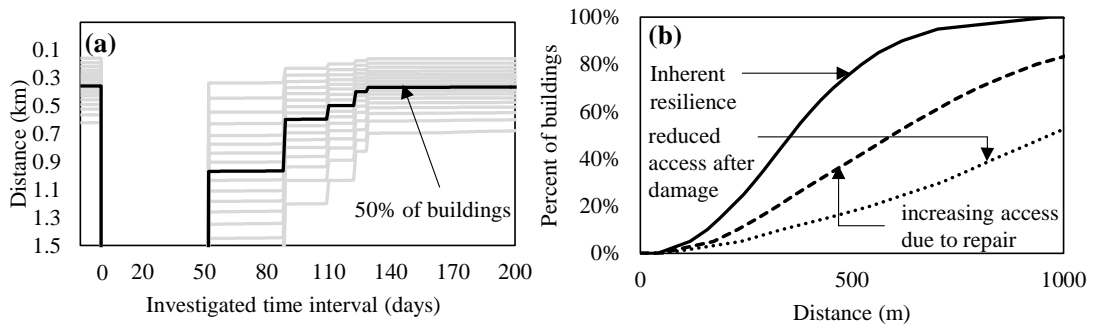


Figure 6-5 Inherent resilience and access to essential facilities (a) during the investigated time, and (b) in terms of percentage of buildings being able to access the facilities within certain distances

6.5.3 Community resilience

The community functionality and access to essential facility indicators are then utilized to assess community resilience. This is achieved by normalizing the two performance indicators and combining them during the investigated time. This would give the community resilience value ranging from zero to one. The maximum value would indicate the full functionality recovery of a community and regain of all the access to essential facilities. Similarly, the reduction in performance would result in the community resilience value less than one. Mathematically, community resilience can be determined as:

$$R(t) = f(CFI_j(t), AE_f(t)) \quad 6-20$$

where $CFI_j(t)$ are the considered community functionality indicators, and $AE_f(t)$ represents normalized access to essential facilities.

6.6 Illustrative example

The proposed resilience assessment framework is illustrated on a community consisting of building portfolios, WN system, and EPN system. The considered community is geographically divided into twenty-one different regions referred to herein as sectors, and each sector is assigned a WN and EPN node. Note that this is the simplified representation of real networks and is considered due to the limited data available and security concerns. The community consists of 16,653 RBs, 591 CBs, and 25 essential facilities. The WN consists of water pipelines distributed throughout the community, a designated pumping plant and water tank for each sector, and a reservoir located adjacent to sector twenty-one. The spatial distributions of the building portfolios, WN, and EPN systems are shown below.

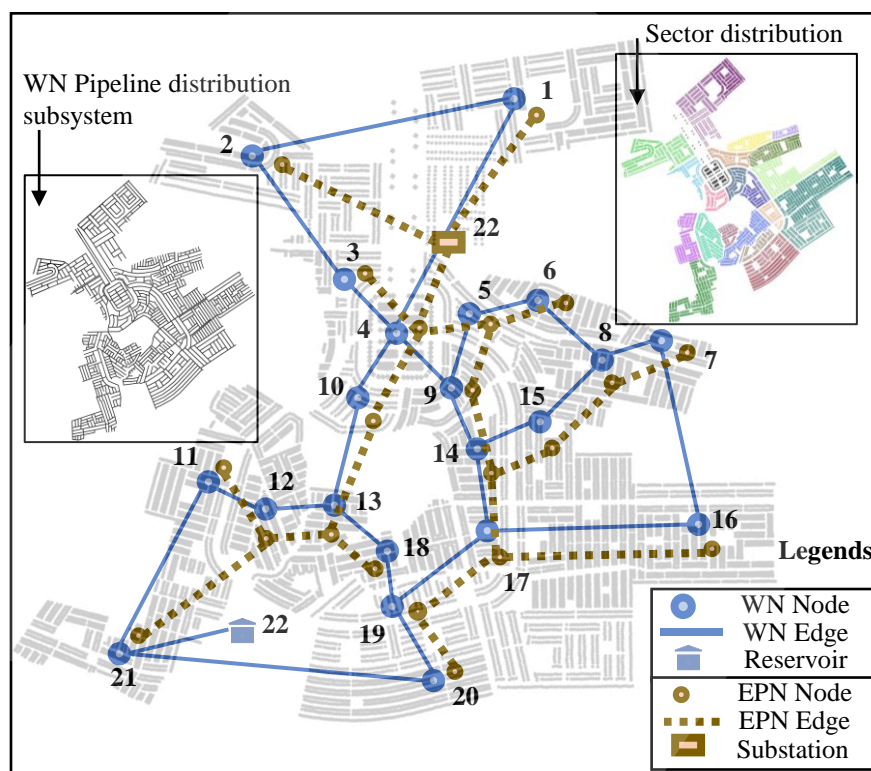


Figure 6-6 Spatial distributions of building portfolios, WN system, and EPN system

6.6.1 Defining hazard scenarios

Ground motion prediction equations are utilized for the spatial distribution of the IMs for an earthquake scenario (Cornell, 1968; Stewart et al., 2015). For instance, in the following Figure, the Kashmir earthquake of October 8, 2005, is simulated which triggered widespread destruction near its epicenter (Rossetto and Peiris, 2009). The illustrative community is located approximately 107 km from the epicenter of the earthquake and experienced a PGA of 0.18. The design seismic hazard PGA value determined for the study region is 0.33 g and the maximum considered PGA is 0.56 g (Waseem et al., 2020). In this illustrative example, a total of four hazard scenarios are considered with return periods of 95-, 475-, 975-, and 2475-years as shown below.

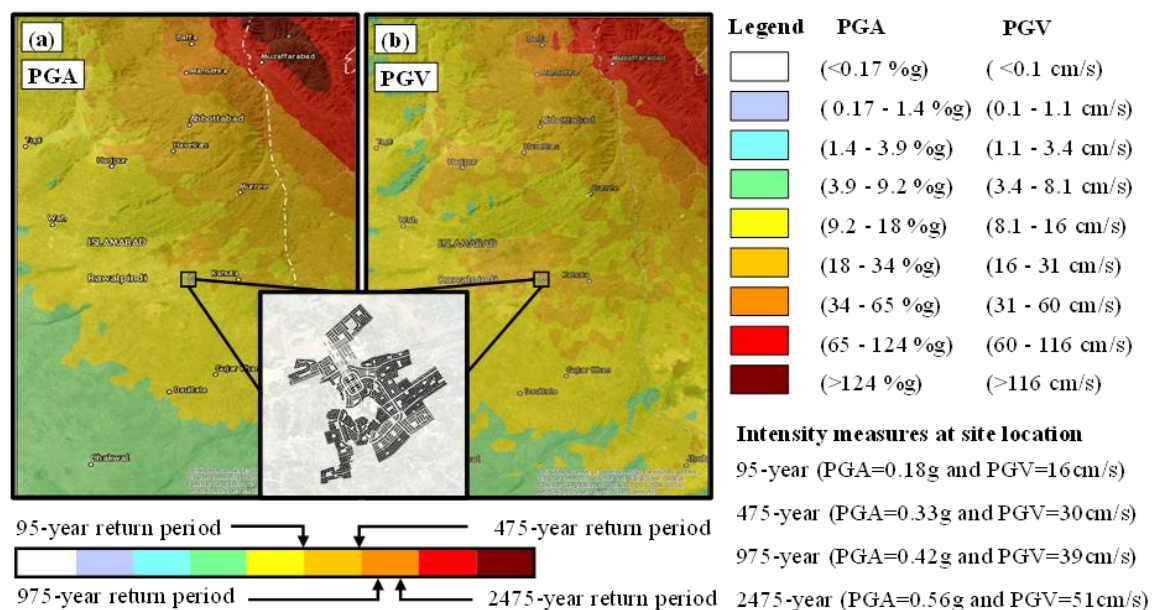


Figure 6-7 Spatial distribution of median (a) PGA under 95-year (b) PGV under 95-year, and considered four hazard scenarios

6.6.2 Component damage and recovery assessment

The first step after an earthquake is to inspect for the damage and it can take between one to five days depending upon the institutional capacity of a community, building importance, among others (Almufti and Willford, 2013). The damage to the buildings will dictate the amount of time needed for engineering mobilization, permitting, and contractor mobilization for the actual repair works. In this illustrative example, the delay times are determined by considering the lognormal CDFs provided by Almufti and Willford (2013).

The WN pipeline distribution recovery assessment requires the estimation of the number of breaks and leaks, WN repair factors, and the number of workers working on the repair works in each sector. The WN repair factors depend on the pipeline size and are determined from (HAZUS, 2003). The total number of repairs required is determined using Equation (6-5) and (6-6), and the total number of days required to repair a pipeline distribution in each sector is determined from Equation (6-7). In the design hazard scenario, the pipelines in sector-sixteen take a maximum time of 258 days to repair, and sector four takes a minimum time of 35 days during the investigated time after an earthquake event. The fragility and consequence functions required for evaluating the damage state probabilities and repair times of all the components are extracted from HAZUS. In the design hazard scenario, the water tanks recover on day 76, the pumping plants recover on day 42, and the water reservoir is recovered on day 32. In the case of EPN, the circuit distributions in different sectors are recovered from day 27 to 67 and the substation is recovered on day 24 after an earthquake event. The WN and EPN recovery for all the sectors under four hazards scenarios is shown in the following Figure. The WN recovery for the hazard scenarios of 95-, 475-, 975-, and

2475-years is at day 77, 258, 449, and 609, respectively. Similarly, the EPN recovery under the four hazard scenarios is at days 23, 67, 92, and 157, respectively. In general, the EPN recovered faster, indicating its higher resilience as compared to WN.

The recovery times for the EPN and WN may appear relatively slower as compared to those observed in the developed countries including the United States. However, in this illustrative example, the utilized fragility functions, adopted consequence functions, impeding delays, and other factors were considered to mimic the community in a developing country. Hence, a relatively longer recovery times are observed, especially for the EPN network. Nonetheless, the community is utilized for the illustration and serve the purpose well in this respect.

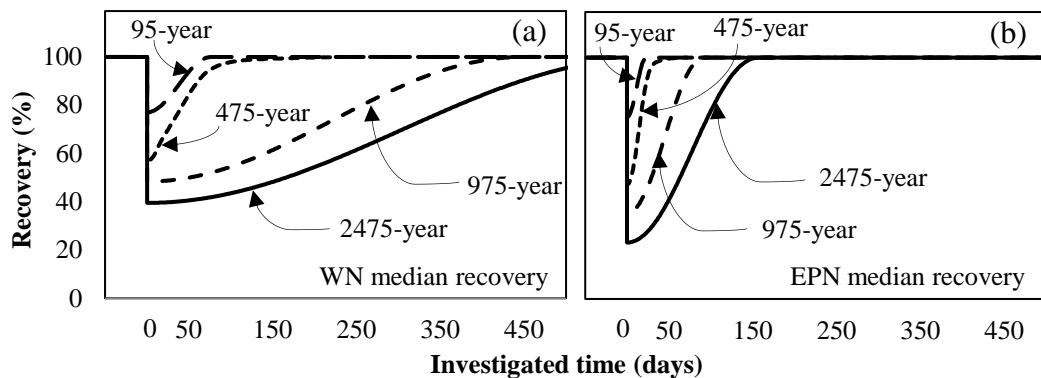


Figure 6-8 Recovery under four hazard scenarios for (a) WN, and (b) EPN

6.6.3 Network modeling and functionality assessment

In this step, the network modeling and functionality assessment are performed to obtain information such as the number of buildings connected with water or electricity, demand, and supply of utilities, utility interdependency, and functionality contribution to buildings, among others. In this illustrative example, the interaction matrix provides

21 interdependent links between two networks, one at each node. In an aftermath of an earthquake, the edges between the nodes will break, but they will start to form again due to the recovery efforts. The supply of water is determined by performing the pressure-dependent flow analysis using a Python package called water network tool for resilience (WNTR), and EPANET (Klise et al., 2017), and for the supply of electricity python package for power system analysis (PyPSA) is utilized (Brown et al., 2017). As an illustration, the WN repair under the design hazard scenario, and the EPN repair are shown in the following Figures. As shown, the water reservoir is repaired and started delivering water to the rest of WN on day 136, and the WN is fully recovered on day 258 after an earthquake event. The EPN under the design hazard scenario started receiving electricity supply on day 36 and is fully repaired on day 67 of the investigated time.

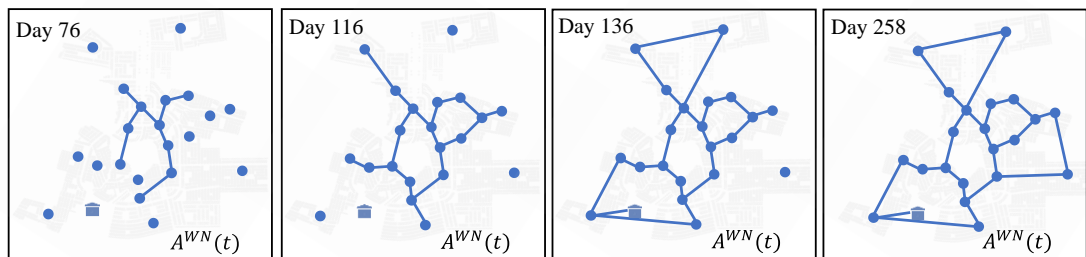


Figure 6-9 WN repair during the investigated time under design hazard scenario

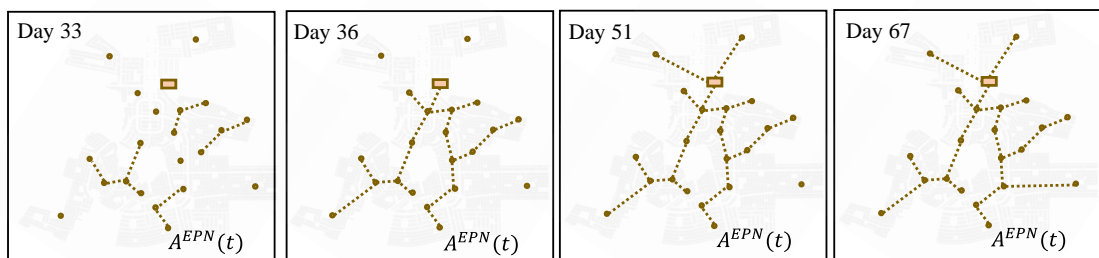


Figure 6-10 EPN repair during the investigated time under four hazard scenarios

The strength of interdependencies between the utility infrastructure systems is extracted from the study conducted by Laugé *et al.*, (Laugé et al., 2015) in which the critical infrastructure experts were asked to rate the interdependencies of various infrastructure systems. The strength of the interdependency utilized in the interaction matrix for EPN on WN is 0.266, and for the WN on EPN is 0.166. Finally, the utility availability factor for all the buildings is utilized to evaluate the functionality contribution of utilities to buildings and the supply and demand of utilities by considering the percentage of buildings needing the utilities versus the percentage of buildings being supplied with the utility.

The residential construction of the community is mostly dominated by unreinforced masonry bearing walls, and few concrete frames with unreinforced masonry bearing walls. The essential buildings are mostly concrete moment frames, while some are concrete frames with unreinforced masonry infill walls. The fragility and consequence functions for the archetype buildings are extracted from HAZUS (HAZUS, 2003). The damage states for all the buildings in the community are determined from the probabilistic method and depending upon the utility availability and the downtime, the building functionality during the investigated time is determined. As an illustration, the building functionality during the investigated time of 0 days, 100 days, 300 days, and 500 days under the design hazard scenario is shown in following Figure. It can be seen that the building functionality improves during the investigated time as a result of recovery efforts and utility availability.

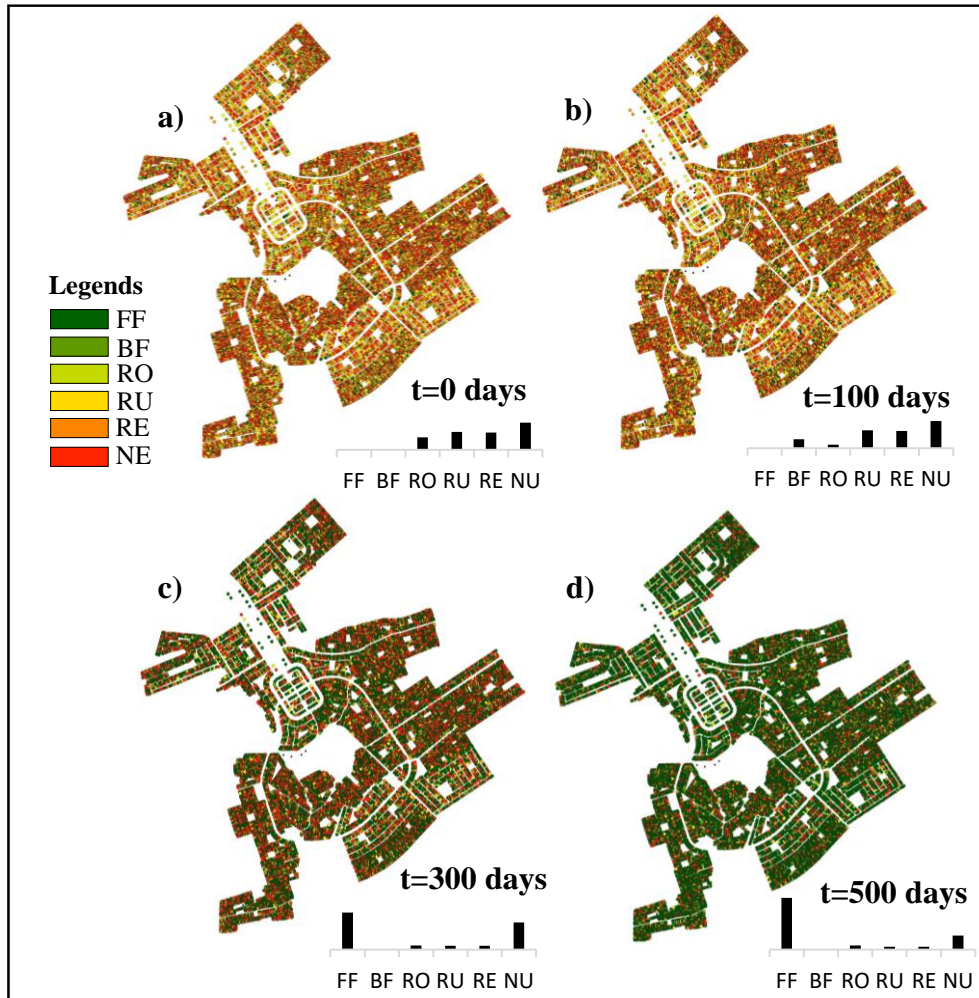


Figure 6-11 Functionality assessment of a community building portfolios under the design hazard scenario during the investigated time of (a) 0 days, (b) 100days, (c) 300 days, and (d) 500 days

6.6.4 Community resilience assessment

The community functionalities measured by different building functionality states (i.e., FF, BF, RO, RU, RE, NU) determined from the damage assessment and utility availability are shown in the following Figure for the design hazard scenario. In this hazard scenario, 90% of the buildings achieve the full functionality at day 708 under the design earthquake, and at that time, 94.32% are in RO, 1.62% are in RU, 1.16% in

RE, and 2.89% are in NU functionality state. The 90% of buildings achieving full functionality for the hazard scenarios of 95-year, 975-year, and 2475-year is at day 479, 755, and 790 of the investigated time, respectively.

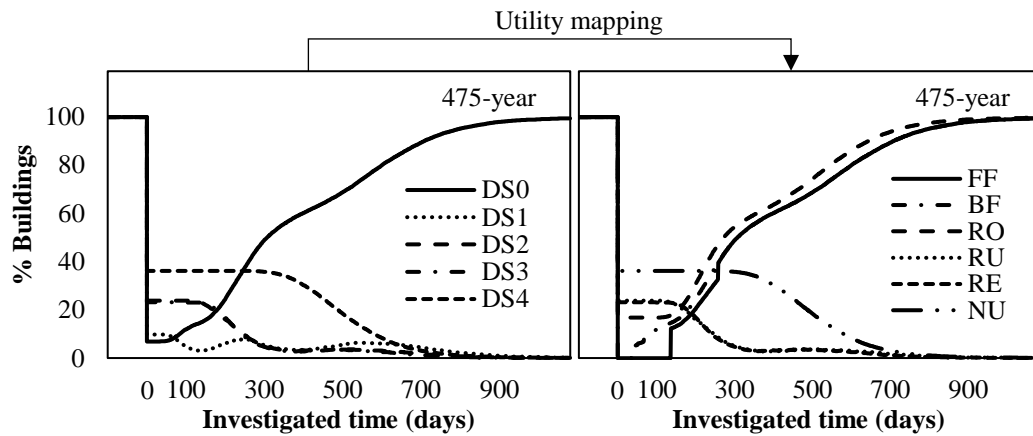


Figure 6-12 Community functionality assessment of building portfolios under the design hazard scenario

In addition to the community achieving full functionality, it is also essential to keep track of the utility availability for the percentage of buildings during the investigated time. The following Figure shows the community-level full functionality recovery indicator for three hazard scenarios considering no utility dependence, baseline utility dependence, and full utility dependence. The baseline utility dependence provides the percentage of buildings having at least one utility available during the investigated time and the full utility dependence provides the percentage of buildings with both utilities available. For instance, in the 95-year hazard scenario, around 30% of the buildings are in a no-damage state during the first 60 days but are provided with electricity on day 21. On day 48, 25% of buildings get water supply and at that time 5% of buildings with no damage are still without water. It is also noted that the effect of utility dependence is higher in low-intensity hazard scenarios, especially

for the baseline utility dependence. For instance, in the 2475-year hazard scenario, there is no significant difference between no-utility dependence and baseline utility dependence.

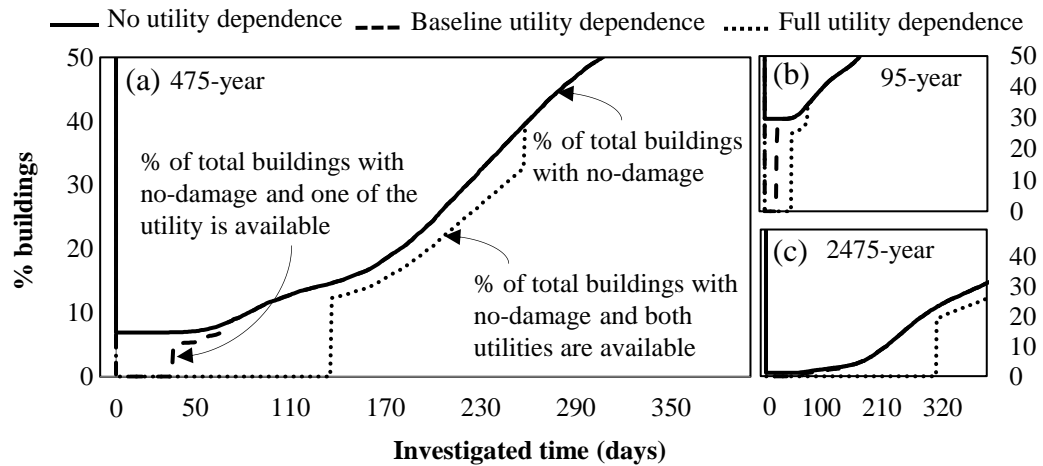


Figure 6-13 Community full functionality assessment showing the effect of utility dependence for different hazard scenarios of (a) 475-year, (b) 95-year, and (c) 2475-year

After an earthquake event, the utility demand will also reduce depending upon the level of damage to the building portfolios. The network modeling and functionality assessment are also utilized to evaluate the supply and demand of utilities (Didier et al., 2018). The loss of resilience due to utility unavailability for essential and non-essential facilities under the design hazard scenario is shown in the Figure below. The percentage of buildings requiring the utilities is referred to as the demand, and the percentage of buildings being provided with the utility is referred to as supply. After an earthquake event, under the design hazard scenario, 6.95% of the total non-essential facility buildings are in a no-damage state and require a utility supply. The demand for the essential facilities starts increasing on day 35, and at that time, 46.7% of the essential

facilities are already connected with electricity. Since the essential facilities recover rapidly, the total demand for the essential facilities also increases as compared to non-essential facilities. This increase is associated with the definition of building functionality provided in Equation (6-18). The electricity supply becomes available for non-essential buildings on day 36 and at that time the EPN network is capable of supplying electricity to 56% of the non-essential buildings, while the demand is 6.95%. The WN is capable of supplying water to 82% of the non-essential buildings on day 136 and at that time the demand is 14.6%.

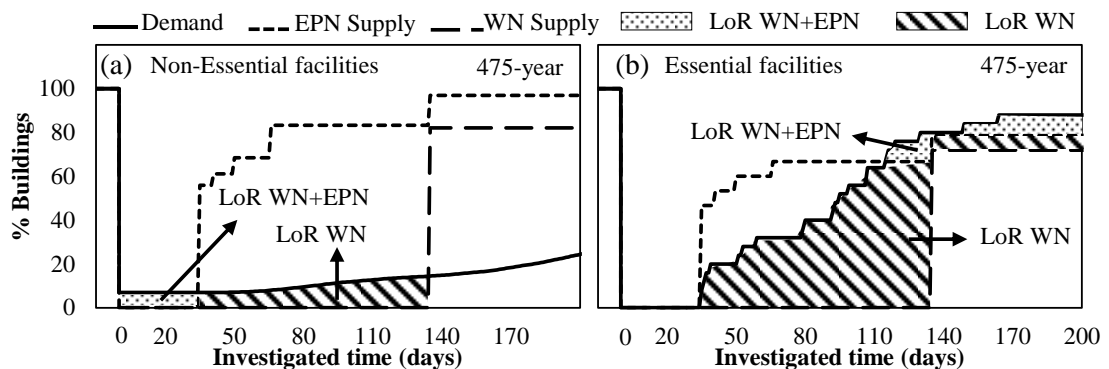


Figure 6-14 Loss of resilience (LoR) due to supply and demand of utilities for (a) Non-essential facilities, and (b) Essential facilities

The inherent resilience for this community is also presented below. Note that, 50% of the RBs have access to CB, EI, MC, and ER within 185, 356, 519, and 1339 meters of distance. After an earthquake, access to essential facilities will change given the functionality of buildings. In this example, we consider the buildings to be accessible if they are at RO state or above. As an illustration, the access to EIs during the investigated time of 0, 60, 100, and 150 days under the design hazard scenario is shown below. The median access (i.e., access to at least 50% of RBs) to essential facilities for all four hazard scenarios is also presented. It is observed that the RBs have

higher access to CBs and even after the 2475-year earthquake, access to CBs is not completely lost indicating better access compared to other essential facilities. The median access to CBs is within 200, 418, 493, and 839 meters of distance under four hazard scenarios at time $t = 0$, which is regained during the investigated time. The access to essential facilities for CB, EI, MC, and ER is restored at days 193, 135, 133, and 129 under the design hazard, and the trend for the rest of the hazard scenarios can be observed accordingly.

Finally, the community functionality recovery and access to essential facility indicators are utilized to evaluate the community resilience, shown in the following Figure. The resilience of a community increases during the investigated time as the access to essential facilities and the community functionality is improved. The increase in resilience is higher for the 95-year hazard scenario and is comparatively slower for the 2475-year earthquake scenario due to severer damage and longer recovery time. The resilience under different investigated time periods for four hazard scenarios can be investigated accordingly.

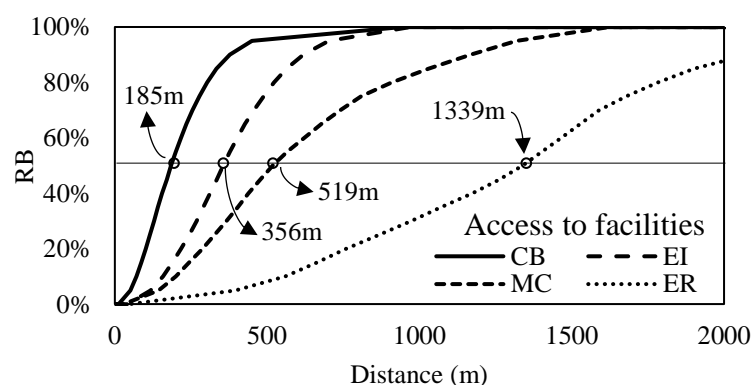


Figure 6-15 Inherent resilience of a community via access to essential facilities

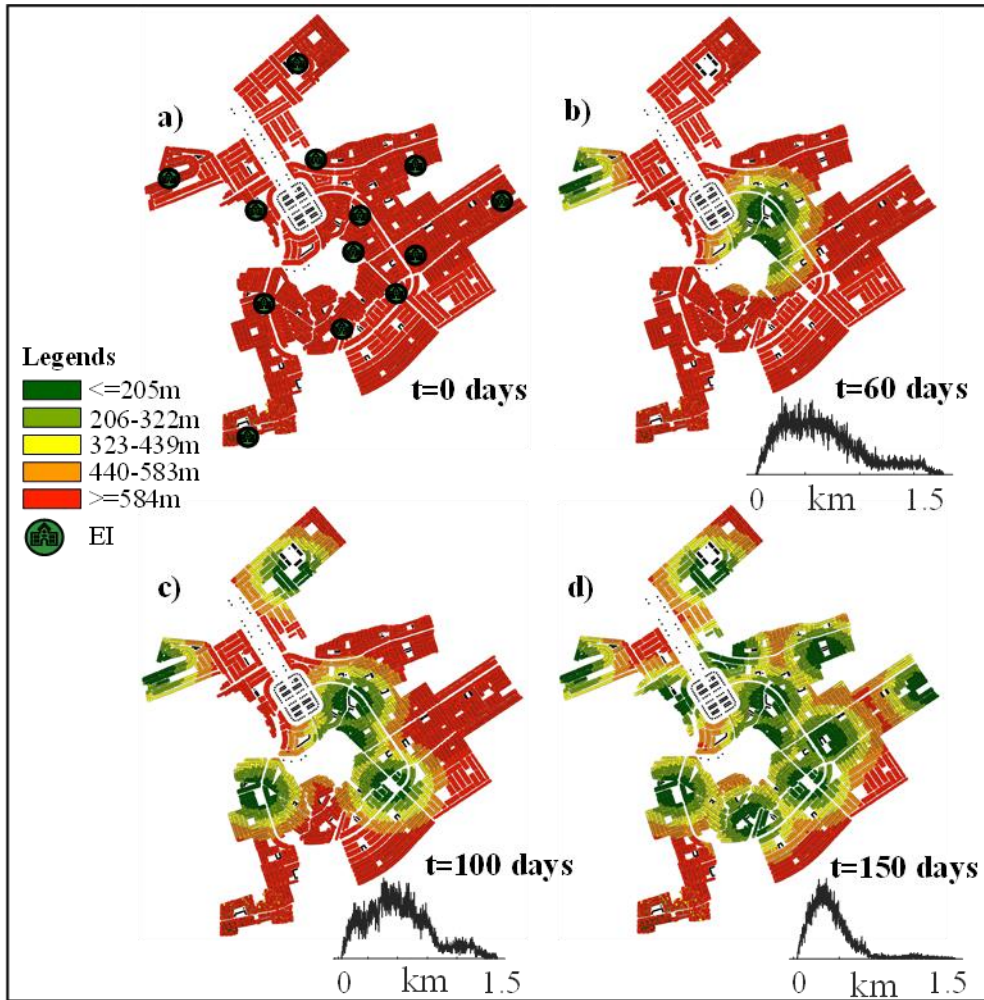


Figure 6-16 Access to EI under design hazard scenario during the investigated time of (a) 0 days, (b) 60 days, (c) 100 days, and (d) 150 days

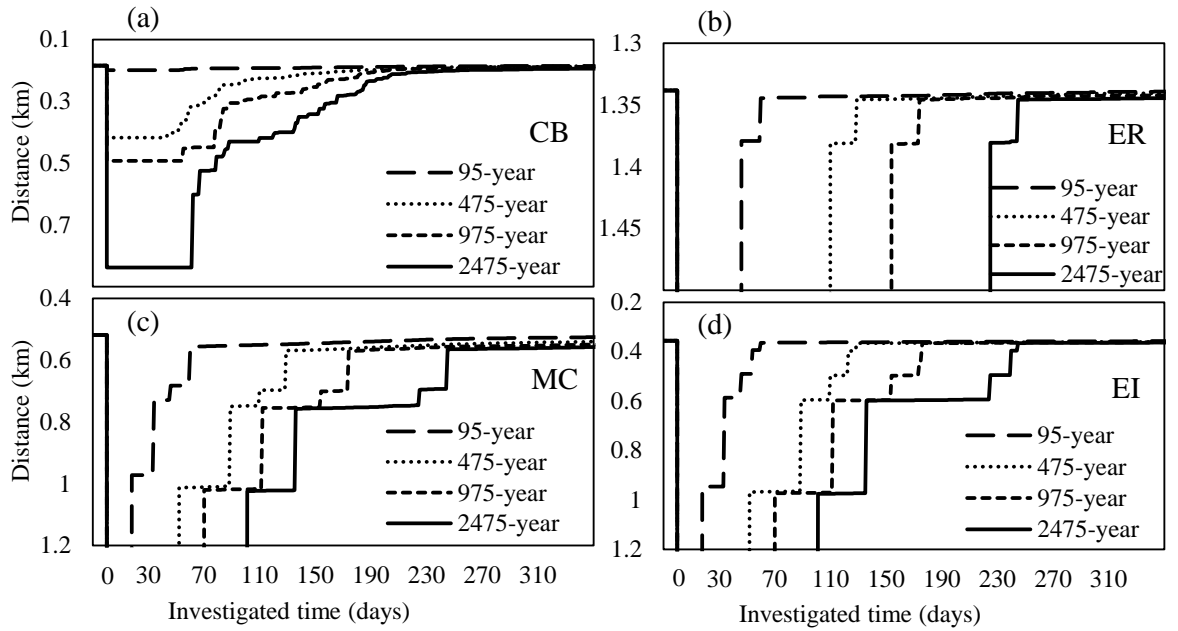


Figure 6-17 Access to essential facilities for (a) CB, (b) ER, (c) MC, and (d) EI

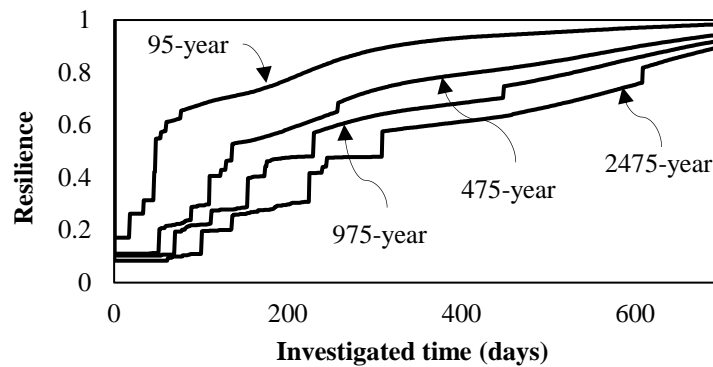


Figure 6-18 Community resilience assessment under the four hazard scenarios

6.7 Conclusions

This chapter proposed a community resilience assessment framework under seismic hazards. The following conclusions can be drawn based on the illustrative example.

1. The EPN under the four hazard scenarios fully recovered at days 23, 67, 92, and 157, respectively, while the WN recovered at days 77, 258, 449, and 609, respectively. Although many utility network components were repaired during the investigated time, it was until days 48, 136, 230, and 309 of the investigated time under the four hazard scenarios that most of the buildings started receiving water as compared to days 21, 36, 44, and 66 for electricity.
2. The utility networks under the considered hazard scenarios fully recovered within 23-609 days of the investigated time, while 90% of the buildings achieved full functionality within 479-790 days. The recovery of the building portfolios took longer as compared to the recovery of utility networks. The EPN was first to get fully recovered among utility networks in all the considered hazard scenarios, followed by the WN and then building portfolios.
3. The pipelines distribution dominated the WN recovery, while the circuit distribution component dominated the EPN full recovery. For instance, in the design hazard scenario, the pipeline distribution per sector started recovering at day 35 and continues till day 258 of the investigated time. The rest of the WN components could recover before the complete recovery of the pipelines. Similarly, the circuit distribution component started recovering at day 27 and continues till day 67 of the investigated time for the design hazard scenario.
4. In the considered community, 90% of the buildings achieved the full functionality at days 479, 708, 755, and 790, and were re-occupiable at days 432, 644, 688, and 719 of the investigated time under the four hazard scenarios. The differences between the full functionality and re-occupancy were not substantial, indicating the higher significance of community full recovery on the total delays and repair times of buildings rather than utility network recovery.

5. The utility dependencies affect the community functionality at an early stage after an earthquake event till the utility networks are fully recovered. These interactions also provide information related to the percentage of buildings with utility availability, demand, and supply of utilities, among others. Hence, considering the building portfolio's dependence on utility networks can provide better decision-making for the community reconstruction during the early stage.
6. The utility demand under the four hazard scenarios was 29.72%, 6.95%, 3.36%, and 1.11%, respectively, at $t=0$ of the investigated time. The higher the earthquake intensity, the lower the demand due to the increased number of damaged buildings after an earthquake event. The utility demand increased with the increasing number of repaired buildings during the investigated time but the increase in demand is comparatively slower as compared to the utility supply due to faster recovery of utility networks as compared to building portfolios. For instance, in the design hazard scenario, the demand increased from 6.95% at $t=0$ to 15.78% at $t=150$ day, while the EPN supply increased to 97% and water supply increased to 82% at $t=150$ day.
7. Access to essential facilities also contributed to the resilience of a community since the increased access may reduce the population outmigration after an earthquake event. For instance, before the earthquake event, 50% of RBs had the access to CBs within 185 meters of distance. This distance increased to 418 meters right after an earthquake event due to the damage to the building portfolios. The access was restored to 185 meters at day 193 of investigated time because of reconstruction efforts..

CHAPTER 7 PERFORMANCE-BASED RETROFIT OPTIMIZATION OF COMMUNITY BUILDINGS

7.1 Introduction

It is essential to assess the performance of a community under probable hazard scenarios and to provide possible performance enhancements. This requires establishing performance indicators, an assessment method, and an optimization technique to provide mitigation alternatives. In this chapter, multiple performance indicators are utilized to assess the performance of a community building portfolio including loss, downtime, and environmental impact (e.g., CO₂ emissions). The performance of a community is assessed by utilizing a performance-based assessment methodology. Then, the performance indicators are utilized as performance objectives to be optimized considering non-dominated sorting and crowding distance evolutionary optimization techniques. The framework utilizes retrofit alternatives for each building in a community and provides Pareto-optimal solutions for considered performance objectives given retrofit cost. This process of performance assessment and optimization is repeated by utilizing the Monte Carlo approach to consider uncertainties. Finally, the Pareto-optimal solutions are utilized to evaluate the retrofit programs for community building portfolios in terms of considered performance indicators.

7.2 Optimization Framework for Community Building Portfolios

The proposed bi-objective retrofit optimization framework can be divided into two main parts: (1) performance assessment part, and (2) evolutionary optimization part. The performance assessment part is utilized to evaluate performance objectives and the evolutionary optimization part is utilized to evaluate the Pareto-optimal solutions by optimizing the performance objectives given retrofit alternatives. The proposed framework is shown in the following Figure, representing a single simulation from start to end. These simulations are repeated N times to incorporate uncertainties by utilizing the Monte Carlo approach (Hammersley, 2013). In each simulation, a random value is extracted from distribution functions utilized in the framework including fragility functions and functions in the consequence assessment part. At the end of all the simulations, the results can be extracted in terms of distributions for damage assessments, consequence assessments, and Pareto-optimal solutions, among others.

The process starts by generating an initial population consisting of a certain number of individuals. Each individual consists of two parts: (1) chromosome, and (2) fitness functions. The fitness functions are utilized as the performance objectives of community building portfolios defined in terms of risk, downtime, and sustainability indicators. The performance objectives provide information related to the performance of a community under hazard events and can be optimized given retrofit costs on a community level. For instance, the fitness function for a risk performance indicator can be the total number of casualties given hazard scenario, or total repair costs of a given hazard event, among others, and will change based on the retrofit costs implemented on a community level. The chromosome can be considered as a scenario of community building portfolio having different types of genes. Each gene can be considered as a

building in a community building portfolio and consists of two main parts: (1) allele, and (2) locus. The allele defines the retrofit alternative implemented for a particular building or no-retrofit implemented in the case of a reference building, and the locus defines the geospatial location of a particular building in a community building portfolio. The geospatial location will help identify the building and all the relevant assigned characteristics such as building type, structural system, code-level, floor area, story heights, among others. These evolutionary optimization terminologies in the context of community building portfolios are also graphically presented as shown below.

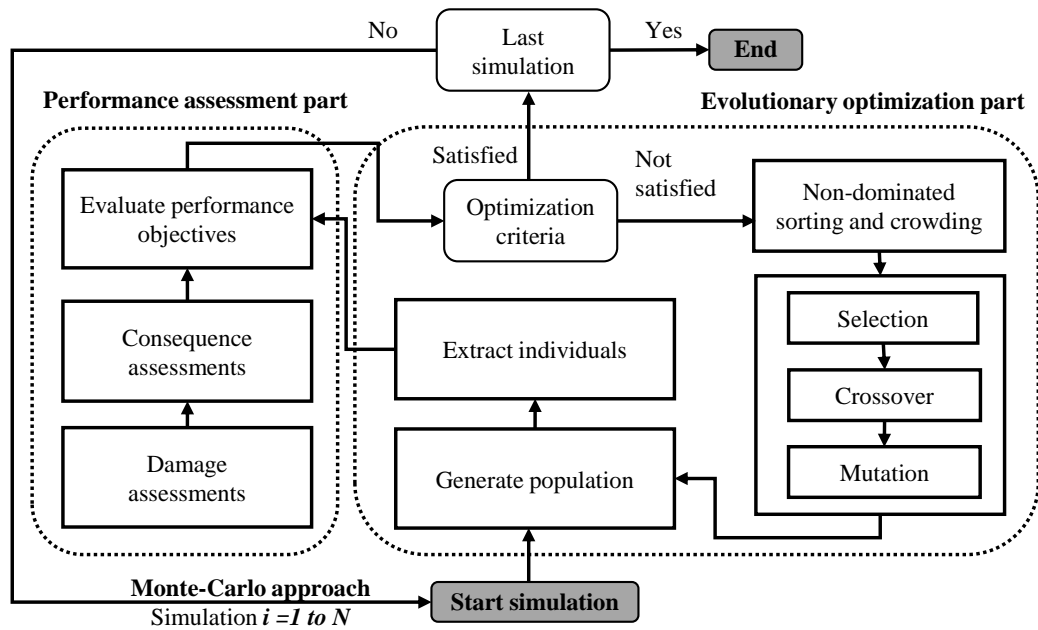


Figure 7-1 Bi-objective retrofit optimization framework for community building portfolio considering uncertainties.

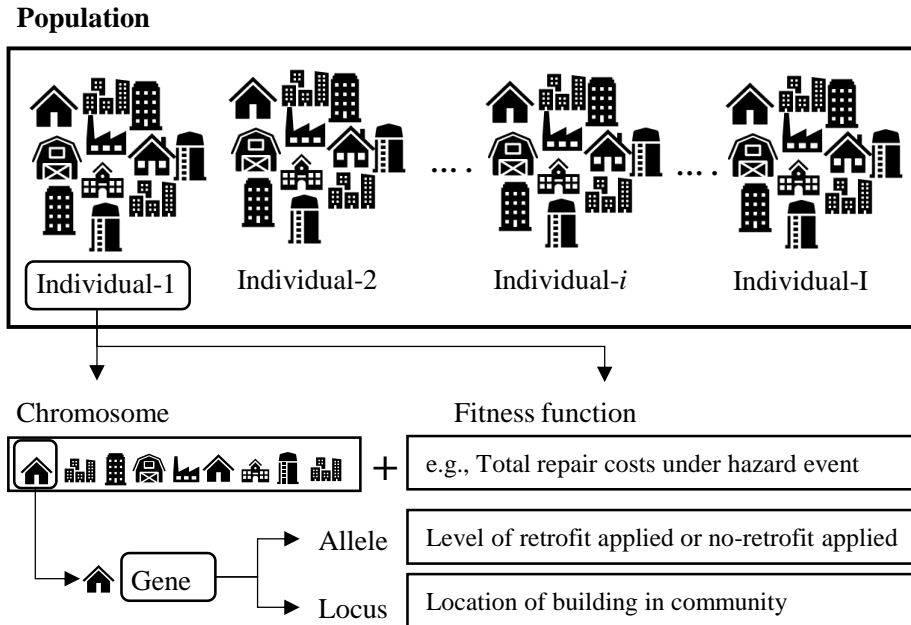


Figure 7-2 Evolutionary optimization terminologies in the context of community building portfolio.

The genes of all the individuals in the initial population are randomly assigned retrofit alternatives or no-retrofit, and fitness functions for all the individuals are determined utilizing a performance-based assessment approach. These individuals are then optimized by utilizing non-dominated sorting and crowding distance genetic algorithm and Pareto-optimal solutions are determined for all the simulations to incorporate uncertainties. The Pareto-optimal solutions are then utilized to assess the performance enhancement of a community building portfolio by providing retrofit programs. The subsequent sections discuss the two main parts of the framework in detail.

7.3.1 Building-Level Damage Assessments

In the literature, there exist different methods of damage assessments including empirical, analytical, numerical, and hybrid methods (Donà et al., 2021). Different risk assessment frameworks have been developed as a result to provide methodologies for predicting damage given seismic hazards (Carreño et al., 2012; Šipoš and Hadzima-Nyarko, 2017; Zentner et al., 2017). The most prominent ones are FEMA and HAZUS, among others, and require defining damage states for building-level damage assessment (HAZUS, 2003; FEMA-P-58, 2012). In HAZUS, for instance, five discrete damage states are defined including no damage state (DS0), slight damage state (DS1), moderate damage state (DS2), extensive damage state (DS3), and complete damage state (DS4). These damage states provide specific damage conditions of a particular structural system. For instance, in the case of unreinforced masonry bearing walls (URM) structural system, the no damage state would indicate negligible damage to a building after a hazard event; slight damage would indicate diagonal hairline cracks on masonry walls, and a few large cracks around the windows and doors; moderate damage state may include diagonal cracks in almost all the masonry walls with few walls having larger cracks; extensive damage state would indicate widespread cracking of masonry walls along with displacement of beams and trusses; and complete damage state would indicate structural collapse or imminent danger of collapse due to in-plane or out-of-plane failure of masonry buildings (HAZUS, 2003; Park et al., 2009; Crowley et al., 2019; da Porto et al., 2021).

These damage states are determined by establishing a fragility function which provides a probability of exceeding each damage state's given intensity measure (Farhan and Bousias, 2020; Qian and Dong, 2020). The intensity measure may include

peak ground accelerations, peak ground velocities, among others, and are correlated with the intensity of hazard scenarios (Wang et al., 2021; Zhang et al., 2021). The damage states of all the buildings in a community are determined by utilizing a probabilistic approach in which a random number is generated from 0 to 1 and depending upon the range of damage state it falls; a relevant damage state is assigned to a particular building as shown in the following Figure illustratively. The process is repeated for all the buildings in a community building portfolio for a single simulation run. The number of simulations is repeated and damage state distribution for each damage state given hazard scenario can be determined.

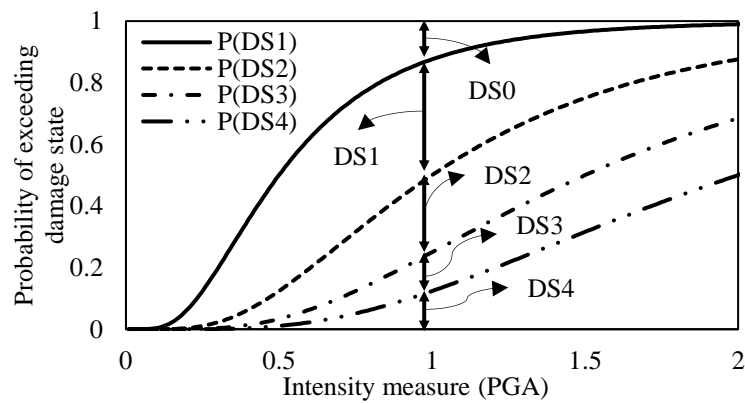


Figure 7-4 Damage state assessment under seismic hazard.

7.3.2 Building-Level Consequence Assessments

The damage states are utilized to evaluate consequences which may include the cost incurred to repair a building, the downtime of a building, equivalent carbon emissions due to the damage, and recovery efforts, among others (Li et al., 2020a). Different methods can be employed to assess the consequences of extreme events on a given damage state of a building (Erdik, 2017; Silva, 2018; Stojadinović et al., 2021). This

requires building information for various building types including the fragility and consequence functions. However, even the same building types can have different fragilities and consequence models based on age, construction materials, geometric properties, material costs, among others, and may require calibration for use in other communities (Erdik et al., 2011).

The HAZUS consequence assessment methodology is utilized in this chapter which starts by evaluating the total material required to be replaced due to the damage of a building. The damaged building material is a function of each damage state and is determined by utilizing percentage damage of different construction materials given the damage state (Kircher et al., 2006). The damaged materials are then correlated with the consequences by utilizing consequence functions (Cardone and Perrone, 2017).

The consequence functions can be uniform, normal, or lognormal cumulative distribution functions defined for each damage state (Molina Hutt et al., 2016). The consequence functions considered in this framework include repair costs, downtime, and equivalent carbon emissions (Mitrani-Reiser, 2007). These consequence functions are evaluated for each building in a single simulation run. The simulations are repeated and the distribution of consequences for each building in a community building portfolio can be evaluated.

The downtime consequence of a building consists of two parts: (1) the repair time, and (2) the delay time. The repair time is determined by lognormal consequence function, which is defined for each damage state, and the delay time is determined by evaluating the additional delays due to financing, engineering mobilization, contractor mobilization, obtaining permits, among others (Almufti and Willford, 2013). These

additional delays are also defined in terms of cumulative distribution functions and added with the repair time to evaluate downtime for each building.

7.3.3 Portfolio-Level Performance Objectives Assessment

The consequences assessed for all the buildings in a community are accumulated into the performance indicators. The risk performance indicator of a community will provide the total cost required to repair a community given a hazard scenario, the downtime indicator will provide total downtime of a community building portfolio, and the sustainability indicator will provide total equivalent carbon dioxide emissions given the hazard scenario. Additional socioeconomic and environmental consequences can also be considered under these performance indicators including total casualties given the hazard, total embodied energy, among others (Asadi et al., 2019).

7.4 Bi-Objective Evolutionary Optimization

The performance indicators will provide meaningful information related to the performance of a community under considered hazard scenarios. The community stakeholders or decision-makers may want to improve the performance of a community. This requires implementing pre-hazard mitigation alternatives which may include retrofitting buildings of a community. The decision-makers may identify various retrofit alternatives to implement but need to assess the number of buildings to be retrofitted, which type of retrofit alternative to be implemented, and how to achieve maximum performance given retrofit alternatives, among others. Briefly, the decision-makers are interested in knowing the performance enhancement of community building portfolios and the cost of supporting the performance enhancements.

There exist many combinations of retrofit alternatives to be implemented on a community building portfolio. Hence, a bi-objective evolutionary approach is utilized to obtain Pareto-optimal solutions that will provide maximized performance of community against the minimized retrofit costs for all the individuals. The performance indicators developed in the performance-based assessment part are utilized here as performance objectives and are optimized utilizing non-dominated sorting and a crowding distance genetic algorithm. It is important to highlight that the proposed performance-based bi-objective evolutionary optimization approach utilized here is heuristic and the optimal solutions are not guaranteed. Nonetheless, the method is sufficient for approximating the Pareto-optimal solutions in a bi-objective space.

The bi-objective optimization problem can be formulated as:

Given:

- The community building portfolio with different structural systems, code-conformance, building heights, fragility, and consequence functions, among others;
- Intensity measure at building locations under a given hazard scenario;
- Probabilistic damage assessment of community building portfolio;
- Consequences of all the buildings in a community building portfolio;
- The damage and consequences of buildings for different retrofit levels.

Find:

- The retrofit actions for all the buildings in a community building portfolio.

So that:

- The retrofit costs associated with the retrofit levels is minimized;
- The performance of a community associated with the retrofit level is maximized.

The first step is to generate an initial population consisting of a certain number of individuals. Each individual is a scenario of a community building portfolio where all the buildings are randomly given one of the retrofit alternatives or no-retrofit. In the next step, the individuals are extracted, and the performance objectives are evaluated by utilizing the performance-based assessment method presented in the previous section. The performance objectives are then checked against the optimization criteria and Pareto-optimal solutions are extracted if the optimization criteria are satisfied, or else the individuals are optimized by utilizing three main steps: performing (1) a fast non-dominated sorting and crowding distances; implementing (2) selection, crossover, and mutation strategies; and finally (3) generating a new population. The process is repeated until the optimization criteria are satisfied and the Pareto-optimal solutions providing performance indicators given retrofit programs can be extracted. The optimization criteria can be the number of allowed generations which may be based on computational costs and accuracy requirements. Subsequent subsections provide more information on the highlighted optimization steps.

7.4.1 Fast Non-Dominated Sorting and Crowding Distances

The individuals in the population have varying performance values against retrofit costs. The fast non-dominated sorting and crowding distances approach is utilized to select the best solutions in the given population. The best solutions are extracted by

utilizing two methods: (1) the dominance depth method to determine the non-dominated and dominated solutions, and (2) the crowding distance algorithm to ensure diversity among the selected solutions. The dominance depth method ranks the individuals based on which front a particular individual lies. For instance, the individuals on a Front-1 would be given the highest rank since they are non-dominated solutions that are not dominated by other individuals. Additionally, the crowding distance algorithm is utilized to measure the relative distances with other individuals lying on the same front. The individuals lying further apart are preferred to ensure the individuals are distributed over the considered Front and are not congested over a localized area. The non-dominated solutions with high diversity are the optimal solutions for a particular generation since these individuals provide the best performance against the least retrofit cost. The dominance depth method and crowding distance assessment given an initial population are shown illustratively as follows.

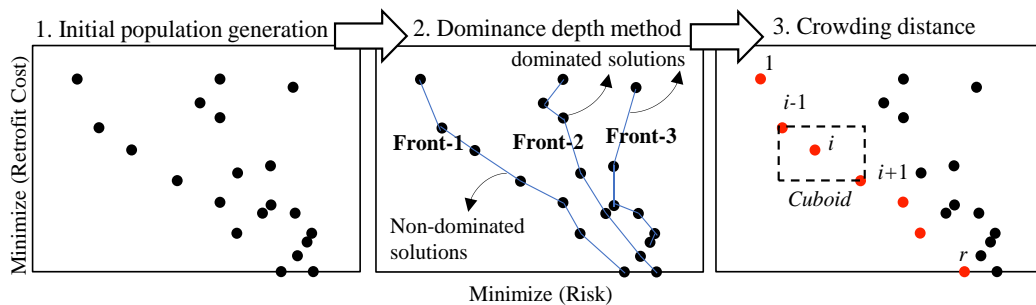


Figure 7-5 Illustration of fast non-dominated sorting and crowding distances.

7.4.2 Selection, Crossover, and Mutation

Once the ranking of all individuals is determined based on the dominance depth method and crowding distance algorithm, the next step is to perform selection, crossover, and mutation to generate new individuals. The purpose of selection is to identify above-

average individuals from the population, based on rank and crowding distances. The crowded binary tournament selection method is utilized to select the parents from the population. This method starts by randomly selecting two individuals from the population and choosing an individual with the better rank to become parent. In the case of two selected individuals having the same rank, then the selection is based on the crowding distances, and in the case that both rank and crowding distances are same, then the selection is performed randomly. This method of selection increases the chance of better individuals being selected from the population.

After selecting parents, the crossover operator is utilized to create new solutions referred as offspring. These offspring are generated by performing a crossover of the two randomly selected parents which helps explore the search in space. In this chapter, a simulated binary crossover operator is utilized to explore the discrete search space. The probability density function of the simulated crossover binary operator is presented as:

$$p(\beta_i) = \begin{cases} 0.5(\eta + 1)\beta_i^\eta, & \text{if } \beta_i \leq 1 \\ \frac{0.5(\eta + 1)}{\beta_i^{\eta+2}}, & \text{else} \end{cases} \quad 7-1$$

where β_i is the spread factor and η is the control parameter that defines the spread of the distribution function. A vector of β_i is determined by integrating the area under the probability distribution curve equal to a random number $u_i \in [0, 1]$, evaluated as:

$$\beta_i = \begin{cases} (2u_i)^{\frac{1}{\eta+1}} & \text{if } u_i \leq 0.5 \\ \left(\frac{1}{2(1-u_i)}\right)^{\frac{1}{\eta+1}} & \text{else} \end{cases} \quad 7-2$$

The vector β_i is utilized to change the allele of the genes. If the β_i is greater than 1, the first child gene is altered to a higher retrofit level as compared to the first parent and the second child gene is altered to a lower retrofit level to that of the parent. Contrarily, if the β_i is lower than 1, the first child gene is altered to a lower retrofit level as compared to the first parent and the second child gene is altered to a higher retrofit level to that of the parent. This process helps to produce fitter offspring from above-average parent population exploring the search space further for optimal solutions.

The mutation operator is adopted with low probability p_m to avoid non-convergence issues. In this chapter, a polynomial distribution operator is utilized for obtaining a solution. The polynomial probability distribution function is presented as:

$$p(\delta) = 0.5(\eta_m + 1)(1 - |\delta|)^{\eta_m} \quad 7-3$$

where δ is the median value and η_m is the factor controlling the spread of the distribution function. A vector of δ is determined by integrating the area under the probability distribution curve equal to a random number $r_i \in [0, 1]$, evaluated as:

$$\delta = \begin{cases} (2r_i)^{\frac{1}{\eta_m+1}} - 1 & \text{if } r_i < 0.5 \\ 1 - [2(1-r_i)]^{\frac{1}{\eta_m+1}} & \text{else} \end{cases} \quad 7-4$$

The polynomial mutation operator works in such a way that if the mutation probability randomly selects a locus where a mutation is required, then the gene is altered to a lower retrofit level if δ is less than zero, or else the gene is altered to a higher retrofit level.

7.4.3 New Population Generation

The resulting solutions include the parent population and the offspring population. The offspring population comprises new individuals extracted by utilizing selection, crossover, and mutation strategies and the parent population comprises previous individuals. The best solutions with the original population size are then selected from the parent and offspring populations such that the total population size is retained at its original size. The best-selected solutions of original population size are referred to as new population or survival population. The next step is to evaluate the performance objectives for all the individuals in a new population, and the process of selection, crossover, mutation, and survival and elimination is repeated until the optimization criteria are satisfied. The resulting Pareto-optimal solutions after the optimization criteria are met are the optimal solutions of the bi-objective optimization problem for a single simulation run. The number of simulations is performed using the Monte Carlo approach and the probability distributions of performance indicators can be extracted. The subsequent section implements the proposed framework on a community building portfolio for illustration of the proposed framework.

7.5 Illustrative Example

The framework is illustrated on a community consisting of residential and commercial buildings. The structural systems consist of unreinforced masonry bearing walls (URM), concrete frames with unreinforced masonry infill walls (C3), and concrete frames (C1). The residential building portfolio is dominated by low-rise (L) construction with story heights ranging from 1–3 stories, and commercial buildings are mid-rise (M) with story heights ranging from 4–7 stories. The building portfolio is a mix of pre-code, low-code, and moderate-code construction with most of the building

comprising low-code construction. The building portfolio is divided into seven different types of buildings depending upon the structural system, height, and code configurations as shown below. The classification of building types follows HAZUS (Kircher et al., 2006) classification system i.e., (1) structural system is highlighted first, (2) followed by story type, and (3) the last symbol denotes the code level. For instance, a URM building with a low-rise story and pre-code configuration is denoted as URML-P.

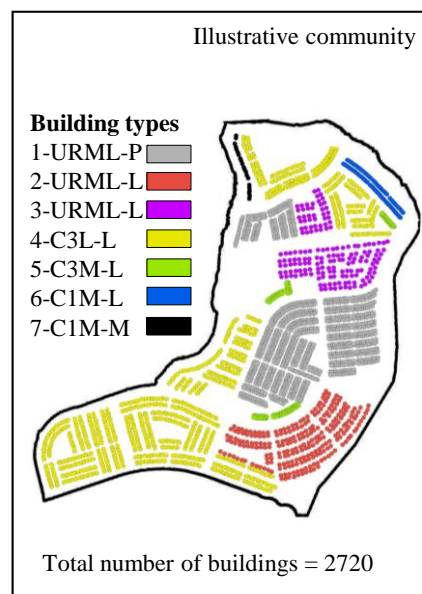


Figure 7-6 Illustrative community consisting of building communities.

To measure the performance of a community building portfolio under an earthquake hazard, three performance indicators are selected: (1) total repair cost incurred on a community because of an earthquake referred herein as risk performance indicator, (2) total downtime of a community as a measure of how long it will take to recover from a hazard, referred herein as a downtime performance indicator, and (3) total equivalent carbon emissions emitted as a result of damage to the community and recovery efforts, referred herein as a sustainability performance indicator.

In this illustrative example, a design hazard scenario is selected with a return period of 475 years, having 10% probability of occurrence in 50 years' service life. The selected hazard scenario will generate a peak ground acceleration of 0.33 g and is considered herein to assess the performance of a community. It is important to note that considering a complete hazard curve along with the relevant mean annual frequency of exceedances for hazard scenarios would provide a better evaluation of retrofit interventions on a community level. Furthermore, it is important to utilize the ground motion prediction equations for the spatial distributions of the intensity measure assessment for a given earthquake scenario. However, considering the small size of the considered illustrative community, uniform distribution of the design hazard scenario is considered, presuming the attenuation will not impact the intensity measures. Also, only a design hazard scenario is considered in this case study to illustrate the proposed framework but can be extended to consider a complete hazard curve. The next section highlights the performance of a community building portfolio under a given hazard without considering any mitigation measures.

7.5.1 Performance-Based Assessment

The first step is to assess the damage states of all the buildings in a community. A total of 4000 simulations are performed to determine the discrete damage states of a community building portfolio considering a probabilistic approach formulated in the methodology section. The resulting damage state distributions under a design hazard scenario are shown below. Four statistical moments are also extracted from the distributions, presented in Table 7-1. As shown, the mean value for buildings having negligible damage is 187.13, and complete damage is 981.57. It is noted that the

damage states have low skewness values and kurtosis values of around 3. The positive kurtosis values around 3 indicate that the damage state distributions are close to the normal distributions.

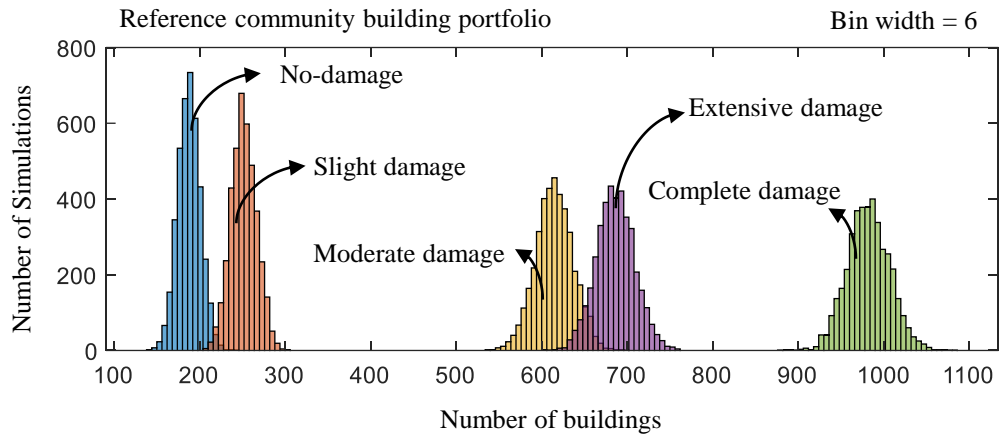


Figure 7-7 Damage states distributions of community building portfolio under given hazard.

Table 7-1 Statistical moments of damage states of community building portfolio given hazard.

Damage States	Mean (Buildings)	Standard Deviation	Skewness	Kurtosis
No-damage	187.13	13.11	0.023	2.996
Slight damage	251.05	14.79	0.051	2.877
Moderate damage	614.41	21.84	-0.012	3.058
Extensive damage	685.84	22.36	0.046	3.045
Complete damage	981.57	24.53	0.078	3.126

The geospatial distribution of damage states of a community building portfolio for a random simulation is shown in the following Figure for illustrative purposes. The simulation represents one of the numerous simulations performed as a part of the Monte Carlo simulation process. In the given simulation (i.e., simulation number 3274), the number of buildings having no damage are 206, and buildings with complete damage are 954 in number. These simulations are repeated and distributions of considered damage states are extracted accordingly.

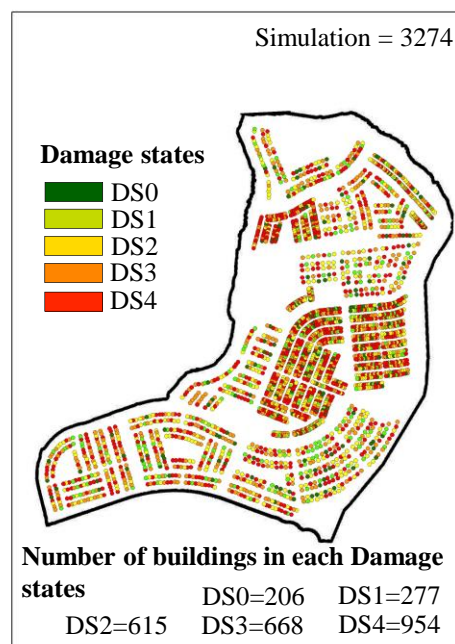


Figure 7-8 Damage states of community building portfolio under a given hazard.

The damage states are then correlated with the consequences to evaluate risk, downtime, and sustainability performance indicators. The consequences in terms of repair cost, downtime, and equivalent tons of kgCO₂ emissions are determined for each building in each simulation. For illustration, the geospatial distribution of consequences in terms of three performance indicators is shown in the following Figure for a random simulation. In this simulation, the number of buildings having repair costs up to

US\$15,000 is 1616, from US\$15,000–50,000 is 707, and from US\$50,000–200,000 is 397. The repair cost for the majority of the buildings is under US\$50,000 per building. Similar observations can be extracted for downtime and equivalent tons of carbon dioxide emissions.

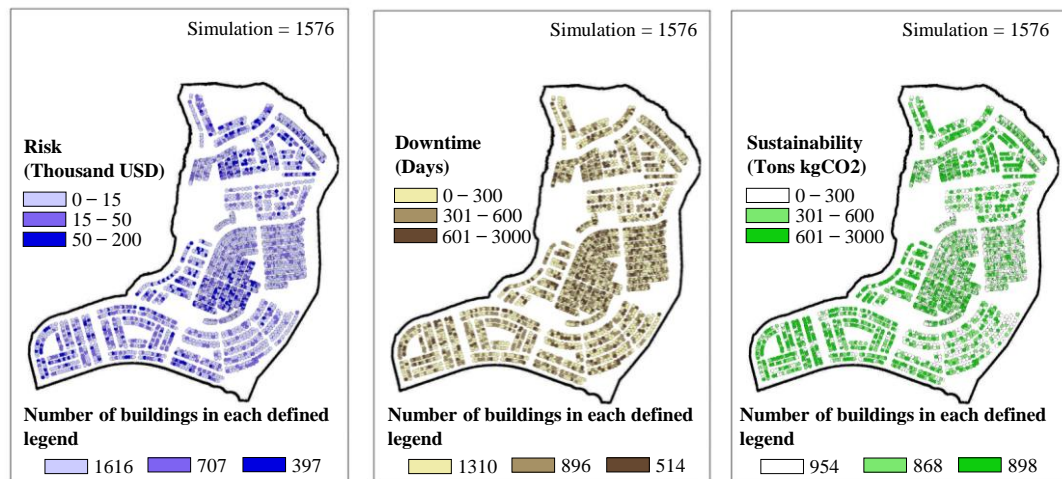


Figure 7-9 Performance indicators of community building portfolio under a given hazard scenario.

The number of simulations is repeated and distributions for three performance indicators on a community level are determined as shown in following Figure. The mean value for risk under a design hazard scenario is US\$63.3 million with a standard deviation of US\$1.42 million, the mean value for downtime is 1.05 million days with a standard deviation of 12,400 days, and the mean value for sustainability is 2.15 million tons of kgCO₂ emissions with a standard deviation of 73,700 tons of kgCO₂. The sustainability performance indicator has a positive skewness of 0.12 and the rest of the performance indicators have negligible skewness. However, all the performance indicators show positive kurtosis values ranging from 2.89–3.10 which shows the performance indicator values are almost normally distributed.

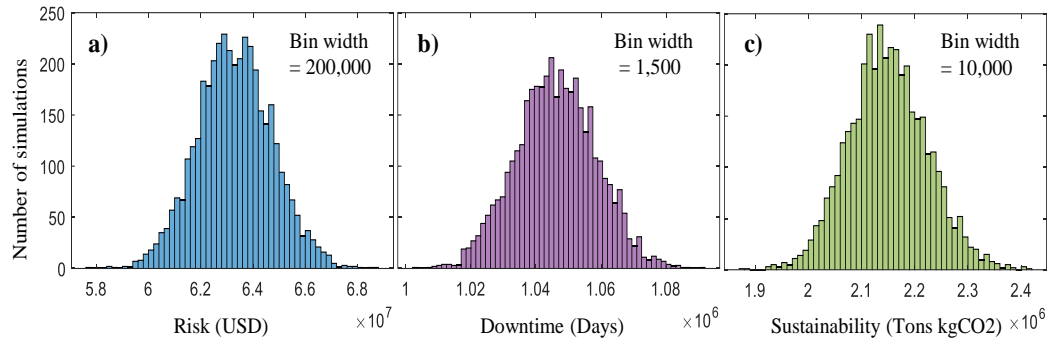


Figure 7-10 Performance indicator distributions of community building portfolio given hazard scenario for (a) Risk, (b) Downtime, and (c) Sustainability

7.5.2 Bi-Objective Evolutionary Optimization

The performance indicators provide total repair costs, an estimation of community recovery time, and total equivalent carbon dioxide emissions under an earthquake hazard scenario. Mitigation alternatives can be implemented to improve the performance of a community building portfolio under a given hazard. The decision-makers are mostly interested in the question related to how much cost is required to improve the required performance of a community. The bi-objective evolutionary optimization technique is utilized to determine retrofit programs which will provide information related to the investment costs needed for retrofitting a community to improve performance to a certain level. Note that the retrofitting buildings can give different performance levels depending upon the type of retrofit implemented and on how many buildings are retrofitted. This optimization technique can provide optimal performance improvements that can be achieved for given retrofit programs in terms of Pareto-optimal solutions.

The performance indicators are utilized as objectives to be optimized for given retrofit alternatives. The initial population with a population size of 20 individuals is selected with an optimization criterion of 20 maximum generations. The higher the number of individuals selected, the more data points will be generated in the Pareto-optimal solutions but as a result, the computational costs would increase. The selection criteria of individuals is based on generating enough data points to appropriately assess the Pareto-optimal solutions at reasonable computational costs. The search space consists of five options for each building which are randomly assigned to all the buildings in the initial population. Option one includes assigning a building with a no-retrofit alternative (i.e., building is not retrofitted), and options two to five consist of an increasing level of retrofit. The increasing level of retrofit would provide increasing performance and would also incur an increasing level of retrofit cost. The fragility functions for all the buildings are extracted from HAZUS (HAZUS, 2003), and the damage state and retrofit cost factors are selected based on the literature review (HAZUS, 2003; FEMA-547, 2006; FEMA-P695, 2009; Anwar and Dong, 2020). The damage state factors are multiplied by the mean values of fragility functions to update the fragility functions for different retrofit levels and retrofit cost factors are multiplied with the construction costs to evaluate retrofit costs. The considered damage state factors for five retrofit levels are 1, 1.27, 1.55, 2.11, and 2.79. Similarly, the considered retrofit cost factors for five retrofit levels are 1, 1.1, 1.15, 1.2, and 1.25. The selection criteria for the damage state factors and retrofit cost factors are based on previous studies conducted on the seismic retrofit of buildings (Anwar and Dong, 2020; Anwar et al., 2020). Nonetheless, the damage state factors and retrofit cost factors are utilized here for illustrative purposes only.

The next step is to evaluate the performance objectives of all the individuals and generate a new population by non-dominated sorting and crowding distances, and through selection, crossover, and mutation strategies discussed in the methodology section. The process is repeated for a new population until the optimization criterion is satisfied. At each generation, the performance of individuals keeps on improving given total retrofit costs and Pareto-optimal solutions can be extracted after the optimization criterion is satisfied.

The Pareto-optimal solutions for a random simulation number are shown in the following Figure for considered performance indicators. As shown, the performance indicators show high risk, downtime, and sustainability values for a reference community with no mitigation alternative implemented. For instance, in this simulation, if all the buildings are given a retrofit level one (i.e., if no mitigation alternative is applied), the risk, downtime, and sustainability values are US\$63.1 million, 1.06 million days, and 2.13 million tons of kgCO₂. Similarly, if all the buildings are retrofitted with the retrofit level five, the maximum performance of US\$9.33 million, 0.41 million days, and 0.3 million tons of kgCO₂ can be achieved. The retrofit cost to achieve this maximum performance level is US\$34.1 million.

Various combinations of retrofit levels on a community building portfolio would result in different levels of performance, and the bi-objective optimization approach is utilized to determine the retrofit-level combinations to achieve optimal performance given the least retrofit costs. For instance, an individual 12 in a population provides risk, downtime, and sustainability values of US\$35.8 million, 0.727 million days, and 1.2 million tons of kgCO₂ with a given retrofit cost of US\$17.5 million. This level of performance is achieved by retrofitting buildings with different retrofit levels

including retrofit level 1 (RL1) having 518 buildings, retrofit level 2 (RL2) having 583 buildings, retrofit level 3 (RL3) having 536 buildings, retrofit level 4 (RL4) having 553 buildings, and retrofit level 5 (RL5) having 530 buildings, accordingly. The determined Pareto-optimal solutions provide an increasing level of performance given increasing retrofit costs for different individuals.

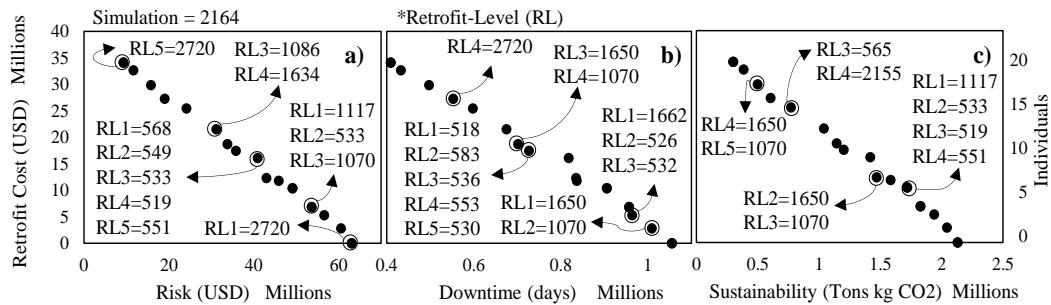


Figure 7-11 Pareto-optimal solutions of performance indicators against retrofit costs for (a) Risk, (b) Downtime, and (c) Sustainability

The uncertainties in the performance enhancement are considered by performing 4000 evolutionary optimization simulations and extracting information including buildings in different retrofit levels, performance indicators, and the required retrofit costs for an optimized population. The mean values of buildings in different retrofit levels for an optimized population are shown in the following Figure. Individual 1 refers to a case scenario of a community building portfolio where all the buildings are at retrofit level one, and individual 20 refers to a case scenario where all the buildings are at retrofit level five. The individuals in between refer to the buildings with different retrofit levels optimized to provide maximized performance objectives at a minimized retrofit cost. Finally, the community stakeholders and decision-makers can utilize the Pareto-optimal solutions and develop retrofit programs to satisfy the required performance of a community under a given hazard.

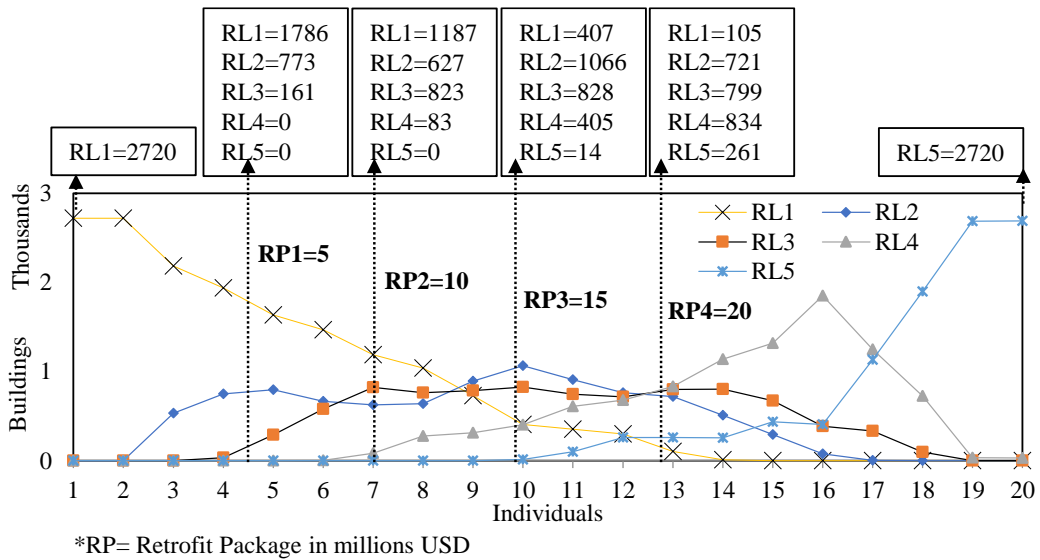


Figure 7-12 Mean values of buildings at different retrofit levels in a population along with considered four retrofit programs.

For illustration purposes, four retrofit programs (RPs) are extracted ranging from retrofit costs of US\$5–20 million. For instance, retrofit package 1 (i.e., US\$5 million cost for retrofitting community building portfolio) requires mean values of 1786 buildings in RL1 (i.e., no-retrofit required), 773 buildings in RL2, and 161 buildings in RL3. Similar observations for other retrofit programs can be made accordingly. The RLs represent mean value of buildings in different retrofit levels averaged over N simulations.

Finally, the distribution of performance indicators under four selected retrofit programs can be determined. For illustration, the statistical moments for the risk performance indicator under four retrofit programs are shown in Table 7-2. As shown, the total repair cost under a design hazard scenario without considering any mitigation alternative is US\$63.3 million which can be reduced to US\$56.78 million by applying a retrofit cost of US\$5 million. Similarly, the retrofit programs costing US\$10, 15, and

20 million would reduce the risk to US\$49.10, 41.74, and 32.34 million. The standard deviation for the risk performance indicator ranges between US\$1.04–1.42 million. In addition, negligible skewness is observed, and the kurtosis values are close to 3 which indicates the distribution is almost normally distributed.

Table 7-2 Statistical moments of risk performance indicator under considered retrofit programs.

Risk Performance Indicator	Mean (Million USD)	Standard Deviation (Million USD)	Skewne ss	Kurto sis
Without a retrofit program	63.30	1.42	0.057	3.03
Retrofit of 5 million USD	56.78	1.33	0.043	2.93
Retrofit of 10 million USD	49.10	1.22	-0.065	2.98
Retrofit of 15 million USD	41.74	1.44	-0.026	2.86
Retrofit of 20 million USD	32.34	1.04	0.211	3.23

Similar observations can be extracted for downtime and sustainability performance indicators given retrofit programs. For instance, implementing the considered four retrofit programs would result in improving mean downtime values from 1.05 million days to 0.977, 0.893, 0.816, and 0.705 million days, and mean sustainability values would improve from 2.15 million tons kgCO₂ to 1.92, 1.65, 1.40, and 1.07 million tons of kgCO₂. The standard deviation for downtime ranges from 11,420–16,930 days and for sustainability ranges from 47,850–73,690 tons of kgCO₂. The kurtosis values for downtime and sustainability range from 2.89–3.26, indicating nearly normal distributions.

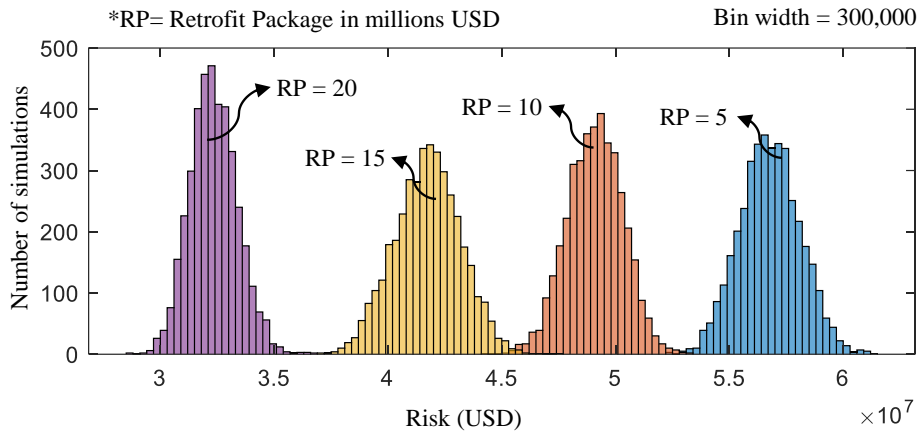


Figure 7-13 Distributions of risk performance indicator under four retrofit programs.

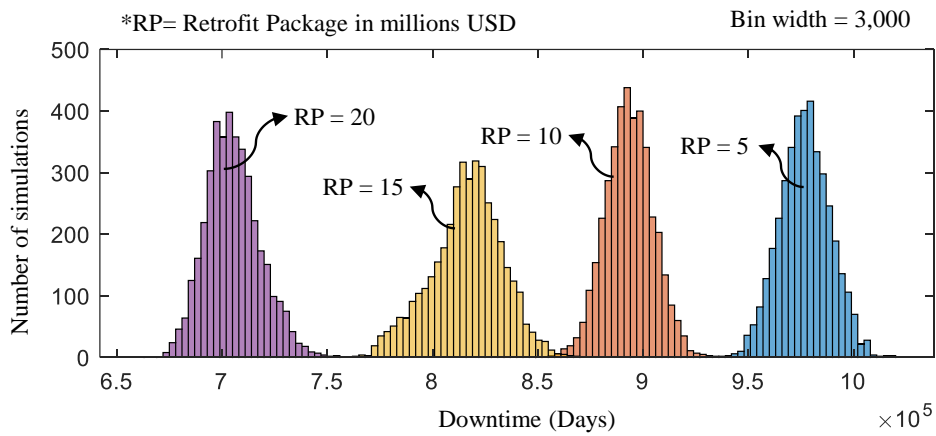


Figure 7-14 Distributions of downtime performance indicator under four retrofit programs.

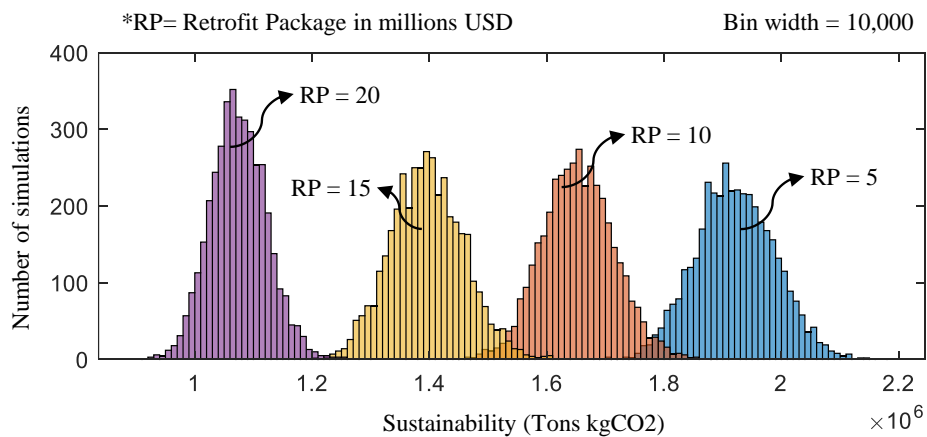


Figure 7-15 Distributions of sustainability performance indicator under four retrofit programs.

7.6 Conclusions

This chapter proposed a performance-based bi-objective optimization framework for community building portfolios considering multiple performance indicators. In addition, the uncertainties in the process were incorporated by utilizing the Monte Carlo approach. The following conclusions can be drawn based on the proposed framework and illustrative example.

1. The proposed bi-objective retrofit optimization framework considered risk, downtime, and sustainability performance indicators for assessment and enhancement of community performance under a designed seismic hazard scenario. The proposed framework optimized the performance objectives for given pre-hazard mitigation alternatives considering uncertainties and provided the decision-makers with retrofit programs to enhance community performance for given retrofit costs.
2. The distributions of discrete damage states and the performance indicators showed negligible skewness with kurtosis values close to three. This showed the distributions were almost normally distributed. The normal distributions were also observed for the retrofit programs extracted after performing performance-based evolutionary optimization.
3. Pareto-optimal solutions were determined by utilizing bi-objective optimization which provided optimal solutions for the considered performance indicators

against the retrofit cost. The number of buildings required to be retrofitted at different retrofit levels to achieve performance enhancements for given retrofit costs was also determined. For instance, in a random simulation, to achieve risk, downtime, and sustainability performance of US\$35.8 million, 0.727 million days, and 1.2 million tons of kgCO₂ emissions, a retrofit cost of US\$17.5 million is required. To achieve this level of performance, the number of buildings needed to be retrofitted in the five retrofit levels ranging from 1–5 were 518, 583, 536, 553, and 530.

4. For an illustration of the proposed framework, four retrofit programs were extracted ranging from US\$5–20 million and the resulting performance enhancements along with the number of buildings required to be retrofitted at different retrofit levels were determined. For instance, by applying a retrofit program of US\$20 million, the mean risk, downtime, and sustainability performance values were reduced to 48.91%, 32.59%, and 50%. Furthermore, to achieve this level of performance enhancement, the mean number of buildings required to be retrofitted ranging from retrofit levels 1–5 were 105, 721, 799, 834, and 261.

CHAPTER 8 BAYESIAN OPTIMIZATION AND DECISION-MAKING OF COMMUNITY BUILDINGS

8.1 Introduction

The performance of community building portfolios under extreme events is increasingly being assessed in terms of socioeconomic and environmental consequences. These multiple consequences are expensive to evaluate, uncertain in nature, and require an efficient optimization and decision-making tool for possible performance enhancements on a community level. In this chapter, an efficient multi-objective performance-based optimization and decision-making framework is proposed to assess and enhance the performance of community building portfolios under uncertain consequences. The proposed approach includes (1) performance-based black-box to evaluate the socioeconomic and environmental consequences given community building portfolios by considering all the possible hazard scenarios, (2) surrogate-based multi-objective optimization to efficiently approximate the Pareto-optimal solutions by exploiting Gaussian process models, spectral sampling, non-dominated crowding and sorting, and hyper improvements, among others, and (3) utility theory-based decision-making of a community building portfolios considering multiple performance-objectives over an entire hazard curve and under different risk attitudes. The proposed methodology is illustrated on community building portfolio under seismic hazards of varying intensities and occurrence probabilities. A performance-based black box is utilized along with a proposed optimization technique to assess community-level

consequences. Finally, the expected utility for Pareto-optimal solutions is assessed and discussed for possible performance enhancements and decision-making.

8.2 Proposed optimization and decision-making framework

The proposed multi-objective surrogate-based optimization and decision-making framework for community building portfolios under uncertain consequences and risk attitudes is shown in Figure 8-1. The framework is divided into three main parts: (1) performance assessment, (2) surrogate-based optimization, and (3) decision-making. The performance-based assessment part considers a range of seismic hazard scenarios and evaluates uncertain socioeconomic and environmental consequences in terms of casualties, repair costs, repair time, carbon emissions, and embodied energy. To reduce uncertain consequences on a community portfolio level, a surrogate-based optimization is proposed that efficiently optimizes the retrofit selection for all the buildings in a community, and consequently, Pareto-optimal solutions are determined for the considered performance objectives. Finally, a utility theory approach is utilized, considering the risk perceptions of the decision-makers to extract ideal solutions from the Pareto-optimal solutions for possible decision-making under varying degrees of risk perceptions of the decision-makers.

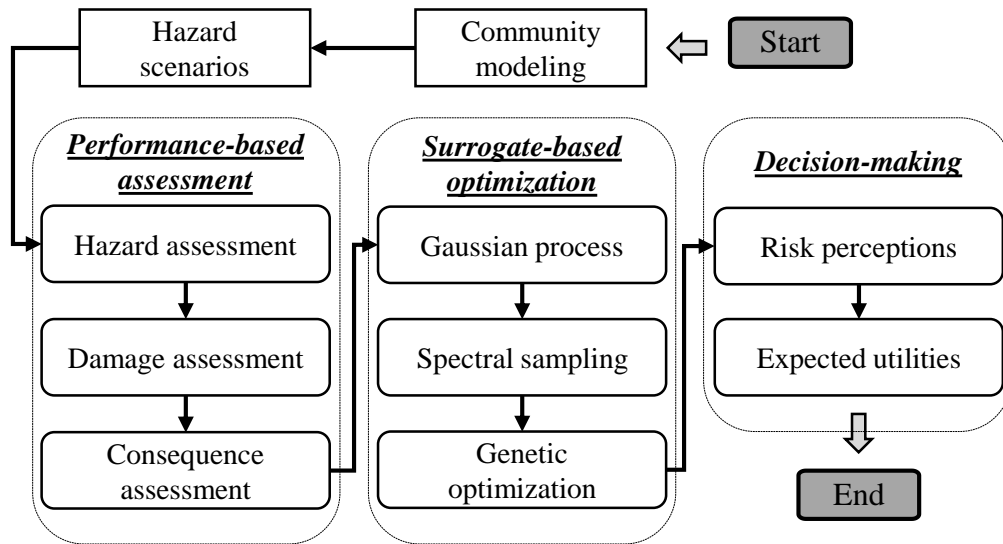


Figure 8-1 Proposed efficient multi-objective performance-based optimization and decision-making framework for community building portfolios under uncertain consequences and risk attitudes

The performance-based assessment part consists of three main steps: (1) hazard assessment, (2) damage assessment, and (3) consequence assessment. The hazard assessment evaluates the intensity measures for all the buildings in a community considering a range of hazard scenarios, also accounting for the varying probability of occurrences and intensity measures. Then, the damage assessment step is utilized to evaluate the damage imparted to the buildings given the hazard. Finally, the damage to the buildings is converted into socioeconomic and environmental consequences that provide a meaningful measure for the decision-makers and key stakeholders for taking necessary actions if any.

The surrogate-based optimization part also consists of three main steps: (1) Gaussian process modeling, (2) spectral sampling, and (3) genetic optimization. Initially, the proposed surrogate-based optimization algorithm randomly assigns the retrofit solutions to all the buildings in a community and creates a scenario referred to

herein as an individual. Several individuals are originally established and the total retrofit costs and uncertain consequences are evaluated by utilizing the performance-based assessment part.

The first step is to build Gaussian process models for all the considered objectives that include: (1) uncertain consequences and (2) retrofit costs on a community level. The Gaussian process models are established by utilizing the considered individuals. The Gaussian process models are utilized as surrogates due to their effectiveness and ability to predict uncertainties by providing distributions of responses instead of a single number as an output. This aspect could aid in quantifying the uncertain consequences and also act as a tool for uncertainty propagation in the various steps of the proposed framework. Furthermore, the Gaussian process has elegant stochastic properties, i.e., apart from providing the predicted values at unexplored points but also providing the variance of the predicted value. Many active learning functions are developed based on the mean value and variance at unexplored points, while other surrogate models can hardly provide statistical information. Also, the Gaussian process models can be applied in a variety of settings and enable efficient hyper parameter selection as compared to other available machine learning models. However, Gaussian process models may need fine-tuning of kernels which may require considerable work. Also, the selection of priors affects the computational efficiency and overall performance of the model along with the hyper parameters that need to be considered. Nonetheless, the Gaussian process models are effective tools to model uncertainties

After Gaussian process modeling, the sample functions for all the objectives are established by utilizing the proposed spectral sampling techniques, providing a computationally inexpensive surrogate replacement of the expensive performance-

based black-box. Finally, genetic optimization is performed to evaluate the Pareto-optimal solutions by utilizing the established surrogate. The number of individuals is increased at each iteration and the surrogates are improved by utilizing the proposed hyper improvement indicator, and hence the Pareto-optimal solutions are improved at each iteration subsequently. After the required number of iterations, the approximate Pareto-optimal solutions for a multi-objective problem can be extracted.

The last part of the proposed framework consists of decision-making and aims to assess the ideal solutions among the Pareto-optimal solutions by utilizing the utility decision theory. The ideal solutions are the solutions among the Pareto-optimal solutions which are selected by the decision-makers considering their risk preferences. The first step in this part consists of evaluating the utility of all the considered objectives by considering the risk perceptions of the decision-makers. Finally, an expected utility can be determined for all the Pareto-optimal solutions considering all the objectives. The particular steps involved in the performance-based assessment, surrogate-based optimization, and decision-making parts are further explained in the subsequent sections.

8.3 Performance-based expensive black-box

The performance-based assessment methodology is utilized to assess the performance of a community building portfolio given vulnerability, value, and exposure (Yamin et al., 2017; Qian and Dong, 2022a). The performance-based module serves as a black-box for the proposed surrogate-based optimization in which community building portfolios related data is provided and performance is extracted as a result. The performance of community building portfolios to extreme events can be improved by

implementing pre-hazard retrofit alternatives. The black-box provides performance in terms of multiple performance objectives covering the entire range of probable seismic hazard scenarios and as a result, it is computationally expensive to evaluate. The community-level performance assessment requires developing a hazard curve, assessing damages, and evaluating consequences over an entire community.

The damage to all the buildings in a community is assessed in terms of discrete damage states. The discrete damage states can be defined as slight, moderate, extensive, and complete damage states and the exact definition of a particular damage state given a structural system can be observed in the HAZUS documentation (HAZUS, 2003). Each damage state translates the intensity measure into the probability of exceeding a particular damage state by utilizing the fragility function (Bao et al., 2019). The intensity measures can be extracted from hazard curve which provides a relationship of mean annual frequency of exceedance for a given intensity measure (Dong and Frangopol, 2016a). The probability of exceedance of all the damage states can then be translated to discrete damage states of community building portfolios (Hashemi et al., 2019; Chen et al., 2021).

The damage state of a building provides information related to the extent of damage which can then be utilized to evaluate consequences by extracting information such as how much material is required for repair, and what are the associated socioeconomic and environmental consequences associated with it (Giouvanidis and Dong, 2020). The associated consequences such as repair cost, downtime, and equivalent carbon emissions are evaluated by utilizing consequence functions and more information can be found in (Anwar et al., 2020).

The consequences for the entire hazard curve can be determined and integrated over a hazard curve to evaluate the expected annual consequences (EAC). The EACs provide consequences considering all the possible hazard scenarios considering their respective probability of occurrences. The resulting performance indicator can then be determined by accumulating the consequences or expected annual consequences of all the buildings in a community.

8.4 Efficient multi-objective surrogate-based optimization

Approximating the Pareto-optimal solutions from a black-box considering multiple performance objectives requires establishing a computationally inexpensive surrogate model for each objective function, spectral sampling from an established surrogate model, finding the Pareto-optimal front from the sampled functions, and evaluating the next point of query from the black-box by utilizing an acquisition function providing largest improvement in the hyper improvement indicator. In this chapter, an efficient multi-objective optimization technique is developed for community building portfolios by first establishing a computationally inexpensive surrogate model and then performing non-dominated sorting and crowding distancing for approximating a Pareto-optimal front, and finally utilizing hyper improvement indicator to evaluate the next query point from performance-based black-box function. The processes utilized in the proposed surrogate-based optimization part is shown in Figure 8-2.

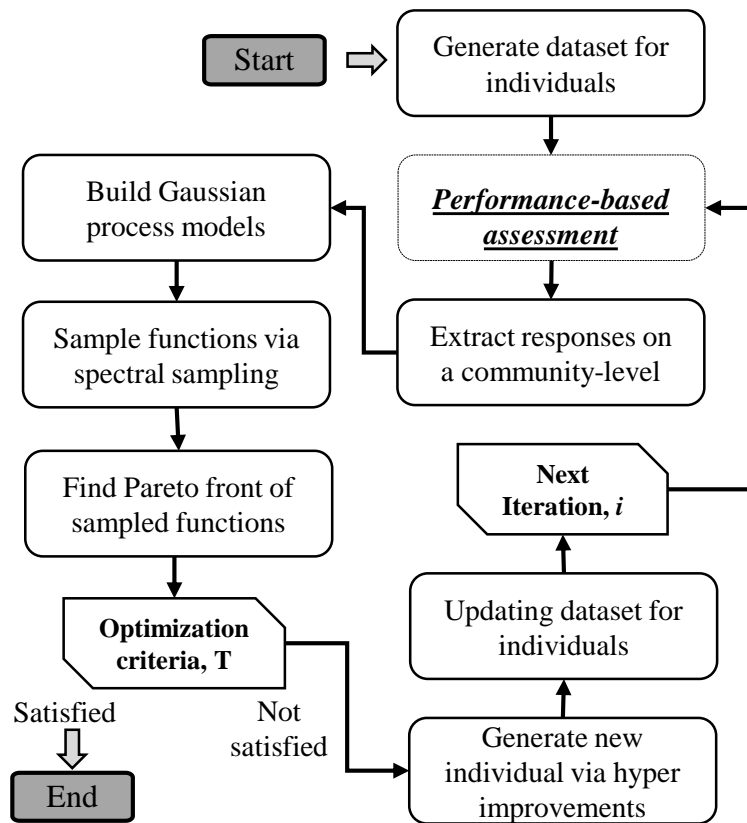


Figure 8-2 Proposed methodology for efficient surrogate-based optimization for community building portfolio

8.4.1 Generating initial dataset for individuals

The first step is to randomly generate an initial dataset for given number of individuals. The dataset for each individual includes information related to the community building portfolio including structural system, number of stories, operational use, and type of retrofit implemented if any, among others. The randomness in the dataset is related to the type of retrofit application on buildings if any. Let n be the number of individuals with the initial data set generated for instance by utilizing the Latin hypercube design (Stein, 1987). Let $X = [x_1, \dots, x_i, \dots, x_n]$ is the initial number of individuals that are utilized to query an expensive objective function $g_j(x)$, where $j = 1, \dots, m$ are the

performance objectives. The expensive objective function is queried by utilizing the performance-based assessment part which serves as a black-box in the considered optimization problem. The resulting responses for each objective function in terms of retrofit costs and consequences, against the considered individuals, are represented as $Y = [y_j^1, \dots, y_j^n]$. These corresponding responses extracted from expensive performance-based black-box are then utilized to build a Gaussian process model.

8.4.2 Building a Gaussian process model

The Gaussian process model is built in each iteration given the individuals and the corresponding responses. Let the total number of individuals is $X^i = [x_1, \dots, x_n, x_{n+1}, \dots, x_{n+i}]$ at iteration i , and the resulting responses for each objective function j is $Y_j^i = [y_j^1, \dots, y_j^n, y_j^{n+1}, \dots, y_j^{n+i}]$. The Gaussian process model is trained for each objective Y_j^i to evaluate $GP_j^i(m^i, k^i | X^i, Y_j^i)$.

The Gaussian process generates data that follows a multivariate Gaussian distribution over functions. It requires formulating a prior which is independent of the observations from the black box function, and the posterior which incorporates the Gaussian process fitted with the observations from black-box (Schulz et al., 2018). The following sub-sections briefly explain the process.

8.4.2.1 Prior of the Gaussian process

The Gaussian process can be defined by a mean and a covariance function as:

$$m(x) := E[f(x)] \quad 8-1$$

$$k(x, x') := E[(y(x) - m(x))(y(x') - m(x')))] \quad 8-2$$

where $m(\cdot)$ is the mean function, $k(\cdot)$ is the covariance function, $x, x' \in R^d$ are arbitrary input vectors, $E[\cdot]$ is the expectation over the function $f(\cdot)$, and $y(\cdot)$ consists of points distributed as a Gaussian process represented as:

$$y(x) \sim GP(m(x), k(x, x')) \quad 8-3$$

where GP denotes Gaussian process over points observed from function $f(\cdot)$ having input vectors x . The mean represents the average value from a function and covariance represents the joint variability of any two values from a function computed at corresponding inputs. The mean of the function is set to zero, and the covariance function is utilized to determine the properties of fitted functions (Rasmussen, 2003b).

8.4.2.2 Posterior of the Gaussian process

The prior of the Gaussian process is independent of the observations from the performance-based black-box function. The prior is updated by utilizing the training data set $X = \{x_1, \dots, x_i, \dots, x_n\}$ having n data points, where each $x_i = [x_{i1}, \dots, x_{iz}]^T$ is a z -dimensional vector. The observations y_i from the black-box function is obtained at x_i to formulate set $Y = \{y_1, \dots, y_n\}$ and the vector $y = [y_1, \dots, y_n]^T$. The posterior of the Gaussian process can then be found based on Bayes' rule as:

$$f(x) \sim GP(m(x), k(x, x')|X, Y) \quad 8-4$$

With

$$m(x)|X, Y = \Sigma(x, X) \Sigma^{-1} y \quad 8-5$$

$$k(x, x')|X, Y = k(x, x') - \Sigma(x, X) \Sigma^{-1} \Sigma(x, X)^T \quad 8-6$$

Where

$$\Sigma = [k(x_i, x_j)]_{nn} \in R^{nn} \quad 8-7$$

$$\Sigma(x, X) = [k(x, x_1), \dots, k(x, x_n)] \in R^{1n} \quad 8-8$$

8.4.2.3 Training of hyper parameters

The hyper parameters are inferred from the data by utilizing the maximum posteriori estimate or maximum likelihood estimate in the case of small data sets. In this chapter, a maximum posteriori estimate is selected due to its better performance as compared to the latter (Sundararajan and Keerthi, 2001). The hyper parameters defining the Gaussian process are represented as:

$$\xi = [\log(\lambda_1), \dots, \log(\lambda_d), \log(\sigma_f), \log(\sigma_n)] \quad 8-9$$

where λ_i are the length scales of the input variable, and σ_f^2 are the output variance. The independent Gaussian distributions are assumed as prior distributions on the log-transformed hyper parameters as:

$$\xi_i \sim \mathcal{N}(\mu_i, \sigma_i^2) \quad 8-10$$

where μ_i is the mean, and σ_i^2 is the variance of the prior Gaussian distribution. The maximum posteriori estimate likelihood is determined as:

$$\mathcal{L}(\xi) = -\frac{1}{2}\log(|\Sigma|) - \frac{1}{2}y^T \Sigma^{-1} y - \frac{n}{2}\log(2\pi) + \sum_i(-\frac{1}{2}\log(2\pi) - \frac{1}{2}\log(\sigma_i^2) - \frac{1}{2\sigma_i^2}(\xi_i - \mu_i)^2) \quad 8-11$$

Finally, the maximum posteriori estimate for hyper parameters is determined by the optimization problem as:

$$\xi_{MAP} \in \arg \max_{\xi} \mathcal{L}_{MAP}(\xi) \quad 8-12$$

8.4.3 Sample functions via spectral sampling

The spectral sampling is utilized to sample m distinct functions $[f_1^i(x), \dots, f_m^i(x)]$ extracted from independent Gaussian process models for each objective. These Gaussian process model samples are computationally inexpensive as compared to expensive black-box and are utilized for multi-objective optimization to extract approximate Pareto-optimal solutions.

8.4.3.1 Spectral sampling from the Gaussian process model

Hernández-Lobato et al. (Hernández-Lobato et al., 2014) initially proposed a method to sample an approximate analytical function from the Gaussian process which can be approximated by utilizing Fourier dual $S(\omega)$ referred as spectral density of stationary covariance function k , expressed as:

$$k(x, x') = \alpha \iint_{\mathbb{R}^d} e^{-j\omega^T(x-x')} p(\omega) d\omega = \alpha E_{\omega}[\xi(x)\overline{\xi(x')}] \quad 8-13$$

where $p(\omega)$ is the associated normalized probability density determined as $p(\omega) = s(\omega)/\alpha$, α is the proportionality constant determined as $\alpha = \int s(\omega)d\omega$, the vector ξ can be determined as $\xi(x) = \sqrt{2\alpha/M}\cos(Wx + b)$, where M is the number of Monte Carlo samples, $[W]_i \sim p(\omega)$, and $[b]_i \sim U(0,2\pi)$.

Hence, the Gaussian process prior can be approximated as:

$$f(x) = \xi(x)^T \theta \quad 8-14$$

where θ is the multivariate Gaussian distribution $\theta \sim \mathcal{N}(0, I)$. Given the data in terms of $\theta \sim \mathcal{N}(m, V)$, where $m = (Z^T Z + \sigma_n^2 I)^{-1} Z^T y$, and $V = (Z^T Z + \sigma_n^2 I)^{-1} \sigma_n^2$, the approximate posterior of the Gaussian process can be approximate as:

$$f^{(i)}(x) = \xi^{(i)}(x)^T \theta^{(i)} \quad 8-15$$

where I is an identity matrix, and $[Z]_i = \xi(x_i)$ are stacked random vectors of ξ given inputs of data.

8.4.4 Evaluating Pareto-optimal solutions from sampled functions

The sampled analytical functions can then be utilized to economically evaluate the approximate Pareto-optimal solutions. Any evolutionary optimization technique can be utilized to allow convergence to the Pareto-set of Gaussian process at a given iteration (Fister Jr et al., 2013). In this chapter non-dominated sorting and crowding distancing algorithm is utilized to evaluate Pareto-set at each given iteration (Deb et al., 2002). The process requires evaluating dominated and non-dominated solutions by utilizing

the tournament selection, dominance depth method, and crowding distance algorithm (Katoch et al., 2021). This allows providing rankings for each individual in a population given each generation within an iteration. The convergence of Pareto-set against Gaussian process samples at each iteration is achieved by utilizing selection, crossover, and mutation strategies (Islam et al., 2011). Finally, after the given number of generations, the Pareto-set converged against Gaussian process samples is extracted.

8.4.5 Generating new points to query expensive black-box function

Since generating a new point from the black-box is expensive, it is essential to match the probability that the next sampled data will provide a Pareto optimal point. In this chapter, a hyper improvement indicator is utilized to sample the next point for querying expensive black-box.

The hyper improvement indicator measures the region between a selected reference point and non-dominated solutions (Beume et al., 2009). The hyper improvement indicator is utilized herein to select the next sampling point from a performance-based expensive black-box function. The larger the region from the previous iteration, the higher the value of hyper improvement indicating higher convergence and better performance between two iterations. Mathematically, the hyper improvement indicator is represented as (Guerreiro et al., 2020):

$$HV(\wp, \mathbf{r}) = \Lambda(\cup_{p \in \wp} [p, \mathbf{r}]) \quad 8-16$$

where $HV(\wp, \mathbf{r})$ denotes the hyper improvement indicator given non-dominated Pareto front \wp at a reference point \mathbf{r} , $\Lambda(\cdot)$ is the Lebesgue measure, $[p, \mathbf{r}]$ is a box delimited below by $p \in \wp$ and above by \mathbf{r} .

Let \wp^i is a converged Pareto-front given iteration i , and current reference point \mathbf{r}^i , the next sample point is to be queried such that it will give maximum hyper improvement ΔHV represented as:

$$x_{n+i+1} \in \arg \max \Delta HV(y_C, \wp^i, \mathbf{r}^i) \quad 8-17$$

where y_C is the set consisting of sampled functions utilizing spectral sampling, and hyper improvement is $\Delta HV(y_C, \wp^i, \mathbf{r}^i) = HV(\wp^i \cup \{y_C\}, \mathbf{r}^i) - HV(\wp^i, \mathbf{r}^i)$. After the sample point is queried, the whole process is repeated to approximate the Pareto-set in the next iteration.

8.4.6 Updating the dataset of individuals

Finally, the dataset is updated with the identified next query point x_{n+i+1} and the resulting response from $g_j(x_{n+i+1})$, such that $X^{i+1} = [x_1, \dots, x_n, x_{n+1}, \dots, x_{n+i}, x_{n+i+1}]$ and $Y_j^i = [y_j^1, \dots, y_j^n, y_j^{n+1}, \dots, y_j^{n+i}, y_j^{n+i+1}]$. The process is repeated with the next iteration $i = i + 1$, until the maximum number of function evaluations is reached and an approximate Pareto-optimal solution is extracted.

8.5 Utility Decision Theory under Uncertainty

The approximate Pareto-optimal solutions provide the performance of community building portfolios in terms of multiple performance objectives. These performance objectives are then utilized to evaluate the expected utility for decision-making under uncertain consequences. The expected utility is determined against the total retrofit cost

of community building portfolios under different risk perceptions. Finally, the ideal solutions can be extracted from the approximate Pareto-optimal solutions.

In community building portfolios under hazard, the cost-benefit analysis provides a ranking of solutions by comparing the mitigation costs and repair costs. However, there are additional factors to consider while making a decision. First, the uncertainties in each step of performance assessment make it difficult to provide an accurate estimation of mitigation and repair costs (Qian and Dong, 2022b). There also exist uncertainties related to the probability of occurrence of an extreme event, the intensity, and frequency of its occurrence (Guo et al., 2022). Also, the considered performance objectives may be different and cannot be directly utilized for decision-making (Mosalam et al., 2018; Asadi et al., 2019). Furthermore, the risk perceptions of the decision-makers under uncertain consequences may affect the cost and benefit estimations (Tversky and Kahneman, 1992; Qin, 2022).

In the context of decision-making under risk perceptions, utility decision theory has been widely utilized. This theory postulates that the decision-makers are rational and select alternatives with maximum utility. The maximum utility is determined by considering multiple performance objectives with a utility function to provide an expected utility value. Mathematically, the expected utility for multiple performance objectives can be determined as:

$$E(U) = \sum_{j=1}^m u(p_j)w_j \quad 8-18$$

where $u(\cdot)$ is the utility function, w_j is the relative importance of the performance objective j , p_j is the j th performance objective, and m is the total number of considered performance objectives such that:

$$\sum_{j=1}^m w_j = 1 \quad 8-19$$

$$p_j \in p (j = 1, 2, \dots, m) \quad 8-20$$

The utility function provides utility for a given performance objective as a subjective evaluation of the decision-maker considering its risk perception. The utility function can be evaluated by utilizing an increasing continuous function as:

$$u(p_j) = \frac{1}{1-e^{-\gamma}} [1 - e^{-\gamma(1-p_j/p_{max})}] \quad 8-21$$

where γ is the shape parameter with $\gamma = 0$ for risk-neutral attitude, $\gamma > 0$ for risk-averse, and $\gamma < 0$ for risk-seeking attitude, p_{max} is the maximum value for a mitigation cost value for normalization purposes.

8.6 Illustrative example

The proposed surrogate-based optimization and decision-making framework is illustrated on a community building portfolio mostly dominated by unreinforced masonry and masonry-filled reinforced concrete structures. The building definitions such as building types, code levels, and building heights, among others are as per HAZUS (Kircher et al., 2006) as shown in Figure 8-3 along with the hazard curve and extracted four hazard scenarios with the probability of occurrences of 50%, 10%, 5%, and 2% considering 50 years of service life of buildings.

It is important to note that different hazard scenarios provide different socioeconomic and environmental consequences. Hence, it is essential to estimate the consequences by taking into account the entire possible hazard scenarios and by also

considering their mean annual frequency of exceedances. These socioeconomic and environmental consequences provide community-level performance objectives which stakeholders can utilize to assess the overall performance of community building portfolios over an entire hazard curve. More information related to these socioeconomic and environmental consequences and expected annual consequences can be found in (Anwar et al., 2020) and is utilized for the surrogate-based optimization and decision-making explained in the subsequent sub-sections.

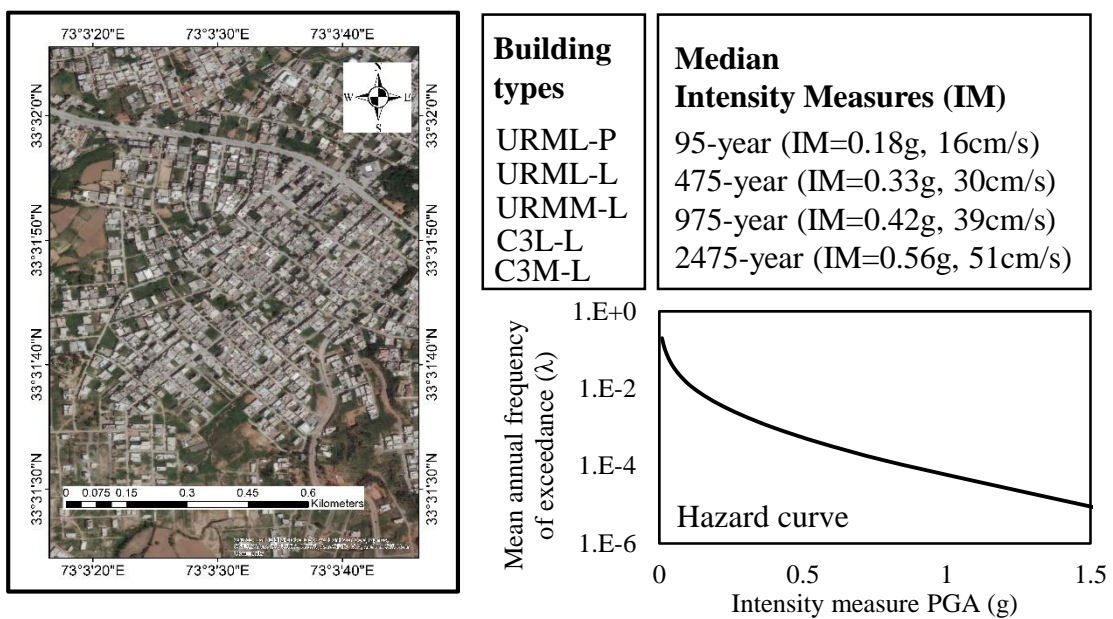


Figure 8-3 The community building portfolio with different structural systems under seismic hazard

In this illustrative example, six performance objectives are considered including retrofit costs, casualties, repair costs, repair time, equivalent carbon emissions, and embodied energy. These performance objectives will provide a holistic understanding of the performance of community building portfolios under seismic hazard scenarios. The considered performance objectives are assessed by utilizing the performance-based assessment methods which also serve as a black-box in the optimization problem. Then,

the selection of the best retrofit alternatives for all the buildings in a community building portfolio providing maximum performance given the least retrofit costs is achieved by utilizing the multi-objective surrogate-based optimization. Finally, the Pareto-optimal solutions are extracted and utilized for decision-making under risk perceptions. The subsequent subsection discusses the performance-based expensive black-box to assess the performance of community building portfolios.

8.6.1 Performance-based expensive black-box

The performance-based assessment requires assessing the damage state of each building given the intensity measures which are then correlated with the socioeconomic and environmental consequences. The methodology utilized to evaluate the discrete damage states, total damaged materials, and resulting consequences along with the relevant data required can be found in (Kircher et al., 2006; Anwar and Dong, 2022). The performance-based black-box will provide consequences given the intensity measures, fragility relationships, and consequence functions for the given community building portfolios.

As an illustration, the probability density functions for the repair cost consequence on a community-level under four hazard scenarios are shown in Figure 8-4, and mean repair costs for all the considered buildings in a community are shown in Figure 8-5. As shown, the mean repair costs under considered four hazard scenarios are 20.15, 48.58, 61.25, and 75.27 million USD with a standard deviation of 3.99, 5.68, 5.56, and 4.82 million USD. The repair costs indicate the amount of monetary value required during the repair works of the damaged buildings after an earthquake event. For instance, in the case of a design hazard scenario, it would mean that there is a 50%

probability that the community will require at least 48.58 million USD for the repair works of damaged buildings to bring the community building portfolios back to a pre-hazard state.

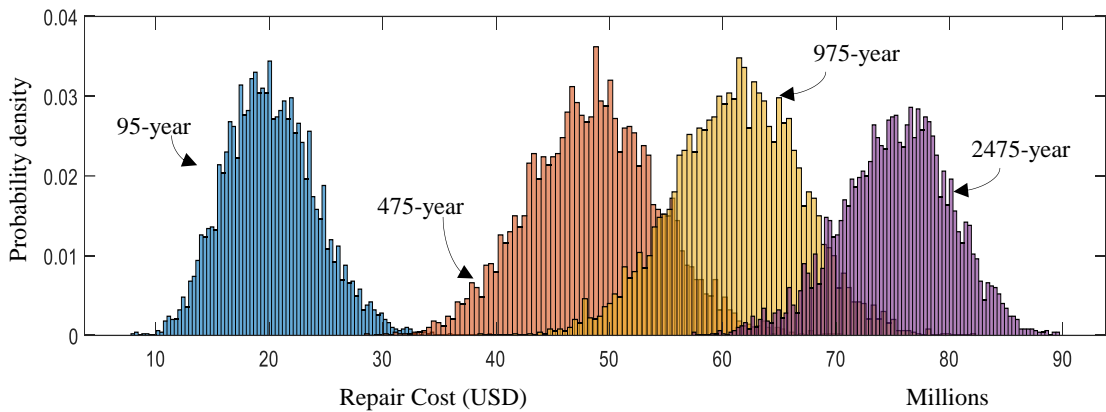


Figure 8-4 The probability density functions of the repair costs under four hazard scenarios

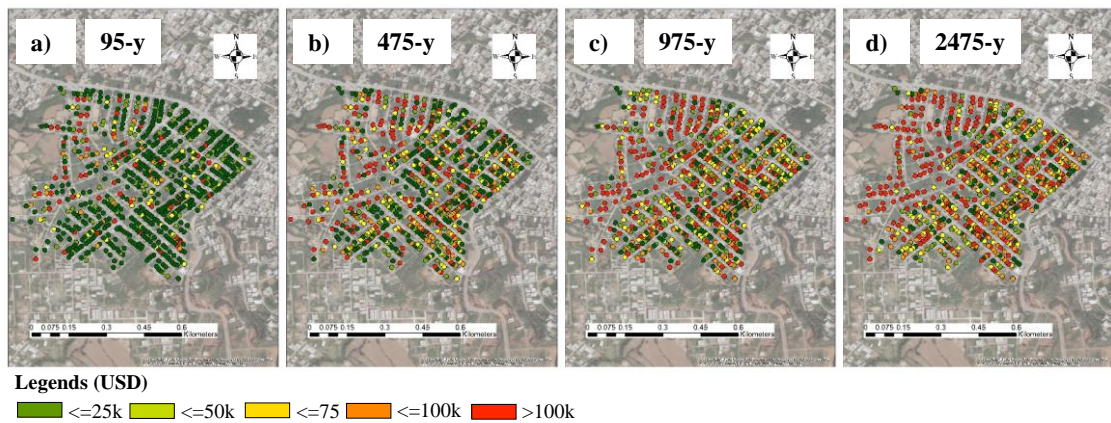


Figure 8-5 Community building portfolios repair costs under hazard scenario of (a) 95-year, (b) 475-year, (c) 975-year, and (d) 2475-year

Similar observations can also be extracted for other socioeconomic and environmental consequences. For illustration, the cumulative distribution functions for casualties, repair costs, equivalent carbon emissions, and embodied energy under four

hazard scenarios are shown in Figure 8-6. Another important performance indicator is related to the recovery of the community building portfolios and can be extracted based on the damage condition of a building during the investigated time. As an illustration, the number of buildings repaired or still in damaged condition during the investigated time after a design hazard scenario is shown in Figure 8-7. This can also be translated into the percentage of buildings repaired during the investigated time as shown in Figure 8-8 for four hazard scenarios. The community building portfolios are considered to be recovered from a hazard event after at least 90% of the buildings are repaired to the pre-hazard state. In the case of four hazard scenarios, the community building portfolios are considered recovered from an extreme event at 468, 711, 752, and 789 days during the investigated time after an earthquake event.

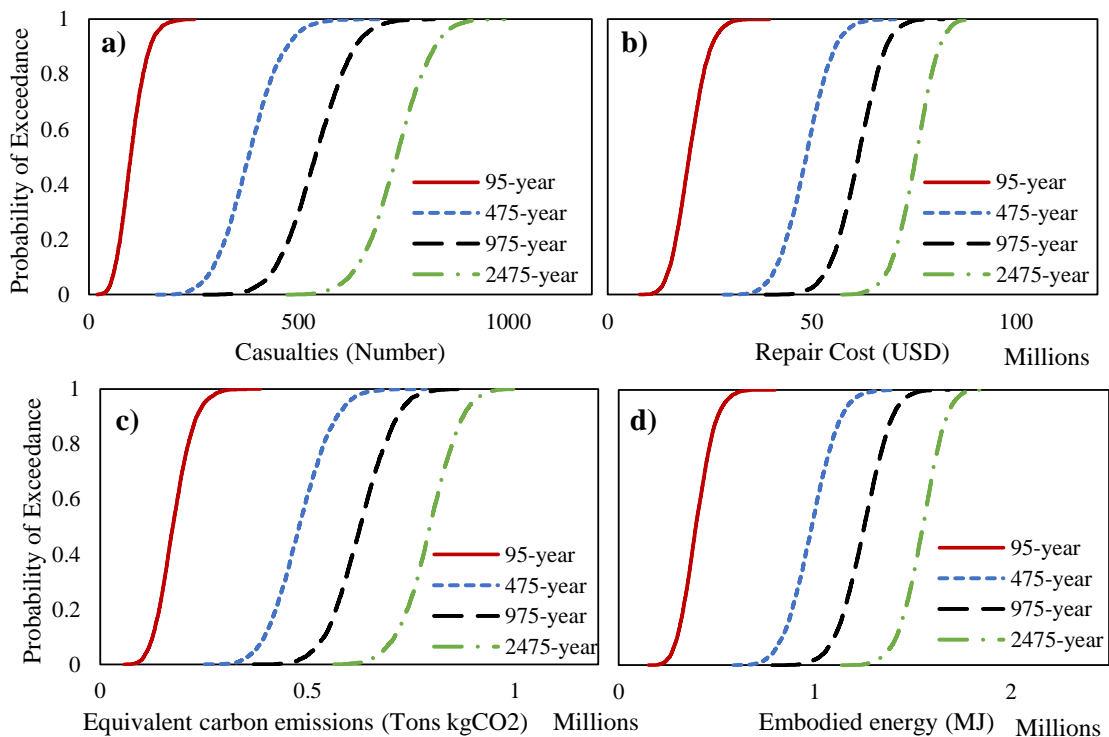


Figure 8-6 Cumulative distribution functions of community building portfolios for (a) casualties, (b) repair costs, (c) equivalent carbon emissions, and (d) embodied energy

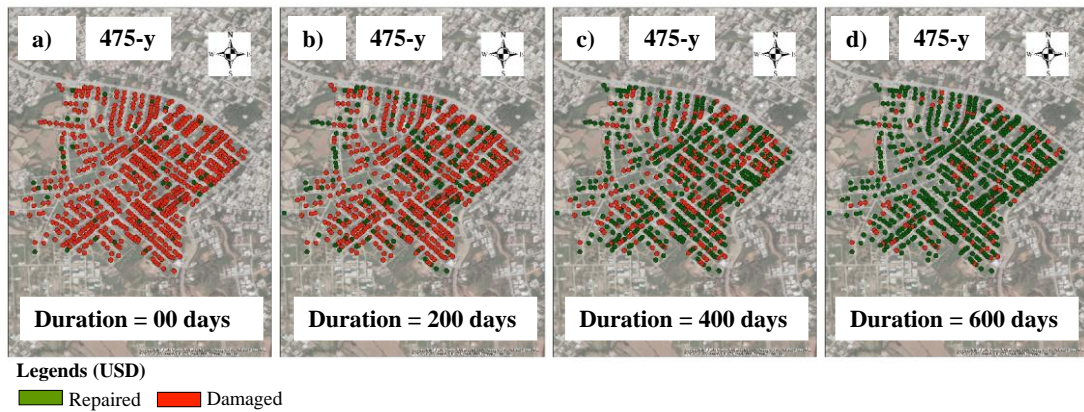


Figure 8-7 Community building portfolios recovery under design hazard scenario during the investigated time of (a) 00 days, (b) 200 days, (c) 400 days, and (d) 600 days

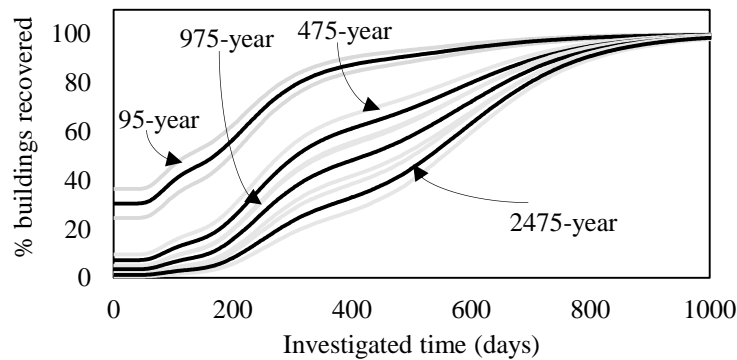


Figure 8-8 Community building portfolios recovery during the investigated time for hazard scenario of (a) 95-year, (b) 475-year, (c) 975-year, and (d) 2475-year

8.6.2 Surrogate-based efficient multi-objective optimization

The decision-makers may be interested in exploring the performance enhancements given the mitigation alternatives. The mitigation alternatives considered herein include retrofitting each building with one of the conventional retrofitting alternatives including reinforced concrete jacketing, steel jacketing, fiber-reinforced polymers, and others, and more details related to the retrofit alternatives can be found in (Anwar and Dong,

2022). The retrofit alternatives adapted with the conventional optimization algorithm are discussed in detail in the recent paper along with the relevant data required to perform consequence assessments (Anwar and Dong, 2020). Additionally, the retrofit implementation costs and the resulting performance enhancements are also discussed to achieve the performance enhancements given retrofit costs.

It is important to note that the community building portfolios consist of numerous buildings and each building can be retrofitted with one of the retrofit options. This results in many combinations of retrofits and assessing the performance on a community level can be computationally expensive. Hence, the proposed surrogate-based optimization algorithm is adopted herein.

In this illustrative example, Latin Hypercube Sampling (LHS) is utilized to generate an initial dataset of ten points. Each point in the dataset is a one-dimensional vector that assigns a random retrofit type to each building in a community building portfolio. The dataset is then utilized to query performance-based expensive black-box which provides community-level consequences in terms of considered performance objectives. Then, a Gaussian process model is fitted for each performance objective followed by spectral sampling, non-dominated sorting, and crowding distancing, and finally generating a new point to query the black-box to refine the Gaussian process model at each iteration. The process is repeated and approximate Pareto-optimal solutions are extracted after a given number of iterations.

As an illustration, the approximate Pareto-optimal solution is shown in Figure 8-9 against retrofit cost and repair cost performance objectives under a design hazard scenario extracted after performing 200 iterations. The initially observed ten solutions

from the dataset established from LHS are shown as purple boxes and the successive query points are shown as evaluations in cross symbol. Each successive evaluation improves the optimal solutions and after a given number of evaluations, the approximate Pareto-optimal solutions can be extracted. A blue dot represents an approximate Pareto-optimal solution and a black bar represents one standard deviation of uncertainty in approximating the Pareto-optimal solution due to the uncertainties in overall consequence assessments. The stationary covariance functions from the Matérn class is utilized as priors and perturbed by the Gaussian distributed noise of variance to represent uncertainties in terms of one standard deviation of the confidence interval.

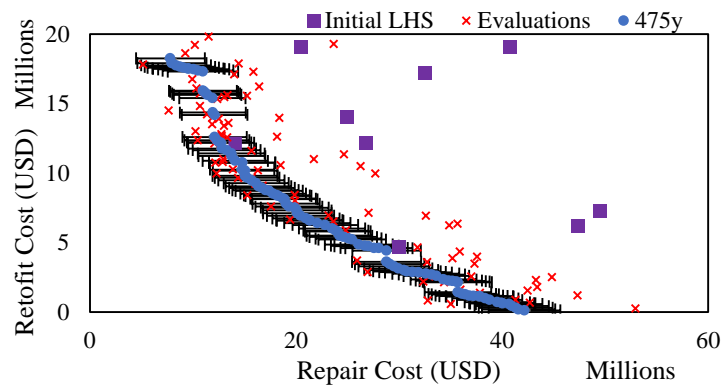


Figure 8-9 Approximate Pareto-optimal solution showing retrofit cost versus repair cost under design hazard scenario

The illustrated Pareto-optimal solution provides repair costs given different implemented retrofit cost solutions on a community-level. It is noted that the repair costs decrease with increasing retrofit costs and also the trend in repair costs reductions tend to decrease with increasing retrofit costs. As an illustration, the reduction in mean repair costs by applying retrofit of 5, 10, and 15 million USD on a community-level is visually shown in Figure 8-10.

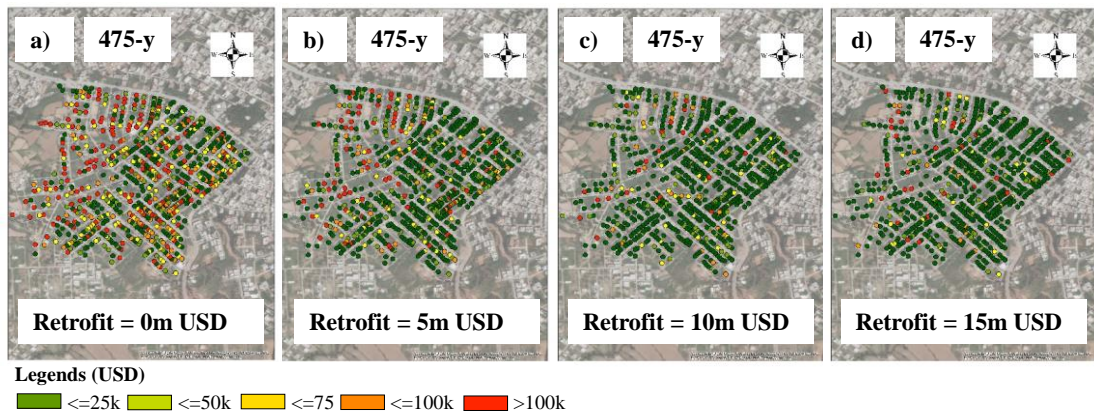


Figure 8-10 Community building portfolio repair costs under the design hazard scenario against the retrofit cost of (a) 0 million USD, (b) 5 million USD, (c) 10 million USD, and (d) 15 million USD

As discussed, the Pareto-optimal solutions from a single hazard scenario may not be sufficient for the decision-making, since the community building portfolios are prone to many hazard scenarios with different intensity measures and with the varying probability of occurrences. Hence, for better decision-making, all the possible hazard scenarios are considered and normalized to the mean annual frequency of occurrences by utilizing a hazard curve. The resulting EACs are determined for considered performance objectives. Illustratively, the approximate Pareto-optimal solutions for four hazard scenarios and resulting EAC considering all the hazard scenarios are shown in Figure 8-11.

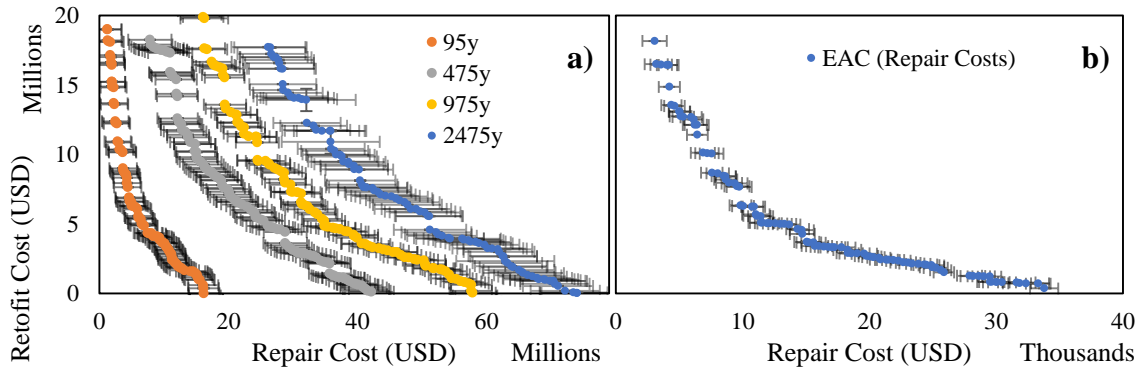


Figure 8-11 Approximate Pareto-optimal solution showing retrofit cost versus repair cost (a) under four hazard scenarios, and (b) Expected annual consequences

The EAC for the repair costs without the retrofit corresponds to 33.8 thousand USD, which reduces to 13.7, 7.56, and 4.22 thousand USD for a community-level retrofit of 5, 10, and 15 million USD. The EAC for the repair cost provides a predictive expected repair cost occurring every year during the service life of buildings considering all the possible hazard scenarios. For instance, in the considered illustrative example, a recurring annual cost of 33.8 thousand USD is required for each building for the repair works considering all the possible hazard scenarios. This information is also crucial for the insurance estimations considering the possible extreme events, among others. The retrofit costs on a community-level will reduce these annual recurring consequences as observed from Figure 8-11 (b) for the repair costs. The overall trend of retrofit costs against the repair costs in terms of EAC can be observed accordingly. The approximate Pareto-optimal solutions for all the considered six objectives in terms of EACs (except the retrofit costs) are shown in Figure 8-12. The retrofit costs are not converted into the EACs since it is an upfront cost in a pre-hazard state required to reduce the consequences determined as annually recurring consequences over the service life of buildings considering all the possible hazard scenarios.

In Figure 8-12, each axis represents a performance objective and each line corresponds to the non-dominated approximate Pareto-optimal solution established by utilizing the proposed surrogate-based optimization approach. The red lines show the solutions with minimal retrofit interventions and the blue lines represent maximum retrofit interventions. The complete spectrum of colors in terms of retrofit interventions can be observed accordingly. It can be seen that increasing the retrofit costs reduces the casualties, repair costs, repair time, emissions, and embodied energy with varying intensity of magnitudes.

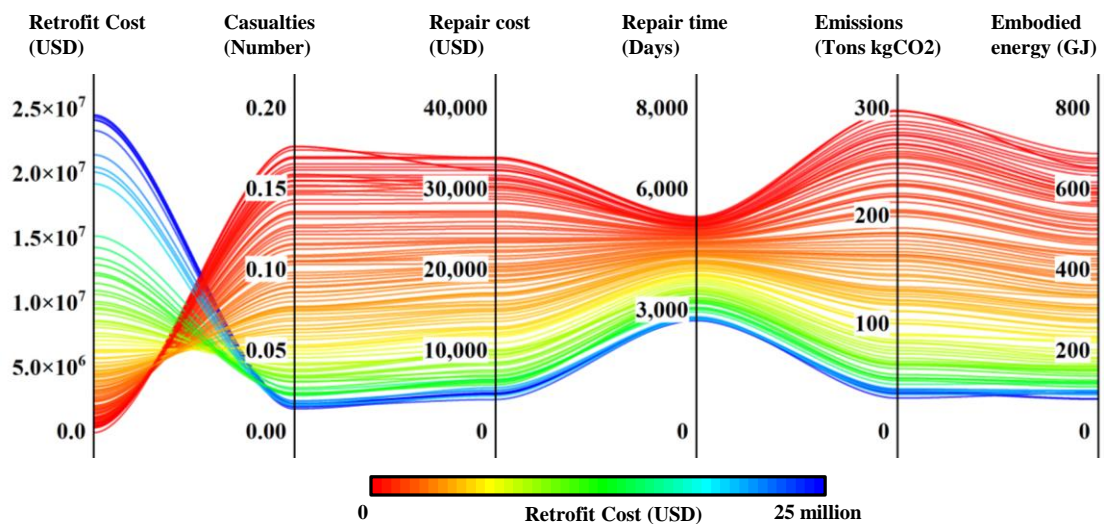


Figure 8-12 Approximate Pareto-optimal solutions for considered performance objectives in terms of EACs

The efficiency of the proposed approach is shown in Figure 8-13 in terms of hyper improvements and the computational time required per iteration. The comparison is made with the conventional non-dominated sorting and crowding distancing genetic algorithm (i.e., NSGA-II). The computations are performed on Intel(R) Core(TM) i7-8700 CPU of 3.20GHz with an installed RAM of 24 GB. It can be seen that the time it takes for the surrogate-based optimization for each iteration is considerably less (22.3-

59.5 seconds) than the NSGA-II (719-1155 seconds). Also, the hyper improvement per iteration is significantly higher for the surrogate-based optimization, especially in the first 50 iterations that suggest the superiority of the proposed approach against the conventional genetic algorithm in terms of efficient convergence to Pareto-optimal solutions for community building portfolios. In the case of NSGA-II, the hyper improvement is somewhat constant throughout the performed 200 iterations, highlighting the need for performing more iterations for convergence to Pareto-optimal solutions as compared to the surrogate-based optimization.

Also, surrogate-based optimization has a negligible effect on the computational time with the increase in the number of individuals. However, the computational time for conventional genetic algorithm increases significantly by increasing the number of individuals. For instance, the computational time in each iteration for individuals ranging from 10-100 is between 18.9-22.3 seconds for proposed surrogate-based optimization, while for conventional genetic algorithm, the computational time for each iteration starts from 95.5 for 10 individuals and goes up to 719 seconds for 100 individuals.

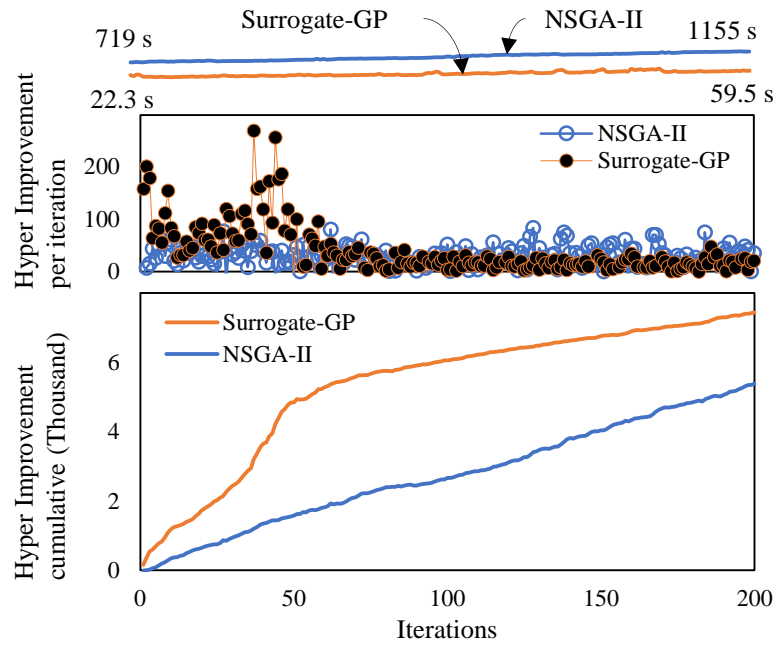


Figure 8-13 The efficiency of the proposed optimization approach against the conventional genetic algorithm in terms of hyper improvement and computational time per iteration

8.6.3 Decision making under Uncertainty

The Pareto-optimal solutions provide community performance for a wide range of retrofit costs. All these solutions are optimal and provide community performances in terms of casualties, repair costs, repair time, emissions, and embodied energy. The utility decision theory is implemented herein to determine the expected utility for each Pareto-optimal solution, by also the risk perceptions of the decision-makers. The Pareto-optimal solutions providing higher expected utility are the ideal solutions and could be implemented considering all the performance objectives and the risk perceptions of the decision-makers.

In this example, equal relative importance is assigned to all the considered performance objectives, and the utility function is utilized to evaluate the expected utility. Shape parameters are selected to consider different types and intensity of risk perceptions including $\gamma = 0$ for risk-neutral, $\gamma = 1, 3, 5$ for risk-averse, and $\gamma = -1, -3, -5$ for risk-seeking attitudes. The resulting expected utility given the retrofit costs under five risk perception scenarios is shown in Figure 8-14. As shown, the risk-seeking attitudes tend to provide higher expected utility for low retrofit cost solutions, and risk-averse attitudes tend to provide higher expected utility to high retrofit cost solutions. For instance, for a risk-seeking attitude having shape parameter $\gamma = -5$, the maximum expected utility of 0.36 can be achieved by selecting a community retrofit cost of 2.6 million USD. The community retrofit cost for a risk-neutral attitude providing maximum utility is 7.92 million USD, and risk-averse attitude with a shape parameter of $\gamma = 5$ provides maximum expected utility at a community retrofit cost of 13.4 million USD. The overall trend of the expected utility under risk perceptions can be observed from Figure 8-14.

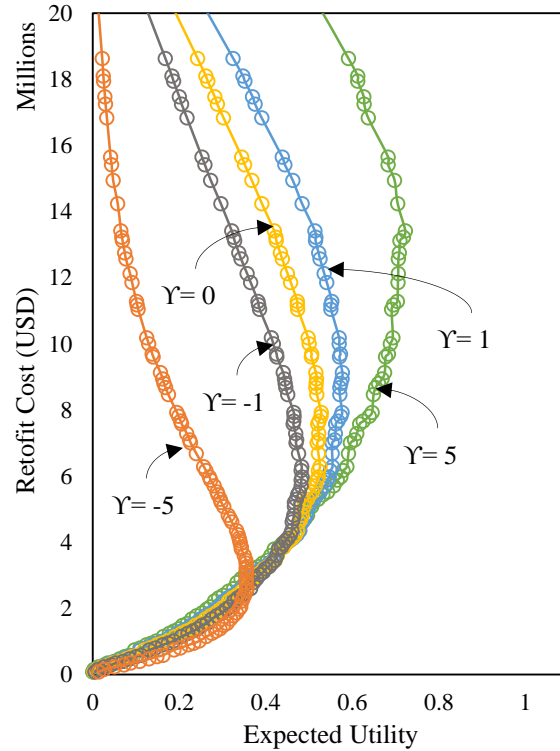


Figure 8-14 The expected utility against the retrofit costs considering risk attitudes

The Pareto-optimal solutions providing maximum utility given risk attitudes at given shape parameters are shown in Figure 8-15. As shown, the risk perceptions of decision-makers can have a significant contribution in deciding the community retrofit costs under uncertain consequences. A risk-seeking decision-maker will opt for a low retrofit cost solution in an uncertain environment, while a risk-averse decision-maker is oriented towards a high retrofit cost solution. For instance, as highlighted before, a risk-seeking decision-maker with a shape parameter of $\gamma = -5$ will opt for a retrofit cost solution of 2.6 million USD. This solution will provide EACs for casualties of around 0.104 in number, the repair cost of 20.9 thousand USD, repair time of 4277 days, equivalent carbon emissions of 195 Tongs KgCO_2 , and an embodied energy of 429 GJs. Contrarily, a risk-averse decision-maker with a shape parameter of $\gamma = 5$ will select a retrofit cost solution of 13.4 million USD which gives an EAC of 0.032 for

casualties, a repair cost of 6870 USD, a repair time of 3044 days, emissions of 62 Tons kgCO₂, and an embodied energy of 118 GJ. Hence, considering the risk profile of the decision-makers and an available retrofit cost budget, a particular retrofit cost solution on a community-level can be selected and implemented accordingly. Also, in the case of a limited retrofit cost budget on a community-level, the associated risk can be determined.

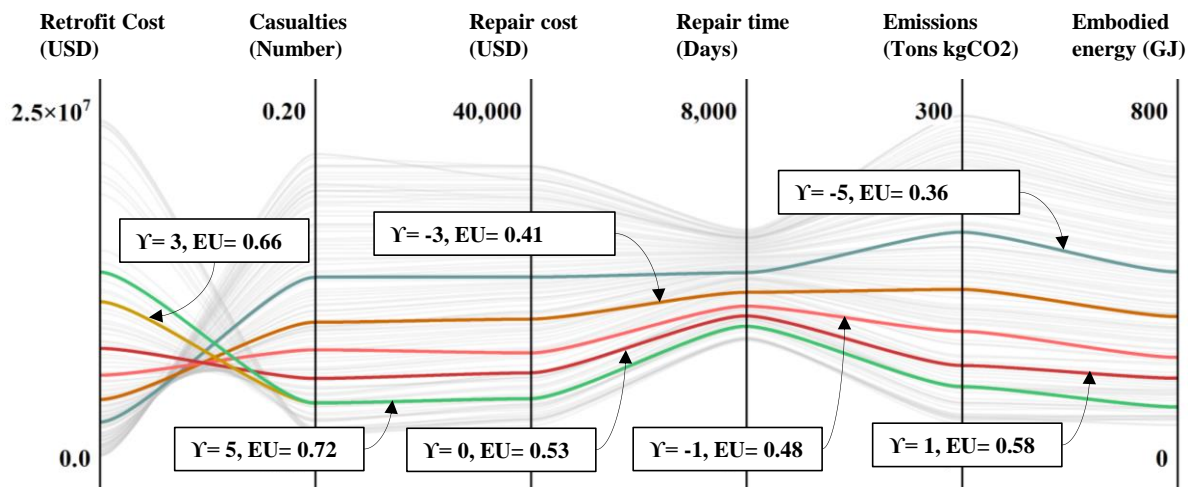


Figure 8-15 The highlighted approximate Pareto-optimal solutions for considered performance objectives in terms of EACs given risk perceptions with maximum expected utility

8.7 Conclusions

This chapter proposed an efficient multi-objective surrogate-based optimization and decision-making framework for community-building portfolios, considering risk perceptions under uncertain consequences. The following conclusions can be drawn:

2. The proposed framework replaced the expensive objective function evaluation part of the community building portfolios with the computationally inexpensive

Gaussian process surrogates, improving the computational efficiency and convergence. For instance, considering 100 individuals, the computational time per iteration was reduced to approximately 32 times, and the convergence to solutions was increased to approximately 3 times in the first 50 iterations.

3. The utility decision theory was implemented to extract ideal solutions from the approximate Pareto-optimal solutions considering risk perceptions. The ideal solutions considering three risk attitudes with shape parameters of $\gamma = -1, 0, -1$ resulted in the retrofit costs ranging from 5.97 million USD to 7.92 million USD. The risk-seeking decision resulted in the lower end of the provided range of retrofit costs while the risk-neutral and risk-averse decisions were inclined towards the higher end.
4. The expected annual consequences for optimization and decision-making were determined by utilizing a complete hazard curve. In the illustrative example, the community was prone to EACs of 33,780 USD of repair cost, 5296 days of repair time, 296 tons kgCO₂ of equivalent carbon emissions, and 686 GJ of embodied energy consumption under considered seismic hazard scenarios.
5. A risk-averse decision resulted in higher reductions in the EACs as compared to risk-neutral or risk-seeking solutions but at increased retrofit costs. Contrarily, the risk-seeking solutions resulted in low retrofit costs, but by compromising on post-hazard consequences. In the illustrative example, considering shape parameters of $\gamma = -1, 0, -1$, a risk-seeking solution required 1.95 million USD less in retrofit costs but with a risk of increased EACs of 0.017 casualties, 2292 USD repair costs, 227 days of repair time, 30 Tons kgCO₂ of equivalent carbon emissions, and 48 GJ of embodied energy.

In summary, the proposed framework provided efficient surrogate-based optimization and decision-making tool to evaluate ideal solutions among the approximate Pareto-optimal solutions considering the risk perceptions. However, the in-depth details including which priors to consider, selection of individuals, the inference of hyper parameters, the variance of Gaussian distributions, and uncertainty information especially in the surrogate establishment, among others were not investigated. Future studies can optimize these parameters to improve the applicability and computational efficiency of the proposed framework even further. Also, the proposed approach can be applied in a post-hazard scenario for recovery and resilience optimization. Furthermore, other infrastructure systems can be considered on a large scale that requires computationally expensive assessments and is provided with limited data points.

CHAPTER 9 CONCLUSIONS AND FUTURE WORK

9.1 Conclusions

This section provides an overall summary of the developed frameworks, mathematical tools, and illustrative examples. Following are the high-level conclusions of this thesis and for the detailed findings, the last section of the individual chapters can be referred:

1. A probabilistic seismic sustainability and resilience assessment methodology was developed and applied to a reinforced concrete frame structure utilizing next-generation performance-based assessment methods. The methodology considered detailed non-linear fiber-based models for accurate prediction of the spread of nonlinearity by utilizing incremental dynamic analysis. A number of non-linear time-history analyses were conducted, and seismic risk and sustainability were quantified in terms of repair cost, carbon emissions, and downtime by considering structural and non-structural components. Finally, the uncertainties associated with consequence functions were incorporated, and probabilistic resilience was assessed.
2. A performance-based seismic resilience enhancement framework was developed and applied to a deficient reinforced concrete building. The increase in seismic resilience was investigated by applying three conventional structural mitigation approaches. The methodology considered a component-level approach that required assembling fragility and consequence functions in building a performance model. The proposed assembly-based component-level

approach adopted the collapse fragility, determined from pushover analysis to reduce the computational costs of time history analyses. Then, social, economic, and environmental consequences were assessed in terms of casualties, monetary loss, and equivalent carbon emissions. Finally, the seismic resilience for retrofit alternatives was assessed by developing a downtime assessment methodology incorporating a sequence of repairs, impeding factors, and utility availability.

3. A performance-based decision-making framework for ranking least to most favorable retrofit alternatives, considering seismic loss, sustainability, and resilience on a long-term perspective was proposed. To achieve this, an improved downtime assessment methodology incorporating utility availability and impeding factors was established to better estimate the post-earthquake functionality loss and recovery. Additionally, the social, economic, and environmental consequences were explored in a long-term context for the decision-making. The consequences were converted into expected annual consequences by integrating the mean annual frequency of occurrence and the total consequence curves considering hazard scenarios. Conventional and modified (e.g., considering a wider gap in performance measures) TOPSIS was used for multi-criteria decision-making to determine the most acceptable solution for retrofit alternatives. The long-term performance-based multi-criteria decision-making considered cost, casualties, equivalent carbon emissions, embodied energy, and repair time as multi-criteria for the decision-making.
4. A system thinking paradigm was explored by considering bi-directional interactions among interconnected physical infrastructure systems to assess the resilience of building portfolios by utilizing indicators such as community

functionality and access to essential facilities. The community resilience was focused on evaluating building functionality by considering functionality contributions from water and electrical power systems. The first step was to identify physical infrastructure systems and key components in a community. The next step was to perform component damage and recovery assessment. Then, the damage and recovery of components were utilized to evaluate the functionality of building portfolios by considering dependencies and interdependencies between buildings and various physical infrastructure systems. Finally, the functionality of individual buildings was utilized to evaluate community resilience by considering community-level indicators such as community functionality, inherent resilience, and access to essential facilities.

5. A performance-based bi-objective optimization framework was proposed to evaluate Pareto-optimal solutions for risk, downtime, and environmental performance indicators against the retrofit costs on a community level. The proposed methodology comprised of a performance-based assessment part to evaluate the performance objectives for all the individuals given each simulation, and the optimization part in which the population with a given number of individuals was utilized to optimize the performance objectives. The simulations were repeated N times to incorporate uncertainties in the damage, consequence assessments, and optimization steps. Finally, Pareto-optimal solutions were determined and utilized to develop retrofit programs to satisfy the required performance of community building portfolios. The framework was also illustrated in a community with residential and commercial buildings

of different structural systems, code configurations, fragility, and consequence functions, among others.

6. An efficient surrogate-based multi-objective optimization and decision-making framework was proposed for computationally expensive black-box optimization problems i.e., performance enhancements of community building portfolios under extreme events considering mitigation alternatives. The framework was divided into three main parts; the performance assessment which served as a multi-objective optimization black-box, the efficient multi-objective surrogate-based optimization, and decision-making considering risk attitudes by utilizing utility decision theory. The proposed framework was later illustrated on a community building portfolio under seismic hazard scenarios to elaborate on the potential of the proposed framework.

9.2 Future directions

The possible future directions are as follows:

1. Although the proposed performance-based multi-criteria decision-making considering seismic loss, sustainability, and resilience provided a systematic way to rank retrofit alternatives but the methodology could be improved further. For instance, the number of criteria, weighting factors, risk attitudes, and investigated period may be based on some logic derived from similar studies, empirical observations, preferences of the stakeholders, engineering judgment, and/or data analytics. In the case of a lack of data or limited preferential knowledge of the stakeholders, a survey can be conducted. Future studies related to establishing a benchmark of these characteristics would help

streamline the ranking process. Additionally, future studies may focus on improving the downtime assessment methodology since the impeding factors, utility availability, and additional delays are based on the lognormal cumulative distribution functions developed from the past data and maybe need adjustment for its wider use.

2. The systems thinking related framework for resilience assessment of community building portfolios provided a holistic approach to community resilience by considering component damage and functionality assessment. The current framework adopted data from HAZUS, REDiTM Rating System, among others (O'Rourke and Ayala, 1993; HAZUS, 2003; Almufti and Willford, 2013; Laugé et al., 2015; Stewart et al., 2015), and future studies may be conducted based on the site-specific data to better calibrate the model parameters for estimating community resilience. Also, there is a need to collect data from future hazard scenarios in a format that would enable researchers and practitioners to further understand the dependencies and interdependencies between systems and their components.
3. The proposed optimization framework considered pre-hazard retrofit alternatives to enhance the performance of community building portfolios under an earthquake scenario and can be extended to other extreme events. The methodology can be extended to optimize the post-hazard scenarios and during the recovery phase after an earthquake event. The study can also be extended to other physical infrastructure systems and new performance indicators can be added including total casualties, and embodied energy consumption, among others.

4. The proposed surrogate-based optimization and decision-making framework considered pre-hazard mitigation alternatives. Future studies can also utilize this approach in a post-hazard scenario for recovery and resilience optimization. Furthermore, other infrastructure systems can be considered on a large-scales which requires computationally expensive assessments and are provided with limited data points.

REFERENCES

- ACI-318 (2011) Building Code Requirements for Structural Concrete. Report no. Report Number|, Date. Place Published|: Institution|.
- Akiyama M, Frangopol DM and Ishibashi H (2020) Toward life-cycle reliability-, risk- and resilience-based design and assessment of bridges and bridge networks under independent and interacting hazards: emphasis on earthquake, tsunami and corrosion. *Structure and Infrastructure Engineering* 16(1): 26-50.
- Aldrich DP (2012) *Building resilience: Social capital in post-disaster recovery*. University of Chicago Press.
- Alisjahbana I and Kiremidjian A (2020) Modeling housing recovery after the 2018 Lombok earthquakes using a stochastic queuing model. *Earthquake Spectra*. 8755293020970972.
- Almufti I and Willford M (2013) REDi™ Rating System: Resilience Based Earthquake Design Initiative for the Next Generation of Buildings. Version 1.0. *October, Arup*.
- Anelli A, Santa-Cruz S, Vona M, et al. (2019) A proactive and resilient seismic risk mitigation strategy for existing school buildings. *Structure and Infrastructure Engineering* 15(2): 137-151.
- Anwar GA and Dong Y (2020) Seismic resilience of retrofitted RC buildings. *Earthquake Engineering and Engineering Vibration* 19(3): 561-571.
- Anwar GA and Dong Y (2022) Surrogate-based decision-making of community building portfolios under uncertain consequences and risk attitudes *Engineering Structures* 268: 114749.
- Anwar GA, Dong Y and Li Y (2020) Performance-based decision-making of buildings under seismic hazard considering long-term loss, sustainability, and resilience. *Structure and Infrastructure Engineering*. DOI: 10.1080/15732479.2020.1845751.
- Anwar GA, Dong Y and Zhai C (2019) Performance-based probabilistic framework for seismic risk, resilience, and sustainability assessment of reinforced concrete structures. *Advances in Structural Engineering*. 1369433219895363.
- Architecture 2030 (2019) *The 2030 Challenge for Products, Architecture 2030, Santa Fe, New Mexico*. Available at: http://www.architecture2030.org/2030_challenge/products (accessed 20/08).

- Asadi E, Salman AM and Li Y (2019) Multi-criteria decision-making for seismic resilience and sustainability assessment of diagrid buildings. *Engineering Structures* 191: 229-246.
- ASCE-41-13 (2013) Seismic evaluation and retrofit of existing buildings. Reportno. Report Number|, Date. Place Published|: Institution|.
- Asprone D and Manfredi G (2015) Linking disaster resilience and urban sustainability: a global approach for future cities. *Disasters* 39(s1): s96-s111.
- Baker JW (2015) Efficient analytical fragility function fitting using dynamic structural analysis. *Earthquake Spectra* 31(1): 579-599.
- Bao X, Zhang M-H and Zhai C-H (2019) Fragility analysis of a containment structure under far-fault and near-fault seismic sequences considering post-mainshock damage states. *Engineering Structures* 198: 109511.
- Barbat AH, Carreño ML, Pujades LG, et al. (2010) Seismic vulnerability and risk evaluation methods for urban areas. A review with application to a pilot area. *Structure & Infrastructure Engineering* 6(1-2): 17-38.
- Battarra M, Balcik B and Xu H (2018) Disaster preparedness using risk-assessment methods from earthquake engineering. *European Journal of Operational Research* 269(2): 423-435.
- Beume N, Fonseca CM, Lopez-Ibanez M, et al. (2009) On the complexity of computing the hypervolume indicator. *IEEE Transactions on Evolutionary Computation* 13(5): 1075-1082.
- Billah AM and Alam MS (2014) Seismic performance evaluation of multi-column bridge bents retrofitted with different alternatives using incremental dynamic analysis. *Engineering Structures* 62: 105-117.
- Bocchini P, Frangopol DM, Ummenhofer T, et al. (2014) Resilience and sustainability of civil infrastructure: Toward a unified approach. *Journal of Infrastructure Systems* 20(2).
- Bristow DN and Hay AH (2017) Graph model for probabilistic resilience and recovery planning of multi-infrastructure systems. *Journal of Infrastructure Systems* 23(3): 04016039.
- Broccardo M, Galanis P, Esposito S, et al. (2015) Probabilistic resilience assessment of civil systems: Analysis and validity of the PEER framework. *Safety and Reliability of Complex Engineered Systems: ESREL* 331.
- Brown C, Milke M and Seville E (2011) Disaster waste management: A review article. *Waste management* 31(6): 1085-1098.
- Brown T, Hörsch J and Schlachtberger D (2017) PyPSA: Python for power system analysis. *arXiv preprint arXiv:1709.09913*.

- Bruneau M, Chang SE, Eguchi RT, et al. (2003) A framework to quantitatively assess and enhance the seismic resilience of communities. *Earthquake Spectra* 19(4): 733-752.
- Burton HV, Deierlein G, Lallemand D, et al. (2015) Framework for incorporating probabilistic building performance in the assessment of community seismic resilience. *Journal of Structural Engineering* 142(8): C4015007.
- Burton HV, Deierlein G, Lallemand D, et al. (2017) Measuring the Impact of Enhanced Building Performance on the Seismic Resilience of a Residential Community. *Earthquake Spectra* 33(4): 1347-1367.
- Calvi G (2013) Choices and criteria for seismic strengthening. *Journal of Earthquake Engineering* 17(6): 769-802.
- Calvi GM, Pinho R, Magenes G, et al. (2006) Development of seismic vulnerability assessment methodologies over the past 30 years. *ISET journal of Earthquake Technology* 43(3): 75-104.
- Cardone D and Perrone G (2017) Damage and loss assessment of pre-70 RC frame buildings with FEMA P-58. *Journal of Earthquake Engineering* 21(1): 23-61.
- Cardone D, Sullivan T, Gesualdi G, et al. (2017) Simplified estimation of the expected annual loss of reinforced concrete buildings. *Earthquake Engineering and Structural Dynamics* 46(12): 2009-2032.
- Carreño ML, Cardona OD and Barbat AH (2012) New methodology for urban seismic risk assessment from a holistic perspective. *Bulletin of Earthquake Engineering* 10(2): 547-565.
- Caspeele R, Frangopol DM and Tsompanakis Y (2020) Life-cycle, risk, resilience and sustainability of civil infrastructure. *Structure and Infrastructure Engineering* 16(4): 517-519.
- Caterino N, Iervolino I, Manfredi G, et al. (2009) Comparative analysis of multi-criteria decision-making methods for seismic structural retrofitting. *Computer - Aided Civil and Infrastructure Engineering* 24(6): 432-445.
- Chang J-R, Chen D-H and Hung C-T (2005) Selecting preventive maintenance treatments in Texas: using the technique for order preference by similarity to the ideal solution for specific pavement study—3 sites. *Transportation research record* 1933(1): 62-71.
- Chen L, Qian J, Tu B, et al. (2021) Performance-based risk assessment of reinforced concrete bridge piers subjected to vehicle collision. *Engineering Structures* 229: 111640.
- Cheng M and Frangopol DM (2021) Life-cycle optimization of structural systems based on cumulative prospect theory: Effects of the reference point and risk attitudes. *Reliability engineering & system safety*. 108100.

- Chhabra JP, Hasik V, Bilec MM, et al. (2017) Probabilistic assessment of the life-cycle environmental performance and functional life of buildings due to seismic events. *Journal of Architectural Engineering* 24(1): 04017035.
- Cimellaro GP and Piqué M (2016) Resilience of a hospital emergency department under seismic event. *Advances in Structural Engineering* 19(5): 825-836.
- Cimellaro GP, Reinhorn AM and Bruneau M (2010a) Framework for analytical quantification of disaster resilience. *Engineering Structures* 32(11): 3639-3649.
- Cimellaro GP, Reinhorn AM and Bruneau M (2010b) Seismic resilience of a hospital system. *Structure & Infrastructure Engineering* 6(1-2): 127-144.
- Cornell CA (1968) Engineering seismic risk analysis. *Bulletin of the seismological society of America* 58(5): 1583-1606.
- Crowley H, Pinho R, van Elk J, et al. (2019) Probabilistic damage assessment of buildings due to induced seismicity. *Bulletin of Earthquake Engineering* 17(8): 4495-4516.
- Cutter SL (2016) The landscape of disaster resilience indicators in the USA. *Natural hazards* 80(2): 741-758.
- Cutter SL (2020) Community resilience, natural hazards, and climate change: Is the present a prologue to the future? *Norsk Geografisk Tidsskrift-Norwegian Journal of Geography* 74(3): 200-208.
- Cutter SL, Ash KD and Emrich CT (2014) The geographies of community disaster resilience. *Global environmental change* 29: 65-77.
- da Porto F, Donà M, Rosti A, et al. (2021) Comparative analysis of the fragility curves for Italian residential masonry and RC buildings. *Bulletin of Earthquake Engineering*. 1-44.
- Deb K, Pratap A, Agarwal S, et al. (2002) A fast and elitist multiobjective genetic algorithm: NSGA-II. *IEEE Transactions on Evolutionary Computation* 6(2): 182-197.
- Decò A, Bocchini P and Frangopol DM (2013) A probabilistic approach for the prediction of seismic resilience of bridges. *Earthquake Engineering & Structural Dynamics* 42(10): 1469-1487.
- Didier M, Broccardo M, Esposito S, et al. (2018) A compositional demand/supply framework to quantify the resilience of civil infrastructure systems (Re-CoDeS). *Sustainable and Resilient Infrastructure* 3(2): 86-102.
- Donà M, Bizzaro L, Carturan F, et al. (2019) Effects of business recovery strategies on seismic risk and cost-effectiveness of structural retrofitting for business enterprises. *Earthquake Spectra* 35(4): 1795-1819.

- Donà M, Carpanese P, Follador V, et al. (2021) Mechanics-based fragility curves for Italian residential URM buildings. *Bulletin of Earthquake Engineering* 19(8): 3099-3127.
- Dong Y and Frangopol DM (2015a) Probabilistic ship collision risk and sustainability assessment considering risk attitudes. *Structural Safety* 53: 75-84.
- Dong Y and Frangopol DM (2015b) Risk and resilience assessment of bridges under mainshock and aftershocks incorporating uncertainties. *Engineering Structures* 83: 198-208.
- Dong Y and Frangopol DM (2016a) Performance-based seismic assessment of conventional and base-isolated steel buildings including environmental impact and resilience. *Earthquake Engineering Structural Dynamics* 45(5): 739-756.
- Dong Y and Frangopol DM (2016b) Probabilistic time-dependent multihazard life-cycle assessment and resilience of bridges considering climate change. *Journal of Performance of Constructed Facilities* 30(5): 04016034.
- Dong Y and Frangopol DM (2017a) Adaptation optimization of residential buildings under hurricane threat considering climate change in a lifecycle context. *Journal of Performance of Constructed Facilities* 31(6): 04017099.
- Dong Y and Frangopol DM (2017b) Probabilistic assessment of an interdependent healthcare–bridge network system under seismic hazard. *Structure and Infrastructure Engineering* 13(1): 160-170.
- Dong Y and Frangopol DM (2020) Resilience of Civil Infrastructure in a Life-Cycle Context. *Resilience of Critical Infrastructure Systems*. CRC Press, pp.43-48.
- Dong Y, Frangopol DM and Sabatino S (2016) A decision support system for mission-based ship routing considering multiple performance criteria. *Reliability Engineering and System Safety* 150: 190-201.
- Dong Y, Frangopol DM and Saydam D (2014) Pre-earthquake multi-objective probabilistic retrofit optimization of bridge networks based on sustainability. *Journal of Bridge Engineering* 19(6): 04014018.
- Eads L, Miranda E, Krawinkler H, et al. (2013) An efficient method for estimating the collapse risk of structures in seismic regions. *Earthquake Engineering and Structural Dynamics* 42(1): 25-41.
- Elkady A and Lignos DG (2015) Effect of gravity framing on the overstrength and collapse capacity of steel frame buildings with perimeter special moment frames. *Earthquake Engineering and Structural Dynamics* 44(8): 1289-1307.
- Elnashai AS and Di Sarno L (2008) *Fundamentals of earthquake engineering*. Wiley Online Library.

- Emmerich M, Yang K, Deutz A, et al. (2016) A multicriteria generalization of bayesian global optimization. *Advances in Stochastic and Deterministic Global Optimization*. Springer, pp.229-242.
- Emmerich MT, Deutz AH and Klinkenberg JW (2011) Hypervolume-based expected improvement: Monotonicity properties and exact computation. *2011 IEEE Congress of Evolutionary Computation (CEC)*. IEEE, 2147-2154.
- Erdik M (2017) Earthquake risk assessment. *Bulletin of Earthquake Engineering* 15(12): 5055-5092.
- Erdik M, Şeşetyan K, Demircioğlu M, et al. (2011) Rapid earthquake loss assessment after damaging earthquakes. *Soil Dynamics and Earthquake Engineering* 31(2): 247-266.
- Faber MH and Stewart MG (2003) Risk assessment for civil engineering facilities: critical overview and discussion. *Reliability engineering & system safety* 80(2): 173-184.
- Fajfar P (2000) A nonlinear analysis method for performance-based seismic design. *Earthquake Spectra* 16(3): 573-592.
- Fang Y-P, Pedroni N and Zio E (2016) Resilience-based component importance measures for critical infrastructure network systems. *IEEE Transactions on Reliability* 65(2): 502-512.
- Farhan M and Bousias S (2020) Seismic fragility analysis of LNG sub-plant accounting for component dynamic interaction. *Bulletin of Earthquake Engineering* 18(10): 5063-5085.
- Feese C, Li Y and Bulleit WM (2014) Assessment of seismic damage of buildings and related environmental impacts. *Journal of Performance of Constructed Facilities* 29(4): 04014106.
- FEMA-547 (2006) Techniques for the seismic rehabilitation of existing buildings. Reportno. Report Number|, Date. Place Published|: Institution|.
- FEMA-P695 (2009) *Quantification of building seismic performance factors*. US Department of Homeland Security, FEMA.
- FEMA-P-58 (2012) Seismic Performance Assessment of Buildings: Vol. 1– Methodology. Reportno. Report Number|, Date. Place Published|: Institution|.
- FEMA (2005) 440, Improvement of nonlinear static seismic analysis procedures. *FEMA-440, Redwood City*.
- Feng K, Wang N, Li Q, et al. (2017) Measuring and enhancing resilience of building portfolios considering the functional interdependence among community sectors. *Structural Safety* 66: 118-126.

- Fister Jr I, Yang X-S, Fister I, et al. (2013) A brief review of nature-inspired algorithms for optimization. *arXiv preprint arXiv*.
- Forrester AI and Keane A (2009) Recent advances in surrogate-based optimization. *Progress in aerospace sciences* 45(1-3): 50-79.
- Frangopol DM, Dong Y and Sabatino S (2017) Bridge life-cycle performance and cost: analysis, prediction, optimisation and decision-making. *Structure and Infrastructure Engineering* 13(10): 1239-1257.
- Frangopol DM, Lin K-Y and Estes AC (1997) Life-cycle cost design of deteriorating structures. *Journal of Structural Engineering* 123(10): 1390-1401.
- Frangopol DM and Soliman M (2016) Life-cycle of structural systems: recent achievements and future directions. *Structure and Infrastructure Engineering* 12(1): 1-20.
- Gambella C, Ghaddar B and Naoum-Sawaya J (2021) Optimization problems for machine learning: A survey. *European Journal of Operational Research* 290(3): 807-828.
- Gautam D and Chaulagain H (2016) Structural performance and associated lessons to be learned from world earthquakes in Nepal after 25 April 2015 (MW 7.8) Gorkha earthquake. *Engineering Failure Analysis* 68: 222-243.
- Gencturk B, Hossain K and Lahourpour S (2016) Life cycle sustainability assessment of RC buildings in seismic regions. *Engineering Structures* 110: 347-362.
- Ghobarah A (2001) Performance-based design in earthquake engineering: state of development. *Engineering Structures* 23(8): 878-884.
- Giouvanidis AI and Dong Y (2020) Seismic loss and resilience assessment of single-column rocking bridges. *Bulletin of Earthquake Engineering*. DOI: 10.1007/s10518-020-00865-5.(18): 4481–4513.
- Godschalk DR (2003) Urban hazard mitigation: creating resilient cities. *Natural Hazards Review* 4(3): 136-143.
- Gong C and Frangopol DM (2020) Condition-based multiobjective maintenance decision making for highway bridges considering risk perceptions. *Journal of Structural Engineering* 146(5): 04020051.
- Gonzalez C, Niño M and Jaimes MA (2020) Event-based assessment of seismic resilience in Mexican school buildings. *Bulletin of Earthquake Engineering* 18(14): 6313-6336.
- Guan M, EERI X, Burton M, EERI H and Shokrabadi M (2021) A database of seismic designs, nonlinear models, and seismic responses for steel moment-resisting frame buildings. *Earthquake Spectra* 37(2): 1199-1222.

- Guerreiro AP, Fonseca CM and Paquete L (2020) The hypervolume indicator: Problems and algorithms. *arXiv*.
- Guidotti R, Chmielewski H, Unnikrishnan V, et al. (2016) Modeling the resilience of critical infrastructure: The role of network dependencies. *Sustainable and Resilient Infrastructure* 1(3-4): 153-168.
- Guirguis D, Aulig N, Picelli R, et al. (2019) Evolutionary black-box topology optimization: challenges and promises. *IEEE Transactions on Evolutionary Computation* 24(4): 613-633.
- Guo H, Dong Y, Bastidas-Arteaga E, et al. (2021) Probabilistic failure analysis, performance assessment, and sensitivity analysis of corroded reinforced concrete structures. *Engineering Failure Analysis* 124: 105328.
- Guo H, Dong Y and Gardoni P (2022) Efficient subset simulation for rare-event integrating point-evolution kernel density and adaptive polynomial chaos kriging. *Mechanical Systems and Signal Processing* 169: 108762.
- Guo T, Xu Z, Song L, et al. (2017) Seismic resilience upgrade of RC frame building using self-centering concrete walls with distributed friction devices. *Journal of Structural Engineering* 143(12): 04017160.
- Hammersley J (2013) *Monte carlo methods*. Springer Science & Business Media.
- Han R, Li Y and van de Lindt J (2017) Probabilistic Assessment and Cost-Benefit Analysis of Nonductile Reinforced Concrete Buildings Retrofitted with Base Isolation: Considering Mainshock–Aftershock Hazards. *Journal of Risk and Uncertainty in Engineering Systems, Part A: Civil Engineering* 3(4): 04017023.
- Hashemi MJ, Al-Attraqchi AY, Kalfat R, et al. (2019) Linking seismic resilience into sustainability assessment of limited-ductility RC buildings. *Engineering Structures* 188: 121-136.
- Hassan EM and Mahmoud H (2020) An integrated socio-technical approach for post-earthquake recovery of interdependent healthcare system. *Reliability engineering & system safety* 201: 106953.
- HAZUS (2003) Multi-hazard loss estimation methodology, earthquake model. Reportno. Report Number|, Date. Place Published|: Institution|.
- Hernández-Lobato JM, Hoffman MW and Ghahramani Z (2014) Predictive entropy search for efficient global optimization of black-box functions. *arXiv*.
- Holland J (1975) *Adaptation in Natural and Artificial Systems*. Ann Arbor: University of Michigan Press.
- Honegger D and Eguchi RJS (1992) Determination of the relative vulnerabilities to Seismic damage for dan diego country water Authority (SDCWA) Water Transmission Pipelines. Reportno. Report Number|, Date. Place Published|: Institution|.

- Horn J, Nafpliotis N and Goldberg DE (1994) A niched Pareto genetic algorithm for multiobjective optimization. *Proceedings of the first IEEE conference on evolutionary computation. IEEE world congress on computational intelligence.* Ieee, 82-87.
- Huang Y-N, Whittaker AS and Hamburger RO (2017) A simplified analysis procedure for performance-based earthquake engineering of buildings. *Engineering Structures* 150: 719-735.
- Hupkens I, Emmerich M and Deutz A (2014) Faster computation of expected hypervolume improvement. *arXiv preprint arXiv.*
- Hutt CM, Almufti I, Willford M, et al. (2015) Seismic loss and downtime assessment of existing tall steel-framed buildings and strategies for increased resilience. *Journal of Structural Engineering* 142(8): C4015005.
- Hwang C-L and Yoon K (1981) Methods for multiple attribute decision making. *Multiple attribute decision making.* Springer, pp.58-191.
- IBC (2012) *International building code.* International Code Council.
- Islam SM, Das S, Ghosh S, et al. (2011) An adaptive differential evolution algorithm with novel mutation and crossover strategies for global numerical optimization. *IEEE Transactions on Systems, Man, and Cybernetics, Part B* 42(2): 482-500.
- Jalayer F, Ebrahimian H and Miano A (2021) Record-to-record variability and code-compatible seismic safety-checking with limited number of records. *Bulletin of Earthquake Engineering.* 1-36.
- Jeong S-H and Elnashai AS (2005) Analytical assessment of an irregular RC frame for full-scale 3D pseudo-dynamic testing part I: Analytical model verification. *Journal of Earthquake Engineering* 9(01): 95-128.
- Jeong S-H, Mwafy AM and Elnashai AS (2012) Probabilistic seismic performance assessment of code-compliant multi-story RC buildings. *Engineering Structures* 34: 527-537.
- Kameshwar S, Cox DT, Barbosa AR, et al. (2019) Probabilistic decision-support framework for community resilience: Incorporating multi-hazards, infrastructure interdependencies, and resilience goals in a Bayesian network. *Reliability Engineering and System Safety* 191: 106568.
- Katoch S, Chauhan SS, Kumar VJMT, et al. (2021) A review on genetic algorithm: past, present, and future. 80(5): 8091-8126.
- Keeble BR (1988) The Brundtland report: 'Our common future'. *MedicineWar* 4(1): 17-25.
- Khanmohammadi S, Farahmand H and Kashani H (2018) A system dynamics approach to the seismic resilience enhancement of hospitals. *International journal of disaster risk reduction* 31: 220-233.

- Kilanitis I and Sextos A (2019) Integrated seismic risk and resilience assessment of roadway networks in earthquake prone areas. *Bulletin of Earthquake Engineering* 17(1): 181-210.
- Kim J-H, Han J-H, Kim Y-H, et al. (2011) Preference-based solution selection algorithm for evolutionary multiobjective optimization. *IEEE Transactions on Evolutionary Computation* 16(1): 20-34.
- Kircher CA, Whitman RV and Holmes WT (2006) HAZUS earthquake loss estimation methods. *Natural Hazards Review* 7(2): 45-59.
- Klise KA, Hart D, Moriarty DM, et al. (2017) Water network tool for resilience (WNTR) user manual. Reportno. Report Number|, Date. Place Published|: Institution|.
- Knowles J (2006) ParEGO: A hybrid algorithm with on-line landscape approximation for expensive multiobjective optimization problems. *IEEE Transactions on Evolutionary Computation* 10(1): 50-66.
- Koliou M, van de Lindt JW, McAllister TP, et al. (2017) State of the research in community resilience: progress and challenges. *Sustainable and Resilient Infrastructure* 5(3): 131-151.
- Konak A, Coit DW and Smith AE (2006) Multi-objective optimization using genetic algorithms: A tutorial. *Reliability engineering & system safety* 91(9): 992-1007.
- Krawinkler H, Zareian F, Medina RA, et al. (2006) Decision support for conceptual performance - based design. *Earthquake Engineering and Structural Dynamics* 35(1): 115-133.
- Larson J, Menickelly M and Wild SM (2019) Derivative-free optimization methods. *Acta Numerica* 28: 287-404.
- Laugé A, Hernantes J and Sarriegi JM (2015) Critical infrastructure dependencies: A holistic, dynamic and quantitative approach. *International Journal of Critical Infrastructure Protection* 8: 16-23.
- Lemma M, Rebelo C and Silva L (2021) Seismic Design and Performance Assessment of Steel Frames Considering Joints' Behaviour. *ce/papers* 4(2-4): 1965-1973.
- Li Y, Dong Y, Frangopol DM, et al. (2020a) Long-term resilience and loss assessment of highway bridges under multiple natural hazards. *Structure and Infrastructure Engineering* 16(4): 626-641.
- Li Y, Dong Y and Qian J (2020b) Higher-Order Analysis of Probabilistic Long-Term Loss under Nonstationary Hazards. *Reliability engineering & system safety* 203: 107092.
- Ligabue V, Pampanin S and Savoia M (2018) Seismic performance of alternative risk-reduction retrofit strategies to support decision making. *Bulletin of Earthquake Engineering* 16(7): 3001-3030.

- Lin P and Wang N (2017a) Stochastic post-disaster functionality recovery of community building portfolios I: Modeling. *Structural Safety* 69: 96-105.
- Lin P and Wang N (2017b) Stochastic post-disaster functionality recovery of community building portfolios II: Application. *Structural Safety* 69: 106-117.
- Liu K, Zhai C and Dong Y (2020) Optimal restoration schedules of transportation network considering resilience. *Structure and Infrastructure Engineering*. 1-14.
- Liu W and Song Z (2020) Review of studies on the resilience of urban critical infrastructure networks. *Reliability engineering & system safety* 193: 106617.
- Logan TM and Guikema SD (2020) Reframing Resilience: Equitable Access to Essential Services. *Risk Analysis*.
- Lounis Z and McAllister TP (2016) Risk-based decision making for sustainable and resilient infrastructure systems. *Journal of Structural Engineering* 142(9): F4016005.
- Ma C-K, Apandi NM, Sofrie CSY, et al. (2017) Repair and rehabilitation of concrete structures using confinement: A review. *Construction and building materials* 133: 502-515.
- Marchese D, Reynolds E, Bates ME, et al. (2018) Resilience and sustainability: Similarities and differences in environmental management applications. *Science of the Total Environment* 613.
- Masoomi H, Burton H, Tomar A, et al. (2020) Simulation-Based Assessment of Postearthquake Functionality of Buildings with Disruptions to Cross-Dependent Utility Networks. *Journal of Structural Engineering* 146(5): 04020070.
- Masoomi H and van de Lindt JW (2018) Community-Resilience-Based Design of the Built Environment. *ASCE-ASME Journal of Risk and Uncertainty in Engineering Systems, Part A: Civil Engineering* 5(1): 04018044.
- Mateo JRSC (2012) Multi-criteria analysis. *Multi criteria analysis in the renewable energy industry*. Springer, pp.7-10.
- McAllister TP (2015) Community resilience planning guide for buildings and infrastructure systems, volume I. Reportno. Report Number|, Date. Place Published|: Institution|.
- McAllister TP and Moddemeyer S (2018) Aligning community resilience and sustainability. *Routledge Handbook of Sustainable and Resilient Infrastructure*. Routledge Abingdon-on-Thames, UK, pp.15-27.
- Miles SB, Burton HV and Kang H (2018) Community of Practice for Modeling Disaster Recovery. *Natural Hazards Review* 20(1): 04018023.

- Miles SB and Chang SE (2006) Modeling community recovery from earthquakes. *Earthquake Spectra* 22(2): 439-458.
- Mitrani-Reiser J (2007) *An ounce of prevention: probabilistic loss estimation for performance-based earthquake engineering*. Doctoral dissertation, California Institute of Technology.
- Moehle JP (2006) Seismic analysis, design, and review for tall buildings. *The Structural Design of Tall and Special Buildings* 15(5): 495-513.
- Molina Hutt C, Almufti I, Willford M, et al. (2016) Seismic loss and downtime assessment of existing tall steel-framed buildings and strategies for increased resilience. *Journal of Structural Engineering* 142(8): C4015005.
- Mosalam KM, Alibrandi U, Lee H, et al. (2018) Performance-based engineering and multi-criteria decision analysis for sustainable and resilient building design. *Structural Safety* 74: 1-13.
- Newman JP, Maier HR, Riddell GA, et al. (2017) Review of literature on decision support systems for natural hazard risk reduction: Current status and future research directions. *Environmental Modelling and Software* 96: 378-409.
- Nozhati S, Rosenheim N, Ellingwood BR, et al. (2019) Probabilistic framework for evaluating food security of households in the aftermath of a disaster. *Structure and Infrastructure Engineering* 15(8): 1060-1074.
- Nurre SG, Cavdaroglu B, Mitchell JE, et al. (2012) Restoring infrastructure systems: An integrated network design and scheduling (INDS) problem. *European Journal of Operational Research* 223(3): 794-806.
- O'Rourke M and Ayala G (1993) Pipeline damage due to wave propagation. *Journal of Geotechnical Engineering* 119(9): 1490-1498.
- O'Rourke M and Deyoe E (2004) Seismic damage to segmented buried pipe. *Earthquake Spectra* 20(4): 1167-1183.
- Ouyang M (2014) Review on modeling and simulation of interdependent critical infrastructure systems. *Reliability Engineering and System Safety* 121: 43-60.
- Ouyang M, Dueñas-Osorio L and Min X (2012) A three-stage resilience analysis framework for urban infrastructure systems. *Structural Safety* 36: 23-31.
- Ouyang M, Liu C and Xu M (2019) Value of resilience-based solutions on critical infrastructure protection: Comparing with robustness-based solutions. *Reliability engineering & system safety* 190: 106506.
- Ouyang M and Wang Z (2015) Resilience assessment of interdependent infrastructure systems: With a focus on joint restoration modeling and analysis. *Reliability Engineering and System Safety* 141: 74-82.

- Padgett JE and Li Y (2014) Risk-based assessment of sustainability and hazard resistance of structural design. *Journal of Performance of Constructed Facilities* 30(2): 04014208.
- Pardalos PM, Rasskazova V and Vrahatis MN (2021) *Black Box Optimization, Machine Learning, and No-Free Lunch Theorems*. Springer.
- Park J, Towashiraporn P, Craig JI, et al. (2009) Seismic fragility analysis of low-rise unreinforced masonry structures. *Engineering Structures* 31(1): 125-137.
- Pekcan G, Itani AM and Linke C (2014) Enhancing seismic resilience using truss girder frame systems with supplemental devices. *Journal of Constructional Steel Research* 94: 23-32.
- Porter KA (2003) An overview of PEER's performance-based earthquake engineering methodology. *Proceedings of ninth international conference on applications of statistics and probability in civil engineering*. 1-8.
- Qian J and Dong Y (2020) Multi-criteria decision making for seismic intensity measure selection considering uncertainty. *Earthquake Engineering and Structural Dynamics* 49(11): 1095-1114.
- Qian J and Dong Y (2022a) Surrogate-assisted seismic performance assessment incorporating vine copula captured dependence. *Engineering Structures* 257: 114073.
- Qian J and Dong Y (2022b) Uncertainty and multi-criteria global sensitivity analysis of structural systems using acceleration algorithm and sparse polynomial chaos expansion. *Mechanical Systems and Signal Processing* 163: 108120.
- Qin H (2022) Decision-making under uncertainty for buildings exposed to environmental hazards. *Journal of Safety Science and Resilience* 3(1): 1-14.
- Rackwitz R (2002) Optimization and risk acceptability based on the life quality index. *Structural Safety* 24(2-4): 297-331.
- Ramirez C, Liel A, Mitrani - Reiser J, et al. (2012) Expected earthquake damage and repair costs in reinforced concrete frame buildings. *Earthquake Engineering & Structural Dynamics* 41(11): 1455-1475.
- Rasmussen CE (2003a) Gaussian processes in machine learning. *Advanced lectures on machine learning*. Springer, pp.63-71.
- Rasmussen CE (2003b) Gaussian processes in machine learning. *Summer school on machine learning*. Springer, 63-71.
- Rodriguez-Nikl T (2015) Linking disaster resilience and sustainability. *Civil Engineering and Environmental Systems* 32(1-2): 157-169.
- Roohi M, van de Lindt JW, Rosenheim N, et al. (2020) Implication of building inventory accuracy on physical and socio-economic resilience metrics for

- informed decision-making in natural hazards. *Structure & Infrastructure Engineering*. 1-21.
- Rossetto T and Peiris N (2009) Observations of damage due to the Kashmir earthquake of October 8, 2005 and study of current seismic provisions for buildings in Pakistan. *Bulletin of Earthquake Engineering* 7(3): 681-699.
- Rousakis TC (2018) Inherent seismic resilience of RC columns externally confined with nonbonded composite ropes. *Composites Part B: Engineering* 135: 142-148.
- Sabatino S, Frangopol DM and Dong Y (2015) Sustainability-informed maintenance optimization of highway bridges considering multi-attribute utility and risk attitude. *Engineering Structures* 102: 310-321.
- Schaffer JD (1985) Multiple objective optimization with vector evaluated genetic algorithms. *Proceedings of the first international conference on genetic algorithms and their applications, 1985*. Lawrence Erlbaum Associates. Inc., Publishers.
- Schulz E, Speekenbrink M and Krause A (2018) A tutorial on Gaussian process regression: Modelling, exploring, and exploiting functions. *Journal of mathematical psychology* 85: 1-16.
- Sen MK, Dutta S, Kabir G, et al. (2021) An integrated approach for modelling and quantifying housing infrastructure resilience against flood hazard. *Journal of Cleaner Production* 288: 125526.
- Sharma N and Gardoni P (2018) Modeling the time-varying performance of electrical infrastructure during post disaster recovery using tensors. *Routledge handbook of sustainable and resilient infrastructure*. pp.263-280.
- Sharma N and Gardoni P (2022) Mathematical modeling of interdependent infrastructure: An object-oriented approach for generalized network-system analysis. *Reliability engineering & system safety* 217: 108042.
- Sharma N, Nocera F and Gardoni P (2021) Classification and mathematical modeling of infrastructure interdependencies. *Sustainable and Resilient Infrastructure* 6(1-2): 4-25.
- Silva V (2018) Critical issues on probabilistic earthquake loss assessment. *Journal of Earthquake Engineering* 22(9): 1683-1709.
- Silva V, Crowley H, Pagani M, et al. (2014) Development of the OpenQuake engine, the Global Earthquake Model's open-source software for seismic risk assessment. *Natural hazards* 72(3): 1409-1427.
- Šipoš TK and Hadzima-Nyarko M (2017) Rapid seismic risk assessment. *International journal of disaster risk reduction* 24: 348-360.

- Stein M (1987) Large sample properties of simulations using Latin hypercube sampling. *Technometrics* 29(2): 143-151.
- Stewart JP, Douglas J, Javanbarg M, et al. (2015) Selection of ground motion prediction equations for the global earthquake model. *Earthquake Spectra* 31(1): 19-45.
- Stojadinović Z, Kovačević M, Marinković D, et al. (2021) Rapid earthquake loss assessment based on machine learning and representative sampling. *Earthquake Spectra*. 87552930211042393.
- Su L, Wan H-P, Dong Y, et al. (2019) Seismic fragility assessment of large-scale pile-supported wharf structures considering soil-pile interaction. *Engineering Structures* 186: 270-281.
- Sundararajan S and Keerthi SS (2001) Predictive approaches for choosing hyperparameters in Gaussian processes. *Neural computation* 13(5): 1103-1118.
- Tesfamariam S and Goda K (2015) Loss estimation for non - ductile reinforced concrete building in Victoria, British Columbia, Canada: effects of mega - thrust Mw9 - class subduction earthquakes and aftershocks. *Earthquake Engineering and Structural Dynamics* 44(13): 2303-2320.
- Thermou G and Elnashai AS (2006) Seismic retrofit schemes for RC structures and local - global consequences. *Progress in Structural Engineering and Materials* 8(1): 1-15.
- Tirca L, Serban O, Lin L, et al. (2016) Improving the seismic resilience of existing braced-frame office buildings. *Journal of Structural Engineering* 142(8): C4015003.
- Tversky A and Kahneman D (1992) Advances in prospect theory: Cumulative representation of uncertainty. *Journal of Risk and Uncertainty* 5(4): 297-323.
- Vamvatsikos D and Cornell A (2006) Direct estimation of the seismic demand and capacity of oscillators with multi-linear static pushovers through IDA. *Earthquake Engineering and Structural Dynamics* 35(9): 1097-1117.
- Vettore M, Donà M, Carpanese P, et al. (2020) A multilevel procedure at urban scale to assess the vulnerability and the exposure of residential masonry buildings: The case study of Pordenone, Northeast Italy. *Heritage* 3(4): 1433-1468.
- Vona M, Mastroberti M, Mitidieri L, et al. (2018) New resilience model of communities based on numerical evaluation and observed post seismic reconstruction process. *International journal of disaster risk reduction* 28: 602-609.
- Voutchkov I and Keane A (2010) Multi-objective optimization using surrogates. *Computational Intelligence in Optimization*. Springer, pp.155-175.

- Wang F, Li Y, Zhang H, et al. (2019) An adaptive weight vector guided evolutionary algorithm for preference-based multi-objective optimization. *Swarm and Evolutionary Computation* 49: 220-233.
- Wang X, Shahzad MM and Wang T (2021) Research on dynamic response characteristics and control effect of mega-sub controlled structural system under long-period ground motions. *Structures*. Elsevier, 225-234.
- Wang Y, Wang N, Lin P, et al. (2020) Life-cycle analysis (LCA) to restore community building portfolios by building back better I: Building portfolio LCA. *Structural Safety* 84: 101919.
- Wang Z, Jin W, Dong Y, et al. (2018) Hierarchical life-cycle design of reinforced concrete structures incorporating durability, economic efficiency and green objectives. *Engineering Structures* 157: 119-131.
- Waseem M, Khan S and Khan MA (2020) Probabilistic Seismic Hazard Assessment of Pakistan Territory Using an Areal Source Model. *Pure and Applied Geophysics*. 1-21.
- Wen W, Zhang M, Zhai C, et al. (2019) Resilience loss factor for evaluation and design considering the effects of aftershocks. *Soil Dynamics and Earthquake Engineering* 116: 43-49.
- Whitman RV, Anagnos T, Kircher CA, et al. (1997) Development of a national earthquake loss estimation methodology. *Earthquake Spectra* 13(4): 643-661.
- Xu M, Ouyang M, Mao Z, et al. (2019) Improving repair sequence scheduling methods for postdisaster critical infrastructure systems. *Computer - Aided Civil and Infrastructure Engineering* 34(6): 506-522.
- Yamin LE, Hurtado A, Rincon R, et al. (2017) Probabilistic seismic vulnerability assessment of buildings in terms of economic losses. *Engineering Structures* 138: 308-323.
- Yang DY and Frangopol DM (2018) Bridging the gap between sustainability and resilience of civil infrastructure using lifetime resilience. *Chapter 23 in Routledge Handbook of Sustainable and Resilient Infrastructure*. Routledge, pp.419-442.
- Yang DY and Frangopol DM (2019) Life-cycle management of deteriorating civil infrastructure considering resilience to lifetime hazards: A general approach based on renewal-reward processes. *Reliability engineering & system safety* 183: 197-212.
- Yeo GL and Cornell CA (2009) Building life-cycle cost analysis due to mainshock and aftershock occurrences. *Structural Safety* 31(5): 396-408.

- Zavadskas EK, Kaklauskas A, Peldschus F, et al. (2007) Multi-attribute assessment of road design solutions by using the COPRAS method. *Baltic Journal of Road Bridge Engineering* 2(4).
- Zentner I, Gündel M and Bonfils N (2017) Fragility analysis methods: Review of existing approaches and application. *Nuclear Engineering and Design* 323: 245-258.
- Zhang N, Gu Q, Dong Y, et al. (2021) Seismic performance of bridges with ECC-reinforced piers. *Soil Dynamics and Earthquake Engineering* 146: 106753.
- Zhao X, Li W and Stanbrook J (2014) A framework for the integration of performance based design and life cycle assessment to design sustainable structures. *Advances in Structural Engineering* 17(4): 461-470.
- Zheng Y and Dong Y (2019) Performance-based assessment of bridges with steel-SMA reinforced piers in a life-cycle context by numerical approach. *Bulletin of Earthquake Engineering* 17(3): 1667-1688.
- Zheng Y, Dong Y, Chen B, et al. (2019) Seismic damage mitigation of bridges with self-adaptive SMA-cable-based bearings. *Smart Structures and Systems* 24(1): 127-139.
- Zheng Y, Dong Y and Li Y (2018) Resilience and life-cycle performance of smart bridges with shape memory alloy (SMA)-cable-based bearings. *Construction and building materials* 158: 389-400.
- Zinke T, Bocchini P, Frangopol D, et al. (2012) Combining resilience and sustainability in infrastructure projects. In: *Life-Cycle and Sustainability of Civil Infrastructure Systems. Proceedings of the Third International Symposium on Life-Cycle Civil Engineering, Vienna, Austria, 3-6 October 2012*, pp.473.
- Zitzler E, Laumanns M and Thiele L (2001) SPEA2: Improving the strength Pareto evolutionary algorithm. *TIK-report* 103.